Fossil Record

25 (2) 2022

PENSOFT

MUSEUM FÜR NATURKUNDE BERLIN

Fossil Record
An International Journal of Palaeontology

Fossil Record

2022. Volume 25. Issue 2

ISSN: 2193-0066 (print), 2193-0074 (online)

In Focus

The cover picture shows *Pterodactylus antiquus* Soemmerring, 1812

See paper of **Augustin FJ, Kampouridis P, Hartung J, Albersdörfer R, Matzke AT** The geologically oldest specimen of Pterodactylus: a new exquisitely preserved skeleton from the Upper Jurassic (Kimmeridgian) Plattenkalk deposits of Painten (Bavaria, Germany).

Cover design

PENSOFT

Fossil Record
An International Journal of Palaeontology

Content of volume **25** (**2**) 2022

Arratia G
The outstanding suction-feeder *Marcopoloichthys furreri* new species (Actinopterygii) from the Middle Triassic Tethys Realm of Europe and its implications for early evolution of neopterygian fishes 231

Joyce WG, Bourque JR, Fernandez V, Rollot Y
An alternative interpretation of small-bodied turtles from the "Middle Purbeck" of England as a new species of compsemydid turtle 236

Adrian B
Stratigraphic range extension of the turtle *Boremys pulchra* (Testudinata, Baenidae) through at least the uppermost Cretaceous 275

Kiesmüller C, Haug JT, Müller P, Hörnig MK
A case of frozen behaviour: A flat wasp female with a beetle larva in its grasp in 100-million-year-old amber 287

Jöst AB, Kim T, Yang H-S, Kang D-H, Karanovic I
Revision of the *Semicytherura henryhowei* group (Crustacea, Ostracoda) with the new records from Korea 307

Augustin FJ, Kampouridis P, Hartung J, Albersdörfer R, Matzke AT
The geologically oldest specimen of *Pterodactylus*: a new exquisitely preserved skeleton from the Upper Jurassic (Kimmeridgian) Plattenkalk deposits of Painten (Bavaria, Germany) 311

Abstract & Indexing Information

Biological Abstracts® (Thompson ISI)
BIOSIS Previews® (Thompson ISI)
Camgridge Scientific Abstracts (CSA/CIG)
Web of Science® (Thompson ISI)
Zoological Record™ (Thompson ISI)

Fossil Record 25 (2) 2022, 231–261 | DOI 10.3897/fr.25.85621

PENSOFT

für Natur MUSEUM FÜR NATURKUNDE BERLIN

The outstanding suction-feeder *Marcopoloichthys furreri* new species (Actinopterygii) from the Middle Triassic Tethys Realm of Europe and its implications for early evolution of neopterygian fishes

Gloria Arratia[1,2]

1 *Biodiversity Institute, University of Kansas, Dyche Hall, 1345 Jayhawk Blvd., Lawrence, Kansas 66045, USA*

2 *Department of Ecology and Evolutionary Biology, University of Kansas, Lawrence, Kansas 66045, USA*

https://zoobank.org/48170AC2-9C0B-42AF-9CCD-3C770113F4CE

Corresponding author: Gloria Arratia (garratia@ku.edu)

Academic editor: Florian Witzmann ♦ **Received** 20 April 2022 ♦ **Accepted** 14 June 2022 ♦ **Published** 5 July 2022

Abstract

Marcopoloichthys furreri **sp. nov.**, a small scaleless fish from the Ladinian of Switzerland, is described based on ten well preserved specimens, which provide outstanding morphological information, allowing the re-study of the family and generic diagnoses that were solely based on a few Eurasian marcopoloichthyids. An exhaustive investigation of morphological features of *M. furreri* provides evidence of new morphological structures not previously known in Triassic neopterygians (e.g., supraneural carrier; two pairs of nasal bones; mesethmoid; series of three bony postcleithra) that are interpreted as autapomorphies of *Marcopoloichthys*, which occur together with some primitive features (e.g., lack of supramaxillae; presence of surangular and coronoid; aspondylous vertebral column; clavicle present). The combination of primitive and advanced characters proved to be critical when *M. furreri* was added to a previous hypothesis of neopterygian relationships, because it provided unquestionable support for *Marcopoloichthys* as a stem teleost or teleosteomorph. Some characters supporting this interpretation are the presence of a mobile premaxilla; an unpaired vomer; and first and last principal rays forming leading margins of caudal fin. Additionally, *Marcopoloichthys furreri*, due to a combination of teleostean synapomorphies (e.g., epineural processes; four pectoral radials; propterygium fused with first pectoral ray), stands in a polytomy with aspidorhynchiforms and more advanced teleosteomorphs in another phylogenetic analysis. Consequently, the combination of characters of *Marcopoloichthys* is relevant for understanding the taxonomy and systematics of crown neopterygians. Marcopoloichthyids were suction-feeding fishes, and the excellent preservation of the new species permits discussion of the anatomical modifications involved in the feeding and resting processes.

Key Words

advanced Neopterygii, Ladinian, morphology, Prosanto Formation, Switzerland, systematics, taxonomy

Introduction

The new material studied here was recovered in Ducanfurgga in a few localities of the Prosanto Formation near Davos, Canton Graubünden (Grisons), Swiss Alps. The Prosanto Formation forms part of the marine Middle Triassic (Ladinian) from the Silvretta Nappe (Fig. 1). The depositional environment of the Prosanto Formation is interpreted as a localized basin with a stratified waterbody that resulted in oxygen-depleted bottom water. Details of the geology, stratigraphy, and paleoecology have been described by Eichenberger (1986), Bürgin et al. (1991), Furrer et al. (1992), and Furrer (1995, 1999, 2004). After reviewing the lithology of the specimens, which is always a finely laminated grey limestone typical of the uppermost Prosanto Formation, it is suggested that all the specimens included in this contribution originated from this uppermost part, about 10 to 20 meters below the upper boundary and a few meters above the volcanic ash layer known as "Ducan I" (Furrer pers. com., December 2021).

Starting in 1989, a large number of new fossils from the Prosanto Formation had been discovered in systematic excavations by Dr. Heinz Furrer and his team from the University of Zurich. The recovered fossils include calcareous algae, bivalves, gastropods, cephalopods, crustaceans (Bürgin et al. 1991), and vertebrates, such as fishes and reptiles, with the fish fauna largely dominated by the actinopterygian *Habroichthys* (Bürgin 1999; Furrer 2019). The fishes that have been described are mainly actinopterygians, such as saurichthyiforms (e.g., *Saurichthys curionii* [Bellotti, 1857], *S. costasquamosus* Rieppel, 1985), perleidiforms (e.g., *Platysiagum minus* Egerton, 1872; *Ctenognathichthys bellotti* Bürgin, 1992; *Ctenognathichthys hattichi* Bürgin & Herzog, 2002; *Peltoperleidus ducanensis* Bürgin et al., 1991), peltopleuriforms (*Peltopleurus lissocephalus* Brough, 1939; *Peripeltopleurus vexillipinnis* Bürgin, 1992; *Peltoperleidus obristi* Herzog, 2001), stem neopterygians (*Habroichthys minimus* Brough, 1939 and Bürgin 1990; *H. griffithi* Bürgin, 1992), and parasemionotiforms (e.g., *Eoeugnathus megalepis* Brough, 1939 and Herzog 2003; and *Prosantichthys buergeni* Arratia & Herzog, 2007). Undescribed actinopterygians include *Colobodus* sp., *Luganoia* sp., *Eosemionotus* sp., *Archaeosemionotus* sp, and many others (see Bürgin 1999: appendix 2 and Furrer 2019), as well as two coelacanthiforms, *Ticinepomis peyeri* (Cavin et al., 2013) and *Foreyia maxkuhni* (Cavin et al., 2017).

Among the fishes mentioned in the literature, there are three specimens from the Prosanto Formation that

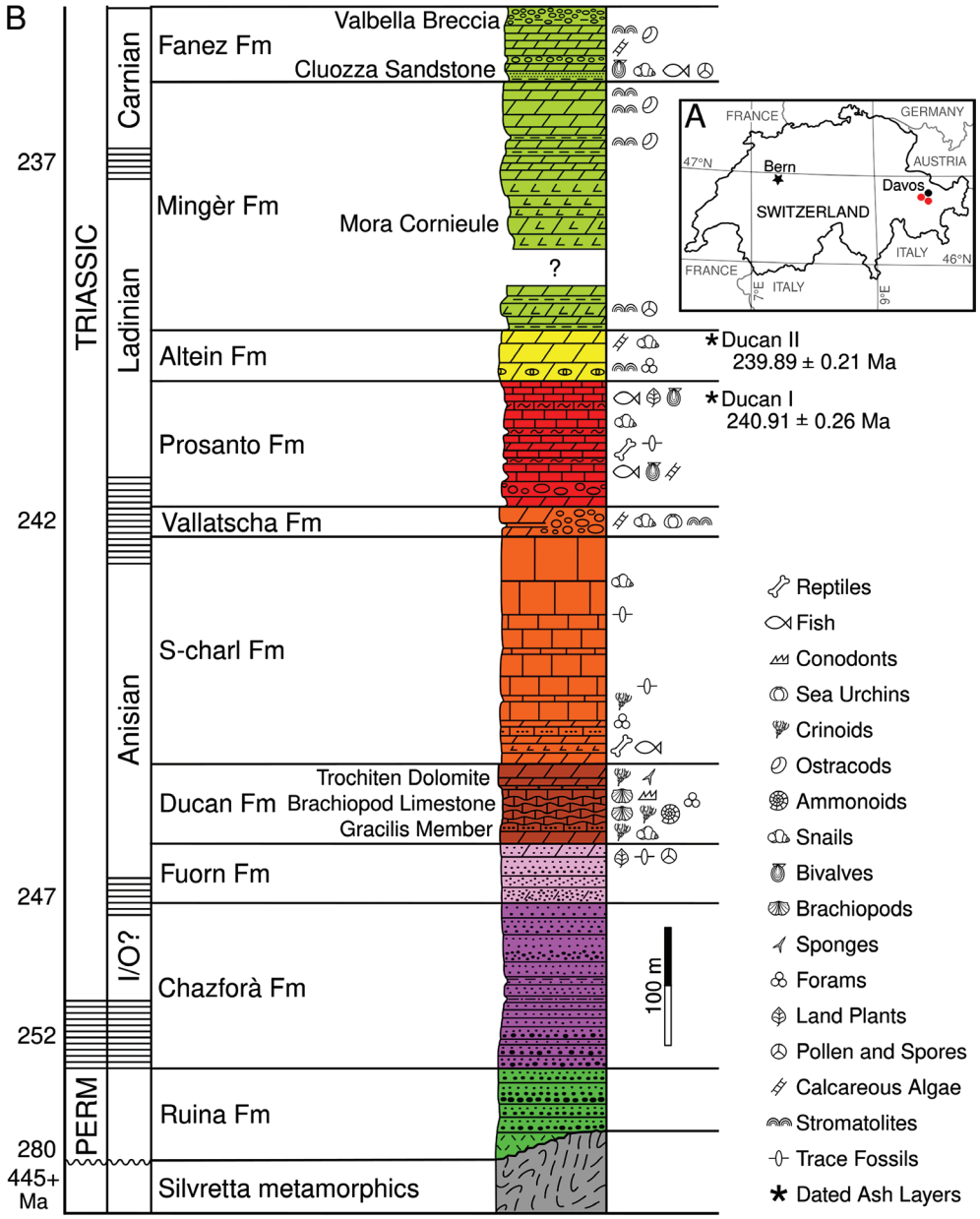

Figure 1. A. Approximate geographic position of localities containing *Marcopoloichthys furreri* sp. nov., indicated with red circles; **B.** Stratigraphy of the Silvreta Nappe with special emphasis of the Prosanto Formation and distribution of faunas and floras. Abbreviated and slightly modified from Furrer (2019: fig. 11).

were previously identified as *Prohalecites* sp. (Bürgin et al. 1991) or Neopterygii incertae sedis gen. et sp. indet. (Bürgin 1999: fig. 8) that are included in this study. These specimens, plus six others collected between 1991 and 2003 in the Early Ladinian strata of the Prosanto Fm., were preliminarily listed in the catalogue as "gen. and sp. indet.", which included a young individual about 23 mm maximum length. Due to their preservation, a long process of careful preparation was required, which revealed features common to all of them. In 2021, a new specimen of this fish was collected. These ten specimens are studied herein, including an extensive anatomical description allowed by the excellent preservation, plus the description of a few anatomical structures previously unreported in fish anatomy. They are assigned to the family Marcopoloichthyidae and its genus *Marcopoloichthys* (Tintori et al., 2007), whose original diagnoses are based on much lesser quality material from the Anisian of China (*Marcopoloichthys ani*) and the Norian of Italy (*M. ani*, *M. andreettii*, and *M. faccii*, which was previously described as *Pholidophorus faccii* by Gortani in 1907). Marcopoloichthyids were broadly interpreted as basal neopterygians by Tintori et al. (2017), following Patterson's (1973) conception of Neopterygii, although the authors mentioned certain similarities with the Middle Triassic teleosteomorph *Prohalecites*.

Marcopoloichthyids, which are small fishes of about 5 cm maximum length, are easy to identify because of their special mouth configuration as suction feeders together with a naked body and a vertebral column with a persistent, functional notochord and well-developed arcocentral vertebral elements. The nice preservation of the new species described herein from the Prosanto Formation in Switzerland allows the description of several cranial and vertebral column characters that were unknown, making this the most completely known species within the family. Additionally, specimens of different sizes exhibit ontogenetic changes that lead to reevaluation of the family and generic diagnoses, and the excellent preservation of specimens with closed and open mouths yields an understanding of the suction feeding mechanism of marcopoloichthyids. A phylogenetic analysis was conducted to investigate the position of these fishes among Neopterygii.

Material and methods

The material studied here consists of ten specimens, nine of which are catalogued in the collections of the Paleontological Institute and Museum, University of Zurich, Switzerland (**PIMUZ**) and one in the Bündner Naturmuseum, Chur, Canton Graubünden (**BNM**). Most of the specimens were found at localities in the so-called "Ducan" mountain chain: Ducanfurgga, Ducantal, Gletscher Ducan and the upper Val da Stugl—all within three km on both sides of the mountain "Gletscher Ducan" (Fig. 1; Table 1).

The older collected specimens used in the description of the new species were mechanically prepared by Angela Ceola and Christian Obrist, whereas the most recently collected were both mechanically prepared by Christin Obrist and acid prepared (3–5% formic acid) by Heinz Furrer.

Wild FM 8 and Leica MZ9 stereomicroscopes equipped with a camera lucida were used by the author to prepare the line drawings of the specimens. Parts of the specimens were photographed under normal light at the Museum für Naturkunde, Leibniz Institute for Evolution and Biodiversity Science (Berlin, Germany); others were photographed at the Paleontological Institute and Museum, University of Zurich. Most illustrations are based directly on specimens; a few are based on photographs. Photographs are not retouched with Photoshop. The latter was only used to label figures.

Anatomical terminology

The terminology of the skull roof bones follows Westoll (1943), Jollie (1962), and Schultze (2008 and literature cited therein) that has been recently confirmed using other evidence (Teng et al. 2019). To avoid confusion, the first time that the parietal and postparietal bones are cited in the text, as well as in all figures, the traditional terminology is shown in square brackets, e.g., parietal bone [= frontal]: pa [= fr]. The terminology of the vertebral column follows Arratia et al. (2001) and Arratia (2015), whereas that of the caudal endoskeletal elements and caudal skeletal types (e.g., polyural or diural) follows Nybelin (1963), Schultze and Arratia (1988, 1989, 2013), and Arratia and Schultze (1992, 2013). The count of vertebrae follows Tintori et al. (2007) to ensure that the results are comparable. The

Table 1. Record of specimens of *Marcopoloichthys furreri* sp. nov. from the Prosanto Formation (Early Ladinian), Switzerland.

Catalogue Nr.	Locality	Community	Date	References
A/I 1194	Valbellahorn 2	Wiesen	21.08.1989	Bürgin et al. (1991); herein
A/I 1924	Ducantal-Mannli-Schutthalde	Davos Sertig	1990	Bürgin et al. (1991); herein
A/I 1958	Gletscher Ducan 3	Stugl-Bergün	21.08.1991	Bürgin (1999); herein
A/I 2841	Gletscher Ducan 3	Stugl-Bergün	21.08.1991	Herein
A/I 2886	Gletscher Ducan	Davos Sertig	30.07.2003	Herein
A/I 2888	Ducanfurgga 4	Davos Sertig	1999	Herein
A/I 2889	Ducanfurgga 4	Davos Sertig	2000	Herein
A/I 2890	Gletscher Ducan	Davos Sertig	2000	Herein
A/I 3209	Ducanfurgga 3	Davos Sertig	17.07.1998	Herzog (2003); herein
BNM 201166	Val da Stugl-NE P. 2523	Stugl-Bergün	2021	Herein

terms fin rays, scutes, fulcra and its different types, procurrent rays, epaxial rudimentary rays, and principal rays follow definitions provided by Arratia (2008, 2009).

Phylogenetic analysis

A phylogenetic analysis was conducted to test the position of *Marcopoloichthys* among neopterygians. This analysis used the list of characters and matrix of Chen and Arratia (2022; Suppl. materials 1, 2), which is an expanded matrix of Xu (2020a) and has a large representation of neopterygian clades. *Boreosomus*, *Moythomasia*, and *Pteronisculus* were included in the outgroup. A second phylogenetic analysis was performed to test the position of *Marcopoloichthys* among teleosteomorphs. This analysis used the list of characters and matrix of Arratia et al. (2021; Suppl. materials 3, 4). *Australosomus*, *Bergeria* and *Polypterus* were used as outgroups. The phylogenetic analyses were conducted using PAUP* 4 (PAUP 4.0a169). All characters are unordered and unweighted.

Systematic paleontology

Superclass Actinopterygii Cope, 1887
Neopterygii Regan, 1923 sensu Xu (2020b)
Infraclass Teleosteomorpha Arratia, 2001

Family Marcopoloichthyidae Tintori et al., 2007

Emended diagnosis. The family diagnosis is based on a unique combination of characters (uniquely derived features among teleosteomorphs are identified with an asterisk [*]): Small fishes about 55 mm maximum length, with naked body, and highly modified protractile upper and lower jaws giving the anterior part of the head a characteristic profile [*]. The body shape is torpedo-like, with a head about 50% deeper than the caudal peduncle [*]. T-shaped mesethmoid with strong lateral processes. Two pairs of nasal bones [*]. Absence of supramaxillae [*]. Absence of dentition [*]. Preopercle L-shaped. Interopercle small triangle-like. Vertebral column with persistent notochord in older forms; chordacentral vertebral column in younger. Vertebral caudal region diplospondylous, with small interdorsal and interventral elements. Ossified ribs absent. Short, stout epineural processes associated to the abdominal neural arches. Large and curved pelvic plates. First dorsal fin proximal radial enlarged and plate-like, resulting from fusion of three or more radials and supporting four or more dorsal rays [*]. Enlarged last dorsal proximal radial supporting several dorsal rays [*]. First anal fin proximal radial basally expanded and very elongate and dorso-anteriorly bent, acting as post-coelomic bone [*]. Last anal fin proximal radial highly modified, expanded, and plate-like, supporting three or more lepidothrichia [*]. No fringing fulcra associated with paired, dorsal, or anal fins. Homocercal caudal fin with both lobes deeply forked. Body lobe of the caudal fin completely reduced. Ural region with five or six broad and short hypurals. Diastema hypural absent or very narrow. Caudal fin with dorsal and ventral scutes; well-developed epaxial and hypaxial basal fulcra; short series of epaxial and hypaxial fringing fulcra reaching about half length of first and last principal rays. Accessory fulcra present in hypaxial caudal lobe. Procurrent rays only present in the hypaxial lobe of caudal fin. Eighteen to 21 principal caudal rays. A few large scales around urogenital opening [*].

Content. One genus and four species known, *Marcopoloichthys ani*, *M. andreetti*, *M. faccii*, and *M. furreri* sp. nov.

Geographic distribution. Eurasian distribution, including Southern China (Yunnan and Guizhou Provinces), Northern Italy (Lombardy and Friuli), and eastern Switzerland (Canton Graubünden). Another undescribed species is present in the Middle Triassic of southern Switzerland, in Monte San Giorgio, Canton Ticino; T. Bürgin, pers. comm., 2022.

Age. From Anisian (Middle Triassic) to Norian (Late Triassic).

Genus *Marcopoloichthys* Tintori et al., 2007

Diagnosis. Same as family diagnosis.

***Marcopoloichthys furreri* sp. nov.**

https://zoobank.org/501280EA-CD8A-4464-96DE-C130D417D05C
Figs 2–14

1991 *Prohalecites* sp. Bürgin et al., p. 964, mention (for specimens PIMUZ A/I 1194 and 1924).
1999 Gen. et sp. indet. Bürgin, p. 487, fig. 8, mention (for specimen PIMUZ A/1 1958).
1999 Neopterygii *incertae sedis*. Bürgin, p. 494, app. 2, mention (for specimen PIMUZ A/1 1958).
2003 Halecostomi gen. et sp. indet. Herzog, p. 93, mention, text-fig. 29 and pl. 18/2 (for specimen PIMUZ A/1 3209).

Diagnosis. The species diagnosis is based on a unique combination of characters: The largest marcopoloichthyid reaching ca 55 mm maximum length. Skull roof covered with small and rounded oval tubercles and a few ridges of ganoine. Premaxilla and maxilla with slightly expanded articular region, spatulate-like and with crenulated anterior margin. Dentary ornamented with strong ridges and deep grooves; anterior margin covered with well-developed tubercles of different shapes. Short vertebral column with 33 to 35 vertebral segments, the first five fused into one element, the supradorsal carrier. With about nine supradorsal bones; the first five expanded distally, followed by sigmoid-shaped supradorsals; last supradorsal bones placed in front of the plate-like first compound dorsal proximal radial. Abdominal and first caudal neural arches with stout epineural processes reaching the next posterior neural arch. Dorsal fin support with first expanded proximal radial a massive squarish plate formed by fusion of four proximal radials. Last anal proximal radial with

long and distally expanded region supporting several lepidotrichia. Five hypurals; no hypural diastema present. Ten or 11 epaxial basal fulcra. Short series of epaxial fringing fulcra. Twenty or 21 principal caudal rays with straight segmentation. One to three short hypaxial procurrent rays; accessory hypaxial fulcra present. About 12 hypaxial basal fulcra. No urodermals present. With three or four large, ovoid scales associated with the urogenital region.

Derivation of name. The species name, *furreri*, honors Dr. Heinz Furrer who has dedicated most of his distinguished professional career to Triassic fossils of Switzerland, especially those of the Prosanto Formation.

Holotype. PIMUZ A/I 2886, an almost complete specimen, very well preserved (Fig. 2A) with a bent abdominal vertebral region; it was collected in Gletscher Ducan, Davos, in the Canton of Graubünden, Switzerland on July 30, 2003. Upper Prosanto Fm., Early Ladinian, Middle Triassic.

Paratypes. PIMUZ A/I 1194, TL about 23 mm; poorly preserved. PIMUZ A/I 1924, almost complete specimen, but it appears longitudinally compressed; poorly preserved. PIMUZ A/I 1958 almost complete, very well-preserved specimen from the same locality as holotype. PIMUZ A/1 2886, complete specimen: TL ca 50 mm. PIMUZ A/I 2888, incomplete, disarticulated specimen with well-preserved disarticulated pectoral girdle and fin. PIMUZ A/I 2889, incomplete specimen; anterior part of body, some abdominal vertebrae, pectoral and pelvic fins poorly preserved. PIMUZ a/1 2890, incomplete specimen missing part of head, paired fins, anal fin and posterior part of caudal fin. PIMUZ A/I 3209, an almost complete specimen of about 54.5 mm maximum length, with nicely preserved head and caudal fin. BNM 201166, almost complete specimen of ca 45 mm total length. See Table 1 for more information concerning specific specimens.

Type locality and age. Gletscher Ducan, Davos, in the Canton Graubünden, Switzerland. Upper Prosanto Fm., Early Ladinian, Middle Triassic. See Table 1 for information on localities and ages of specimens studied.

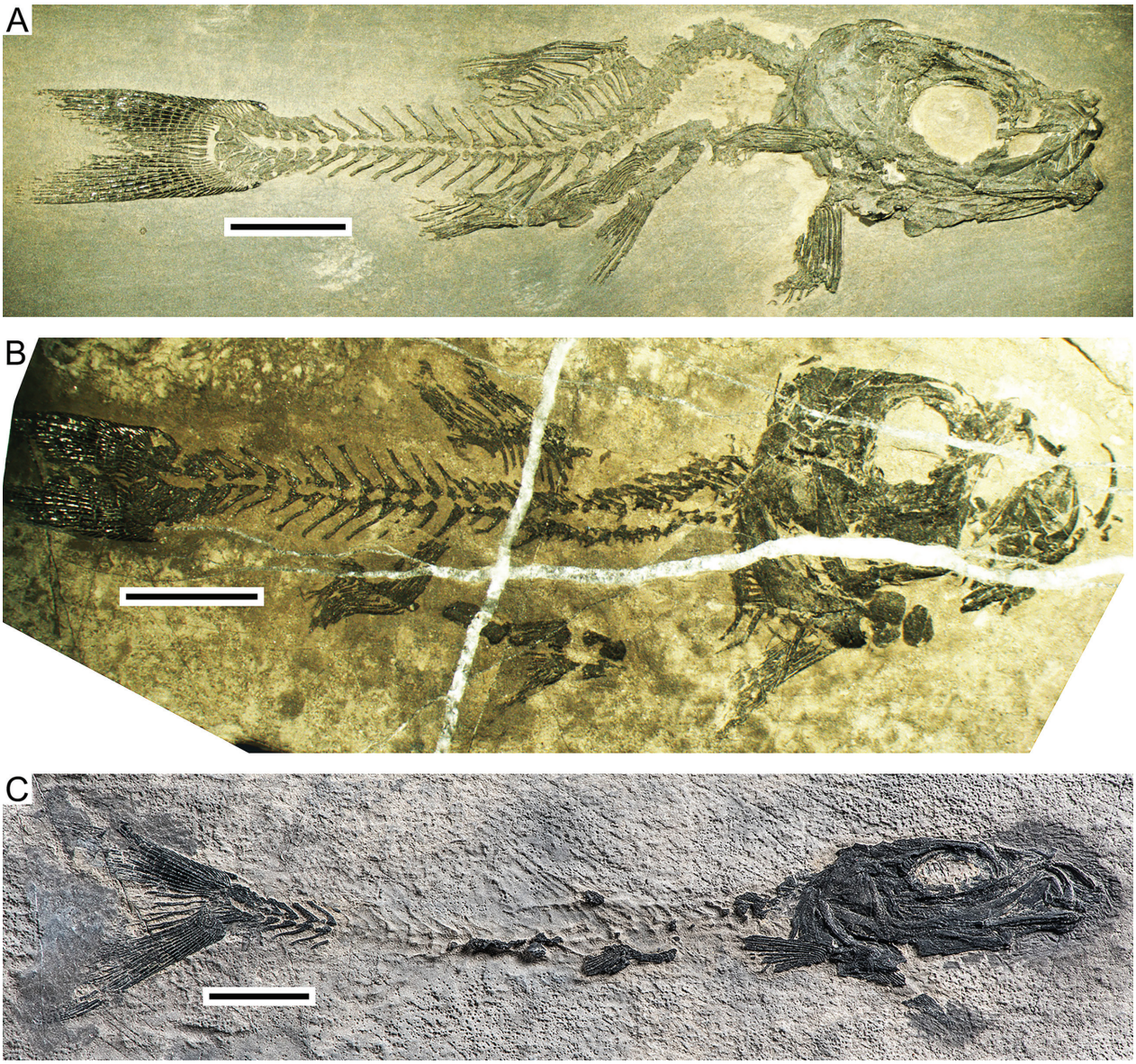

Figure 2. *Marcopoloichthys furreri* sp. nov. in lateral view. **A.** Holotype, PIMUZ A/I 2886; **B.** Paratype BNM 201166; **C.** Paratype PIMUZ A/I 3209. Scale bars: 5 mm. Photographs in **A** and **B** were taken by T. Scheyer and in **C** by C. Radke.

Figure 3. *Marcopoloichthys furreri* sp. nov. in lateral view. **A.** Paratype PIMUZ A/I 1958; **B.** Paratype PIMUZ A/I 2841. Scale bars: 5 mm. Photographs were taken by C. Radke.

Description. ***General description*.** The fish is ca 55 mm total length, slightly torpedo-like form (Fig. 2), with the head about three times deeper than the caudal peduncle. The dorsal fin insertion placed near to or at the midpoint of standard length (51–53% of SL). The pelvic fin insertion is placed at the same level of the dorsal fin insertion, but in one specimen is placed anteriorly (48–54%). The anal fin insertion is closer to the insertion of the pelvic fins than to the caudal fin (60–68% of SL); consequently, the fish has a long peduncle. The head is proportionally large, about 33 to 38% of standard length, and its aspect is very different when the mouth is closed compared to open. When the mouth is closed, most of the dorsal profile of the head looks gently rounded, decreasing in depth anteriorly (Fig. 3A; PIMUZ A/I 1958). When the fish is preserved in "feeding mode", the mouth is extended anteriorly, as well as the bones supporting the lower jaw, giving the head a characteristic profile (Figs 2C, 4; PIMUZ A/I 3209). The orbit is moderately large, about 28 to 39% of head length, and the preorbital region is moderately short, ca 25% of head length (specimens with closed mouth). The pectoral fins have a low position, closer to the ventral margin of the body than to the middle region of the flank (Figs 2, 3). The caudal fin is homocercal with both lobes almost the same size and with its posterior margin deeply forked. All exposed surfaces of cranial bones are ornamented with tubercles and longitudinal ridges covered with a thin layer of ganoine. The lateral surface of fin rays and fulcra is covered with a thin layer of ganoine. The body is naked, except for a few large scales (or scutes?) around the urogenital region, probably one in front of the dorsal fin, and dorsal and ventral scutes in the caudal fin.

***Skull roof and braincase*.** Although the skull roof is preserved in several specimens, it is almost impossible to trace each bone, because sutures are not visible due to fusion (Figs 4, 5). As the preservation permits, the bones of the skull roof apparently have smooth surfaces; however, under magnification, the bony surfaces may be densely ornamented with small, round or oval tubercles and short, longitudinal ridges (Fig. 5B). The ornamentation is covered by a thin layer of ganoine.

The parietal [= frontal] region is about 2.5–3 times longer than the postparietal [= parietal] region, and the limit between dermopterotic and postparietal cannot be traced (Figs 4, 5A, B). Consequently, it is assumed here that the postparietal and dermopterotic are fused to each other. This possibility is supported by the skull roof of the paratypes PIMUZ A/I 2887 and PIMUZ A/I 3209 (Figs 4, 5). According to available information, no specimen illustrates a complete fusion involving left and right sides of the skull roof, but each side is independent from its antimere.

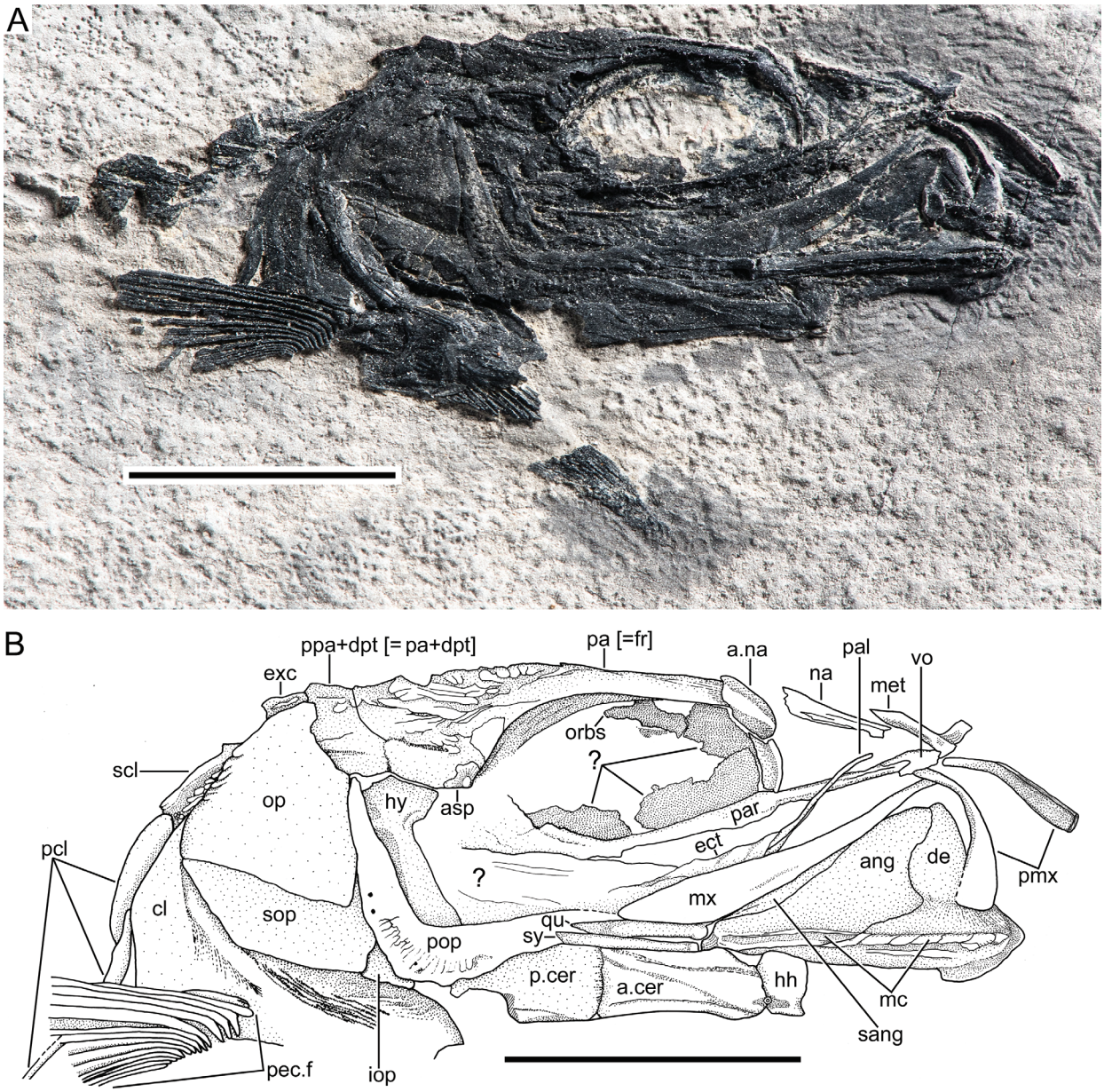

Figure 4. *Marcopoloichthys furreri* sp. nov. **A.** Photograph of right side of the skull roof of paratype PIMUZ A/I 2887 (photograph was taken by C. Radke); **B.** Interpretative drawing. Abbreviations: a.cer, anterior ceratohyal; a.na, accessory nasal bone; ang, angular; asp, autosphenotic; cl, cleitrum; de, dentary; ect, ectopterygoid; exc, extrascapular; hh, hypohyal; iop, interopercle; mx, maxilla; na, nasal bone; mc, mandibular canal; met, mesethmoid; mx, maxilla; pa[=fr], parietal [= frontal] bone; op, opercle; orbs, orbitosphenoid; pal, palatine; p.cer, posterior ceratohyal; par, parasphenoid; pcl, postcleitra 1–3; pec.f, pectoral fin; pmx, premaxilla; pop, preopercle; ppa+dpt [= pa + dpt], postparietal + dermopterotic bone; qu, quadrate; sang, surangular; scl, supracleithrum; sop, subopercle; sy, symplectic; vo, vomer; ?, uncertain or unknown. Scale bars: 5 mm.

From posteriad to rostrad, the skull roof is formed by the broadly and latero-ventrally expanded dermopterotic fused with the postparietal (postparietal + dermopterotic), which are densely covered with small tubercles (Fig. 5A, B). Apparently left and right bones are contacting each other through a straight suture (= *sutura harmonica*). It is unclear whether the parietal branch of the supraorbital canal extends into the compound bone, or the anterior middle pit-line is the one placed from the anterior margin to almost the half of the bone almost reaching the middle pit-line (Fig. 5B). The middle pit-line, as well as the anterior pit-line, are placed in conspicuous grooves. A posterior pit-line has not been observed. It is unclear if the supraorbital canal was covered by thin bone that collapsed after death and burial. The trajectory of the otic canal is not evident in the available specimens. The latero-ventral region of the postparietal + dermopterotic together with the autosphenotic are the main elements that articulate with the hyomandibula. Posterior to the postparietal + dermopterotic is a narrow, triangular bone that it is interpreted as an extrascapular (Fig. 5B). Although the extrascapular is incomplete in the available material,

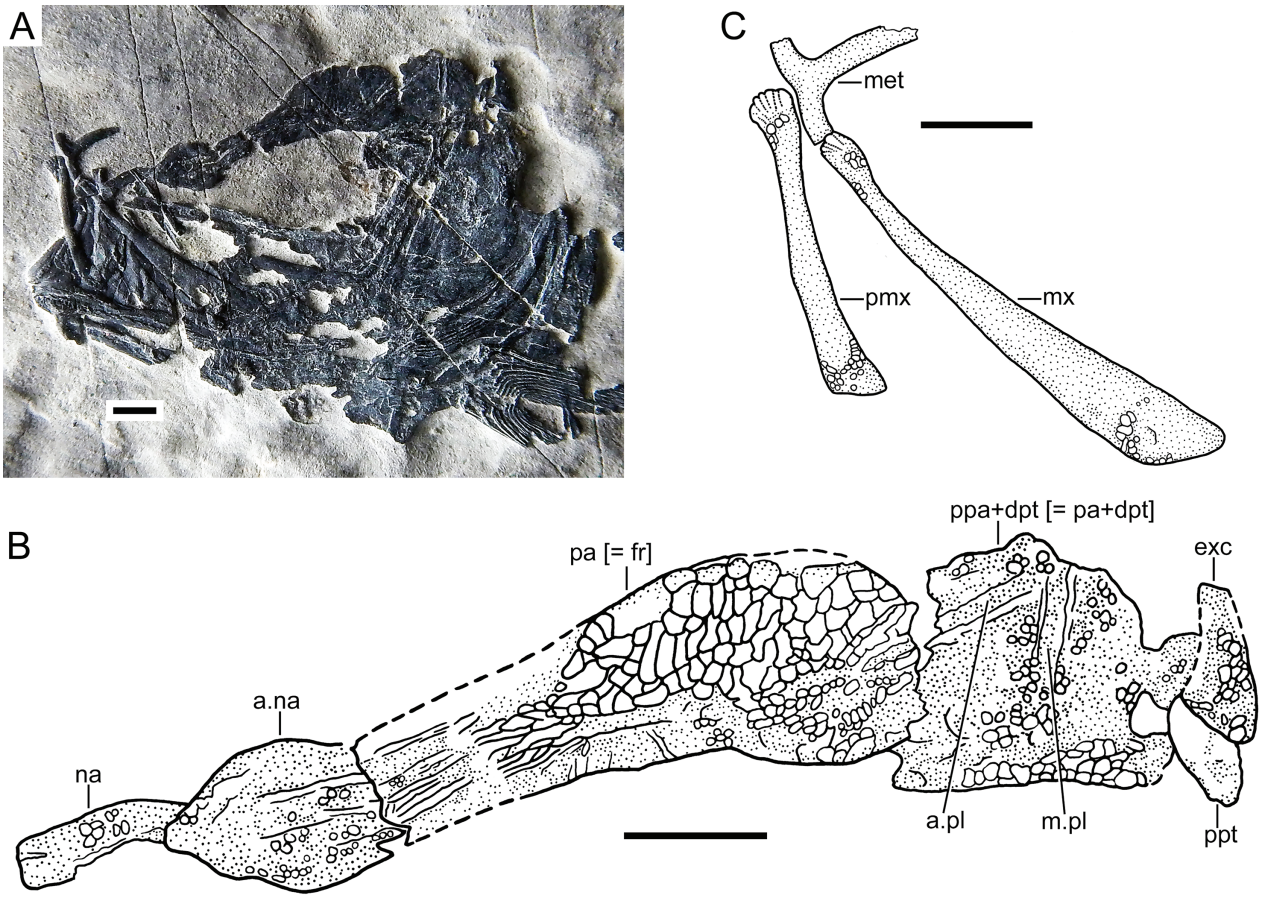

Figure 5. *Marcopoloichthys furreri* sp. nov. in lateral view illustrating some cranial bones in paratype PIMIZ A/I 2887. **A.** Cranium and pectoral girdle and fin in lateral view; photograph was taken by T. Scheyer; **B.** Skull roof bones illustrating ornamentation; **C.** Upper jaw bones; ornamentation on bones is damaged. Abbreviations: a.na, accessory or additional nasal bone; a.pl, anterior pit-line; exc, extrascapular; met, mesethmoid; m-pl, middle pit-line; mx, maxilla; na, nasal bone; pa[=fr], parietal [= frontal] bone; pmx, premaxilla; ppa+dpt [= pa + dpt], postparietal + dermopterotic bone; ptt, posttemporal. Scale bars: 1 mm.

it appears to be in contact, or at least becomes closer, to its antimere medially. The postero-median region of the skull roof is not preserved in any specimen, hence it is unknown whether a supraoccipital bone was present.

The short lateral process of the autosphenotic is well-ossified, but its dorso-lateral walls are not well preserved (Fig. 4). The autosphenotic seems to be fused with the postparietal + dermopterotic region posteriorly in the holotype (Fig. 2A), whereas it is not preserved in PIMUZ A/I 2887 (Fig. 5), which raises the possibility that the autosphenotic is not fused to any of its surrounding bones in this specimen.

The parietal [= frontal] is the longest bone of the skull roof, about twice the length of the postparietal + dermopterotic, and it ends just short of the postero-dorsal corner of the orbit; anteriorly it ends near the antero-dorsal corner of the orbit. Due to conditions of preservation, the interparietal [= frontal] and postparietal [= parietal] sutures are not discernable in most specimens, except for PIMUZ A/I 2887 that shows straight sutural borders (Fig. 5A, B). Because of the parietal preservation, it looks like a fontanelle was partially separating both left and right bones medially. The trajectory of the supraorbital canal is partially visible in PIMUZ A/I 2887 (Fig. 5), and no lateral sensory tubules or pores are observed. It is unclear whether the sensory canal was placed in a groove or whether the groove was covered by thin bone that has collapsed. The bones described above are part of the immovable region of the skull roof. In contrast, the so-called snout is formed by bones that are loosely articulated and changed position during the suction feeding process.

The anterior movable region of the skull roof includes, from posteriad to rostrad, an extra bone identified here as a posterior nasal or additional nasal, a nasal bone, and the mesethmoid (Figs 4A, A, 5A, B, 6, and 7). The first two are paired, whereas the latter is an unpaired bone. The additional nasal is a somewhat ovoid-shaped bone with slightly irregular anterior and posterior margins loosely articulated with the parietal posteriorly and the nasal bone anteriorly; when the fish is not feeding, this bone is placed downward, forming a kind of anterior margin to the parietal bone, and because of its position, it can be confused with the lateral ethmoid. This additional nasal is preceded by the nasal that is almost as long as the additional nasal in PIMUZ A/I 2887 (Figs 5, 6), but is about twice the length in the holotype (Fig. 6) and is almost rectangular-shaped. Unfortunately, its lateral margins are damaged in most specimens.

Both nasals seem to be loosely articulated medially. The supraorbital sensory canal is positioned almost in the mid-region of the additional nasal and nasal bones. Part of the surface of the nasal bone is covered by rounded tubercles in the holotype (Fig. 6). Forming the tip of the snout is a T-shaped median bone, the mesethmoid (Figs 4–7), with strongly ossified lateral processes, as well as a strongly ossified and elongate posteromedian process. There is no evidence of a rostral commissure. The holotype, PIMUZ A/I 2886, has an outstanding element preserved, which by comparison with some living atherinomorphs and cyprinodontiforms with suction feeding mechanisms, is interpreted as the rostral cartilage (Fig. 6). The rostral cartilage can be a continuous element extending in front of the parietal to the mesethmoid anteriorly. It can be perforated or not. In this case, only one ovoid foramen is observed, and because of this, I interpret that the rostral cartilage was broader, and its right side is incompletely preserved.

Morphologically, the anterior tip of the skull roof looks very different when the mouth is not open (e.g., Figs 5–7) compared to open (Figs 4, 7). When the mouth is closed, the anterior articular margin of the parietals together with the additional nasals produce a marked curved, downward region where the additional nasals lie. When the upper jaw is protracted, the profile of the anterior part of the head changes with the additional nasals, nasals, and mesethmoid placed almost in a straight line in front of the anterior margin of the parietal bones and the well-ossified lateral ethmoids. Since the mentioned bones are loosely connected, it is assumed here that the bones involved in the suction mechanism were kept in their position by the aid of ligaments and the rostral cartilage, but due to their soft structure, they were lost after death and burial.

The orbitosphenoid is not preserved in most specimens, but apparently both eyes are separated by an incomplete interorbital septum as shown by specimen PIMUZ A/I 3209 (Fig. 4). The lateral ethmoid is well-ossified and slightly bent, but its preservation does not allow a proper description.

The antero-middle region of the parasphenoid is visible in one of the fishes (Fig. 4), permitting its partial description. The parasphenoid is narrow anteriorly, it expands slightly posteriorly, and part of its ascendant process is poorly preserved just posterior to the orbital region. There are no teeth associated with the ventral surface of the bone or scattered below the parasphenoid. The parasphenoid joins anteriorly a small, narrow, triangular-shaped, and unpaired vomer (Fig. 4). No teeth are associated with the vomer either.

Orbit and circumorbital series. The fish has a moderately large orbit (Figs 2, 3A, 7), ranging from 28 to 39% of head length. When the fish was not feeding, the orbit was almost rounded, but when the fish was in feeding action, and the mouth protracted anteriorly, the orbit became oval-shaped.

The series of circumorbital bones is incomplete; supraorbital bones are absent dorsally, as well as an antorbital that seems to be missing at the antero-dorsal margin of the orbit in most specimens. Since I do not feel confident about the presence of an antorbital in this fish, I consider its presence uncertain. The infraorbital bones are thin and fragile and destroyed in most specimens. They are partially preserved in the paratype PIMUZ A/I 1958 (Fig. 2B); however, their delicate preservation makes their description difficult. Their total number is probably five plus a small dermosphenotic (Fig. 7). It is unclear whether the small flat bone placed between the dermosphenotic and

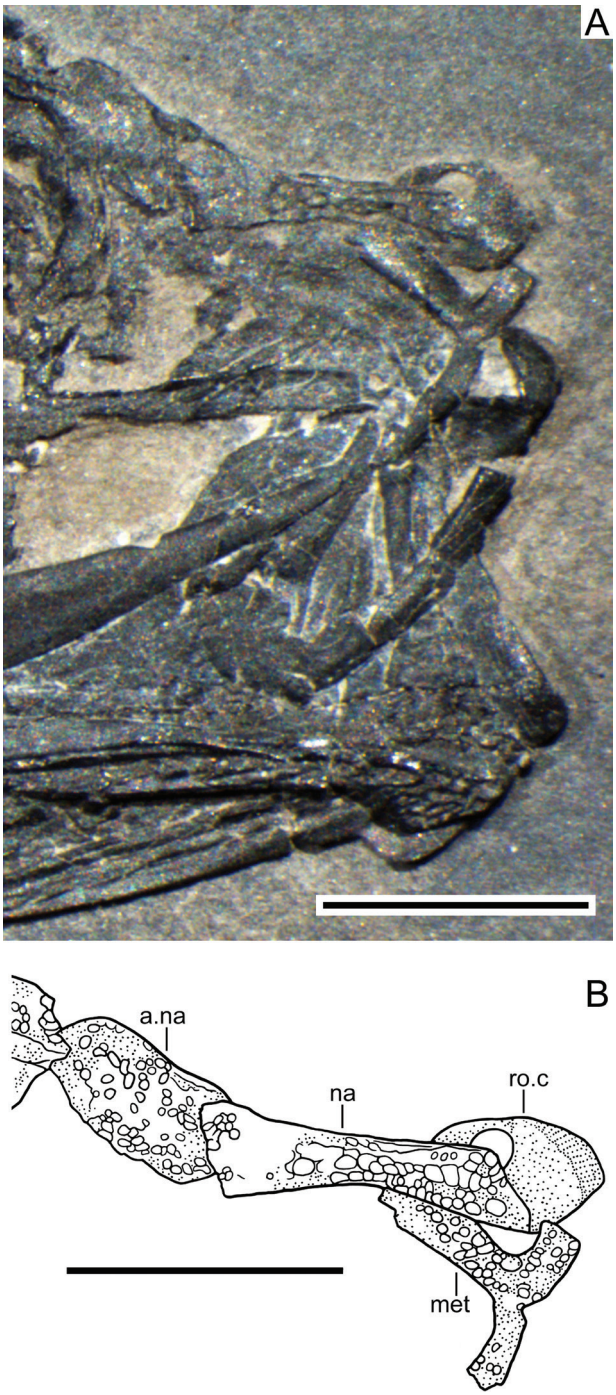

Figure 6. *Marcopoloichthys furreri* sp. nov. Anterior region of skull roof of holotype, PIMUZ A/I 2886. **A.** Photograph; it was taken by T. Scheyer; **B.** Interpretative drawing. Abbreviations: a.na, accessory or additional nasal; met, mesethmoid; na, nasal bone; ro.c, rostral cartilage. Scale bars: 2 mm.

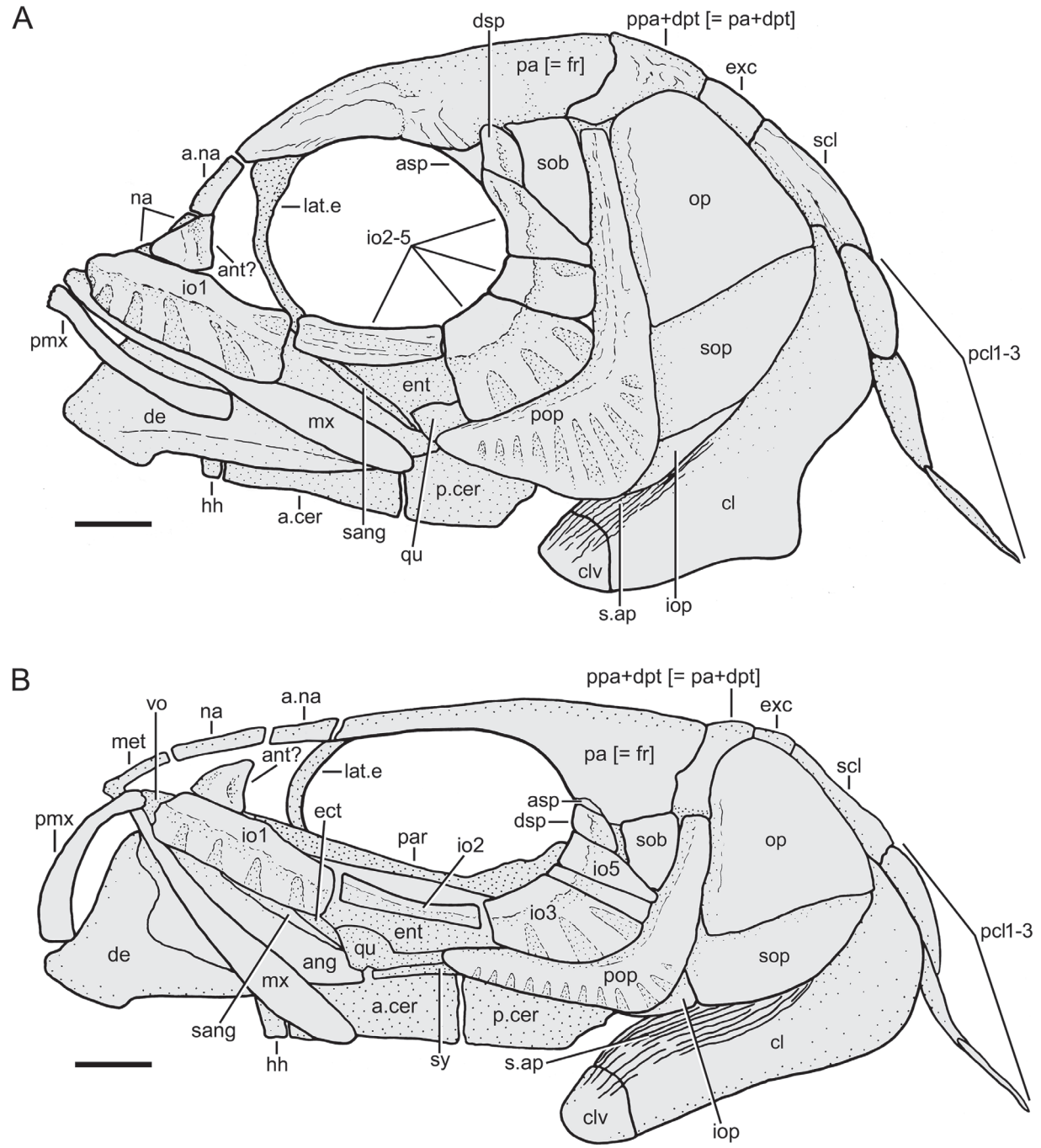

Figure 7. *Marcopoloichthys furreri* sp. nov. Restorations of head in lateral view. Heads reversed to the left. **A.** Fish during rest, based mainly on specimens PIMUZ A/I 1958, PIMUZ A/I 2841, PIMUZ A/I 2886; and BNM 201166; **B.** Fish during feeding, based mainly on specimen PIMUZ A/I 1958, PIMUZ A/I 2887; and BNH 201166. Abbreviations: a.cer, anterior ceratohyal; a.na, accessory or additional nasal bone; ant? antorbital?; asp, autosphenotic; cl, cleitrum; clv, clavicle; de, dentary or dentosplenial; dsp, dermosphenotic; ect, ectopterygoid; ent, entopterygoid; exc, extrascapular; hh, hypohyal; io1–5, infraorbitals 1–5; iop, interopercle; lat.e, lateral ethmoid; met, mesethmoid; mx, maxilla; na, nasal bone; op, opercle; pa [=fr], parietal bone [=frontal bone]; par, parasphenoid; ppa+dpt [= pa+dpt], postparietal bone + dermopterotic [= parietal bone + dermopterotic]; p.cer, posterior ceratohyal; pcl 1–3, postcleithrum 1–3; pmx, premaxilla; pop, preopercle; qu, quadrate; sang, surangular; s.ap, serrated appendage; scl, supracleithrum; sob, suborbital; sy, symplectic; vo, vomer. Scale bars: 1 mm.

anterior margin of the preopercle is a suborbital or part of the most dorsal infraorbital, but it is interpreted here as a suborbital.

Infraorbital 1 is the largest bone of the series, somewhat rectangular-shaped and with some broad sensory tubules that are difficult to count (Fig. 2B; PIMUZ A/I 1958); infraorbital 1 is incompletely preserved in PIMUZ A/I 2887, and the main infraorbital canal seems to be placed in a groove, but this could be misleading, since a groove is not observed in PIMUZ A/I 1958. Infraorbital

2 is an elongate, narrow bone, bearing a groove for the infraorbital canal (or the outer wall of the sensory tube is broken away). Infraorbital 3, at the posteroventral corner of the orbit, is slightly enlarged, reaching the anterior margin of the preopercle and its circumorbital margin, as well as that of the dorsal most infraorbital(s); it is well-ossified, and its few sensory tubules seem to be positioned in grooves. Infraorbital 4 is square-shaped, with its margin heavily ossified and with at least one sensory tubule. If a fifth infraorbital is present, it should be mainly represented by the thickened orbital margin. A description of the dermosphenotic is not possible because of poor preservation. The possible suborbital is a narrow, squarish bone dorsally and triangular-shaped ventrally, but this also could be the flat laminar surface of infraorbital 5. Unfortunately, there is not another specimen preserving the infraorbital series, so these uncertainties cannot be clarified with the available material.

In most specimens there are no orbitosphenoid or sclerotic bones preserved, and the orbital space looks "clean". It is uncertain whether this condition is the result of the preparation of this area, but one specimen (PIMUZ A/I 3209; Fig. 4) shows remnants of bones preserved. Due the flatness of the bones, it is unclear if these can be considered sclerotic bones or parts of a broken orbitosphenoid. In another specimen (Fig. 3A), there is one elongate bone at the anterior part of the orbit, giving the impression of the presence of an enlarged, slightly concave anterior sclerotic bone, but a possible posterior sclerotic is not preserved.

Upper jaw. Premaxilla and maxilla form the upper jaw. A supramaxilla has not been observed in any specimen, and it is assumed here to be absent. Both bones lack teeth, and their ventral margin is smooth. The premaxilla is about half of the length of the maxilla, and when the mouth is closed, the premaxilla is placed ventral to the ventral border of the maxilla, but when the mouth is open, both premaxillae project anteriorly in a very distinct position (compare Figs 2A and 3A with 2C and 4; and Fig. 7A with 7B).

The premaxilla (Figs 4, 5C) is a slightly bent bone, with its proximal end slimmer than the main section of the bone, which expands gently distally, ending in a straight margin. The slightly curved proximal region of the bone (Fig. 5C) lacks an ascendant process or any other process and is slightly spatulate, with a few short interdigitating ridges separated from each other by short grooves, giving this region a characteristic surface.

The maxilla (Figs 4, 5C) is an elongate bone, ending below the posterior half of the orbit and about the level of the articulation of the quadrate-lower jaw when the mouth is closed. It is narrower in its anterior half and slightly expanded at its anterior tip, with similar interdigitations as in the anterior tip of the premaxilla; in contrast, the maxilla expands gently posteriorly, keeping an elongate, straight aspect in its middle region, and then expands posteriorly, ending in a slightly triangular or rounded tip. A supramaxillary process is absent on the dorsal margin of the bone. The ventral margin is almost straight. The surface of the maxilla is covered with longitudinal bony ridges, which in some specimens retain remnants of ganoine. When the mouth is open, the maxilla is displaced anteriorly (compare Fig. 2A with Fig. 4 and Fig. 7A with 7B).

Lower jaw. The jaw (Figs 4, 8) is massive, relatively short, deep, and somehow triangular-shaped, with the quadrate-mandibular articulation placed below the posterior half of the orbit when the mouth is closed and displaced anteriorly, below the anterior half of the orbit, when the mouth is open (compare Figs 2A, 7A, 8 and 4, 7B). The jaw is formed laterally by three bones: dentary (= dentalosplenial or dentosplenial), angular, and surangular. Medially, an ossification interpreted here as a coronoid bone is present (Fig. 8). Since the medial view reveals only one bone posteriorly, it is assumed here that the angular, articular and retroarticular are fused into an angulo+articulo+retroarticular (Fig. 8). The lower jaw is toothless, and no evidence of sockets for teeth has been observed in any specimen.

The sutures between angular, surangular and dentary reveal that the dentary forms most of the jaw (Figs 7, 8). From a narrow but thick mandibular symphysis, the dentary expands abruptly dorso-posteriad, producing a massive and high coronoid process that is thicker and strongly ossified at its antero-dorsal region. The latter has a large contribution of the surangular. The antero-ventral portion of the dentary projects anteriorly and ventrally in a kind of flap or broad process (Figs 6A, 8) that commonly is broken, but it is well-preserved in A/I 3209 (Fig. 4). The postero-ventral process of the dentary narrows posteriorly and extends ventrally, almost reaching the posterior corner of the angular. A notch is absent in the ascending margin of the dentary. The surangular is an elongate bone, suturing ventrally with the dorsal region of the angular portion of the angulo + articulo + retroarticular and the postero-dorsal region of the dentary. The postarticular process is short.

The mandibular sensory canal is placed near the ventral margin of the jaw, and its trajectory is marked by a conspicuous ornamentation that has preserved remnants of ganoine. Sensory pores have not been observed in the postero-ventral region of the angulo + articulo + retroarticular, so it is assumed that the mandibular canal exits medially.

The lateral surface of the lower jaw of certain specimens presents a curious ornamentation at its antero-dorsal region of the dentary along the oral margin (Fig. 8). The ornamentation consists of well-developed, massive protuberances of various sizes and shapes that make the oral margin uneven. In other specimens such ornaments are missing (Figs 3A, 4, 6). It is unclear if these differences in ornamentation are sexual dimorphism, a hypothesis that should be tested when more specimens become available. The surface of the postero-ventral process of the dentary presents marked longitudinal ridges in most specimens; the deep ridges are also observed in the medial view of the jaw. Both the external protuberances and ridges are partially covered with a thin layer of ganoine.

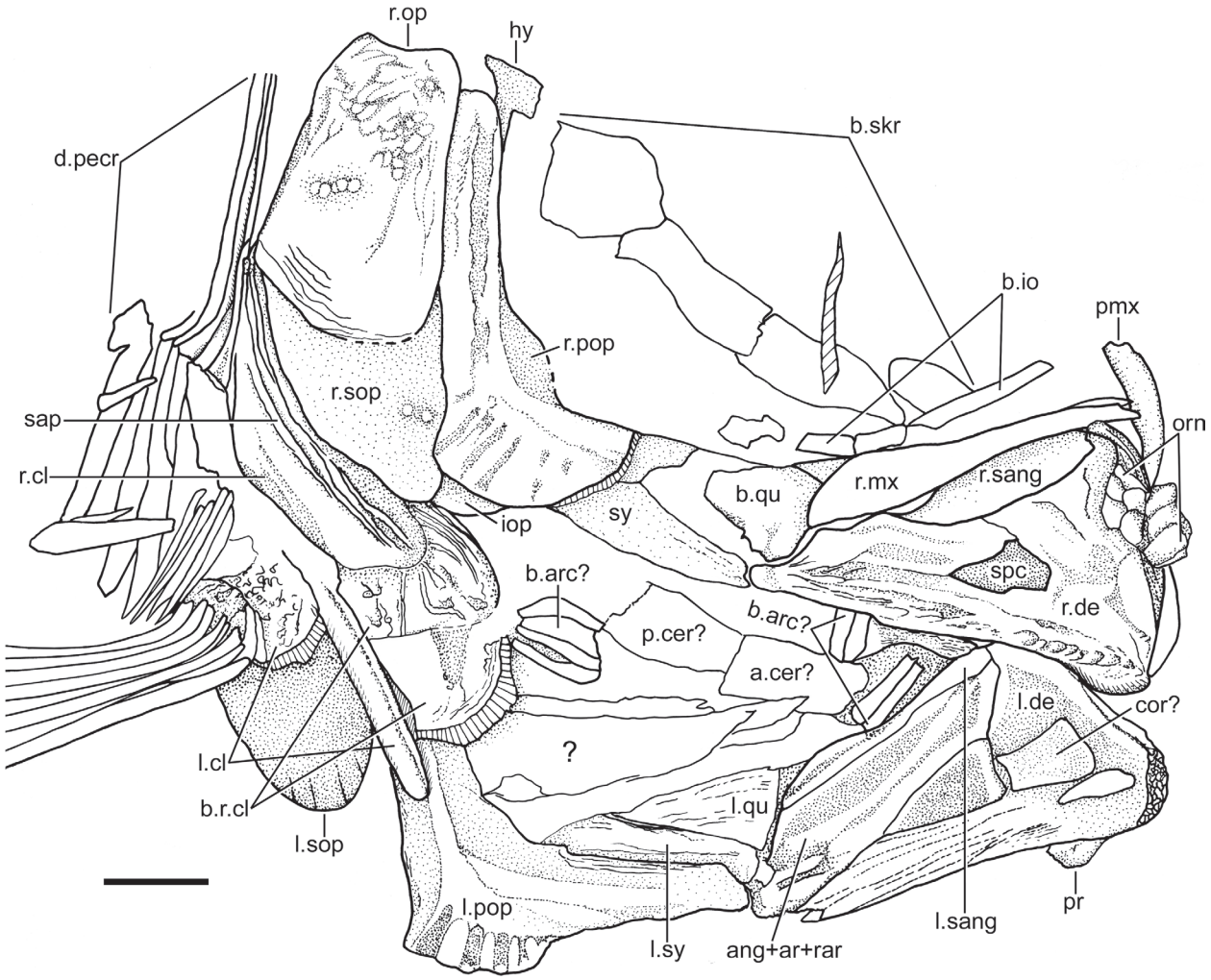

Figure 8. *Marcopoloichthys furreri* sp. nov., partially preserved cranium and pectoral girdle and fins in latero-ventral view of paratype, PIMUZ A/I 2841. Abbreviations: ang+ar+rar, angular+articular+retroarticular; b.io, broken infraorbital bones; b.arc?, broken branchial arches?; b.r.cl, broken anterior part of right cleithrum; b.qu, broken quadrate; b.skr, broken skull roof bones; cor?, coronoid?; d.pecr, displaced pectoral rays of left fin; hy, hyomandibula; iop, interopercle; l.cl, left cleithrum; l.de, left dentary; l.pop, left preopercle; l.qu, left quadrate; l.sang, left surangular; l.sop, left subopercle; l.sy, left symplectic; orn, ornaments; pmx, premaxilla; pr, ventral process of lower jaw; r. cl, right cleitrum; r.de, right dentary; r.mx, right maxilla; r.op, right opercle; r.pop, right preopercle; r.sang, right surangular; sap, serrated appendage; spc, space; sy, symplectic; ?, unidentified element. Scale bar: 1 mm.

The medial view of the lower jaw (Fig. 8) is somehow concave, with a deep triangular depression at the anterior confluence of the dentary and the angular portions. In some jaws, this region gives the impression of the presence of a space between bones. In front of the depression/space, a rectangular, well-ossified bone is positioned. Because of its position, I interpret this bone as a coronoid devoid of teeth.

Palatoquadrate, suspensorium, hyoid arch, and urohyal. Most of these elements are partially hidden by other bones or are destroyed so that the description is restricted to a few of them.

The regions where the metapterygoid, entopterygoid and ectopterygoid would be placed are damaged in most specimens, but a section of a bone that is interpreted here as the ectopterygoid is preserved in PIMUZ A/I 3209, anterior to the anterior margin of the quadrate (Fig. 4). Because of the size of the preserved areas, it is assumed here that the metapterygoid, as well as the entopterygoid, was a narrow bone. Another long, thin, and narrow bone anteriorly placed to the ectopterygoid is interpreted here as a palatine. Under the present conditions of preservation, it is impossible to clarify whether this is a dermal (dermopalatine) or a chondral bone (= autopalatine).

The quadrate is hidden by the anterior arm or ramus of the preopercle and the posterior region of the maxilla when the mouth is closed (Fig. 3A) and is partially exposed when the mouth is open, because the lower jaw displaces anteriorly (Figs 4, 7). The main body of the quadrate (Fig. 8) is slightly triangular close to its articular condyle with the lower jaw. The articular condyle is strong and slightly laterally projected to articulate with the lower jaw. The posterior margin of the quadrate, which shifts to a horizontal position in continuation with the jaw, when the mouth is open, is massive, and together with the symplectic, which lies ventrally to the quadrate,

provide a strong support for the lower jaw. The quadrate seems to continue posteriorly in a flat, almost rectangular process in the holotype, whereas the process ends in a sharp tip in PIMUZ A/I 3209 (Fig. 4). The complete length of the symplectic is unknown, because the bone is covered by the anterior margin of the preopercle or is broken, but considering its position and that of the hyomandibula, it is assumed here that it was a long bone. A quadratojugal has not been observed, and it is interpreted as absent.

The hyomandibula is incompletely preserved in all specimens, but in some its contour is visible throughout the preopercle. In specimen PIMUZ A/I 3209, it appears as a long, columnar bone that is inclined ventro-anteriorly when the mouth is open, and together with the long symplectic gives support to the jaw; the hyomandibula is placed in an almost straight line when the mouth is closed. Its dorsal region articulating with the cranium is broader and well-ossified and continues ventrally as a well-ossified shaft; it is unclear whether an anterior membranous flange is present or not. The dorsal articular region of the hyomandibula (Fig. 4) apparently has only one elongate articular condyle with the latero-ventral articular facets of the dermopterotic and autosphenotic regions laterally. Nothing can be said about the opercular process. Considering the length of the jaw and the position of the quadrate-mandibular articulation, the symplectic is assumed to be a long and strong bone that is partially exposed in PIMUZ A/I 3209 and PIMUZ A/I 2841; an alternative possibility is the presence of an elongate cartilaginous articular region filling the space between the ventral margin of the hyomandibula and the dorso-posterior margin of the symplectic.

The lower part of the hyoid arch preserves a posterior ceratohyal (Fig. 4C, D) that is almost as long as the anterior ceratohyal, which is an almost rectangular bone, lacking a foramen or a notch close to its smooth, dorsal margin. Only one massive, squarish hypohyal articulating with the anterior margin of the anterior ceratohyal (Fig. 4C, D) is present. A urohyal has not been observed in any specimen, and it is assumed here to be absent.

Opercular and branchiostegal series, and gular plate. Although the preopercle is an element associated with the suspensorium, it is included here to describe the opercular series together. The preopercle (Figs 2C, 3A, 4, 8) is a large and L-shaped bone, which is slightly expanded postero-ventrad. The dorsal lobe is slightly longer than the ventral one when the mouth is closed (PIMUZ A/I 1958); however, when the mouth is open, the angle of the preopercle changes, and both arms are about the same length (Figs 4, 7B). Its dorsal arm is about 57% longer than the ventral one, almost reaching the ventro-lateral margin of the dermopterotic region. When the mouth is closed, both arms form an almost right angle, whereas the angle increases to over 100 degrees when the mouth is open, as a result of the anterior extension of the mouth and the action of assumed ligaments joining the posterior margin of the lower jaw and the anterior margin of the anterior arm of the preopercle and interopercle. The preopercle has a gentle flange just anterior to the confluence of both arms where a curvature of the preopercular canal is present. A notch at the posterior margin of the bone is absent. The preopercular canal (Fig. 8) apparently only bears the main preopercular canal, because no tubules are conspicuous at is dorsal arm. A few tubules (Figs 3A, 4, 7, 8) fill the preopercular ventral arm; more precise information is not available because of incomplete preservation of the available preopercles. The sensory tubules are delicate, simple and narrow, and open irregularly near to or at the ventral margin of the bone.

The opercle (Figs 3A, 4, 8) is not very well preserved in the available specimens, but still, it is possible to observe that is the largest element of the series, slightly deeper than broad, and slightly narrower at its dorsal margin, whereas the ventral margin is slightly broader. Dorsally, the opercle reaches the latero-ventral margin of the dermopterotic region, the extrascapular and the posttemporal, and posteriorly, the supracleithrum and cleithrum. Its dorsal and anterior margins are almost straight, whereas the posterior margin in gently curved, and the ventral margin is markedly oblique. Anteriorly, the margin of the opercle is thickened and joins the dorsal limb of the preopercle, whereas it joins the subopercle postero-ventrally and the interopercle antero-ventrally. The opercular surface is irregularly covered with short ridges and rounded and oval tubercles. The subopercle (Figs 3A, 4, 8) is large, as broad as the opercle, and slightly shorter. The general aspect of the bone is not easy to describe, because it is gently curved ventrally in some and markedly rounded in others. Information on the size of the antero-dorsal process is not possible based on the available specimens. A small interopercle (Figs 4, 8) is partially covered by the postero-ventral margin of the preopercle so that its complete shape and size remains unknown.

Branchiostegal rays are not preserved, except for one specimen (holotype PIMUZ A/I 2886) with two narrow and spine-like posterior branchiostegals associated with the posterior ceratohyal. The absence of branchiostegals or their low number in one specimen could simply indicate that the fish has very few that are usually not preserved. Only one short and rounded branchiostegal ray was mentioned and illustrated for *Marcopoloichthys ani* by Tintori et al. (2007: p. 16, fig. 3). A gular plate has not been observed, and it is assumed here that it is absent.

Vertebral column, intermuscular bones, and ribs. The information on the whole vertebral column is incomplete, because most specimens provide partial or no information. An almost complete vertebral column is preserved in several specimens, including the holotype (PIMUZ A/I 2886; Fig. 2A) and paratypes (BNM 201166 and PIMUZ A/I 19568; Figs 2B, 3A), while the caudal region is well-preserved in PIMUZ A/I 2890 and several other specimens.

The vertebral column is aspondylous (see Arratia et al. 2001 for different types of the vertebral column), with well-developed arcocentral elements forming the centra,

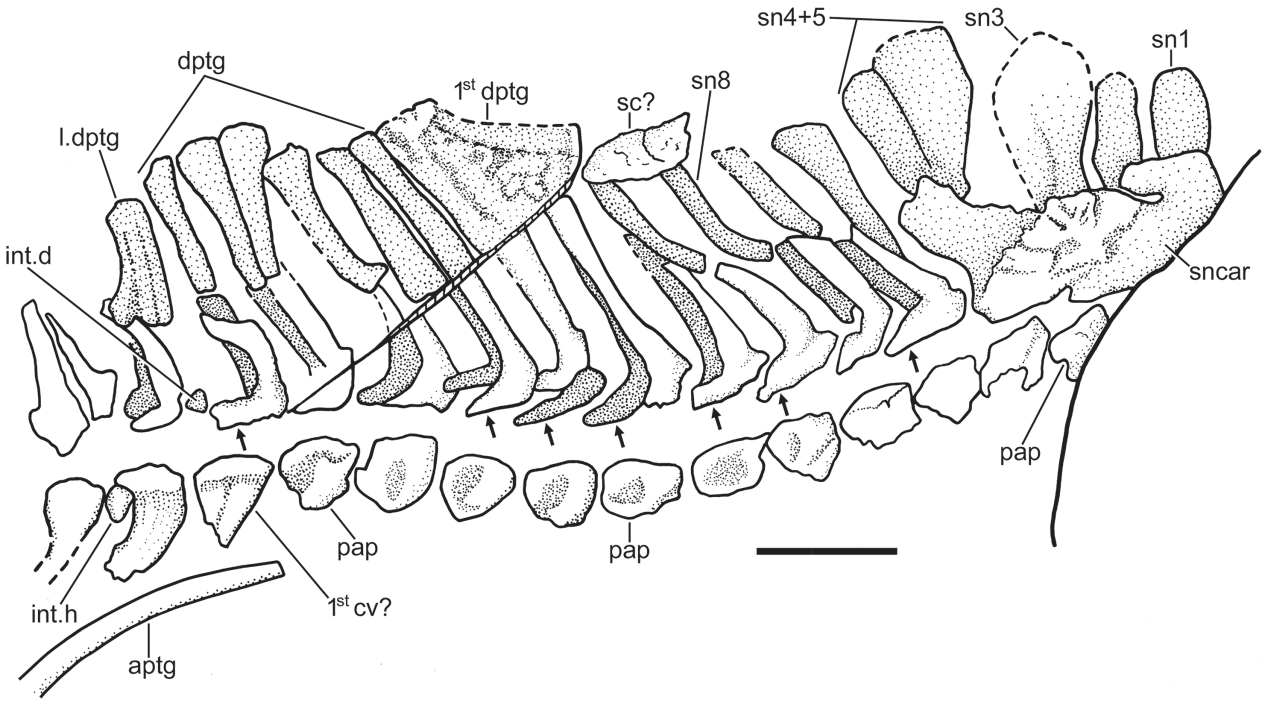

Figure 9. *Marcopoloichthys furreri* sp. nov., illustrating a lateral view of the abdominal or precaudal region of the vertebral column and associated elements and the dorsal fin and endoskeletal support (paratype PIMUZ A/I 1958). Small arrows point to the epineural processes. Abbreviations: aptg, 1st anal pterygiophore or proximal radial; dptg, dorsal pterygiophores or proximal radials; int.d, interdorsal arcocentrum; int.v, interventral arcocentrum; l.dptg, last dorsal pterygiophore; pap, parapophyses; sc?: scale or scute?; sncar, supraneural carrier; sn1–8, supraneurals 1–8; 1st cv?, first caudal vertebra?; 1stdptg, first dorsal pterygiophore or fused proximal radials. Scale bar: 1 mm.

but the notochord remains persistent and functional in adults. There are about 33 to 35 vertebral segments, including those of the hypurals. About 13 to 18 are abdominal, monospondylous vertebral segments, whereas the caudal region is diplospondylous, with very small interdorsal and interventral arcocentral elements alternating with the well-developed basidorsal and basiventral arcocentral elements. Because of their small sizes, many of the interdorsal and interventral elements have not been preserved. No remains of centra are present in the ural region.

The first five neural arches and spines are fused into one special, previously unreported element that is preserved in the holotype PIMUZ A/1 2886, as well as in PIMUZ A/1 1958 (Figs 2, 3, 9). This compound bone is named here "supradorsal carrier" and is formed by the lateral, fused expansions of the neural arches and hemispines of the first abdominal vertebrae, forming two lateral wings (Fig. 9). Five supraneurals are in a median position between the two lateral wings of the supradorsal carrier. I expect that this special structure is a synapomorphy of marcopoloichthyids, a character that should be checked in other species when better-preserved material becomes available.

There are about 13 or 14 parapophyses (Figs 3, 9), the first ones covered by the opercle and the dorsal bones of the pectoral girdle. The parapophyses are comparatively large for the size of the fish, and they are well-ossified; they are squarish in shape and each bear a small cavity close to its ventral margin. No ribs are preserved in the available material, and they were not reported or illustrated in *Marcopoloichthys ani* (Tintori et al. 2007: fig. 4) either; thus, it is accepted here that marcopoloichthyids do not have ossified ribs.

The neural arches of the abdominal vertebrae (Figs 3, 9) are slightly expanded, and the halves of each arch, plus their elongate neural spines, are unfused medially. The lateral wall of each neural arch projects in a stout and short epineural process (= epineural bone; see Arratia 1997 or 1999 on the terminology) emerging at the postero-lateral margin of the arch. They are easily broken because of their position and structure.

The neural arches of the first caudal vertebrae (Figs 2, 3A, 9) are slighter broader than those of the abdominal vertebrae, and each has an epineural process until the third or fourth vertebra posterior to the last anal pterygiophore. The neural and haemal spines of the caudal region are narrow, except for those of the preural centra (see below). The neural and haemal spines are moderately inclined toward the body axis in the precaudal region, increasing their inclination caudally (Figs 10, 11). The first haemal spines (Figs 10, 11) are short, not extending between the anal pterygiophores or just reaching them. The neural and haemal spines of the mid and caudal regions are ossified, showing an internal core of cartilage where the bones are broken.

The series of supraneural bones is commonly not preserved, distorted, or covered by other structures. The series is formed by nine bones in the paratype (PIMUZ A/I 1958), with the first five associated with the supradorsal carrier. These anterior supradorsals are slightly ovoidal and expanded, especially supraneural 3, whereas supraneural 4 and 5 are partially fused proximally. The

subsequent supradorsals are slightly sigmoid-shaped. The series extends up to the expanded, plate-like, compound first dorsal proximal radial, and it does not extend between the most anterior proximal radials as in *Marcopoloichthys ani* (Tintori et al. 2007: fig. 4).

The epineural processes of the neural arches (Figs 9, 11) extend along the abdominal region, ending posterior to the last dorsal pterygiophore. The broad and well-ossified epineural processes are short, extending laterally on the neural arch of the next vertebral segment. Epipleural bones are absent.

Pectoral girdle and fins. The pectoral girdle includes dermal and chondral bones. The dermal bones are the posttemporal (linking the girdle with the cranium), supracleithrum, cleithrum, and postcleithra. It is unclear whether a clavicle was present, but see below. The chondral bones are the scapula, coracoid, and proximal and distal radials. The posttemporal is incompletely preserved in the available material (Figs 4, 5B). Apparently, it is a relatively small and narrow bone, placed laterally to the extrascapular; it is unclear whether a dorsal process for articulating with the cranium is present. The main lateral line is not observed.

The supracleithrum (Figs 4, 7) is incompletely preserved or covered by the opercle, but it seems to be an elongate bone. The trajectory of the lateral line is not observed. The sigmoidal-shaped cleithrum (Figs 4, 5A, 7–9) is a heavily ossified bone, with a moderately long dorsal limb and markedly developed, expanded and curved ventral limb, which is partially broken in the available material, making identification of its complete area difficult. The cleithrum is slightly expanded at its postero-dorsal corner and becomes narrower at its dorsal region. The anterior surface of the cleithrum is covered by a long and broad serrated appendage that is almost completely preserved in the paratypes PIMUZ A/I 2841 and 2887 (Figs 5A, 8). The external surface of the cleithrum in PIMUZ A/I 2888 (Fig. 10) is abraded so that the serrated appendage is not preserved. A broad clavicle in front of the antero-ventral region of the cleithrum is observed in specimen BNM 201166.

Three postcleithra are present (Figs 4, 7). Postcleithrum 1, the uppermost element of the series, is elongated, with a slightly rounded posterior margin. Dorsally, it articulates with the supracleithrum and anteriorly with the upper part of the cleithrum and ventrally with postcleithrum 2. Postcleithrum 2 is slightly narrower than postcleithrum 1 and is curved postero-distally. Postcleithrum 3 is a splint-like bone. By comparison with other teleosteomorphs, it is assumed here that the three bones were not externally placed, but they were covered by the body hypaxial musculature.

The scapula and coracoid (Fig. 10) are incompletely preserved in the available material, and they are not informative. Four proximal radials are observed in the paratype PIMUZ A/I 2888 (Fig. 10), with the first two being larger than the third and fourth proximal radials, which are square-shaped. At least three small distal radials are preserved between the broken proximal region of some pectoral rays.

The pectoral fin (Figs 2, 3, 5A) is positioned near the ventral margin of the body. The total number of pectoral rays is unknown, because commonly the fins are incomplete, but 15 rays are preserved in the right fin in PIMUZ A/I 2841, and most fins in other specimens have ca 12 rays preserved. All rays have very long bases, are scarcely branched, and segmented distally; a few last rays, closer to the body, are smaller than the lateral ones. The first pectoral ray, which is exposed in PIMUZ A/I 2888 (with the pectoral girdle and fin displaced), merits a description. The first ray is a massive ray formed by the fusion of three rays at least (Fig. 10). These rays are fused at their

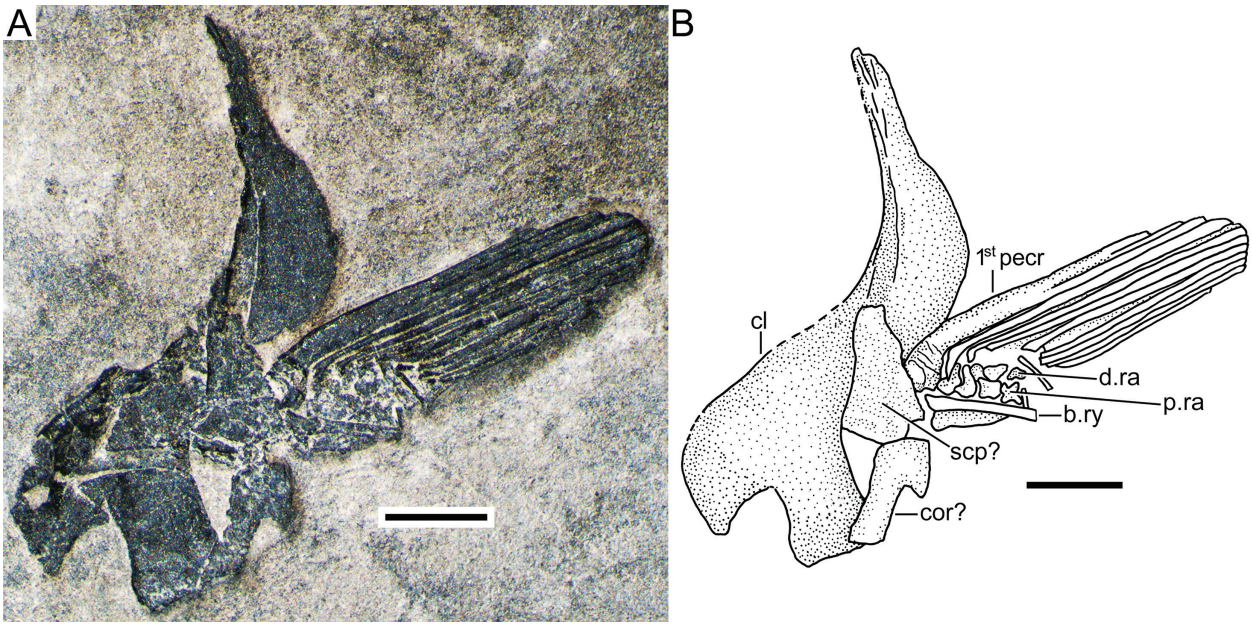

Figure 10. *Marcopoloichthys furreri* sp. nov., illustrating part of the pectoral girdle and fin (paratype PIMUZ A/I 2888). Abbreviations: b.ry, broken ray; cl, cleithrum with antero-ventral part broken; cor?, coracoid?; d.ra, distal radials; p.ra, proximal radials; scp?, scapula?; 1st pecr, first pectoral ray. Scale bars: 1 mm.

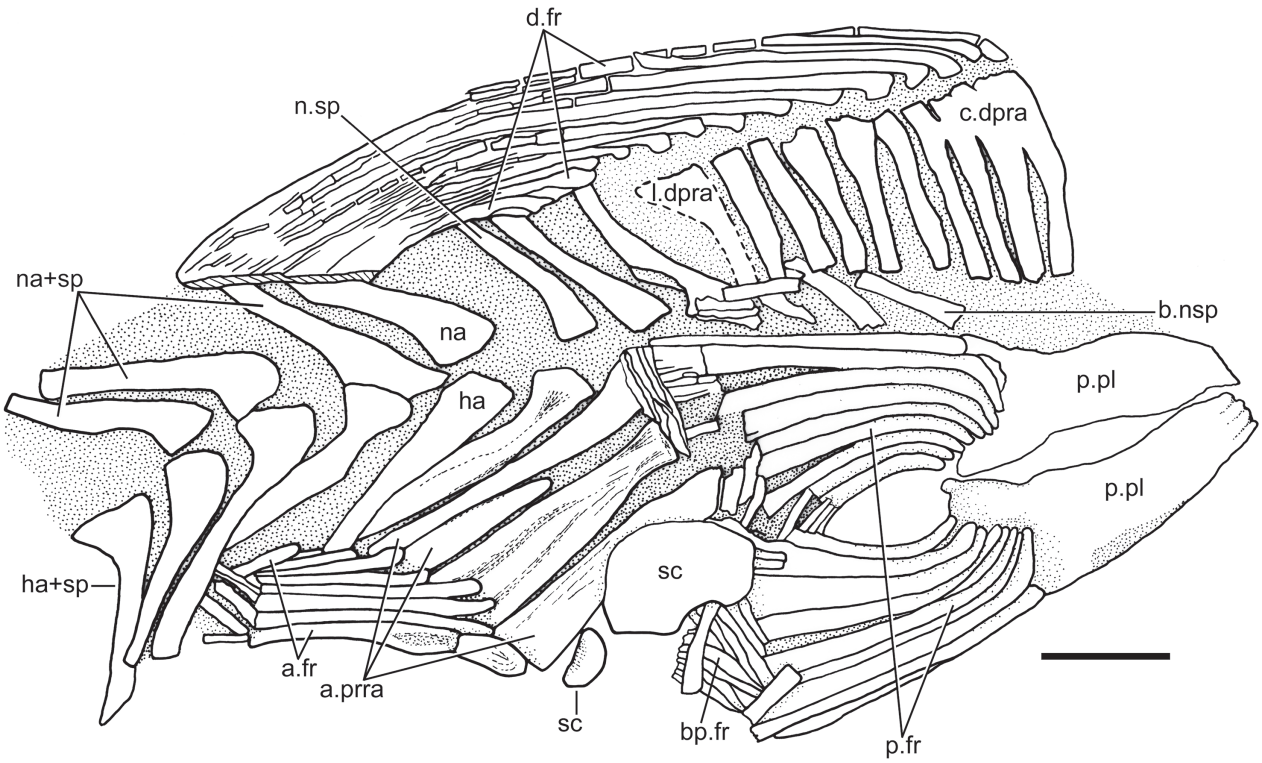

Figure 11. *Marcopoloichthys furreri* sp. nov., illustrating the dorsal, anal, and pelvic fins and associated structures (paratype PIMUZ A/I 2841). Abbreviations: a.fr, anal fin rays; a.prra, anal proximal radials; bp.fr, broken pelvic rays; b.nsp, broken neural spines; c.dpra, compound dorsal proximal radial element; d.fr, dorsal fin rays; ha, haemal arch; ha+sp, haemal arch plus spine; l.dpra, last dorsal proximal radial; na, neural arch; na+sp, neural arch plus spine; n.sp, neural spine; p.fr, pelvic rays; p.pl, pelvic plate or basipterygium; sc, scales. Scale bar: 1 mm.

bases, being separated distally. This first compound ray is slightly expanded and thicker at its proximal portion where the propterygium is fused with its base.

Pelvic girdles and fins. The pelvic girdles are partially exposed in several specimens (Figs 2A, B, 3A, B, 11). A large, elongate plate-like basipterygium (or pelvic plate) is slightly curved medially, with its lateral margin more strongly ossified than the rest of the plate. The posterior part of the basipterygium is slightly broader than the anterior margin and presents a short postero-medial process. The number of rays per fin are difficult to count, due to preservation. Ten or 11 rays are present in the holotype; eight of them are thicker and longer than the two or three medial rays. In contrast, nine long pelvic rays are preserved in each fin in specimen PIMUZ A/I 2888. Eleven rays were mentioned for *Marcopoloichthys ani*, but the number of rays remains unknown for *M. andreetti* and *M. faccii* (Tintori et al. 2007). The pelvic rays of *M. furreri* sp. nov. have long bases, are distally segmented, and apparently branched only once. This information is collected from the holotype, with one ray distally exposed (Fig. 2A). In other specimens, the distal parts of the fin rays are disarticulated or overlapping so that they are not informative (Fig. 11). Because of the position of the articular region of each ray, it is unknown whether proximal radials were present.

Dorsal fin and radials. The dorsal fin (Figs 2, 3, 11, 12) is commonly not well preserved with its rays partially displaced or damaged so that a precise total number of dorsal fin rays cannot be provided, but considering that the paratype PIMUZ A/I 2841 has 15 rays preserved, including a short, thin one segmented anteriorly, this could indicate that the fin has ca 15 rays.

Commonly, the dorsal pterygiophores preserved the proximal radials, however in the holotype, some of the anterior middle and distal radials are also preserved (Fig. 12). The series of proximal radials presents distinct features characterizing marcopoloichthyids, for instance, the modifications in the first and last proximal radials. In *M. furreri* sp. nov., the first proximal radial can be plate-like and square, but in others, the proximal radials are incompletely fused so that the elements forming this complex structure can be counted (Fig. 11). There are six intermediate proximal radials followed by one modified last radial bearing an undetermined number of rays in PIMUZ A/I 2841 and holotype (Figs 11, 12). This last proximal radial has an expanded distal articular region that projects ventrally in a narrow, markedly curved process. The complex plate-like first proximal radial in *Marcopoloichthys ani* is ax-shaped, whereas it is pear-shaped in *M. andreetti* (Tintori et al. 2007); in addition, *M. ani* has an ax-shaped proximal radial and nine to 10 proximal radials posterior to the first, which is a higher number than in *Marcopoloichthys furreri* sp. nov.

Anal fin and radials. The anal fin and its pterygiophores are not well preserved in the available material, and because of this, a description is difficult, and a total

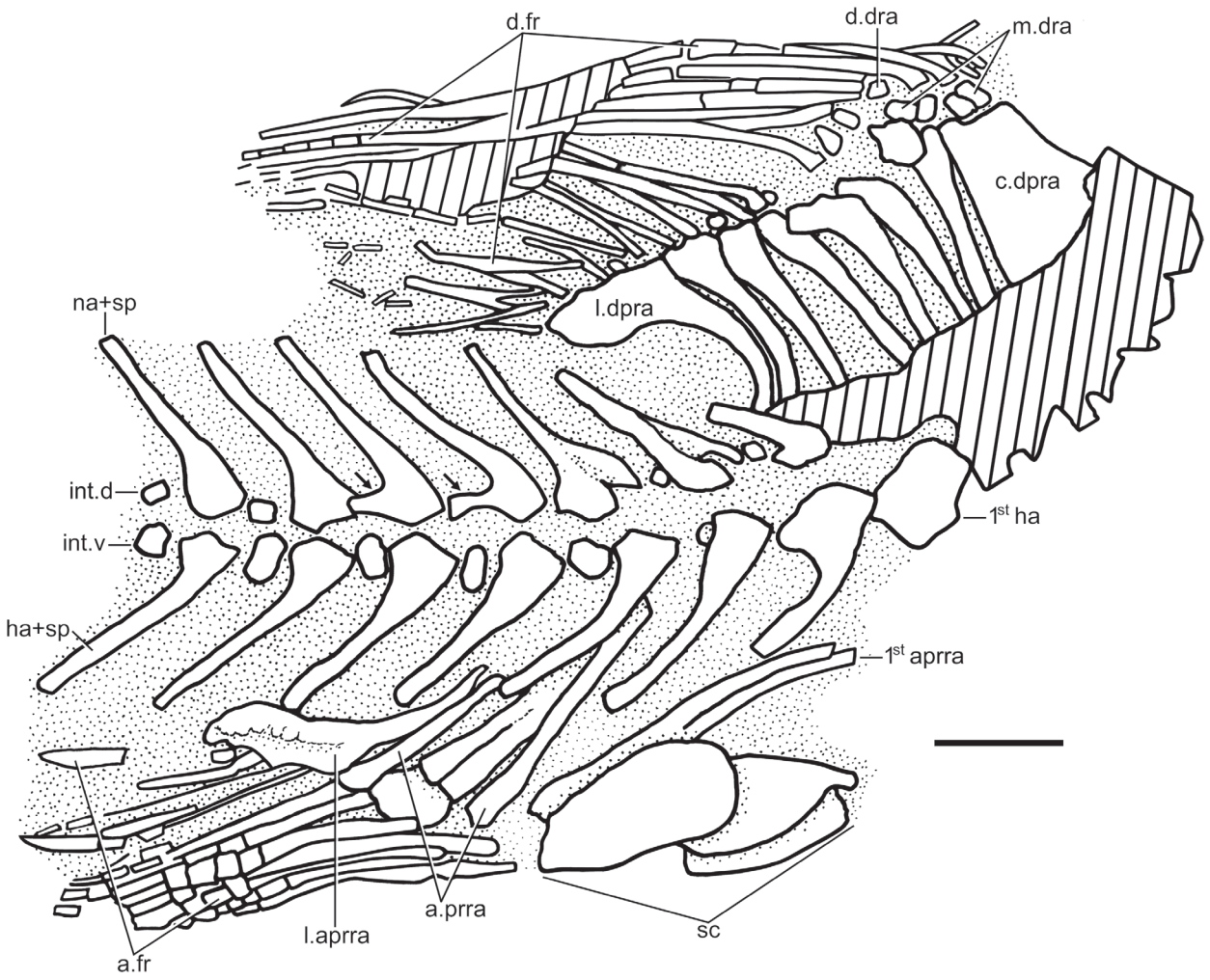

Figure 12. *Marcopoloichthys furreri* sp. nov., illustrating the dorsal, anal, and pelvic fins and associated structures (holotype PIMUZ A/I 2886). Oblique lines represent damaged areas. Abbreviations: a.fr, anal fin rays; a.prra, anal proximal radials; c.dpra, compound dorsal proximal radial element; d. dra, distal dorsal radial; d.fr, dorsal fin rays; ha+sp, haemal arch plus spine; int.d, interdorsal element; int.v, interventral element; l.aprra, last anal proximal radial; l.dpra, last dorsal proximal radial; m.dra?, middle dorsal radial; na+sp, neural arch plus spine; sc, scales; 1st aprra, first anal proximal radial; 1st ha, first haemal arch. Scale bar: 1 mm.

count of fin rays is not available. Additionally, there is variation in the number and amount of fusion of the proximal radials. The most complete series of proximal anal radials, or the most informative, is that present in the holotype (Fig. 12). In this specimen, the first anal proximal radial is a compound element resulting from the incomplete fusion of two proximal radials. This first element curves antero-dorsally giving the radial a characteristic shape, reminiscent of the postcoelomic bone of pycnodontiforms (Tintori et al. 2007). The first anal proximal radial is followed by a second, long, narrow radial, that is followed by a third element that results from the partial fusion of two proximal radials which are broken at their bases. Behind this element is one simple proximal radial that is followed by the last radial. The last radial is an elongate element bearing a narrow, thin anterior process that extends dorsally between the distal tips of the haemal spines and has a broad distal portion for articulation with several lepidotrichia (Fig. 12). In total, the anal series of proximal radials in the holotype included five separate elements. In the paratype PIMUZ A/I 2841, only three proximal radials are preserved, and the first and last are not preserved.

Caudal fin and endoskeleton. The caudal fin and endoskeleton are preserved in several specimens, but the dorsal elements of the ural region are poorly or not preserved at all. The homocercal caudal fin (Figs 2, 3) is deeply forked, with few short middle principal rays compared to the long first and last leading marginal ray that frame the segmented and branched principal rays. Many rays preserve a thin layer of ganoine.

One or two preural vertebrae support the most anterior basal fulcra. The preural vertebrae, as well as the ural ones, are supported by a functional notochord. Consequently, except by the arcocentra, no centra are formed, and the region is monospondylous, in contrast to diplospondylous vertebral segments in anterior and mid-caudal vertebrae (Figs 2, 13, 14). The two preural segments (corresponding to preural centra 1 and 2) are characterized by the presence of well-developed ventral arcocentra

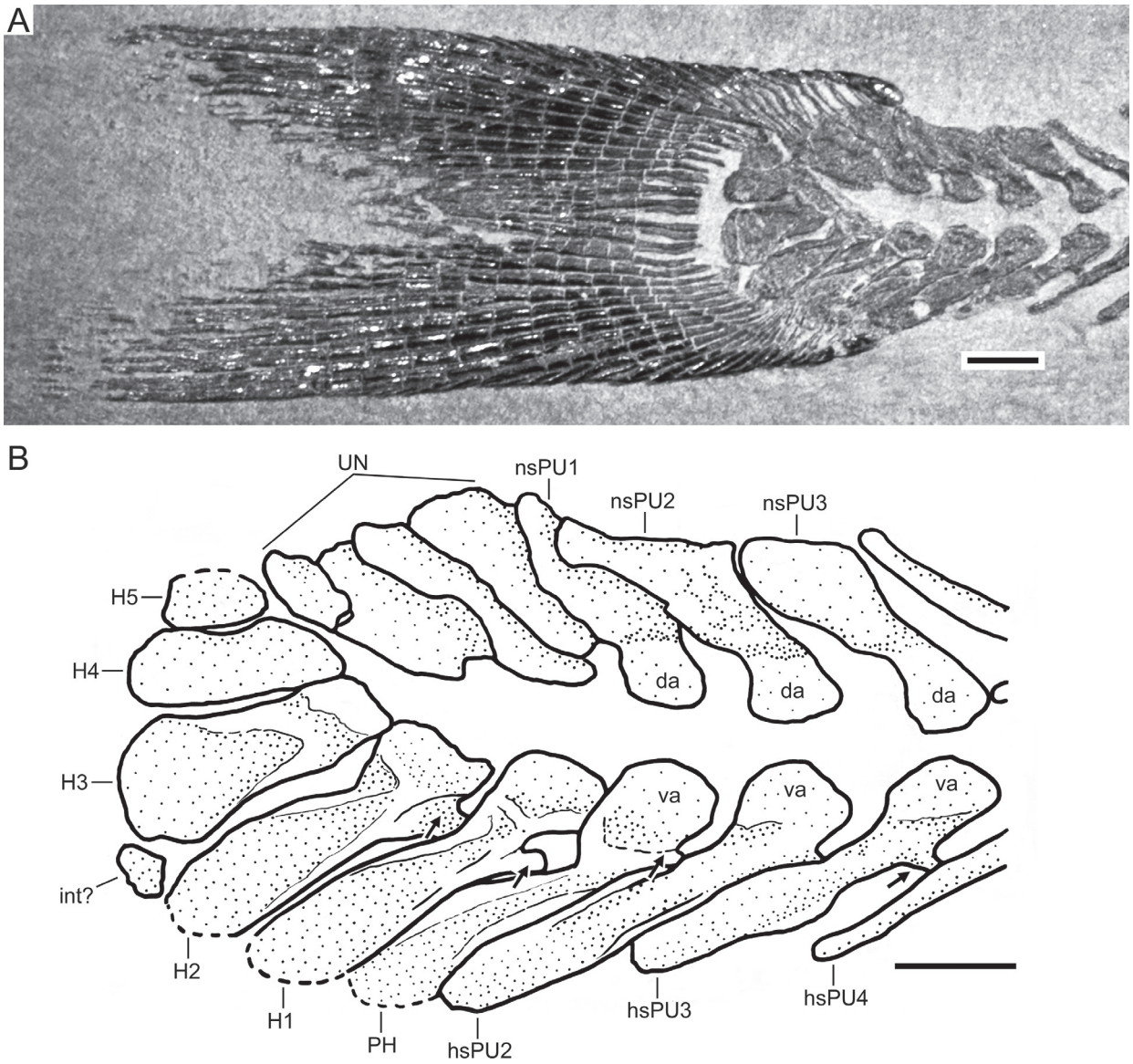

Figure 13. *Marcopoloichthys furreri* sp. nov., illustrating the caudal fin and its endoskeleton. **A.** Photograph of holotype, PIMUZ A/I 2886; photograph was taken by T. Scheyer; **B.** Drawing of endoskeleton. Abbreviations: da, dorsal arcocentra; H1–5, hypurals 1–5; hsPU2–4, haemal spine of preural centra 2–4; int, interhaemal; PH, parhypural ot haemal spine of preural centrum 1; nsPU1–3, neural spine of preural centra 1–3; UN, uroneurals; va, ventral arcocentra. Small arrows point to a series of anterior processes. Scale bars: 1 mm.

with broad and flat haemal spines, which distally support the last principal rays, one procurrent ray, and the series of hypaxial basal fulcra (Figs 13, 14). Dorsally, the neural arches or arcocentra of these two vertebrae are well-developed, and their neural spines are broad and of similar length. The neural spines of the last caudal and preural vertebrae are inclined posteriorly, closer to the body axis, and they do not support the most anterior basal fulcra.

The preservation of the neural spines of preural vertebrae 1–5 suggests they have a central core of cartilage surrounded by a thin, perichondral ossification. In the vertebrae that are completely preserved, an anterior process at the base of neural spines 1–5 is apparently absent. The haemal spines of preural centra 1–3 are moderately broad, but narrower than their respective neural spines. The haemal spine of preural vertebra 4 and more anterior ones are narrower. The haemal spines of the most preural vertebrae are perichondrally ossified thinly. The haemal spines of preural vertebrae 1–3 (Fig. 13) bear a short and narrow anterior process dorsally, at their limit with the expanded ventral arcocentra. A complete neural arch or dorsal arcocentrum, with a well-developed spine, is present on preural centrum 1. A hypurapophysis on the lateral wall of the ventral arcocentrum or haemal arch of preural centrum1 is absent.

Posterior to the neural spine of preural centrum 1, a series of slightly modified chondral neural elements is positioned (Fig. 13). In most specimens, this region is damaged or badly preserved, except for the holotype, which is illustrated in Fig. 13. The first two are elongate laminar elements resembling neural spines, and lacking the ural arcocentra; a third broad, laminar element, also lacking an arcocentrum follows. There is a fourth small, plate-like element posteroventral to the third, which extends caudally between the bases of the epaxial basal fulcra, but it is

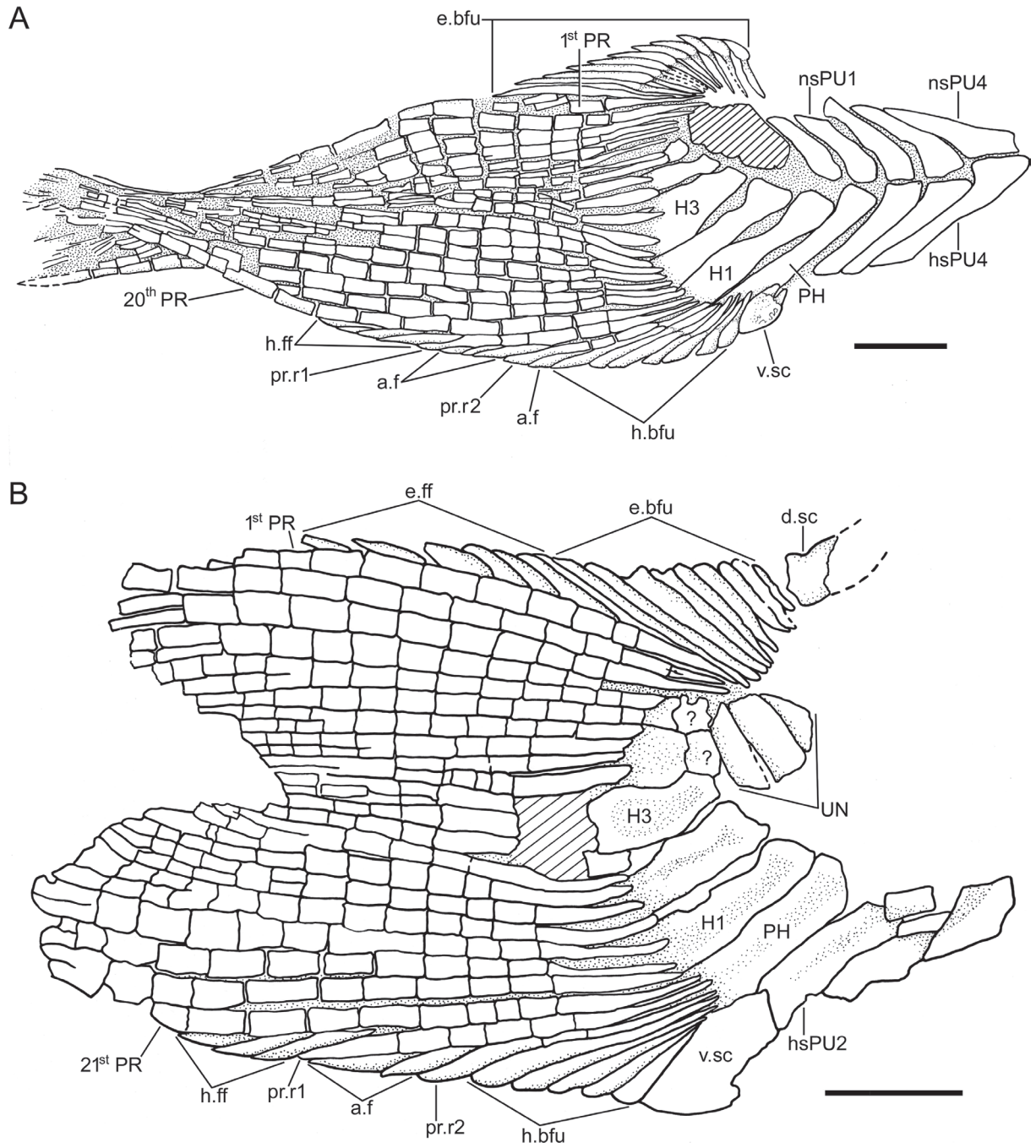

Figure 14. *Marcopoloichthys furreri* sp. nov., illustrating the caudal fin and its endoskeleton. **A.** paratype PIMUZ A/I 2841; area with oblique lines represent a damaged region; **B.** paratype PIMUZ A/I 1958. Abbreviations: a.f, accessory fulcra; d.sc, dorsal caudal scute; e.bfu, epaxial basal fulcra; h.bfu, hypaxial basal fulcra; h.ff, hypaxial fringing fulcra; hsPU4, haemal spine of preural vertebra 4; H1–3, hypurals 1–3; nsPU1, 4, neural spine of preural vertebrae 1, 4; PH, parhypural; pr.r1–2, procurrents rays 1–2; UN, uroneurals; v.sc, ventral caudal scute; 1stPR, first principal caudal ray; 20thPR, principal caudal ray numbered 20; 21stPR, principal caudal ray numbered 21; ?, broken bases of hypurals 4 and 5? Scale bars: 1 mm.

unclear if this could be a broken section of the enlarged third bone. Because of their position as part of the ural region and the lack of their ural neural arches or arcocentra, these bones are considered here as uroneurals "of a special kind". They are different from the uroneural-like elements present in pachycormiforms or some present in aspidorhynchiforms and *Eurycormus*, which are modifications of spines of the preural region. They also differ in shape from the uroneurals of *Leptolepis coryphaenoides* plus more advanced teleosts (see Discussion below). Certainly, these elements in *Marcopoloichthys furreri* sp. nov., because of their position and shape, increase the stiffness of the tail during locomotion, which is a function of the uroneurals.

No epurals are present in the holotype, and there is no space left for them between the distal tips of the enlarged uroneurals and the bases of the epaxial basal fulcra.

Five hypurals (Figs 13, 14) are present, all of them close together so that a diastema between hypurals 2 and

3 is absent. Hypurals 1–4 are slightly expanded at their proximal regions and seem to have preserved part of the ventral arcocentrum. Hypurals 1 and 2 are the longest elements of the series, and hypural 3 is the broadest. A small element is positioned between the distal portions of hypural 2 and 3, and it is interpreted here as an interhemal. Hypural 5 is the smallest of the series of hypurals. Hypurals 1 and 2 (Fig. 13) are weakly supporting the thin bases of part of the hypaxial basal fulcra, the procurrent ray, and the lowest principal rays. Several thin and narrow bases of the principal rays articulate directly with one hypural without producing a special angle.

There are ten or eleven epaxial basal fulcra, which are followed by 10 or 11 fringing fulcra and only reach to the mid-region of the dorsal margin of the first unsegmented principal ray. There are 20 or 21 principal rays that are segmented and branched distally, and their bases are narrow. The articulation between segments of the principal rays is straight. Ventrally, the basal fulcra are usually incompletely preserved so that a total count cannot be given, but the holotype presents 12 hypaxial basal fulcra. There are one or two short procurrent rays that are followed by a short series of hypaxial fringing fulcra; however, PIMUZ A/I 3209 has a third short procurrent ray (Fig. 14). In addition, accessory fulcra are present between the principal rays and the hypaxial basal fulcra (Figs 13, 14). The external surface of the different kind of fulcra and rays is covered by a thin layer of ganoine.

One elongate and slightly oval dorsal scute and a slightly shorter ventral scute (Figs 13, 14) precede the epaxial and hypaxial lobes, respectively. No urodermals have been observed in the available material.

***Scales*.** The body is devoid of scales, with the exception of two to four large oval scales (Figs 2, 3, 10) placed around or close to the urogenital region and a possible elongate one in front of the dorsal fin in one specimen (Fig. 9).

Taxonomic comments

A comparison between the first described marcopoloichthyids from China and Italy (Tintori et al. 2007) and the new species described here is difficult because of the different states of preservation and information provided by the fossil specimens. *Marcopoloichthys ani* from Yunnan Province, S China, is based on four specimens, whereas *M. andreetti* from Lombardy, Italy is based on one complete specimen; *M. faccii* from Fruli, N Italy, is also based on one specimen. Although the holotypes of *M. ani* and *M. andreetti* were described as complete, the illustrations of *M. ani* (the only species illustrated in Tintori et al. 2007) show that several features are poorly preserved. These facts make it difficult for any comparison among them and with *Marcopoloichthys furreri* sp. nov. Although marcopoloichthyids are known from the Middle Triassic, their age differs, with the Chinese *M. ani* being the oldest (Anisian; Tintori et al. 2007), *M. facii* and *M. furreri* sp. nov. lying in the middle (Ladinian; Tintori et al. 2007; present paper, Table 1), and *M. faccii* being the youngest (Early Carnian; Tintori et al. 2007; Dalla Vecchia 2008). Additionally, there are younger (Carnian) specimens reported by Dalla Vecchia (2008) from the middle-late Norian Dolomia di Forni Formation of Friuli Region of NE Italy (Dalla Vecchia 2012, fig. 8.87; pers. comm. May, 2021) that remain undescribed (work in progress together with A. Tintori). Additionally, a possible new species (still undescribed) has been recovered in the Middle Triassic of Monte San Giorgio, Canton Ticino, southern Switzerland (T. Bürgin pers. comm., 2022).

Marcopoloichthys furreri sp. nov. presents the diagnostic characters of the family Marcopoloichthyidae and its only known genus, *Marcopoloichthys*: a naked, torpedo-like body; highly modified protractile upper and lower jaws; vertebral column with persistent notochord and well-developed arcocentral elements; vertebral caudal region diplospondylous, with small interdorsal and interventral elements; ossified ribs absent; large and curved pelvic plates; enlarged, plate-like first dorsal fin proximal radial supporting four or more dorsal rays; enlarged last dorsal proximal radial supporting several dorsal rays; first anal fin proximal radial basally expanded and very elongate; last anal fin proximal radial highly modified into an expanded plate supporting three or more lepidotrichia; no fringing fulcra associated with paired, dorsal, and anal fins; homocercal caudal fin with both lobes deeply forked; body-lobe of caudal fin completely reduced; and a few large scales around urogenital opening.

The new species presents an unreported feature that I have named here supradorsal carrier, which is the result of the fusion of at least the five most anterior abdominal vertebrae in *M. furreri*, with modified expanded hemi-neural spines, and the five expanded anterior supraneurals sit in a median position. I expect that this feature is present in other marcopoloichthyids and diagnostic for the family, a claim that should be checked when better specimens become available.

There are several diagnostic characters supporting *Marcopoloichthys ani* as a new species according to Tintori et al. (2007), but few supporting other species so that the comparison below does not always includes all recognized species. For example, (1) The postparietal and dermopterotic are separate elements in the skull roof of *M. ani*, as illustrated by Tintori et al. (2007: fig. 3), whereas these bones are fused in *M. furreri* sp. nov. (Fig. 5A, B). (2) The anterior articular region of the maxilla is expanded into an oval region in *M. ani*, whereas it is not expanded anteriorly in *M. andreetti*, but is slightly expanded in *M. furreri* sp. nov. (Fig. 5C). The condition is unknown in *M. faccii*. (3) The lower jaw of *M. ani* is "short and deep, with an ascending anterior margin ending with a tip bending downwards" (Tintori et al. 2007: p. 16), and its ventral margin is markedly bent (my interpretation of Tintori et al. 2007: fig. 3A–C). In contrast, the lower jaw in *M. furreri* (Figs 3, 4, 8) has a high dorsal

margin as a result of a well-developed, oval-shaped coronoid process, and its ventral margin is almost straight, with a rounded antero-ventral process. (4) *M. ani* has 37 to 39 vertebral segments, and this means a comparatively longer vertebral column than in *M. furreri* with 33 to 35 vertebral segments. There is no available information for the other species. (5) The last supradorsal bones are positioned between the most anterior proximal dorsal radials in *M. ani*, whereas the last one is placed in front of the large compound first proximal radial in *M. furreri* (Fig. 9). (6) The pectoral fin of *M. ani* has 13 pectoral rays, whereas *M. faccii* has 15 or 16 principal rays; 15 rays seem to be present in *M. furreri*, with the inner ones thinner and shorter than the most lateral ones, a feature not mentioned for the Chinese and Italian species. (7) Eleven pelvic rays are present in *M. ani*, whereas 10 or 11 rays are in *M. furreri*. (8) The first compound proximal dorsal radial in *M. ani* is ax-shaped; it is pear-shaped in *M. andreetti*; it is a massive, compact, rectangular-shaped plate in *M. furreri* that may be formed by the complete or partial fusion of four proximal radials (Fig. 10). (9) The last dorsal proximal radial is boomerang-shaped in *M. ani*, whereas it is regularly arched with the horizontal limb larger than the vertical one in *M. andreetti*. In contrast, the horizontal limb in *M. furreri* is expanded to support several last dorsal rays, and the vertical limb is markedly arched (Fig. 11). (10) The last proximal anal radial has a similar boomerang shape as the last proximal dorsal radial in *M. ani*; whereas it has an elongate and broad distal portion and a thin elongate anterior vertical limb in *M. furreri* (Fig. 11). (11) There are 10 epaxial and seven to 10 hypaxial basal fulcra in *M. ani*, whereas 10 or 11 epaxial basal fulcra and 12 hypaxial basal fulcra are present in *M. furreri*. (12) Eighteen principal rays are present in the caudal fin of *M. ani*; in contrast, 20 or 21 rays are present in *M. furreri*. (13) Three or four hypaxial procurrent rays are present in *M. ani*; in contrast one or two, occasionally three, are present in *M. furreri*. (14) Two urodermals are apparently present in *M. ani*, whereas no urodermals are found in *M. furreri*.

Although the Triassic *Marcopoloichthys* show similarities with another small, scaleless Triassic fish of similar age—*Prohalecites*—major differences separate them, as for example, the dentition presents in *Prohalecites* (Tintori 1990: text-fig. 2) that is lacking in marcopoloichthyids, the round profile of the head with a rostral bone in *Prohalecites* instead of a mesethmoid, one pair of nasal bones instead of two, weak and simple first and last dorsal pterygiophores in *Prohalecites* in contrast to special bony plates resulting from fusion of several proximal dorsal radials in marcopoloichthyids, ossified ribs in *Prohalecites* versus absence in *Marcopoloichthys*, and numerous other differences.

The above list of morphological differences illustrates differences among *Marcopolichthys ani*, *M. andreetti*, and *M. faccii* as described by Tintori et al. (2007) and *Marcopolichthys furreri*, which support *M. furreri* as a new species.

Phylogenetic analysis

First phylogenetic analysis

Two phylogenetic analyses were performed. The first phylogenetic analysis was conducted using a matrix containing numerous neopterygians to test the position of *Marcopoloichthys furreri* sp. nov. within Neopterygii. For this purpose, the matrix of Shen and Arratia (2022) which is a partially modified matrix of Xu (2020a) and contains 55 taxa scored for 137 characters, was used. One character (Ch. 138, absence versus presence of uroneurals) was added. For the details concerning the characters and their coding, see Suppl. material 1, and for the matrix, see Suppl. material 2. *Moythomasia durgaringa*, *Pteronisculus stensioi*, and *Boreosomus piveteaui* represent the outgroup.

The parsimony phylogenetic analysis was performed using PAUP 4.0a169. The topology of the strict consensus is shown in Fig. 15 and is based on 84 most parsimonious trees. The tree length is 382. Consistency index (CI) is 0.4241, and the retention index (RI) is 0.7598. For the description of node support for *Marcopoloichthys furreri* and phylogenetic related taxa, see below and Fig. 15 (Node A, crown-group Neopterygii, and Node B, Teleosteomorpha). An asterisk [*] identifies a character interpreted as uniquely derived.

Nodes 1 and 2, showing unresolved polytomies, represent (Fig. 15) a different topology of the consensus than in Xu (2020a), but the same topology as in Shen and Arratia (2022). Node 1 represents the unresolved polytomies including [*Teffichthys madagascariensis* + *Perleidus altolepis* + [*Plesiofuro mingshuica* + *Meidiichthys browni*] plus [[Louwoichthyiformes + Luganoiiformes + Peltopleuriformes] + [*Venusichthys comptus* + *Habroichthys minimus* + crown Neopterygii]] and is weakly supported by four homoplasies: dermosphenotic does not contact with preopercle (Ch. 36[0]); opercle is nearly equal to, or smaller than, subopercle (Ch. 89[1]); four to six branchiostegal rays present (Ch. 93[2]); and 24 or less principal caudal fin rays (Ch. 111[1]).

Node 2 represents the unresolved polytomy formed by [[Louwoichthyiformes + Luganoiiformes + Peltopleuriformes] + [*Venusichthys comptus* + *Habroichthys minimus* + [crown Neopterygii]] and is weakly supported by two homoplastic characters: ratio of dermopterotic [= or supratemporotabular] or pterotic length to parietal length is less than two (Ch. 12[0]); and teeth only present on the anterior portion of oral margin of maxilla (Ch. 65[1]).

Node A (Holostei plus Teleosteomorpha) is supported by nine synapomorphies, only one being uniquely derived: expanded dorsal lamina in the maxilla lost (Ch. 59[1]*). Eight homoplastic characters also support this node: nasal bones joined in midline (Ch. 8[1]); supraorbital bone present (Ch. 43[1]); supramaxilla present (Ch. 54[1]); and interopercle present (Ch. 83[1]). The following five characters are interpreted as reversals by the parsimony analysis at this phylogenetic level: broad width of posttemporal,

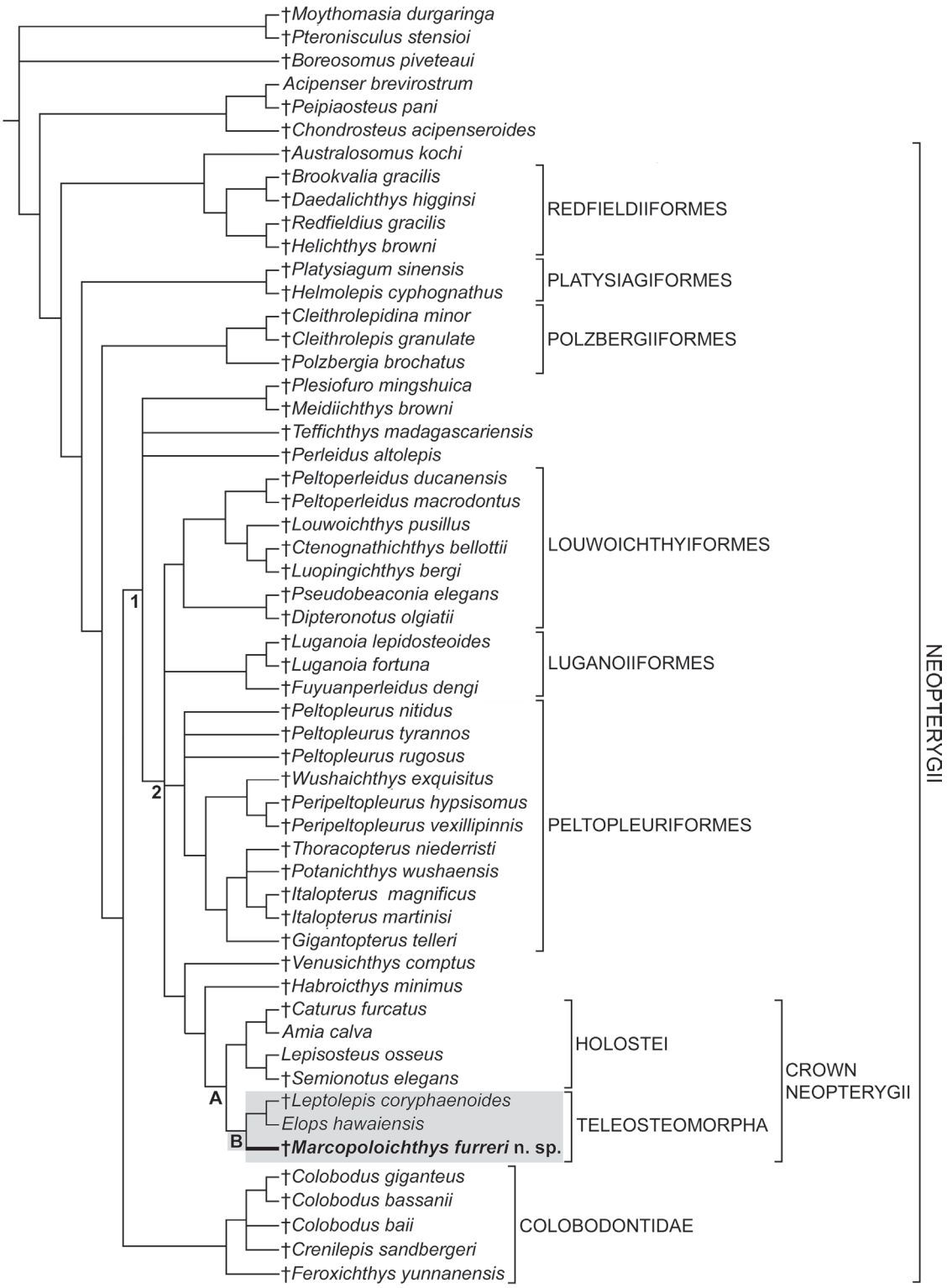

Figure 15. Hypothesis of phylogenetic relationships of *Marcopoloichthys furreri* sp. nov. among neopterygians based on 138 characters and three outgroup taxa. Strict consensus tree of 84 most parsimonious trees: three length 464 steps, consistency index (CI) = 0.3491 and retention index (RI) = 0.6696. An asterisk identifies a uniquely derived character. **Node A** (crown Neopterygii) is supported by the following synapomorphies: supraorbital bone present; supramaxilla present; expanded dorsal lamina in the maxilla lost (*); nasal bones joined in midline; interopercle present; supracleithrum nearly as deep as posterior margin of opercle (Ch. 102[0]); no segmented procurrent rays in dorsal lobe of caudal fin (Ch. 109[0]); and lateral line scales as deep as, or slightly deeper than, those scales above and below (Ch. 124[0]). **Node B** (Teleosteomorpha): supraoccipital present (*); mobile premaxilla present (*); two supramaxillae present (*); vomers fused in adults into a single bone (*); elongated posteroventral process of quadrate present (*); uroneural(s) present (*); cycloid type of scales present (*); and leading margins of the caudal fins formed by the first and last principal rays (*). Homoplasies supporting this node are: basipterygoid process absent; internal carotid foramen on parasphenoid present; single supraorbital bone; suture between opercle and subopercle greatly inclined; origin of dorsal fin slightly posterior or just in front to pelvic fin origin; and fringing fulcra absent on pectoral fins.

nearly as wide as extrascapular (Ch. 100[0]); supracleithrum nearly as deep as posterior margin of opercle (Ch. 102[0]); no segmented procurrent rays in dorsal lobe of caudal fin (Ch. 109[0]); and lateral line scales as deep as or slightly deeper than those scales above and below (Ch. 124[0]). It is interesting to note that according to this analysis, character 8[1], 43[1], and 54[1] are not present in *Marcopoloichthys furreri* and are interpreted by the parsimony analysis as losses. Character 124[0] is not applicable in *M. furreri*, because the fish has a naked body.

Node B (Teleosteomorpha or total group teleosts) is supported by 14 synapomorphies, eight of which are uniquely derived traits: supraoccipital present (19[1]*); mobile premaxilla present (48[1]*); two supramaxillae present (55[1]*); vomers fused in adults into a single bone (72[1]*); elongated posteroventral process of quadrate present (80[1]*); uroneural(s) present (97[1]*); cycloid type of scales present (128[2]*); and leading margins of the caudal fins formed by the first and last principal rays (138[1]*). Homoplasies supporting this node are the following: basipterygoid process absent (Ch. 26[1]); internal carotid foramen on parasphenoid present (Ch. 27[1]); single supraorbital bone (Ch. 44[0]); suture between opercle and subopercle greatly inclined (Ch. 90[1]); origin of dorsal fin slightly posterior or just anterior to pelvic fin origin (Ch. 107[3]); and fringing fulcra absent on pectoral fins (Ch. 120[1]). The condition of characters 19[1], 27[1], and 80[1] is still unknown in *Marcopoloichthys furreri* sp. nov. because of incomplete preservation, and characters 44[0], 55[1], and 128[2] are not applicable to this taxon, because the fish lacks supraorbitals, supramaxillae, and scales and the parsimony analysis interpret them as a synapomorphy of this node that has been lost in *Marcopoloichthys furreri* sp. nov. The parsimony analysis interprets these losses as autapomorphies of *Marcopoloichthys*. *Marcopoloichthys furreri* sp. nov. stands as the sister group of (*Leptolepis coryphaenoides* + *Elops saurus*). Thus, the phylogenetic analysis unambiguously confirms *Marcopoloichthys* as a member of the Teleosteomorpha.

Second phylogenetic analysis

The second phylogenetic analysis was conducted using a matrix containing numerous teleosteomorphs to test the position of *Marcopoloichthys furreri* sp. nov. For this purpose, the matrix of Arratia et al. (2021) which contains 36 taxa scored for 130 characters, was used. Two characters (Ch. 131: absence versus presence of short, stout epineural processes and Ch. 132: presence versus absence of scales on body) were added. For the details concerning the characters and their coding, see Suppl. material 3, and for the matrix, see Suppl. material 4. *Australosomus*, *Birgeria*, and *Polypterus* represent the outgroup.

The parsimony phylogenetic analysis was performed using PAUP 4.0a169. The topology of the strict consensus is shown in Fig. 16 and is based on two most parsimonious trees. The tree length is 374. Consistency index (CI) is 0.4599, and the retention index (RI) is 0.7534. For the description of node support for *Marcopoloichthys furreri* and phylogenetic related taxa, see below and Fig. 16 (Node C, Teleosteomorpha). An asterisk [*] identifies a character interpreted as uniquely derived.

The clade Teleosteomorpha (Pachycormiformes plus more advanced teleosteomorphs) is supported by 15 synapomorphies, six of which are interpreted as uniquely derived: Foramen for glossopharyngeal nerve placed in prootic or prootic-exoccipital suture (Ch. 34[1]*); four pectoral proximal radials present (Ch. 93[1]*); olfactory organ with accessory nasal sacs (Ch. 122[1]*); craniotemporal muscle present (Ch. 123[1]*); heart with two arterial valves (in the conus arteriosus) present (Ch. 124[1]*); and muscles at the basal arteria (ventral aorta) absent (Ch. 125[1]*). Seven homoplasies also support this node: pectoral propterygium fused with first pectoral-fin ray (Ch. [94[1]); dorsal or epaxial leading margin of caudal fin with basal fulcra (Ch. 114[1]); and quadratojugal absent (Ch.127[1]). Characters 122, 123, 124, and 125 are interpreted by the parsimony analysis to be present at this phylogenetic level although they are unknown in fossils due to preservation.

Node D represents the trichotomy including *Marcopoloichthys*, Aspidorhynchiformes, and *Prohalecites* plus more advanced teleosteomorphs. This node is weakly supported by two synapomorphies: supramaxillary bone or most posterior supramaxilla dorsal to maxilla (Ch.58[0]) and mid-caudal centra (adults) with diplospondylous centra (Ch. 87[0]). The parsimony analysis interprets the absence of a supramaxilla in *Marcopoloichthys* as an autapomorphy of this fish.

While in one tree Aspidorhynchiformes, *Marcopoloichthys*, and *Prohalecites* plus more advanced teleosts have resolved relationships, in the second tree, *Marcopoloichthys* is interpreted by the parsimony analysis as the sister of Aspidorhynchiformes.

Node E represents the branching of *Prohalecites* plus more advanced teleosteomorphs. This node is supported by five homoplasies: interparietal [= interfrontal] suture absent (Ch. 22[2]); nasal bones separated from each other by parietal bones [= frontals] (Ch. 23[2]); supraorbital canal with branched tubules (Ch. 35[1]); one supramaxillary bone (Ch. 57[1]); and three or four epurals present (Ch.109[1]).

The consensus tree in Fig. 16, Node F (*Atacamichthys* plus more advanced teleosteomorphs) has an identical topology to that in figure 9 in Arratia et al. (2021).

Discussion and conclusions

Marcopoloichthys and Neopterygii

In the original description of the family Marcopoloichthyidae and its genus *Marcopoloichthys* with three species, Tintori et al. (2007) assigned the family to Neopterygii sensu Patterson (1973), but without assigning the new fish to any neopterygian major taxon. The authors specifically stated in the abstract (p. 13) that “Lack of

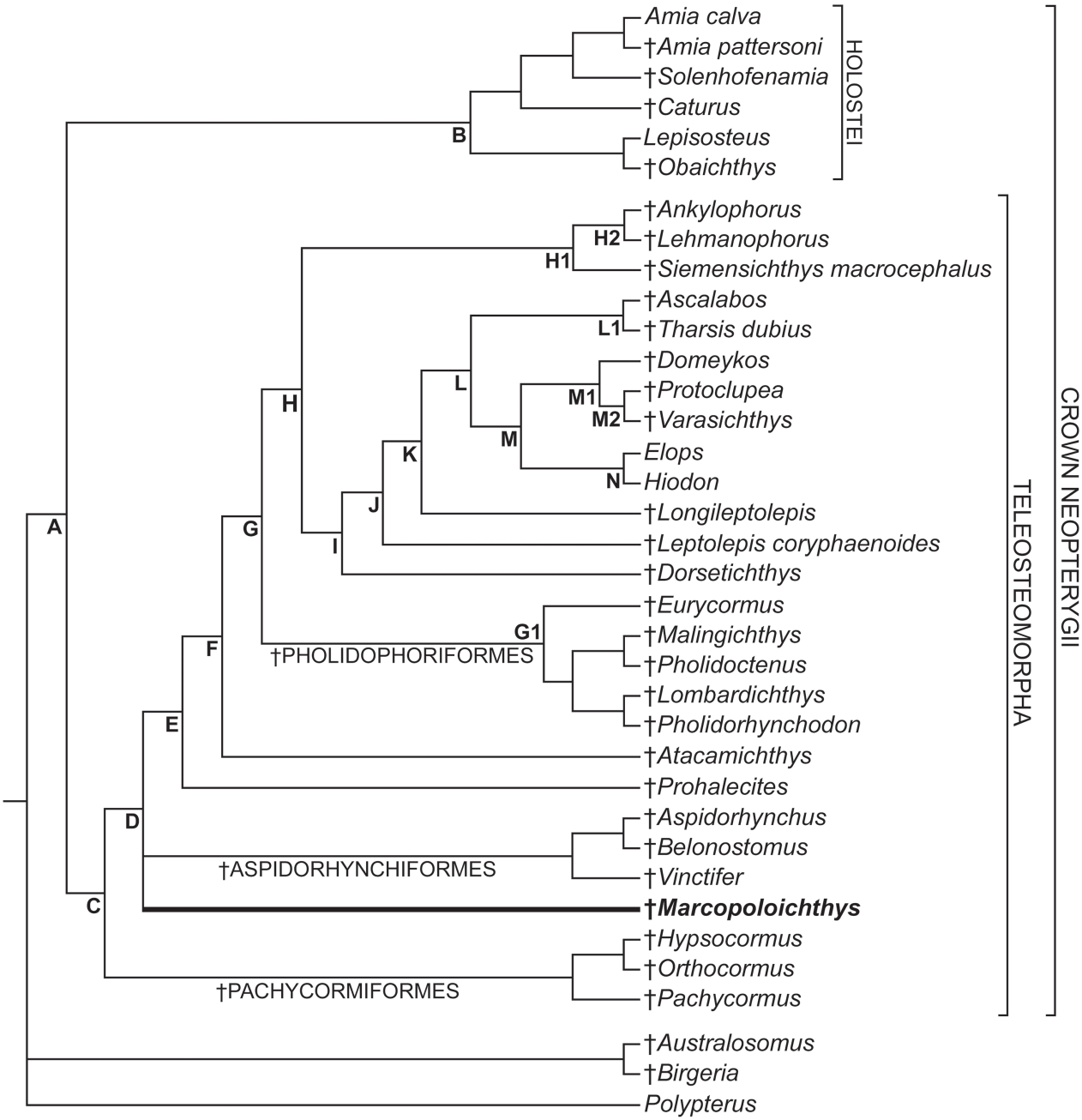

Figure 16. Hypothesis of phylogenetic relationships of *Marcopoloichthys furreri* sp. nov. among crown neopterygians based on 132 characters and three outgroup taxa. Strict consensus tree of two most parsimonious trees: three length 374 steps, consistency index (CI) = 0.4599 and retention index (RI) = 0.7534. An asterisk identifies a uniquely derived character. Teleosteomorphs (**Node C**) are supported by the following synapomorphies: foramen for glossopharyngeal nerve placed in prootic or prootic-exoccipital suture (*); four pectoral proximal radials present (*); olfactory organ with accessory nasal sacs (*); craniotemporal muscle present (*); heart with two arterial valves (in the conus arteriosus) present (]*); muscles at the basal arteria (ventral aorta) absent (*); propterygium fused with first pectoral-fin ray; dorsal or epaxial leading margin of caudal fin with basal fulcra; and quadratojugal absent (Ch.127[1]). **Node D** is supported by two synapomorphies: supramaxilla or most posterior supramaxilla dorsal to maxilla and mid-caudal centra (adults) with diplospondylous centra. For other nodes see text and Arratia et al. (2021).

vertebral centra and epineurals, among others, makes the new taxa quite distinct from true Teleosts, even if some characters may recall the corresponding in Teleosts themselves." Considering their statement and how the understanding of neopterygians has changed, the taxonomic position of *Marcopoloichthys*, as well as its phylogenetic position, were tested based on the new information provided by *Marcopoloichthys furreri* sp. nov. (the best preserved marcopoloichthyid).

Up to 1973, the neopterygians contained the holosteans, but Patterson (1973) proposed a new classification that did not recognize the Holostei as part of the Neopterygii. Later, Grande (2010), based on fossil and living lepisosteiforms, demonstrated the validity of the taxon

Holostei, which has been confirmed in subsequent phylogenetic hypotheses based on morphological (e.g., Arratia 2013; López-Arbarello and Sferco 2018; Xu 2020a, 2020b; 2021; Gouiric-Cavalli and Arratia 2022) and molecular evidence (e.g., Near et al. 2013; Betancur-R. et al. 2013; Betancur-R. et al. 2017). What seems resolved for extant neopterygians has been not so clear for fossil neopterygians with a large and varied record, and whose knowledge has improved during the last years due to new findings, especially in the Triassic of Eurasia (e.g., Xu et al. 2013; Xu and Ma 2016; Xu 2020a, 2020b, 2021).

Although the phylogenetic relationships seem to be resolved for many neopterygian clades, and numerous stem- and crown-group neopterygians are now recognized in recent phylogenetic hypotheses (e.g., López-Arbarello and Sferco 2018; Xu et al. 2015; Xu and Ma 2016; Xu 2020a, 2020b, 2021), the phylogenetic analysis of thoracopteroids by Shen and Arratia (2022), who used the matrix of Xu (2020a), proved to be devastating (see their fig. 3, node 2; Fig. 15 herein) because numerous clades have an unresolved positions within neopterygians. The inclusion of *Marcolopoichthys ferreri* sp. nov. did not change the topology of the consensus (see Fig. 14, node 2) that is similar to that of Shen and Arratia (2022). Nevertheless, we should be aware of the fact that many characters still remain unknown or ambiguous (coded with a question mark) for many of the neopterygians included in the phylogenetic analyses due to incomplete preservation and many nodes are weakly supported so that the phylogenetic position of several taxa still remain controversial and requires further investigation. For instance, Redfieldiiformes (Triassic to Early Jurassic age) have been controversial since the establishment of the family Catopteridae (= Redfieldiidae Berg, 1940) by Woodward in 1890. Discussions on redfieldiiform relationships or phylogenetic analyses including them can be found in Stensiö (1921), Brough (1931, 1936), Schaeffer (1955, 1967, 1984), Hutchinson (1973, 1978), Gardiner and Schaeffer (1989), and more recently in Xu (2021). Redfieldiiformes and Platysiagiformes have been referred as subholosteans, a clade that has not had recognition in fish classification (e.g., Nelson et al. 2016; Arratia 2021). Redfieldiiformes (= family Redfieldiidae) and Platysiagiformes have recently been interpreted as primitive neopterygians by Xu (2020a, 2021; Fig. 15 herein), but as crown actinopterygians, Palaeoniscimorpha, by Schultze et al. (2022).

Finally, the present results suggest marcopoloichthyids as part of the crown-group neopterygians (Fig. 15, node A) and as stem teleosts (Fig. 15, node B), disagreeing with Tintori et al.'s (2007) interpretation that marcopoloichthyids are basal neopterygians.

Marcopoloichthys and Teleosteomorpha

Among Triassic fishes, *Marcopoloichthys* is unique in showing a combination of characters as those in the jaws, endoskeleton of the median fins, or in the reduction of the caudal fin (Tintori et al. 2007). Furthermore, the authors mentioned specifically (p. 13) that "the lack of vertebral centra and epineurals" are characters that question a possible interpretation with "true" teleosts (= *Leptolepis coryphaenoides* plus more advanced teleosts sensu Arratia 1996, 1997, 1999). The presence of a functional notochord or an aspondylous type of vertebral column is true for Ladinian marcopoloichthyids, but a character shared with other teleosteomorphs, such as the Triassic *Prohalecites* (Tintori 1990; Arratia and Tintori 1999) and most pachycormiforms (e.g., Arratia and Schultze 2013; Gouiric-Cavalli 2022). In contrast, other teleosteomorphs, such as Triassic pholidophorids, *Eurycormus* and *Leptolepis coryphaenoides* plus more advanced teleosts, possess vertebral centra formed either by chordacentra or autocentra or both (Arratia 1997, 2013, 2015; Arratia et al. 2001). The statement that marcopoloichthyids lack epineurals is a result of incomplete preservation in the specimens studied by Tintori et al. (2007), but *Marcopoloichthys furreri* sp. nov. has short epineural processes in the abdominal vertebrae and first caudal vertebrae (Figs 3A, 9, 12), and the presence of epineural processes, either short or long, is an undisputed synapomorphy of the apomorphy-based teleosts. Similar short epineural processes are found in another Triassic stem teleost, *Prohalecites*. In addition, *Marcopoloichthys furreri* sp. nov. shares with other teleosteomorphs several undisputed synapomorphies, such as an unpaired vomer (Fig. 4), a mobile premaxilla (Figs 4, 5), lack of prearticular bone in the lower jaw (Fig. 4), four proximal pectoral radials (Fig. 10), propterygium fused with the base of first pectoral ray (Fig. 10), presence of modified ural neural arches or uroneurals (Fig. 13), and first and last principal caudal rays (Fig. 14A) forming the leading margins of the caudal fin (see Patterson 1977 and Arratia 1997, 1999, 2013, 2015 for explanations of these synapomorphies). Because of preservation conditions, it is unknown if other teleostean synapomorphies could be present, such as a supraoccipital bone (Patterson 1975) or a postero-ventral or dorsal process of the quadrate (Arratia and Schultze 1991; Arratia 2013, 2015).

The phylogenetic hypothesis shown in Fig. 15, node B (and descriptions above) confirms *Marcopoloichthys* as a teleosteomorph, phylogenetically closer to *Leptolepis coryphaenoides* and *Elops saurus* than to any other neopterygian clade. The phylogenetic hypothesis shown in Fig. 16, node D confirms *Marcopoloichthys* as a teleosteomorph, with an unresolved phylogenetic position with Aspidorhynchiformes, and [*Prohalecites* plus more advanced teleosteomorphs].

Marcopoloichthys furreri sp. nov. and its complex morphology

Although I refer especially to the new *Marcopoloichthys* from Switzerland, I would expect that some of the morphological characters discussed below are also in other marcopoloichthyids, but due to incomplete preservation

they have not been observed yet. A discussion on selected morphological structures follows.

A strongly ossified T-shaped mesethmoid forming the anterior tip of the snout is an uncommon bone in Triassic and Jurassic teleosteomorphs, which usually have a rostral bone carrying the ethmoidal commissure as in pholidophoriforms (Arratia 2013, 2017) or a special compound rostrodermethmoid as in pachycormiforms (e.g., Lambert 1992; Gouiric-Cavalli and Arratia 2022). The condition in *Marcopoloichthys*, including shape and development of the mesethmoid, resembles that of *Leptolepis coryphaenoides* and *Tharsis dubius* plus more advanced teleosts, such as Elopiformes, Clupeiformes, Ostariophysi, Salmoniformes and many others (Arratia pers. obs.); it differs from them in that the marcopoloichthyid mesethmoid is not sutured with the anterior margin of the parietal [= frontal] bones—it is a free bone.

Marcopoloichthys furreri sp. nov. is remarkable in having two pairs of nasal bones (Figs 4, 5, 6), which are identified here as nasal bones (the anterior pair) that are loosely articulated with the mesethmoid, and an "accessory pair" loosely articulated with the parietal [= frontal] bones posteriorly. The accessory nasal is also a special bone that lies in an almost vertical position in front of the lateral ethmoid when the mouth is closed, and then moving forward in a horizontal position when the mouth is opened (Fig. 7). To my best knowledge, no other teleosteomorph has two pairs of nasal bones; additionally, the bones are unique for the loose articulation between the two pairs and between antimeres, a condition that would permit them to change position during resting and suction feeding. An accessory nasal bone is an autapomorphic feature of *Marcopoloichthys furreri*, and it is expected to be a family character.

An additional structure, named here "rostral cartilage" (Fig. 6), because of its position and structure, is placed below the mesethmoid, probably supporting the latter and offering a smooth surface facilitating the movements of the mesethmoid during feeding.

Marcopoloichthyids lack supramaxillae, in contrast to neopterygians that have one or two supramaxillae on the dorsal margin of the maxilla. In this trait, marcopoloichthyids resemble primitive actinopterygians (Schultze et al. 2022), a feature that becomes a synapomorphy of Marcopoloichthyidae.

The presence of two hypohyals is a common condition in crown teleosts and is also present in such fossils as *Leptolepis coryphaenoides* and more advanced teleosts. The condition remains obscure for several stem teleosts, but among them *Marcopoloichthys furreri* has one hypohyal resembling the condition in holosteans.

A supraneural carrier is a compound structure formed by the fusion of the most anterior neural elements of the vertebral column, bearing five expanded supraneurals (Fig. 9). To the best of my knowledge, this structure is only known in *Marcopoloichthys furreri* but it is expected to be present in other marcopoloichthyids and be a family synapomorphy. See below concerning possible interpretations about the feeding mechanism in *Marcopoloichthys furreri*.

It is interesting that *Marcopoloichthys* specimens show a series of parapophyses in specimens with the abdominal region of the vertebral column well-preserved, but ossified ribs or their remains have not been found in any specimen (Tintori et al. 2007: figs 2, 4; Figs 2, 3, 4, 9 herein). According to the available information, ossified ribs are found in other teleosteomorphs, making this absence a synapomorphy of Marcopoloichthyidae.

Marcopoloichthys furreri sp. nov. possesses three bony postcleithra (Fig. 4) that are mainly positioned in the hypaxial body musculature, forming a series similar to those found in *Leptolepis coryphaenoides*, *Tharsis* and other ascalaboids, and more advanced teleosts, such as crown groups elopiforms, clupeomorphs, many ostariophysans and euteleosts. Certainly, this is a different condition to that found in *Prohalecites* with one bony postcleithrum and neopterygians with modified ganoid scales that are also named postcleithra. Among stem teleosts, the postcleithra of *Marcopoloichthys furreri* appears to be another autapomorphic feature that should be confirmed in other marcopoloichthyids.

The first three or four proximal radials of the dorsal fin fused together forming a broad bony plate that supports the anterior most dorsal fin in marcopoloichthyids is an unquestionable synapomorphy of the group, apparently unique among neopterygians. Additionally, the differences in shape and numbers of radials included in the fusion is of taxonomic value, characterizing some species of marcopoloichthyids. Usually, in teleosteomorphs and crown teleosts, the first dorsal pterygiophore may have one to three processes.

The last dorsal pterygiophore in stem teleosteomorphs and crown teleosts is slightly expanded and supports two dorsal lepidotrichia that are counted as one. The last element in marcopoloichthyids is enlarged and supports more than two lepidotrichia; this is another synapomorphy of the family. The current information concerning the number of lepidotrichia involved is incomplete for all marcopoloichthyid species. A similar situation concerns the last anal pterygiophore, which is also expanded and supports more than two rays, but the total number involved for each species is unclear due to preservation.

Although it is clear that *Marcopoloichthys furreri* represents a new species and that marcopoloichthyids are a well diagnosed taxon, their unique combination of primitive and advanced characters makes it difficult to place them phylogenetically among teleosteomorphs (a study that will be addressed when the youngest marcopoloichthyids from Italy can be added to the study).

Comments on suction feeding mechanism

Studies on the suction mechanism in extant teleosts is a complicated subject that requires a combination of experimental and modeling approaches (e.g., Gibb and Ferry-Graham 2005; Day et al. 2015). It is not my intention to analyze the biomechanics of the feeding suction of *Marcopoloichthys furreri* sp. nov., but the sample of

specimens under study have individuals that died with the mouth closed, whereas others were feeding. It is interesting to analyze the morphological differences between both stages trying to understand, somehow, the positional changes of the bones, the function of additional bones, and the massive ossification of some bones. Because conditions of preservation, soft structures (ligaments, tendons, or muscles) are missing in the fossils.

One of the noteworthy changes that I should mention is the differences in the shape of the head; it is somewhat triangular when the mouth was closed, whereas there is an antero-posterior elongation of the cranium that is accompanied with a dorso-ventral compression during suction (compare Figs 3A and 4; Fig. 7A and 7B), which is often referred to as "functional integration" (Olson and Miller 1951, 1958; Klingenberg 2014). For example, changes in the shape of the upper and lower jaws and expansion of the skull in *Marcopoloichthys* were integrated to generate an intraoral pressure to draw water and prey into the mouth, as has been shown for extant fishes (Lauder 1985; Day et al. 2015; Wainwright et al. 2015). Such action involved multiple integral components: the mesethmoid; nasals; accessory nasals; upper and lower jaws; the whole suspensorium, including the preopercle, and the strong and heavily ossified ceratohyals, which changed position during suction; integration of the cleithrum—strongly expanded antero-ventrally—as well as the clavicle; and support of the pectoral fins by the scapula and coracoid, whose integrated kinetic movements maximized forces and the chance to engulf prey. In this context, I can suggest an explanation for the presence of a previously unreported structure, the supraneural carrier (Fig. 9) in *Marcopoloichthys*. The large head of the fish in comparison to a narrower body with an aspondylous vertebral column (Fig. 4) would need some kind of support for expansion of the cranium during feeding, and it is possible that this was the function of the fused vertebrae forming the supradorsal carrier. A mechanism that in extant teleosts is replaced by an ossified vertebral column, which may include chordacentrum surrounded by autocentrum or autocentrum alone, depending on the taxon.

The integration of these mechanisms in extant teleosts during prey capture also involves lower jaw length and the length of the ascending process of the premaxilla (Kane et al. 2019). Interestingly, the lower jaw of *Marcopoloichthys furreri* has a moderate length and its articular region with the quadrate (and also symplectic in this case) is placed at about the level of the posterior half of the orbit (Fig. 3A), but when the fish was feeding, the lower jaw displaced anteriorly to below the anterior half of the orbit, closer to the anterior orbital margin (Figs 4, 7). *Marcopoloichthys* lacked an ascending process in the premaxilla, which is present with different degrees of development in extant teleosts. The articular regions of the premaxilla and maxilla were weakly developed (Fig. 5A, C), and when the fish was feeding, both bones displaced anteriorly, forming the lateral walls of the buccal tube (Figs 4, 7B). The dorsal part of the buccal tube was formed by a median and strongly ossified mesethmoid (and the rostral cartilage; Fig. 6), which was loosely articulated postero-laterally with the nasals, and which turn were loosely articulated with the accessory nasals and parietal [= frontal] bones posteriorly. I assume that the bones of the snout region and the upper jaw were kept in position by the action of ligaments.

Independent of the evolutionary changes in bone lengths and the presence of specific bones playing a role in the feeding of teleosteomorphs, *Marcopoloichthys furreri* sp. nov. and its exceptional preservation are an outstanding example of the suction feeding mechanism 242–235 million years ago.

Acknowledgements

Special thanks to Heinz Furrer for making specimens of *Marcopoloichthys furreri* sp. nov. available for this study, providing detailed information for each specimen and its collecting data, and valuable assistance with literature on the Prosanto Formation. To Florian Witzmann (Museum für Naturkunde, Berlin, Germany) for assistance with loans of *Marcopoloichthys* specimens. For loan of valuable specimens used in the phylogenetic analyses, I am grateful to H. Bjerring (Stockholm); R. Böttcher and E. Maxwell (Stuttgart); the late C.H. von Daniels (Hannover); H. Jahnke (Göttingen); W. Mette and W. Resch (Innsbruck); G. Viohl, M. Kölbl-Ebert and M. Ebert (Eichstätt); P. Wellnhofer, O. Rauhut, and M. Moser (München); F. Westphal and the late W.-E. Reif (Tübingen); F. Witzmann (Berlin); U. Goehlich (Vienna); A. Paganoni (Bergamo); A. Tintori (Milan); the late C. Patterson and A. Longbottom (London); D. Berman (Cleveland, Ohio); W. Eschmeyer and D. Catania (San Francisco, California); L. Grande, W. Simpson, W. Westneat, and M.A. Rogers (Chicago); A. Simons and V. Hirt (Saint Paul, Minnesota); E. O. Wiley and A. Bentley (Lawrence, Kansas); the late L. Martin and D. Miao (Lawrence, Kansas); the late K. Liem, K. Hartel, the late F. Jenkins, J. Cundiff, and C. Byrd (Cambridge, Massachusetts); J. McEacharan and M. Retzer (Texas); W. Saul (Philadelphia, Pennsylvania); and J.-Y. Zhang (Beijing). Photographs of specimens were kindly taken by Mrs. Carola Radke (Museum für Naturkunde, Berlin, Germany) and by Torsten Scheyer (University of Zurich, Switzerland) as indicated in the respective figures. Flavio Dalla Vecchia (Institut Català de Paleontologia Miquel Crusafont, Spain) helped with photographs on undescribed specimens of *Marcopoloichthys* illustrated in his (2012) book. To Terry Meehan (Lawrence, Kansas, USA) for revision of the style and grammar of the ms. Special thanks to Toni Bürgin (St. Gallen, Switzerland), Giorgio Carnevale (Torino, Italy), and Florian Witzmann (Chief-Editor) for reviewing the manuscript. Many thanks to the private collectors who donated interesting specimens: Alex Dübendorfer (BNM 201166), Christian Obrist (A/I 2888, 2889, 2890) and Elisabeth Schaufelberger (A/I 1923).

References

Arratia G (1997) Basal teleosts and teleostean phylogeny. Palaeo Ichthyologica 7: 5–168.

Arratia G (1999) The monophyly of Teleostei and stem group teleosts. Consensus and disagreements. In: Arratia G, Schultze H-P (Eds) Mesozoic Fishes 2 – Systematics and the Fossil Record. Verlag Dr. Friedrich Pfeil, München, 265–334.

Arratia G (2001) The sister-group of Teleostei: Consensus and disagreements. Journal of Vertebrate Paleontology 21: 767–773. https://doi.org/10.1671/0272-4634(2001)021[0767:TSGOTC]2.0.CO;2

Arratia G (2008) Actinopterygian postcranial skeleton with special reference to the diversity of fin ray elements, and the problem of identifying homologies. In: Arratia G, Schultze H-P, Wilson MVH (Eds) Mesozoic Fishes 4 – Homology and Phylogeny. Verlag. Dr. Friedrich Pfeil, München, 40–101.

Arratia G (2009) Identifying patterns of diversity of the actinopterygian fulcra. Acta Zoologica, Stockholm 90: 220–235. https://doi.org/10.1111/j.1463-6395.2008.00375.x

Arratia G (2013) Morphology, taxonomy, and phylogeny of Triassic pholidophorid fishes (Actinopterygii, Teleostei). Journal of Vertebrate Paleontology, Memoir 13, 33: 1–138. https://doi.org/10.1080/02724634.2013.835642

Arratia G (2015) Complexities of early Teleostei and the evolution of particular morphological structures through time. Copeia 103: 999–1025. https://doi.org/10.1643/CG-14-184

Arratia G (2016) New remarkable Late Jurassic teleosts from southern Germany: Ascalaboidae n. fam., its content, morphology, and phylogenetic relationships. Fossil Record 19(1): 31–59. https://doi.org/10.5194/fr-19-31-2016

Arratia G (2017) New Triassic teleosts (Actinopterygii, Teleosteomorpha) from northern Italy and their phylogenetic relationships among the most basal teleosts. Journal of Vertebrate Paleontology 37(6): e131269. https://doi.org/10.1080/02724634.2017.1312690

Arratia G (2021) Osteichthyes or Bony Fishes. In: Elias S, Alderton D (Eds) Encyclopedia of Geology, 2nd Edn. Elsevier Inc., New York, 121–137. https://doi.org/10.1016/B978-0-12-409548-9.12082-2

Arratia G, Herzog A (2007) A new halecomorph fish from the Middle Triassic of Switzerland and its systematic implications. Journal of Vertebrate Paleontology 27(4): 838–849. https://doi.org/10.1671/0272-4634(2007)27[838:ANHFFT]2.0.CO;2

Arratia G, Schultze H-P (1991) The palatoquadrate and its ossifications: Development and homology within osteichthyans. Journal of Morphology 208: 1–81. https://doi.org/10.1002/jmor.1052080102

Arratia G, Schultze H-P (2013) Outstanding features of a new Late Jurassic pachycormiform fish from the Kimmeridgian of Brunn, Germany and comments on current understanding of pachycormiforms. In: Arratia G, Schultze H-P, Wilson MVH (Eds) Mesozoic Fishes 5 – Global Diversity and Evolution. Verlag Dr. Friedrich Pfeil, München, 87–120.

Arratia G, Schultze H-P, Casciotta J (2001) Vertebral column and associated elements in dipnoans and comparison with other fishes: development and homology. Journal of Morphology 250: 101–172. https://doi.org/10.1002/jmor.1062

Arratia G, Schultze H-P, Gouiric-Cavalli S, Quezada-Romegialli C (2021) The intriguing *Atacamichthys* fish from the Middle Jurassic of Chile – an amiiform or a teleosteomorph? In: Pradel A, Denton J, Janvier P (Eds) Ancient Fishes and their Living Relatives: a tribute to John G. Maisey. Verlag Dr. Friedrich Pfeil, München, 19–36. https://doi.org/10.1080/14772019.2022.2049382

Bellotti C (1857) Descrizione di alcune nuove specie di pesci fossili di Perledo e di alter localita Lombarde. In: Stoppani A (Ed.) Studii Geologici Paleontologici sulla Lombardia. Turati, Milano, 419–438.

Berg LS (1940) Classification of fishes both recent and fossil. Travaux de l'Institut de l'Académie des sciences de l'URSS, 52: 87–517.

Betancur-R R, Broughton RE, Wiley EO, Carpenter K, Lopez JA, Li C, Holcroft NI, Arcila D, Sanciangco M, Cureton JC, Zhang F, Buser T, Campbell MA, Ballesteros JA, Roa-Varon A, Willis S, Borden WC, Rowley T, Reneau PC, Hough DJ, Lu G, Grande T, Arratia G, Orti G (2013) The tree of life and new classification of bony fishes. PLoS Currents 5. https://doi.org/10.1371/currents.tol.53ba26640df0ccaee75bb165c8c26288

Betancur-R R, Wiley EO, Arratia G, Acero A, Bailly N, Miya M, Lecointre G, Orti G (2017) Phylogenetic Classification of Bony fishes. BMC Evolutionary Biology 17: e162. https://doi.org/10.1186/s12862-017-0958-3

Brough J (1931) On fossil fishes from the Karoo system and some general considerations on the bony fishes of the Triassic period. Proceedings of the Zoological Society of London 101: 235–296. https://doi.org/10.1111/j.1469-7998.1931.tb06193.x

Brough J (1936) On the evolution of bony fishes during the Triassic period. Biological Review 11: 385–405. https://doi.org/10.1111/j.1469-185X.1936.tb00912.x

Brough J (1939) The Triassic fishes of Besano, Lombardy. British Museum of Natural History, London, 117 pp.

Bürgin T (1990) Der Schuppenpanzer von *Habroichthys minimus*, einem ungewönlichen Strahlenflosser (Actinopterygii: Peltopleuriformes) aus der Mittleren Trias der Südalpen. Neues Jahrbuch für Geologie und Paläontologie, Monatshefte 1990(11): 647–658. https://doi.org/10.1127/njgpm/1990/1990/647

Bürgin T (1992) Basal ray-finned fishes (Osteichthyes; Actinopterygii) from the Middle Triassic of Monte San Giorgio (Canton Tessin, Switzerland). Schweizerische Paläontologische Abhandlungen, 114: 1–164.

Bürgin T (1999) Middle Triassic marine fish faunas from Switzerland. In: Arratia G, Schultze H-P (Eds) Mesozoic Fishes 2 – Systematics and Fossil Record. Verlag Dr. Friedrich Pfeil, München, 481–494.

Bürgin T, Herzog A (2002) Die Gattung *Ctenognathichthys* (Actinopterygii; Perleidiformes) aus der Prosanto-Formation (Ladin, Mitteltrias) Graubündens (Schweiz), mit der Beschreibung einer neuen Art, *C. hattichi* sp. nov. Eclogae Geologicae Helvetiae 95: 461–469.

Bürgin T, Eichenberger U, Furrer H, Tschanz K (1991) Die Prosanto-Formation—eine fischreiche Fossil-Lagerstätte in der Mittel-trias der Silvretta-Decke (Kanton Graubünden, Schweiz). Eclogae geologicae Helvetiae 84(3): 921–990.

Cavin L, Furrer H, Obrist C (2013) New coelacanth material from the Middle Triassic of eastern Switzerland, and comments on the taxic diversity of actinistians. Swiss Journal of Geosciences 106: 101–177. https://doi.org/10.1007/s00015-013-0143-7

Cavin L, Mennecart B, Obrist C, Costeur L, Furrer H (2017) Heterochronic evolution explains unusual body shape in a Triassic coelacanth from Switzerland. Scientific Reports 7: e13695. https://doi.org/10.1038/s41598-017-13796-0

Cope ED (1887) Zittel's Manual of Paleontology. American Naturalist 17: 1014–1019.

Dalla Vecchia FM (2008) Vertebrati Fossili del Friuli – 450 milioni di anni di evoluzione. Edizione del Museo Friulano di Storia Naturale, Udine, 303 pp.

Dalla Vecchia FM (2012) Friuli 215 milioni di anni fa – Gli straordinari fossili di Preone finestra su di un mondo scomparso. Municipality of Preone, 224 pp.

Day SW, Higham TE, Holzman R, Van Wassenbergh S (2015) Morphology, kinematics, and dynamics: the mechanics of suction feeding in fishes. Integrative and Comparative Biology 55: 21–35. https://doi.org/10.1093/icb/icv032

Egerton MG (1872) Figures and descriptions of British organic remains. Memoirs of the Geological Survey of the United Kingdom 1872(13): 5–35.

Eichenberger U (1986) Die Mitteltrias der Silvretta-Decke (Ducankette und Landwassertal, Ostalpin). Mitteilungen aus den Geologischen Institut der Eidgenössischen Technischen Hochschule und der Universität Zürich, Neue Folge 252, 196 pp.

Furrer H (1995) The Prosanto Formation, a marine Middle Triassic Fossil Lagerstätte near Davos (Canton Graubünden, Eastern Swiss Alps). Eclogae geologicae Helvetiae 88(3): 681–683.

Furrer H (1999) New excavations in marine Middle Triassic Fossil Lagerstätte at Monte San Giorgio (Canton Ticino, Southern Switzerland) and the Ducan Mountains near Davos (Canton Graubünden, Eastern Switzerland). Rivista Museo Civico di Scienze Naturali "Enrico Caffi" 20: 85–88.

Furrer H (2004) So kam der Fisch auf den Berg—Eine Broschüre zur Sonderausstellung über die Fossilfunde am Ducan. Bündner Natur-Museum Chur und Paläontologisches Institut und Museum der Universität Zürich, 32 pp.

Furrer H (2019) Fische und Saurier aus dem Hochgebirge. Fossilien aus der mittleren Trias bei Davos. Neujahrsblatt der Naturforschenden Gesellschaft in Zürich NGZH221, 112 pp.

Furrer H, Froitzheim U, Wurster D (1992) Geologie, Stratigraphie und Fossilien der Ducankette und des Landwassergebiets (Silvretta-Decke, Ostalpin). Eclogae geologicae Helvetiae 85(1): 245–256.

Gardiner BG, Schaeffer B (1989) Interrelationships of lower actinopterygian fishes. Zoological Journal of the Linnean Society 97: 135–187. https://doi.org/10.1111/j.1096-3642.1989.tb00550.x

Gibb A, Ferry-Graham L (2005) Cranial movements during suction feeding in teleost fishes: Are they modified to enhance suction production? Zoology 108: 141–153. https://doi.org/10.1016/j.zool.2005.03.004

Gortani M (1907) *Pholidophorus faccii* nel Raibliano di Cazzaso in Carnia. Rivista Italiana de Paleontologia 13: 117–124.

Gouiric-Cavalli S, Arratia G (2022) A new †Pachycormiformes (Actinopterygii) from the Upper Jurassic of Gondwana sheds light on the evolutionary history of the group. Journal of Systematic Palaeontology 19(21): 1517–1550. https://doi.org/10.1080/14772019.2022.2049382

Grande L (2010) An empirical synthesis pattern study of gars (Lepisosteiformes) and closely related species, based mostly on skeletal anatomy. The resurrection of Holostei. American Society of Ichthyologists and Herpetologists. Special publication 6, Suppl. Copeia 10(2A), [x +] 871 pp. [ISBN: ISSN 0045-8511]

Herzog A (2001) *Peltoperleidus obristi* sp. nov., ein neuer kleiner Strahlenflosser (Actinopterygii, Perleidiformes) aus der Prosanto-Formation (Mitteltrias) von Graubünden (Schweiz). Eclogae Geologicae Helvetiae 94: 495–507.

Herzog A (2003) Die Knochenfische der Prosanto-Formation (Mitteltrias, GR) - Systematik, Funktionsmorphologie und Paläoökologie. PhD Thesis, University of Zürich, Switzerland.

Hutchinson P (1973) A revision of the redfieldiiform and perleidiform fishes from the Triassic of Bekker's Kraal (South Africa) and Brookvale (New South Wales). Bulletin of the British Museum of Natural History (Geology) 22: 235–354.

Hutchinson P (1978) The anatomy and phylogenetic position of *Helychthys*, a redfieldiiform fish from the Triassic of South Africa. Palaeontology 21: 881–891.

Jollie M (1962) Chordate Morphology. Reinhold Publishing Corporation, New York, 478 pp. https://doi.org/10.5962/bhl.title.6408

Kane EA, Cohen HE, Hicks WR, Mahoney ER, Marshall CD (2019) Beyond suction-feeding fishes: Identifying new approaches to performance integration during prey capture in aquatic vertebrates. Integrative and Comparative Biology 59: 456–472. https://doi.org/10.1093/icb/icz094

Klingenberg CP (2014) Studying morphological integration and modularity at multiple levels: concepts and analysis. Philosophical Transactions of the Royal Society B, Biological Sciences 369: e20130249. https://doi.org/10.1098/rstb.2013.0249

Lauder GV (1985) Aquatic feeding in lower vertebrates. In: Hildebrand M, Bramble DM, Liem KF, Wake DB (Eds) Functional Vertebrate Morphology. Harvard University Press, Cambridge, 210–229. https://doi.org/10.4159/harvard.9780674184404.c12

Lambers P (1992) On the ichthyofauna of the Solnhofen Lithographic Limestones (Upper Jurassic), Germany. Unpublished PhD Thesis, University of Gröningen, The Netherlands.

López-Arbarello A, Sferco E (2018) Neopterygian phylogeny; the merger assay. Royal Society Open Science 5: 172337. https://doi.org/10.1098/rsos.172337

Near TJ, Dornburg A, Eytan RI, Keck BP, Smith WL, Kuhn KL, Moore JA, Price SA, Burbrink FT, Friedman M, Wainwright PC (2013) Phylogeny and tempo of diversification in the super radiation of spiny-rayed fishes. Proceedings of the National Academy of Sciences 110(31): 12738–12743. https://doi.org/10.1073/pnas.1304661110

Nelson JS, Grande T, Wilson MVH (2016) Fishes of the World. Fifth edition. J. Wiley & Sons, Hoboken, New Jersey, [XLI +] 707 pp.

Nybelin O (1963) Zur Morphologie und Terminologie des Schwanzskelettes der Actinopterygier. Arkiv for Zoologi 15: 485–516.

Patterson C (1973) Interrelationships of holosteans. In: Greenwood PH, Miles RS, Patterson C (Eds) Interrelationships of Fishes. Zoological Journal of the Linnean Society, London, 233–305.

Patterson C (1975) The braincase of pholidophorid and leptolepid fishes, with a review of the actinopterygian braincase. Philosophical Transactions of the Royal Society of London, Series B, 269: 275–579. https://doi.org/10.1098/rstb.1975.0001

Patterson C (1977) Contributions of paleontology to teleostean phylogeny. In: Hecht MK, Goody PC, Hetch BM (Eds) Major Patterns in Vertebrate Evolution. NATO Advances Study Institute Series, Serie A: 579–643. https://doi.org/10.1007/978-1-4684-8851-7_21

Regan CT (1923) On the skeleton of *Lepidosteus*, with remarks on the origin and evolution of the lower neopterygian fishes. Proceedings of the Zoological Society of London, pt 1–2: 445–461. https://doi.org/10.1111/j.1096-3642.1923.tb02191.x

Rieppel O (1985) Die Trias Fauna der Tessiner Kalpalpen. XXV. Die Gattung *Saurichthys* (Pisces, Actinopterygii) aus der mittleren Trias des Monte San Giorgio, Kanton Tessin. Schweizerische Paläontologische Abhandlungen 108: 1–103.

Schaeffer B (1955) *Mendocinia*, a subholostean fish from the Triassic of Argentina. American Museum Novitates 1737: 1–23.

Schaeffer B (1984) On the relationships of the Triassic and Liassic redfieldiiform fishes. American Museum Novitates 2795: 1–18.

Schaeffer B, McDonald NG (1978) Redfieldiid fishes from the Triassic-Liassic Newark Supergroup of eastern North America. Bulletin of the American Museum of Natural History 159: 129–174.

Schultze H-P (1966) Morphologische und histologische Untersuchungen an den Schuppen mesozoischer Actinopterygier (Übergang von Ganoid- zu Rundschuppen). Neues Jahrbuch für Geologie und Paläontologie, Abhandlungen 126: 232–312.

Schultze H-P (1996) The scales of Mesozoic actinopterygians. In: Arratia G, Viohl G (Eds) Mesozoic Fishes – Systematics and Paleoecology. Verlag Dr. Friedrich Pfeil, München, 83–93.

Schultze H-P (2008) Nomenclature and homologization of cranial bones in actinopterygians. In: Arratia G, Schultze H-P, Wilson MVH (Eds) Mesozoic Fishes 4 –Homology and Phylogeny. Verlag Dr. Friedrich Pfeil, München, 23–48.

Schultze H-P, Arratia G (1988) Reevaluation of the caudal skeleton of some actinopterygian fishes. II. *Hiodon*, *Elops* and *Albula*. Journal of Morphology 195: 257–303. https://doi.org/10.1002/jmor.1051950304

Schultze H-P, Arratia G (1989) The composition of the caudal skeleton of teleosts (Actinopterygii: Osteichthyes). Zoological Journal of the Linnean Society 97: 189–231. https://doi.org/10.1111/j.1096-3642.1989.tb00547.x

Schultze H-P, Arratia G (2013) The caudal skeleton of basal teleosts, its conventions, and some of its major evolutionary novelties in a temporal dimension. In: Arratia G, Schultze H-P, Wilson MVH (Eds) Mesozoic Fishes 5 – Global Diversity and Evolution. Verlag Dr. Friedrich Pfeil, München, 187–246.

Schultze H-P, Mickle KE, Poplin C, Hilton EJ, Grande L (2022) Actinopterygii I. In: Schultze H-P (Ed.) Handbook of Paleoichthyology, vol. 8A. Verlag Dr. Friedrich Pfeil, München, 1–299.

Shen C, Arratia G (2022) Re-description of the sexually dimorphic peltopleuriform fish *Wushaichthys exquisitus* (Middle Triassic, China): taxonomic implications and phylogenetic relationships. Journal of Systematic Palaeontology 19(19): 1317–1342. https://doi.org/10.1080/14772019.2022.2029595

Stensiö E (1921) Triassic fishes from Spitzbergen. Part I. Verlag Holzhausen: Wien, 307 pp. https://doi.org/10.5962/bhl.title.159141

Teng CS, Cavin L, Maxon Jr RE, Sánchez-Villagra MS, Crump JG (2019) Resolving homology in the face of shifting germ layer origins: Lessons from a major skull vault boundary. eLife 8: e52814. https://doi.org/10.7554/eLife.52814

Tintori A (1990) The actinopterygian fish *Prohalecites* from the Triassic of Northern Italy. Palaeontology 33: 155–174.

Tintori A, Sun Z-Y, Lombardo C, Jiang D-Y, Sun Y-L, Rusconi M, Hao W-C (2007) New specialized basal neopterygians (Actinopterygii) from Triassic of the Tethys realm. Geologia Insubrica 10(2): 13–19.

Tintori A, Lombardo C, Jiang D-Y, Sun Z-Y (2011) "*Pholidophorus*" *faccii* Gortani 1907: nuovi dati tassonomici. Gortania 32: 45–52.

Wainwright PC, McGee MD, Longo SJ, Hernandez LP (2015) Origins, innovations, and diversifications of suction feeding in vertebrates. Integrative and Comparative Biology 55: 134–145. https://doi.org/10.1093/icb/icv026

Westoll S (1943) The origin of the tetrapods. Biological Reviews 18: 78–98. https://doi.org/10.1111/j.1469-185X.1943.tb00289.x

Woodward AS (1890) The fossil fishes of the Hawkesbury series of Gosford. Memoirs of the Geological Survey of New South Wales, Paleontology 4: 1–55.

Xu G-H (2020a) *Feroxichthys yunnanensis* gen. et sp. nov. (Colobodontidae, Neopterygii), a large durophagous predator from the Middle Triassic (Anisian) Luoping Biota, eastern YunnaChina. PeerJ 8: e10229. https://doi.org/10.7717/peerj.10229

Xu G-H (2020b) A new stem-neopterygian fish from the Middle Triassic (Anisian) of Yunnan, China, with a reassessment of the relationships of early neopterygian clades. Zoological Journal of the Linnean Society 191: 375–394. https://doi.org/10.1093/zoolinnean/zlaa053

Xu G-H (2021) The oldest species of *Peltoperleidus* (Louwoichthyiformes, Neopterygii) from the Middle Triassic (Anisian) of China, with phylogenetic and biogeographic implications. PeerJ 9: e12225. https://doi.org/10.7717/peerj.12225

Xu G-H, Ma X-Y (2016) A Middle Triassic stem-neopterygian fish from China sheds new light on the peltopleuriform phylogeny and internal fertilization. Science Bulletin 61: 1766–1774. https://doi.org/10.1007/S11434-016-1189-5

Xu G-H, Zhao L-J, Shen C-C (2015) A Middle Triassic thoracopterid from China highlights the evolutionary origin of overwater gliding in early ray-finned fishes. Biology Letters 11: 183–191. https://doi.org/10.1098/rsbl.2014.0960

Supplementary material 1

List of characters and coding used in First Phylogenetic Analysis

Authors: Gloria Arratia
Data type: Characters and their coding (docx. file)
Explanation note: Characters and their coding used in the First Phylogenetic Analysis.

Link: https://doi.org/10.3897/fr.25.85621.suppl1

Supplementary material 2

Matrix used in First Phylogenetic Analysis

Authors: Gloria Arratia
Data type: Matrix, coding of characters (excel file)
Explanation note: Matrix used in the first phylogenetic analysis.

Link: https://doi.org/10.3897/fr.25.85621.suppl2

Supplementary material 3

List of characters and their coding used in Second Phylogenetic Analysis

Authors: Gloria Arratia
Data type: Characters and their coding (docx. file)
Explanation note: List of characters and coding used in the second phylogenetic analysis.

Link: https://doi.org/10.3897/fr.25.85621.suppl3

Supplementary material 4

Matrix with coding of characters used in Second Phylogenetic Analysis

Authors: Gloria Arratia
Data type: Matrix, coding of characters (excel file)
Explanation note: Matrix with coding of characters used in Second Phylogenetic Analysis.

Link: https://doi.org/10.3897/fr.25.85621.suppl4

Fossil Record 25 (2) 2022, 263–274 | DOI 10.3897/fr.25.85334

PENSOFT

MUSEUM FÜR NATURKUNDE BERLIN

An alternative interpretation of small-bodied turtles from the "Middle Purbeck" of England as a new species of compsemydid turtle

Walter G. Joyce[1], Jason R. Bourque[2], Vincent Fernandez[3], Yann Rollot[1]

1 *Department of Geosciences, University of Fribourg, 1700 Fribourg, Switzerland*
2 *Florida Museum of Natural History, University of Florida, Gainesville, FL 32611, USA*
3 *Core Research Laboratories, Natural History Museum, London, SW7, UK*

https://zoobank.org/347E8CB2-6D5C-46C1-8269-C60629424822

Corresponding author: Walter G. Joyce (walter.joyce@unifr.ch)

Academic editor: Torsten Scheyer ♦ **Received** 14 April 2022 ♦ **Accepted** 9 August 2022 ♦ **Published** 17 August 2022

Abstract

A series of small-sized fossil turtles were collected from Beckles' Pit, Durlston Bay, Dorset, United Kingdom in 1856 from a sediment package referable to the Early Cretaceous (Berriasian) Purbeck Group. The two primary accounts that previously documented these turtles concluded that they represent the juveniles of the coeval early pleurosternid *Pleurosternon bullockii*. A brief, third account, however, suggested that these may represent a new species of compsemydid turtle. We here highlight a series of discrete morphological characters that consistently distinguish the small-bodied turtles from Beckles' Pit from large-bodied *Pleurosternon bullockii*, in particular the arrangement of the bones and scutes along the anterior margin of the shell. As these characters are otherwise used to diagnose new species of turtles, in particular compsemydids, and to establish the phylogeny of fossil turtles, we side with the latter interpretation and name a new taxon of early compsemydid, *Tongemys enigmatica* **gen. et sp. nov.** The early record of compsemydid is restricted to the Early Cretaceous of Europe, but is extremely fragmentary. We suggest that this may be a bias towards the collection and identification of small turtle remains, but also that a re-study of Early Cretaceous continental turtle faunas is likely to yield further material.

Key Words

Berriasian, Compsemydidae, Early Cretaceous, Paracryptodira, Testudinata, United Kingdom

Introduction

Late Jurassic (Tithonian) to Early Cretaceous (Berriasian) sediments of the Purbeck Group, which are broadly exposed along the southern coast of England, have yielded a particularly rich collection of fossil turtles over the course of the last two centuries (Owen 1842, 1853; Mantell 1844; Seeley 1869; Lydekker 1889a, b; Woodward 1909; Watson 1910a, b; Evans and Kemp 1975, 1976; Barrett et al. 2002). At present, at least five species are recognized as valid from these strata: the abundant pleurosternid *Pleurosternon bullockii* Owen, 1842, which is known from a single cranium and rich shell remains (Milner 2004; Evers et al. 2020; Guerrero and Pérez-García 2021a), the indeterminate paracryptodire *Dorsetochelys typocardium* (Seeley, 1869) (Milner 2004; Pérez-García 2014), two helochelydrids, including "*Helochelydra*" *anglica* (Lydekker, 1889b) and an undefined form (Barrett et al. 2002; Joyce 2017) and the shell taxon *Hylaeochelys belli* (Mantell, 1844), which is a plausible thalassochelydian turtle, synonymous with the skull taxon *Dorsetochelys delairi* Evans & Kemp, 1976 (Anquetin and André 2020).

Lydekker (1889a) was the first to figure and describe the well-preserved, but crushed shell of a small-bodied turtle from the Middle Purbeck. The specimen was part of a collection that had been assembled by Samuel H. Beckles in what is now known to be part of the Marly Freshwater and Cherty Freshwater Members of the Purbeck Group (Sweetman et al. 2017, see below). Although Lydekker (1889a) noted numerous differences

with far larger specimens of *Pleurosternon bullockii* from the overlying Intermarine Member of the Purbeck Group, he ultimately concluded the small-bodied turtle to represent juveniles of that species, because he believed that subadult individuals would document an intermediate morphology. This conclusion was soon after reiterated by Lydekker (1889b), who attributed nearly two dozen additional small specimens from Beckles' collection to *Pleurosternon bullockii*. More than a century later, Lapparent de Broin and Murelaga (1999) listed a number of characteristics that distinguish the small-bodied material from Beckles' collection from large-bodied *Pleurosternon bullockii* and suggested that the small-bodied form might represent a new species of compsemydid turtle, but they refrained from naming it, likely because this was not the focus of their study. Guerrero and Pérez-García (2021b) recently figured and described most of the small-sized turtles available from the Beckles' collections. Similar to Lydekker (1889a) and Lapparent de Broin and Murelaga (1999), Guerrero and Pérez-García (2021b) highlighted numerous differences between these small-sized turtles and *Pleurosternon bullockii*, but sided with Lydekker (1889a) by interpreting the differences as ontogenetic. In our estimation, the analyses of Guerrero and Pérez-García (2021b) are insufficient to suggest conspecificity of the material at hand. Instead, the small-bodied turtles can readily be diagnosed as a new species of extinct turtle using a series of discrete characters otherwise used for this purpose. The primary goal of this contribution, therefore, is to name this taxon as a new species of fossil turtle, *Tongemys enigmatica* gen. et sp. nov. and to investigate its phylogenetic and biogeographic significance. All specimens discussed herein are house at the Natural History Museum in London, United Kingdom (NHMUK).

Materials and methods

Geological settings

The vast majority of small-bodied turtles discussed herein (i.e. NHMUK PV OR 48262, 48263, 48263a, 48263c, 48263e, 48343, 48344, 48347 and 48354), including all specimens unambiguously referred to *Tongemys enigmatica* gen. et sp. nov., were explicitly listed by Lydekker (1889b) as originating from the collection of Samuel H. Beckles. The overall similarity of the remaining material referred herein (i.e. NHMUK PV OR 48264, 48345, 48351 and 48355) in their preservation and the adjacency of their catalog numbers make it highly plausible that these originate from this collection as well. This collection of fossil turtles was the by-product of an extensive excavation that had been carried out in search of mammalian remains under the supervision of Beckles in 1856 at Durlston Bay (Kingsley 1857) at a locality now known as "Beckles' Pit" (Milner 2004). To reach the target of this excavation, a single layer known as the mammal bed (bed DB 83 in the terminology of Clements 1993), Beckles had up to 16 m of overburden removed from an area of more than 650 m^2 (Kingsley 1857). It is unclear, however, if the resulting small-bodied turtles were collected from the mammal bed per se or from the overburden. The latter conclusion is supported by the heterogeneity of the matrix in which non-turtle specimens are preserved (Sweetman et al. 2017). We, therefore, conclude that these specimens either originated from the Marly Freshwater Member, which includes the mammal bed or the overlying Cherty Freshwater Member, the two members exposed at Beckles' Pit (Sweetman et al. 2017). These two Members are generally interpreted as representing lacustrine environments without marine influence. Among turtles, they otherwise yielded fragmentary helochelydrid remains (Barrett et al. 2002).

The best documented specimens of *Pleurosternon bullockii*, *Dorsetochelys typocardium* and *Hylaeochelys belli*, in contrast, originate from the overlying Intermarine Member (Milner 2004). This member is interpreted as ranging from lacustrine to lagoonal.

Although the exact location of the Jurassic-Cretaceous boundary within the Purbeck Group is still contentious, ammonite zonation, sequence stratigraphy and magnetostratigraphy suggest that the Marly and Cherty Freshwater Members are early Berriasian, while the Intermarine Member is middle to late Berriasian in age (Ogg et al. 1994).

Visualization

The best-preserved small-bodied turtles from Beckles' Pit were recently figured by Guerrero and Pérez-García (2021b). Although we here disagree with their interpretation of this material representing juveniles of *Pleurosternon bullockii*, we fully agree with their anatomical observations. To aid the reader, we, nevertheless, re-figure the two most telling specimens, NHMUK PV OR 48262/48265, the holotype (Fig. 1) and NHMUK PV OR 48343, the specimen with the best-preserved plastron (Fig. 2). In the rare instance where referred material provides important insights, we refer the reader to the figures of Guerrero and Pérez-García (2021b).

In the hope of recovering anatomical information from the ventral side of the holotype, which is covered in matrix, we subjected this specimen to high-resolution X-ray micro-computed tomography using a Nikon Metrology XTH 225 ST scanner at the NHMUK Imaging and Analysis Centre. The system set-up consisted of: a tungsten rotating reflection target; X-ray source set to 215 kV and 660 µA; source filtered with 1.5 mm of copper; detector gain of 24 dB; source-object distance of 358.7 mm and object-detector distance of 619.4 mm generating data with isotropic voxels with an edge length of 55.00 µm. Both parts of the specimen (NHMUK PV OR 48262 and 48265) were put together for the acquisition, which consisted of 4476 projections over a 360° rotation of the object, using the minimize ring artefact option of the instrument; each projection had a total integration time of 1 second resulting from 4 frame averaging of 250 msec

exposure each. 3D mesh models were generated using the software Amira 2020.2 (Thermo Fisher Scientific, Hillsborough, USA). Data segmentation was performed combining manual masking every sixth slice with the interpolation tool in the z-axis. The 3D mesh models were generated and exported as .ply-files. The images used in Fig. 1 were taken as screen shots from SPIERSview 3.1.0. The original set of coronal slices and the 3D mesh models are available at MorphoSource (https://www.morphosource.org/projects/000434697).

Comparisons

Our primary comparative sources are as follows: *Compsemys* (a.k.a. *Berruchelus*) *russelli* (Pérez-García, 2012) from the Paleocene of France, as described by Pérez-García (2012); *Calissounemys matheroni* Tong et al., 2022 from the Campanian of France, as described by Tong et al. (2022); *Compsemys victa* Leidy, 1856 from the Paleocene of New Mexico, as described by Gilmore (1919); *Peltochelys duchastelii* Dollo, 1884 from the Early Cretaceous (middle Barremian to early Aptian) of Belgium, as described by Joyce and Rollot (2020); *Pleurosternon bullockii* from the Early Cretaceous (Berriasian) of England, as described by Guerrero and Pérez-García (2021a); and *Selenemys lusitanica* Pérez-García & Ortega, 2011 from the Late Jurassic (Kimmeridgian) of Portugal, as described by Pérez-García and Ortega (2011).

Phylogenetic analysis

To investigate the phylogenetic relationships of compsemydids, we integrated *Tongemys enigmatica* gen. et sp. nov. into the paracryptodire character/taxon matrix of Rollot et al. (2021). The new turtle could be scored for 35 of 107 characters. The matrix was otherwise adjusted, by re-scoring the early compsemydids *Peltochelys duchastelii* and *Selenemys lusitanica* as "0," not "1," for characters 86 and 87, as they clearly do not exhibit extensive contacts between the inguinal and axillary buttresses with the costals, in contrast to the derived compsemydids *Compsemys russelli*, *Compsemys victa* and *Kallokibotion bajazidi*. The updated character taxon matrix is provided in the Suppl. material 1.

The expanded matrix was subjected to a parsimony analysis using TNT (Goloboff et al. 2008). Twenty-one characters (i.e. characters 6, 14, 16, 18, 27, 28, 31, 34, 39, 40, 41, 46, 48, 60, 63, 80, 88, 95, 97, 98 and 101) were run ordered because they form morphoclines. *Proganochelys quenstedti* served as the outgroup. One thousand random addition sequences were followed by a round of tree bisection reconnection. Trees suboptimal by 10 steps and with a relative fit difference of 0.1 were retained as part of the first search. A tree-collapsing rule was implemented with a minimum length of 0. Our analysis under equal-weighting resulted in 48 most parsimonious trees with 301 character-state transitions. The Pruned Trees function of TNT identified *Riodevemys inumbragigas* and *Scabremys ornata* as rogue taxa, which were subsequently removed. The 50% majority-rule tree is shown in Fig. 3. *Tongemys enigmatica* gen. et sp. nov. is retrieved as the most basal branching compsemydid.

Nomenclature

We use phylogenetic nomenclature throughout this manuscript. All names of taxa, including clades, are therefore highlighted using italics.

Systematic paleontology

***Testudinata* Klein, 1760**
***Compsemydidae* Pérez-García et al., 2015**

***Tongemys enigmatica* gen. nov.**
https://zoobank.org/92EBB8E9-9FDB-403E-A619-170CC9936568

Type species. *Tongemys enigmatica* Joyce, Bourque, Fernandez & Rollot, sp. nov.

***Tongemys enigmatica* gen. et sp. nov.**
https://zoobank.org/5E4C6B25-01B6-4237-8C59-6DBC8DFBB978
Figs 1, 2

Holotype. NHMUK PV OR 48262/48265, a near complete shell preserved on two separately catalogued slabs (Lydekker 1889a, fig. 3; Guerrero and Pérez-García 2021b, fig. 1a–c; Fig. 1).

Type locality. Beckles' Pit, Durlston Bay, Dorset, United Kingdom; Marly Freshwater or Cherty Freshwater Members, Purbeck Group, early Berriasian, Early Cretaceous (see Geological Settings above).

Nomenclatural acts. This publication and its nomenclatural acts were registered at ZooBank on 2 August 2022, prior to publication. The LSID of the publication is urn:lsid:zoobank.org:pub:347E8CB2-6D5C-46C1-8269-C60629424822, that of the new genus LSID urn:lsid:zoobank.org:act:92EBB8E9-9FDB-403E-A619-170CC9936568 and that of the new species LSID urn:lsid:zoobank.org:act:5E4C6B25-01B6-4237-8C59-6DBC8DFBB978.

Etymology. The genus name, *Tongemys*, is formed in honor of Haiyan Tong, a paleontologist who has consistently contributed to the field of descriptive turtle paleontology and systematics over the course of the last three decades. The epithet, *enigmatica*, alludes to 150 years of taxonomic uncertainty obscuring the validity of this new taxon. The epithet is formed as a noun in apposition, not an adjective.

Diagnosis. *Tongemys enigmatica* gen. et sp. nov. can be diagnosed as a representative of *Compsemydidae* by its relatively small size (carapace length smaller than

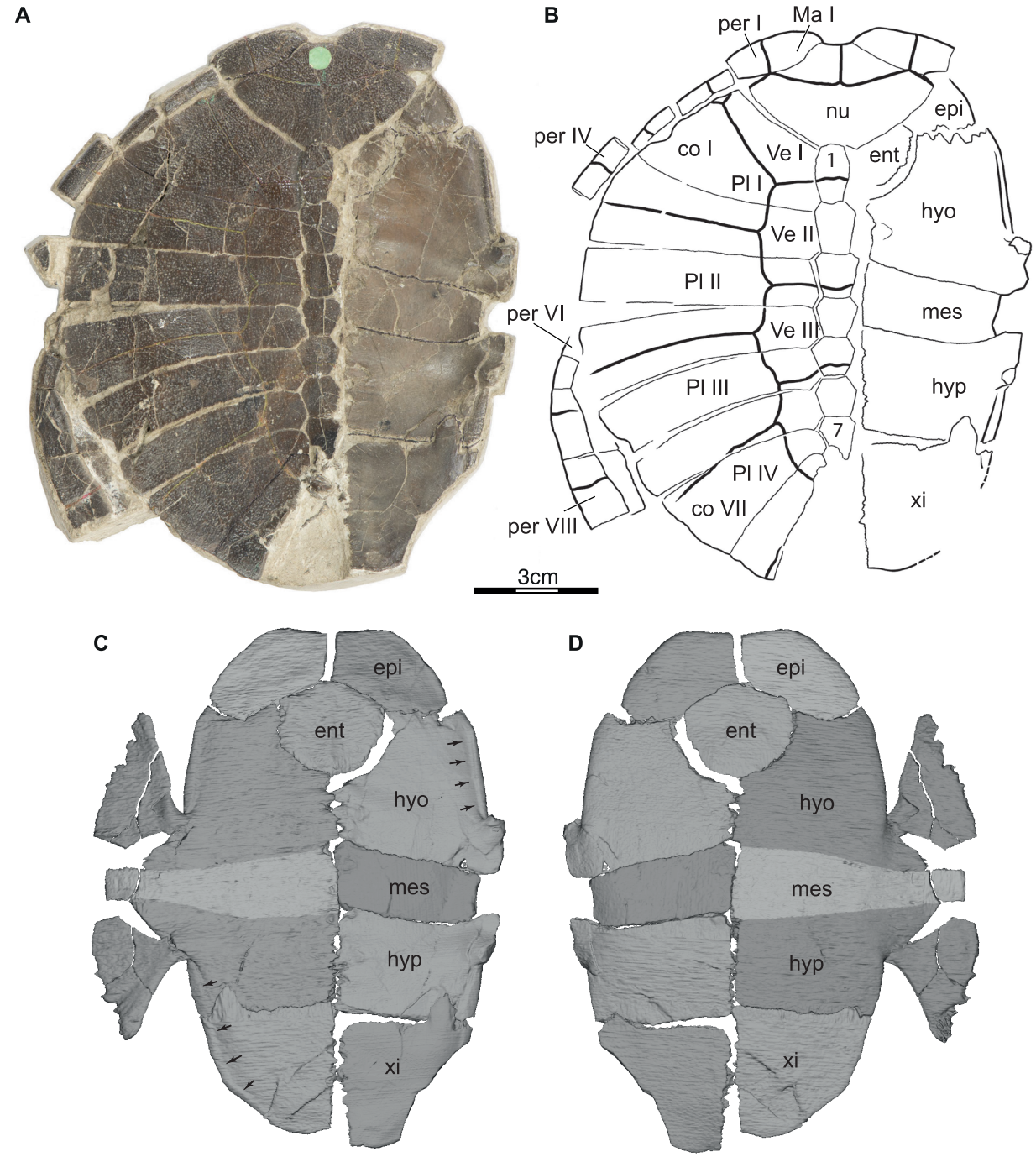

Figure 1. NHMUK PV OR 48262/48265, *Tongemys enigmatica*, holotype, Early Cretaceous (Barremian) of England: **A.** Photograph in dorsal view; **B**. Interpretive line drawing in dorsal view; **C**. 3D model of plastron in dorsal view; **D.** 3D model of plastron in ventral view. Abbreviations: co, costal; ent, entoplastron; epi, epiplastron; hyo, hyoplastron; hyp, hypoplastron; Ma, marginal scute; mes, mesoplastron; per, peripheral; Pl, pleural scute; Ve, vertebral scute; xi, xiphiplastron.

30 cm), a finely textured shell, a sutured bridge, the reduction to absence of a nuchal contribution to the anterior carapace margin, the reduction to absence of a contact between peripheral I and costal I resulting in a contact between the nuchal and peripheral II, the absence of a cervical and a posterolaterally sloping gular-humeral sulcus. *Tongemys enigmatica* gen. et sp. nov. differs from other compsemydids by the presence of a distinct nuchal notch, which is formed by an anterior protrusion of peripheral I, a residual contribution of the nuchal to the anterior carapacial margin, a laterally expanded nuchal that is wider than costal I (also in *Selenemys lusitanica*), the convergence of the nuchal, peripheral I, peripheral II and costal I on to a single point, neurals II–VII as broad as long (also in *Compsemys russelli* and *Compsemys victa*), four-sided neural I (also in *Compsemys russelli* and *Compsemys victa*), narrow anterior peripherals (also in *Peltochelys duchastelii*) that are much wider than tall,

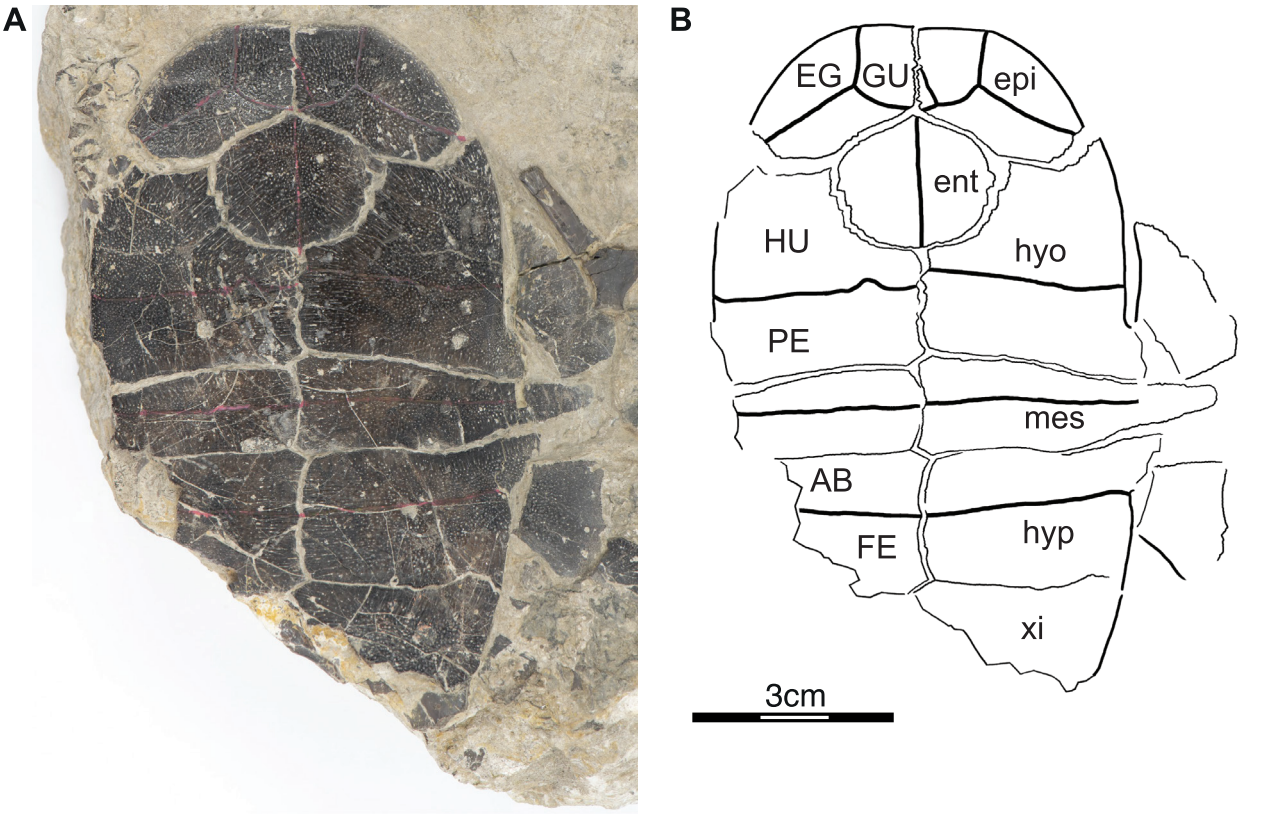

Figure 2. NHMUK PV OR 48343, *Tongemys enigmatica*, referred specimen, Early Cretaceous (Barremian) of England: **A**. Photograph in ventral view; **B.** Interpretive line drawing in ventral view. Abbreviations: AB, abdominal scute; EG, extragular scute; ent, entoplastron; epi, epiplastron; FE, femoral scute; GU, gular scute; HU, humeral scute; hyo, hyoplastron; hyp, hypoplastron; mes, mesoplastron; PE, pectoral scute; xi, xiphiplastron.

V-shaped peripherals in cross section, anterior and posterior to the bridge, a straight medial margin of costal VIII resulting in a trapezoidal space for the suprapygals (also in *Peltochelys duchastelii*), restriction of vertebral I to the nuchal and costals (also in *Selenemys lusitanica*), the convergence of vertebral I, marginal II, marginal III and pleural I on to a single point, development of a shallow anal notch only (also in *Selenemys lusitanica* and *Peltochelys duchastelii*), lack of a sinuous mid-line sulcus (also in *Peltochelys duchastelii*), a posterolaterally sloping gular/humeral sulcus that nearly crosses the epi-hyoplastral suture and restriction of gulars to epiplastra. The available material is not sufficient to allow differentiating *Tongemys enigmatica* from *Calissounemys matheroni*, but the latter appears to be larger and have a finer and more striated surface texture.

Referred material. The following specimens from the type locality are referred, based on their small size and the presence of a nuchal that is wider than costal I and that shows a reduced contribution to the anterior carapacial margin: NHMUK PV OR 48263, a carapacial disc lacking peripherals (Guerrero and Pérez-García 2021b, fig. 2d); NHMUK PV OR 48263c, the anterior half of a carapacial disk lacking the peripherals (Guerrero and Pérez-García 2021b, fig. 2b); NHMUK PV OR 48263e, a partial carapacial disk lacking peripherals (Guerrero and Pérez-García 2021b, fig. 2c); NHMUK PV OR 48264, a carapacial disk lacking peripherals (Guerrero and Pérez-García 2021b, fig. 3b, c). The following specimens are referred, based on their small size and the presence of a laterally contracting mesoplastron: NHMUK PV OR 48343, a near complete plastron (Fig. 2; Guerrero and Pérez-García 2021b, fig. 4a); NHMUK PV OR 48344, a near complete plastron lacking much of the lobes (Guerrero and Pérez-García 2021b, fig. 4b); NHMUK PV OR 48347, a partial plastron lacking the anterior and posterior lobes (Guerrero and Pérez-García 2021b, fig. 4c); NHMUK PV OR 48355, a partial plastron lacking the anterior and posterior lobes (Guerrero and Pérez-García 2021b, fig. 3d); NHMUK PV OR 48354, a disarticulated shell lacking nuchal, peripherals and most of the anterior and posterior plastral lobes (Guerrero and Pérez-García 2021b, fig. 3a). The following specimens, also from the type locality, but too incomplete to yield much taxonomic information, are referred, based on their small size: NHMUK PV OR 48263a, a carapacial disk lacking the nuchal and the peripherals (Guerrero and Pérez-García 2021b, fig. 2a); NHMUK PV OR 48345, a heavily-eroded carapace (Guerrero and Pérez-García 2021b, fig. 1f); NHMUK PV OR 48351, a partially disarticulated carapacial disk lacking the nuchal and the peripherals (Guerrero and Pérez-García 2021b fig. 2e). Although all referred specimens are incomplete, all provide sufficient character evidence to assess their taxonomic referral.

Description.

***Carapacial bones*.** The exact number of elements that comprise the carapace of *Tongemys enigmatica* is not known. No complete carapace is preserved, but the available material preserves a nuchal, eight neurals, eight pairs of costals, the anterior eight pairs of peripherals and one to two suprapygals. Three pairs of posterior peripherals and the pygal were likely present as well. Though incomplete, the shell looks to have been rounded, with exception of a distinct nuchal notch, which is framed by peripherals I (Fig. 1A, B). In the smallest specimens (e.g. NHMUK PV OR 48263a; Guerrero and Pérez-García 2021b, fig. 2a), elongate distal rib ends suggest that fontanelles were present, but in more skeletally mature specimens, including the holotype, the costals appear to contact the peripherals, with the exception of a minor gap between the nuchal, costal I and peripherals I and II (Fig. 1A, B). The surface of the shell is decorated by a fine texture consisting of small, evenly-spaced pits (Figs 1, 2). The holotype, one of the largest available specimens, has an estimate carapace length of 14 to 15 cm. Smaller specimens, such as NHMUK PV OR 48264, had an estimated carapace length of only 8 cm.

The nuchal is wide and hexagonal with long anterolateral and posterolateral contacts with peripheral I and costal I, a short anterior contribution to the margin of the shell and a short posterior contact with neural I (Fig. 1A, B). A lateral corner contact with peripheral II is interrupted by what looks to be a minute fontanelle. Among compsemydids, the nuchal of *Tongemys enigmatica* resembles that of *Selenemys lusitanica* by being wider than costal I, but differs by symplesiomorphically contributing to the anterior margin of the carapace. A clear lateral contact with peripheral II is present in all other compsemydids.

The available material suggests that eight neurals are present, of which the last is typically fused with the suprapygals. The former presence of an asymmetric, abnormal element in the holotype is hinted at by a notch at its posterior end (Fig. 1A, B). The variable fusion of neural VIII with suprapygal I is not only documented for other compsemydids, such as *Compsemys russelli*, *Compsemys victa* and *Selenemys lusitanica*, but also *Pleurosternon bullockii*. The neurals resemble those of *Compsemys russelli* and *Compsemys victa* by being nearly as wide as long. The holotype resembles *Compsemys russelli* and *Compsemys victa* by possessing a four-sided neural I, while the remaining parts of the sequence are hexagonal with symmetrically short anterior sides. The remaining specimens, though fragmentary, are consistent with this arrangement, with the exception of NHMUK PV OR 48263 (Guerrero and Pérez-García 2021b, fig. 2d), which resembles *Peltochelys duchastelii* by exhibiting a preneural, a hexagonal neural I with symmetrically short posterior sides and a square neural II. A square neural II also seems to have been present in *Selenemys lusitanica*.

Eight pairs of costals are present that are fully separated from their counterparts by the contiguous neural series (Fig. 1A, B). As in all turtles, the costals evenly fan out from the anterior to the posterior. All costals have similar anteroposterior dimensions to one another, with the exception of costal I, which is considerably longer anteroposteriorly than costal II and costal VIII, which is much smaller and almost rudimentary relative to costal VII. The costals typically contact two neurals medially (see above). Costal I contacts peripheral II and III anterolaterally. A point contact may have existed with peripheral I anteriorly and peripheral IV posterolaterally. Costal VIII otherwise contacted the suprapygal complex posteromedially. The remaining contacts of the costals with the peripherals are not preserved.

The holotype is the only specimen to preserve a meaningful sample of peripherals (Fig. 1A, B). As in most species of compsemydids, peripheral I is located anterolaterally to the nuchal and the two bones broadly contact the entirety of one another. As a result, peripheral I lacks a posterior contact with costal I. This characteristic is present among all unambiguous compsemydids. In contrast to other compsemydids, however, peripheral I is not a wedge-shaped element that forms a rounded anterior carapace margin, but rather is a rectangular element that forms minor anterior protrusions that frame a narrow anterior nuchal notch. The anterior margin of peripheral II lines up with the anterior margin of costal I. A medial contact with the nuchal is, therefore, absent. A short contact between these two bones is present in *Selenemys lusitanica* and *Peltochelys duchastelii*, a more extensive one in *Compsemys russelli* and *Compsemys victa*. The remaining peripheral elements are disarticulated from the rest of the shell, likely because they were not tightly sutured to the costals. The peripheral III–IV and peripheral VIII–IX contacts, however, seem to have aligned with the costal I–II and costal VI/VII contacts. The anterior peripherals are notably narrow, like those of *Peltochelys duchastelii*. The CT data reveal that all available peripherals have a V-shaped cross section, not just the bridge peripherals. This is a previously under-reported characteristic not only apparent among other European compsemydids, such as *Peltochelys duchastelii*, but also the pleurosternid *Pleurosternon bullockii* (clearly visible in NHMUK PV R 1891) and the helochelydrid *Aragochersis lignitesta* (Pérez-García et al. 2020).

The suprapygals are not preserved in the holotype (Fig. 1A, B). In three specimens, a single suprapygal is apparent that is fused with neural VIII (NHMUK PV OR 48263a, 48263 and 48354, Guerrero and Pérez-García 2021b, fig. 2a, c and fig. 3a, respectively). In two other specimens, two suprapygal elements are present, of which the anterior is fused with neural VIII (NHMUK PV OR 48351, 48264, Guerrero and Pérez-García 2021b, fig. 2e and fig. 3b and c, respectively). The fusion of the suprapygal element to neural VIII is alluded to by the unusual polygonal form of the resulting compound element, including angular concavities. The suprapygal elements in concert fill the triangular space between costals VIII. The medial margin of costal VIII is, therefore, straight, not stepped to account for differently-sized anterior and posterior suprapygals. A similar arrangement is seen in *Peltochelys duchastelii*.

Carapacial scutes. The carapace was likely covered by five vertebrals, four pairs of pleurals and twelve pairs of marginals (Fig. 1A, B). As in all other compsemydids, but also *Pleurosternon bullockii*, a cervical is clearly absent. In the holotype, the intervertebral contacts are located over the middle of neural I, the posterior thirds of neural III and V and neural VIII (Fig. 1A, B). Other specimens generally agree, although minor deviations are apparent. As a more extreme abnormality, at least one specimen exhibits medially split vertebrals (NHMUK PV OR 48263c, Guerrero and Pérez-García 2021b, fig. 2b), also noted by Guerrero and Pérez-García 2021c (fig. 2c). Vertebral I is the broadest vertebral element. It has straight anterior contacts with marginal I, which jointly form a moderate convexity. Furthermore, it contacts the full length of marginal II anterolaterally, pleural I posterolaterally and vertebral II posteriorly. The near contact of vertebral I with marginal III hinders marginal II from broadly contacting pleural II, the condition seen in most other turtles. Vertebral I resembles that of *Selenemys lusitanica* by not lapping on to the peripherals. An overlap on to peripherals I and II is developed in *Compsemys russelli*, *Compsemys victa* and *Peltochelys duchastelii*. An overlap on to peripheral I only is exhibited in *Pleurosternon bullockii*. Vertebrals II to IV are hexagonal elements (Fig. 1A, B). They each have two lateral contacts with the adjacent pleurals and relatively straight anterior and posterior contacts with the adjacent vertebrals. Of the three, vertebral III is the widest, vertebral IV the narrowest. In the holotype, these vertebrals are distinctly narrower than the pleurals (Fig. 1A, B), but in the most juvenile specimens, they are wider (e.g. NHMUK PV OR 48263a, Guerrero and Pérez-García 2021b, fig. 2a). This differs significantly from the condition seen in *Pleurosternon bullockii*, where the vertebrals are much broader than the pleurals, even though all known individuals have a much greater size. The outlines of vertebral V are not well preserved in any specimen, but the holotype suggests that this element was about as wide as vertebral IV, but trapezoidal in outline, as its anterior sulcus with vertebral IV is narrow (Fig. 1A, B). This element appears to be particularly narrow in the holotype, as the vertebral V-pleural IV sulcus barely overlaps the most posterodistal portion of costal VIII, but is clearly located on costal VIII in other specimens. This is not confirmed to be regular by the remaining material (e.g. NHMUK PV OR 48263, Guerrero and Pérez-García 2021b, fig. 2d).

In the holotype, the interpleural sulci are straight, but, while the anterior two evenly cross costals II and IV (as in most turtles), the posterior one laterally crosses from costal VI on to costal VII (Fig. 1A, B). This unusual position is not seen in other specimens (e.g. NHMUK PV OR 48263, Guerrero and Pérez-García 2021b, fig. 2d).

The holotype best preserves the marginals (Fig. 1A, B). Marginal I is relatively broad and contacts its counterpart medially, marginal II laterally and vertebral I posteriorly. It evenly covers the medial two-thirds of peripheral I and the anterior portions of the nuchal. The median intermarginal sulcus is symplesiomorphically located on the nuchal as in *Selenemys lusitanica*, but also *Pleurosternon bullockii*. Only remnants of the remaining intermarginal sulci are otherwise apparent. This, in return, suggests that the marginal-pleural sulcus was located near the peripheral-costal suture. In this regard, *Tongemys enigmatica* resembles other compsemydids, but differs markedly from *Pleurosternon bullockii*, where the marginals broadly overlap the costals.

Plastral bones. The plastron consists of an entoplastron and paired epi-, hyo-, meso-, hypo- and xiphiplastra (Figs 1, 2). The plastral fore-lobe is relatively straight along the hyoplastral margin and has a transverse anterior margin, but otherwise is broadly rounded. The plastral hind-lobe is shorter than the fore-lobe and more evenly rounded. Only a shallow anal notch is apparent, as in *Selenemys lusitanica*. On the visceral side of the plastron, the skin-scute sulcus is located just medial inside the margin of the plastron (see black arrows in Fig. 1C) and, therefore, lacks broad overlap, in contrast to the plastral hind-lobe of *Pleurosternon bullockii*. The space between the inguinal and axillary notches is significantly shorter than either lobe. There is no evidence of plastral fontanelles.

The epiplastron broadly contacts its counterpart along the mid-line, the entoplastron posteromedially and the hyoplastron along a posteriorly convex contact posteriorly (Figs 1, 2). The hyo-, meso- and hypoplastron jointly form the bridge region. Possible dorsal contacts of the wing-like axillary and inguinal buttresses with the carapace are unclear, even in the CT data, because the plastron is displaced relative to the carapace, but the lack of extensive sutural surfaces on the underside of the costals suggest that a contact would have been minor, if present at all. As in other compsemydids and *Pleurosternon bullockii*, the plastral bones do not align to meet exactly at the mid-line. The mesoplastron narrows laterally to a tip. This condition is otherwise hinted at in *Selenemys lusitanica*. The mesoplastron is lacking in *Peltochelys duchastelii*. The hypoplastron is only about two-thirds the anteroposterior length of the hyoplastron. The xiphiplastron is attached to the hypoplastron along a transversely straight suture, which is stabilized on the visceral side by a pronounced process of the xiphiplastron that overlies the hypoplastron.

Plastral scutes. In NHMUK PV OR 48343, the only specimen that preserves the plastral scutes well, the plastron is covered by paired gulars, extragulars, humerals, pectorals, abdominals, femorals and presumably anals (Fig. 2). There is no evidence of inframarginals, but we cannot be certain of this observation. The gulars are large, blocky elements that do not overlap the entoplastron ventrally, but exhibit an asymmetric mid-line contact. Similar asymmetries are polymorphically developed in *Pleurosternon bullockii* as well. As in other compsemydids, but not *Pleurosternon bullockii*, the extragular/humeral sulcus slopes posteriorly and may have even lapped on to the hyoplastron posterolaterally. There is no evidence of a deeply sinuous mid-line sulcus. The humeral-pectoral,

pectoral-abdominal and abdominal-femoral sulci are arranged relatively straight transversely. The humeral-pectoral sulcus is located mid-length between the entoplastron and the axillary notch, the pectoral-abdominal crosses the mesoplastron, and the abdominal-femoral laterally aligns with the inguinal notch. The anal-femoral sulcus is not preserved, but a telling break in the holotype suggests that it is orientated diagonally and did not cross on to the hypoplastron.

Discussion

Alpha taxonomy

The taxon represented by the small-sized turtle material recovered from Beckles' Pit has a somewhat unique taxonomic history, as authors have noted its morphological distinction ever since it was first reported in the 19th century, but either interpreted it as the juvenile morph of *Pleurosternon bullockii* nevertheless (Lydekker 1889a, b; Guerrero and Pérez-García 2021b) or as a new species of compsemydid (Lapparent de Broin and Murelaga 1999).

Although we here conclude that the turtles from Beckles' Pit represent a new species of compsemydid turtle, *Tongemys enigmatica* gen. et sp. nov., we agree that a number of characters are present that unite it with the coeval *Pleurosternon bullockii*, including a broadly similar surface texture, the number and arrangement of bones in the shell, a complete neural series, a four-sided neural I, the common fusion of neural VIII with suprapygal I, peripherals that are V-shaped anteriorly and posteriorly to the bridge, the absence of a cervical scute and a straight mid-line plastral sulcus. As our phylogenetic analysis cannot resolve the interrelationships of compsemydids, pleurosternids and baenids, it is unclear if these characters represent symplesiomorphies or homoplasies, although biogeographic arguments provide support for the former hypothesis, as early pleurosternids and compsemydids are best known from Europe.

In spite of the above listed similarities, we find considerable character evidence that distinguishes *Tongemys enigmatica* from *Pleurosternon bullockii*: much smaller size (a carapace length of ca. 15 cm versus ca. 55 cm); the development of a distinct nuchal notch that is framed by anterior protrusions of the first peripherals, instead of a rounded anterior margin; the near complete retraction of the nuchal from the anterior margin of the shell (ca. 20% of nuchal width contributes to the margin, instead of 50%), a nuchal that is laterally expanded to the approximate width of costal I resulting in a near contact of the nuchal with peripheral II which, in turn, hinders a clear contact between peripheral I and costal I, in contrast to a narrow nuchal and a broad contact between peripheral I and costal I; presence of neurals that are about as long as wide, not longer than wide; notably narrow peripherals; presence of a costal VIII that is significantly smaller than costal VII, not similar in size; a straight medial margin of costal VIII resulting in a triangular space for the suprapygals, not an angular margin; restriction of vertebral I on to the costals, instead of a clear overlap on to peripheral I; a near contact of vertebral I with marginal III, resulting in a short, not expanded contact between marginal II and pleural I; marginals that are restricted to the peripherals, broad pleurals and narrow vertebrals, instead of wide marginals that lap on to the costals, narrow pleurals and broad vertebrals; a distance between the axillary and inguinal notch that is less, not greater than the length of the plastral lobes; plastral lobes with parallel, not evenly converging sides; absence, not presence of a deep anal notch; absence, not presence of broad scute overlap on the dorsal side of the plastral hind-lobe; laterally contracting mesoplastra, instead of rectangular elements; hypoplastron much shorter than hyoplastron, not equal in anteroposterior length; extragular-humeral sulcus not orientated transversely, but rather sloping posterolaterally to nearly contact the epiplastral-hyoplastral suture; and restriction of the gulars to the epiplastron, instead of overlapping the entoplastron.

The vast majority of characters listed above were noted by Guerrero and Pérez-García (2021b), but attributed to ontogeny, as they felt that most differences pertain to proportions. While we agree with Guerrero and Pérez-García (2021b) that proportions change during the ontogeny of turtles, we disagree that this has been documented in literature for the shell of turtles beyond matter-of-fact statements. Indeed, we are only aware of very few morphometric studies that rigorously document shell growth for turtles beyond simple plots of length, width or height against age (e.g. Chiari and Claude 2011; Casale et al. 2017).

As part of their study, Guerrero and Pérez-García (2021b) gathered novel morphometric data from unambiguous *Pleurosternon bullockii* versus *Tongemys enigmatica*, in particular 2D landmarks that approximate the outlines of the nuchal, entoplastron, vertebral III and the anterior plastral lobe. In our estimation, the resulting principal component plots are insufficient to serve as taxonomy evidence for two primary reasons. First and foremost, the use of morphometrics of single shell elements for taxonomic purposes has never been used before and has not been tested by reference to known examples. Is it possible to distinguish extant species using these measurements, even closely related ones? If so, what patterns should we look for? Is this source of data sufficient to distinguish between taxonomic versus ontogenetic effects? These basic questions remain unanswered. As is, the small-bodied turtles variously plot within, outside or beyond the range of the large-bodied ones, which does not correspond to any particular hypothesis in a self-apparent way. Secondly, the nuchal, entoplastron, vertebral III and the anterior plastral lobe of the vast majority of turtles globally have a similar shape, being trapezoidal, lozenge-shaped, hexagonal and tongue-shaped, respectively. Therefore, we do not expect these elements by themselves to yield useful taxonomic data, in contrast perhaps to the morphometrics of all shell elements combined (e.g.

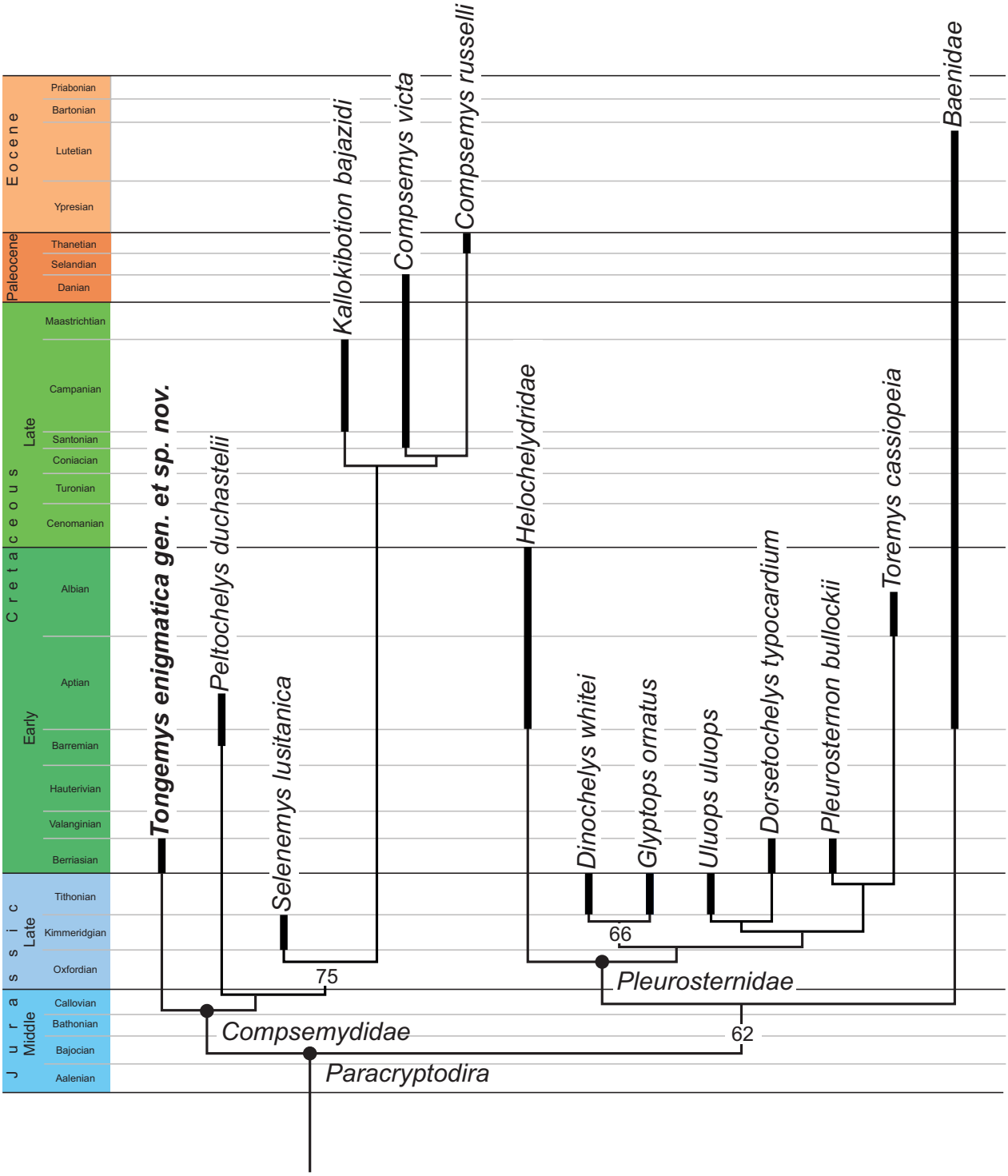

Figure 3. Time-calibrated 50% majority-rule tree obtained from the phylogenetic analysis under equal-weighting, without rogue taxa. Unless otherwise stated, all nodes were found in 100% of all trees.

Claude et al. 2003). Guerrero and Pérez-García (2021b) also plot regression scores of these elements against their centroid size, but here also we are unable to interpret the resulting graphs for the same reasons as listed above.

The available morphometric studies do highlight the tendency for the vertebral scutes to become relatively narrower during ontogeny, at least in the testudinid *Chelonoidis nigra* (Chiari and Claude 2011) and the cheloniid *Caretta caretta* (Casale et al. 2017). To explore if this is universally true among turtles, we collected linear morphometric measurements from a series of eight extant turtles representing all major lineages (see Suppl. material 1 for data and plots). Although the available data are not sufficient to undertake meaningful statistical analyses, we find a notable gradual decrease in vertebral width is found in all species. In contrast to the morphometric data mentioned above, this observed morphometric trend explicitly favors the taxonomic distinctness of *Tongemys enigmatica*

and *Pleurosternon bullockii*, as the largest individuals of the smaller species have proportionally narrower vertebrals than the smallest individual of the latter species.

A number of studies exist that document ontogenetic variation in the shell of some extinct turtles (e.g. Brinkman 2003; Lichtig and Lucas 2015; Joyce et al. 2019; Garbin et al. 2019; Limaverde et al. 2020), but none observes ontogenetic trends among discrete characters beyond the closure of fontanelles or the loss of keels. Indeed, an underlying principle in fossil turtle taxonomy is that the shell of turtles more or less faithfully represents their species and are not influenced by ontogeny beyond changes to the level of ossification. Although we agree that this axiom has perhaps not been tested sufficiently, the very observation that no significant literature is available that might test this tenet is indirect confirmation that is seems to hold true. This is relevant for the taxonomic case at hand: if the turtle material from Beckles' Pit were juveniles of *Pleurosternon bullockii*, it would imply ontogenetic changes that far outpace what is normally observed between species, such as the relative contraction of the nuchal and vertebral I, which would cause the loss of contacts and the creation of others during ontogeny. Incidentally, all of the affected characters were used in the more recent literature to diagnose other compsemydid species as being distinct, including *Compsemys russelli*, *Peltochelys duchastelii* and *Selenemys lusitanica* (Pérez-García and Ortega 2011; Pérez-García 2012; Joyce and Rollot 2020). Therefore, we find it inconsistent to use these characters on the one side to diagnose new species, but to push them aside as an ontogenetic nuisance at other times. The turtle material from Beckles' Pit is easily distinguished from all other named compsemydids, particularly in the topological relationships of the nuchal and vertebral I relative to the surrounding elements and we feel justified in naming a new species, *Tongemys enigmatica*.

Tongemys enigmatica is intermediate in morphology between *Selenemys lusitanica* and *Peltochelys duchastelii*. This is supported by our phylogenetic hypothesis, which depicts them as a paraphyletic grade (see below). A notable difference with these species is the incomplete retraction of the nuchal from the carapacial margin and the retention of a mesoplastron, respectively. As such, we feel further justified in assigning our new species to a new genus as well.

Phylogeny, biogeography and paleoecology

Our phylogeny broadly corresponds to previous hypotheses (e.g. Rollot et al. 2021) by covering *Compsemys russelli*, *Compsemys victa*, *Kallokibotion bajazidi*, *Peltochelys duchastelii* and *Selenemys lusitanica* as members of *Compsemydidae*, in addition to the newly-added *Tongemys enigmatica*, which is recovered as the most basal representative of the clade (Fig. 3). The synapomorphies that unite this clade are the absence of cervicals, placement of marginal I mostly over peripheral I, absence of a contact between peripheral I and costal I and the presence of an entoplastron that is broader than long. All compsemydids more derived than *Tongemys enigmatica* are united by the absence of the nuchal from the anterior margin of the carapace and the presence of a sinuous mid-line sulcus. The novel placement of *Kallokibotion bajazidi* as sister to *Compsemys russelli* and *Compsemys victa* is supported by the novel recognition that only these compsemydids possess extensive contacts of the axillary and inguinal buttresses with the overlying costals. This topology further supports the notion that the clade originated in Europe during the Late Jurassic, but secondarily dispersed to North America during an uncertain time (Joyce and Rollot 2020).

Guerrero and Pérez-García (2021b) noted that the material we refer to *Tongemys enigmatica* originates from a more lacustrine facies, while classic *Pleurosternon bullockii* originate from a setting with marine influence (see Geological settings above). As they concluded all material to represent the same taxon, they reasonably inferred that the juveniles of the species (i.e. *Tongemys enigmatica*) inhabited inland areas, while the adults (i.e. *Pleurosternon bullockii*) were more towards the shore. We conclude, instead, that two taxa are present and that these turtles occupied separate ecological niches. A more ponded, inland habitat for *Tongemys enigmatica* is consistent with the inferred habitat preferences of other basal compsemydids, as both *Selenemys lusitanica* and *Peltochelys duchastelli* were collected from formations otherwise known for their dinosaurs (Baele et al. 2012; Mateus et al. 2017).

At present, compsemydids are only known from three localities throughout the Late Jurassic and Early Cretaceous of Europe, despite a rich record of coeval dinosaurs, particularly in France, Germany and Spain. We suspect this is a taphonomic filter, as the three available forms are notably small in size (carapace length less than 20 cm) and, therefore, likely easily overlooked. We, nevertheless, suspect that careful study of existing collections will yield additional remains from across the continent.

Data availability

All specimens described herein are housed in the Paleontology Collections of the Natural History Museum, London, United Kingdom. The CT data and the 3D mesh models generated from it are available at MorphoSource (https://www.morphosource.org/projects/000434697).

Author contributions

WGJ designed the study. VF scanned the holotype using micro-CT. JRB obtained shell measurements of extant turtles. YR segmented CT data and exported 3D mesh models. WGJ photographed specimens, illustrated them and assembled figures. WGJ and YR assembled the character matrix and conducted phylogenetic analyses. WGJ, YR, JRB and VF prepared the manuscript and contributed to editing.

Competing interests

The authors declare that they have no conflicts of interest.

Financial support

This research was supported by a grant from the Swiss National Science Foundation to WGJ (SNF 200021_178780/1).

Acknowledgements

We would like to thank Michael Day (NHM) for providing access to the specimens that are the focus of this study and Coleman Sheehey and Dave Blackburn for access to the FLMNH Herpetology Collection. Julien Claude and Torsten Scheyer are thanked for meaningful insights that helped improve the quality of the manuscript.

References

Anquetin J, André C (2020) The last surviving *Thalassochelydia* — A new turtle cranium from the Early Cretaceous of the Purbeck Group (Dorset, UK). PaleorXiv 7pa5c. https://doi.org/10.31233/osf.io/7pa5c

Baele JM, Bolotsky YL, Bonde N, Botfalvai G, Buffetaut E, Bugdaeva EV, Bultynck P, Canudo JI, Carlier P, Jun C, Codrea VA (2012) Bernissart dinosaurs and Early Cretaceous terrestrial ecosystems. Bloomington, Indiana University Press, 630 pp.

Barrett PM, Clarke JB, Brinkman DB, Chapman SD, Enson PC (2002) Morphology, histology and identification of the 'granicones' from the Purbeck Limestone Formation (Lower Cretaceous: Berriasian) of Dorset, southern England. Cretaceous Research 23: 279–295. https://doi.org/10.1006/cres.2002.1002

Brinkman DB (2003) A review of nonmarine turtles from the Late Cretaceous of Alberta. Canadian Journal of Earth Sciences 40, 557–571. https://doi.org/10.1139/e02-080

Casale P, Freggi D, Rigoli A, Ciccocioppo A, Luschi P (2017) Geometric morphometrics, scute patterns and biometrics of loggerhead turtles (*Caretta caretta*) in the central Mediterranean. Amphibia-Reptilia 38: 145–156. https://doi.org/10.1163/15685381-00003096

Chiari Y, Claude J (2011) Study of the carapace shape and growth in two Galapagos tortoise lineages. Journal of Morphology 272: 379–386. https://doi.org/10.1002/jmor.10923

Claude J, Paradis E, Tong H, Auffray J-C (2003) A geometric morphometric assessment of the effects of environment and cladogenesis on the evolution of the turtle shell. Biological Journal of the Linnean Society 79: 485–501. https://doi.org/10.1046/j.1095-8312.2003.00198.x

Clements RG (1993) Type-section of the Purbeck Limestone Group, Durlston Bay, Swanage. Proceedings of the Dorset Natural History and Archaeological Society 114: 181–206.

Dollo L (1884) Première note sur les chèloniens de Bernissart. Bulletin du Musée Royal d'Histoire Naturelle de Belgique 3: 63–79.

Evans J, Kemp TS (1975) The cranial morphology of a new Lower Cretaceous turtle from Southern England. Palaeontology 18: 25–40.

Evans J, Kemp TS (1976) A new turtle skull from the Purbeckian of England and a note on the early dichotomies of cryptodire turtles Palaeontology 19: 317–324.

Evers SW, Rollot Y, Joyce WG (2020) Cranial osteology of the Early Cretaceous turtle *Pleurosternon bullockii* (Paracryptodira: Pleurosternidae). PeerJ 8: e9454. https://doi.org/10.7717/peerj.9454

Garbin RC, Böhme M, Joyce WG (2019) A new testudinoid turtle from the middle to late Eocene of Vietnam. PeerJ 7: e6280. https://doi.org/10.7717/peerj.6280

Gilmore CW (1919) Reptilian faunas of the Torrejon, Puerco, and underlying Upper Cretaceous formations of San Juan County, New Mexico. United States Geological Survey Professional Papers 119: 1–68. https://doi.org/10.3133/pp119

Goloboff PA, Farris JS, Nixon K (2008) TNT: a free program for phylogenetic analysis. Cladistics 24: 774–786. https://doi.org/10.1111/j.1096-0031.2008.00217.x

Guerrero A, Pérez-García A (2021a) Morphological variability and shell characterization of the European uppermost Jurassic to lowermost Cretaceous stem turtle *Pleurosternon bullockii* (Paracryptodira, Pleurosternidae). Cretaceous Research 125: 104872. https://doi.org/10.1016/j.cretres.2021.104872

Guerrero A, Pérez-García A (2021b) Ontogenetic development of the European basal aquatic turtle *Pleurosternon bullockii* (Paracryptodira, Pleurosternidae). Fossil Record 24: 357–377. https://doi.org/10.5194/fr-24-357-2021

Guerrero A, Pérez-García A (2021c) Shell anomalies in the European aquatic stem turtle *Pleurosternon bullockii* (Paracryptodira, Pleurosternidae). Diversity 2021 13: e518. [10 pp] https://doi.org/10.3390/d13110518

Joyce WG (2017) A review of the fossil record of basal Mesozoic turtles. Bulletin of the Peabody Museum of Natural History 58: 65–113. https://doi.org/10.3374/014.058.0105

Joyce WG, Rollot Y (2020) An alternative interpretation of *Peltochelys duchastelii* as a paracryptodire. Fossil Record 23: 83–93. https://doi.org/10.5194/fr-23-83-2020

Joyce WG, Brinkman DB, Lyson TR (2019) A new species of trionychid turtle, *Axestemys infernalis* sp. nov., from the Late Cretaceous (Maastrichtian) Hell Creek and Lance formations of the Northern Great Plains, USA. Palaeontologia Electronica 22.3.72. https://doi.org/10.26879/949

Kingsley C (1857) Geological discoveries at Swanage. Illustrated London News, Dec. 26th, 637–638.

Klein IT (1760) Klassification und kurze Geschichte der vierfüßigen Thiere. Jonas Schmidt, Lübeck, 381 pp.

Lapparent de Broin F de, Murelaga X (1999) Turtles from the Upper Cretaceous of Laño (Iberian peninsula). Estudios del Museo de Ciencias Naturales de Alava 14: 135–211.

Leidy J (1856) Notices of extinct Vertebrata discovered by Dr. F. V. Hayden, during the expedition to the Sioux country under the command of Lieut. G. K. Warren. Proceedings of the Academy of Natural Sciences of Philadelphia 8: 311–312.

Lichtig AJ, Lucas SG (2015) Paleocene-Eocene turtles of the Piceance Creek Basin, Colorado. New Mexico Museum of Natural History and Science Bulletins 67: 145–152.

Limaverde S, Pêgas RV, Damasceno R, Villa C, Oliveira GR, Bonde N, Leal MEC (2020) Interpreting character variation in turtles: *Araripemys barretoi* (Pleurodira: Pelomedusoides) from the Araripe Basin, Early Cretaceous of Northeastern Brazil. PeerJ 8: e9840. https://doi.org/10.7717/peerj.9840

Lydekker R (1889a) On certain chelonian remains from the Wealden and Purbeck. Quarterly Journal of the Geological Society of London 45: 511–518. https://doi.org/10.1144/GSL.JGS.1889.045.01-04.34

Lydekker R (1889b) Catalogue of the Fossil Reptilia and Amphibia in the British Museum (Natural History), Part III, The Order Chelonia. Trustees of the British Museum, London, 239 pp.

Mantell GA (1844) The Medals of Creation: or First Lessons in Geology and in the Study of Organic Remains. Private edition, London, 587–876.

Mateus O, Dinis J, Cunha P (2017) The Lourinhã Formation: the Upper Jurassic to lower most Cretaceous of the Lusitanian Basin, Portugal – landscapes where dinosaurs walked. Ciências da Terra 19: 75–97. https://doi.org/10.21695/cterra/esj.v19i1.355

Milner AR (2004) The turtles of the Purbeck Limestone Group of Dorset, southern England. Palaeontology 47: 1441–1467. https://doi.org/10.1111/j.0031-0239.2004.00418.x

Ogg JG, Hasenyager RW, Wimbledon WA (1994) Jurassic-Cretaceous boundary: Portland-Purbeck magnetostratigraphy and possible correlation to the Tethyan faunal realm. Geobios 17: 519–527. https://doi.org/10.1016/S0016-6995(94)80217-3

Owen R (1842) Report on British fossil reptiles, part II. Report of the British Association for the Advancement of Science 11: 60–204.

Owen R (1853) Monograph on the fossil Reptilia of the Wealden and Purbeck formations, Part 1, Chelonia. Palaeontographical Society Monograph 7: 1–12. https://doi.org/10.1080/02693445.1853.12113207

Pérez-García A (2012) *Berruchelus russelli*, gen. et sp. nov, a paracryptodiran turtle from the Cenozoic of Europe. Journal of Vertebrate Paleontology 32: 545–556. https://doi.org/10.1080/02724634.2012.658933

Pérez-García A (2014) Revision of the poorly known *Dorsetochelys typocardium*, a relatively abundant pleurosternid turtle (Paracryptodira) in the Early Cretaceous of Europe. Cretaceous Research 49: 152–162. https://doi.org/10.1016/j.cretres.2014.02.015

Pérez-García A, Espílez E, Mampel L, Alcalá L (2020) A new basal turtle represented by the two most complete skeletons of Helochelydridae in Europe. Cretaceous Research 107: 104291. https://doi.org/10.1016/j.cretres.2019.104291

Pérez-García A, Ortega F (2011) *Selenemys lusitanica*, gen. et sp. nov, a new pleurosternid turtle (Testudines: Paracryptodira) from the Upper Jurassic of Portugal. Journal of Vertebrate Paleontology 31: 60–69. https://doi.org/10.1080/02724634.2011.540054

Pérez-García A, Royo-Torres R, Cobos AA (2015) New European Late Jurassic pleurosternid (Testudines, Paracryptodira) and a new hypothesis of paracryptodiran phylogeny. Journal of Systematic Palaeontology 13: 351–369. https://doi.org/10.1080/14772019.2014.911212

Rollot Y, Evers S, Joyce WG (2021) A redescription of the Late Jurassic turtle *Uluops uluops* and a new phylogenetic hypothesis of Paracryptodira. Swiss Journal of Paleontology 140: 1–23. https://doi.org/10.1186/s13358-021-00234-y

Seeley HG (1869) Index to the fossil remains of Aves, Ornithosauria, and Reptilia, from the Secondary system of strata arranged in the Woodwardian Museum of the University of Cambridge. Deighton, Bell, and Co, Cambridge, UK, 143 pp.

Sweetman SC, Smith G, Martill DM (2017) Highly derived eutherian mammals from the earliest Cretaceous of southern Britain. Acta Palaeontologica Polonica 62: 657–665. https://doi.org/10.4202/app.00408.2017

Tong H, Tortosa T, Buffetaut E, Dutour Y, Turini E, Claude J (2022). A compsemydid turtle from the Upper Cretaceous of Var, southern France. Annales de Paléontologie 108, 102536. https://doi.org/10.1016/j.annpal.2022.102536

Watson DMS (1910a) *Glyptops ruetimeyeri* (Lyd.), a chelonian from the Purbeck of Swanage. Geological Magazine 7: 311–314. https://doi.org/10.1017/S0016756800134600

Watson DMS (1910b) A chelonian from the Purbeck of Swanage, Dorset. Geological Magazine 7, 381, 1910b. https://doi.org/10.1017/S0016756800134892

Woodward AS (1909) Note on a chelonian skull from the Purbeck beds at Swanage. Proceedings of the Dorset Natural History Society 30: 143–144.

Supplementary material 1

File S1

Authors: Walter G. Joyce, Jason R. Bourque, Vincent Fernandez, Yann Rollot

Data type: shell measurement data (EXCEL file)

Explanation note: Extant Turtle Taxa; all measurements in mm taken direction from specimens; UF/H = University of Florida, Herpetology, Gainesville, Florida. Fossils; all measurements in mm taken indirectly using ImageJ; NHM = Natural History Museum, London, UK.

Link: https://doi.org/10.3897/fr.25.85334.suppl1

Fossil Record 25 (2) 2022, 275–285 | DOI 10.3897/fr.25.85563

PENSOFT

für Natur MUSEUM FÜR NATURKUNDE BERLIN

Stratigraphic range extension of the turtle *Boremys pulchra* (Testudinata, Baenidae) through at least the uppermost Cretaceous

Brent Adrian[1]

1 *School of Human Evolution and Social Change, Arizona State University, Tempe, Arizona 85287, USA*

https://zoobank.org/1B122F9D-B355-4D4B-808D-A0345404370B

Corresponding author: Brent Adrian (brentonadrian@gmail.com)

Academic editor: Florian Witzmann ♦ **Received** 19 April 2022 ♦ **Accepted** 8 August 2022 ♦ **Published** 25 August 2022

Abstract

New material of the derived baenid turtle *Boremys pulchra* from the Hell Creek Formation of Montana extends the stratigraphic range of the taxon through at minimum the latest Maastrichtian. Previously, the species was constrained to the Campanian of Montana and Alberta, so this extension constitutes at least 5 million years. Due to fossil reworking at the Bug Creek Anthills assemblage, where Maastrichtian and Paleocene deposits are mixed, a definitive extension for *B. pulchra* cannot currently include Paleocene strata. However, the presence of *B. pulchra* in latest Cretaceous strata, previous identification of Paleocene *Boremys* sp. and the general success of baenid taxa across the K–Pg boundary, make it quite plausible that *B. pulchra* survived the extinction event and that previously described Maastrichtian and Paleocene *Boremys* sp. material probably represents a new taxon. A stratigraphic extension beyond the Campanian indicates that *B. pulchra* survived the paleoenvironmental conditions of the latest Cretaceous, where adaptation to locally heterogeneous aquatic habitats and paleotemperature fluctuations may have facilitated latest Cretaceous and K–Pg survivorship. Additionally, ectoparasitic bore marks on the *Boremys pulchra* specimen described here can be attributed to the ichnotaxon *Karethraichnus lakkos*.

Key Words

Biostratigraphy, Bug Creek Anthills, Hell Creek Formation, *Karethraichnus lakkos*, K–Pg boundary, Montana

Introduction

Boremys Lambe, 1906a is a genus of eubaenine baenodd turtle known primarily from the Campanian of Utah (Kaiparowits Formation [Fm.]) and New Mexico (upper Kirtland Formation), as well as the Judith River Group in Alberta and Montana (Lambe et al. 1906a; Lambe 1914; Gilmore 1920; Parks 1933; Gaffney 1972; Brinkman and Nicholls 1991; Hutchison et al. 2013; Sullivan et al. 2013; Joyce and Lyson 2015). Of particular interest presently, Lyson and colleagues (2011) referred material to *Boremys* sp. from the Maastrichtian Hell Creek Formation of North Dakota and eastern Montana and the Paleocene Fort Union Formation of North Dakota (Puercan North American land mammal "age" [NALMA]), but did not reach a species designation due to missing key areas of the shell (Lyson et al. 2011; Joyce and Lyson 2015). A partial eubaenine nuchal from the early Paleocene Denver Basin of Colorado has also been attributed to *Boremys* sp. (Hutchison and Holroyd 2003; Joyce and Lyson 2015). Additionally, undescribed partial specimens of *Boremys* sp. (e.g. RSKM P3135.68, RSKM P3143.36, RSKM P3150.41, RSKM P3173.11, RSKM P3174.16, RSKM P3174.37, RSKM P3175.14, RSKM P3176.25 and RSKM 2618.44) from the Maastrichtian Frenchman Fm. of southern Saskatchewan, which is coeval with the Upper Hell Creek Fm., could correspond with the *Boremys* sp. described by Lyson et al. (2011). Several other published referrals of *Boremys* were not supported by the comprehensive baenid review of Joyce and Lyson (2015) and I follow their assessment of this material. No *Boremys pulchra* material was identified in the survey of Montana Hell Creek/Fort Union Formation turtle faunas by Holroyd et al. (2014) and the total number of referred

B. pulchra specimens is small, suggesting that it was a rare turtle, as proposed for *B. grandis* in New Mexico and Utah (Lively 2016).

Previously, all *Boremys* specimens were synonymised into *B. pulchra*, distributed from Alberta to New Mexico, including *Boremys albertensis* Gilmore 1920 from the Belly River Group of Alberta (Gaffney 1972; Joyce and Lyson 2015). Currently, *Boremys* is comprised of two valid species, the northern Laramidian *Boremys pulchra* Lambe, 1906a and southern Laramidian *Boremys grandis* Gilmore, 1935, which differ systematically (Brinkman and Nicholls 1991; Joyce and Lyson 2015). The most dramatic difference is shell size, with *B. grandis* nearly twice as large as *B. pulchra* (Brinkman and Nicholls 1991; Joyce and Lyson 2015). Sandy crevasse splays, followed by channels, were determined as the preferred paleoenvironment inhabited by *Boremys* sp., based on the material evaluated by Lyson et al. (2011). A paleobiogeographical analysis of Cretaceous baenids suggests that a southern *B. grandis* and *B. pulchra* in Montana are the result of an allopatric speciation event, with subsequent southern dispersal of *B. grandis* and *B. pulchra* into Alberta (Lively 2013).

Geological setting

The turtle specimen described here (RAM 27109) was discovered in 1994 in the Bug Creek Anthills assemblage (Locality V-1994096), near the Cretaceous-Paleogene (K–Pg) boundary in McCone County, Montana (Lofgren 1995) (Fig. 1). Unlike similarly-aged exposures in nearby Garfield County, where the Hell Creek-Tullock Formation contact approximates the K–Pg boundary, the upper part of the Hell Creek Formation in McCone County is Paleocene (Lofgren 1995). Fossils at Bug Creek Anthills locality V-1994096 (Fig. 1) occur in abundance as disarticulated elements within a pebble conglomerate, which is composed of clay–mud clasts with a light brown to tan sandstone matrix. The fossiliferous conglomerate–sandstone is scoured into a grey sandstone with red–brown ironstone lenses. Conglomerate is exposed along the north-facing side of a prairie-capped flat area, 0.6–1.5 m (2–5 ft) below the prairie cap.

The greater Bug Creek assemblages are comprised of several localities that have been historically challenging to categorise temporally, due to reworking of their fossils–see detailed history in Lofgren (1995) and summary in Cifelli et al. (2004). One of these assemblages, Bug Creek Anthills, was originally described as the oldest in a series of three (followed by Bug Creek West and Harbicht Hill) (Cifelli et al. 2004). Extensive fossil reworking in these strata was determined to be caused by the incision of large Paleocene sandstone channels into fossiliferous Cretaceous strata, resulting in older (uppermost Maastrichtian) fossils that are present as sedimentary particles in younger channel fills deposited during the Puercan NALMA (Lofgren 1995; Cifelli et al. 2004). Central to the age determination of Bug Creek Anthills is the presence of the "archaic ungulate" index taxon *Protungulatum donnae* Sloan and Van Valen, 1965 as the FAD (First Appearance Datum) for the advent of the initial interval zone of the Puercan NALMA (Archibald 1981, 1982; Archibald and Lofgren 1990; Cifelli et al. 2004). Lithofacies analyses of the Bug Creek localities show exclusive association with lag deposits of large channel facies, which are deeply entrenched into older floodplain deposits yielding in situ dinosaur remains (Lofgren 1995). Channel facies are arranged within a complex stratigraphic interval and locally traceable erosion surfaces were formed within channelling events (Lofgren 1995). The channels can only rarely be ordered temporally, based on superposition or crosscutting relationships (Lofgren 1995).

Some North American fossil sites near the K-Pg transition represent restricted and homogenous habitats, with faunal and floral content that can vary with depositional facies (see the Gryde Local Fauna of the Frenchman Formation in Saskatchewan; Storer 1991). This is the case in the Bug Creek assemblages of the Hell Creek Formation, where faunal remains are restricted to large, sandy channel fillings that reflect multiple episodes of deep channel entrenchment into older floodplains (Fastovsky 1987; Lofgren 1995). As in many terrestrial microvertebrate localities formed by fluvial regimes, the majority of bone material at Bug Creek is concentrated into lags in channel facies and abrupt faunal and floral changes in these strata may be, at least in part, artefacts of the depositional system (Fastovsky 1987; Eaton et al. 1989). Fluvial sedimentation also produces patterns of lenticular, interfingering and laterally discontinuous facies, none of which has extensive spatial or temporal continuity (Fastovsky 1987). Individual channels at Bug Creek are frequently lithologically and petrographically indistinguishable, sedimentary hiatuses are numerous and correlation between discontinuous outcrops is often uncertain, as the scale of the gaps between exposures can exceed that of the predicted scale of the fluvial components (Fastovsky 1987). Taphonomic analysis assessing the degree of abrasion on fossil specimens from reworked sediments may approximate distance of transport or the energy and abrasive capacity of a channel, but cannot distinguish between heterochronous faunas (Eaton et al. 1989). Overall, the depositional history of the Hell Creek Formation at Bug Creek Anthills presents a complex suite of depositional and taphonomic biases that confound characterisation and limit detailed channel and paleoenvironmental reconstructions.

Baenidae is represented by at least 11 taxa in the Hell Creek Formation, accounting for much of the diversity in the considerable turtle assemblage of the unit (Lyson et al. 2019). At least seven other family level clades of turtles are also known from the Hell Creek Fm.: Adocidae, Chelydridae, Kinosternoidea, Macrobaenidae, Nanhsiungchelyidae, Pleurosternidae and Trionychidae (see faunal list of Holroyd et al. 2014: table 2). As previously stated, no specimens of *Boremys pulchra* were identified

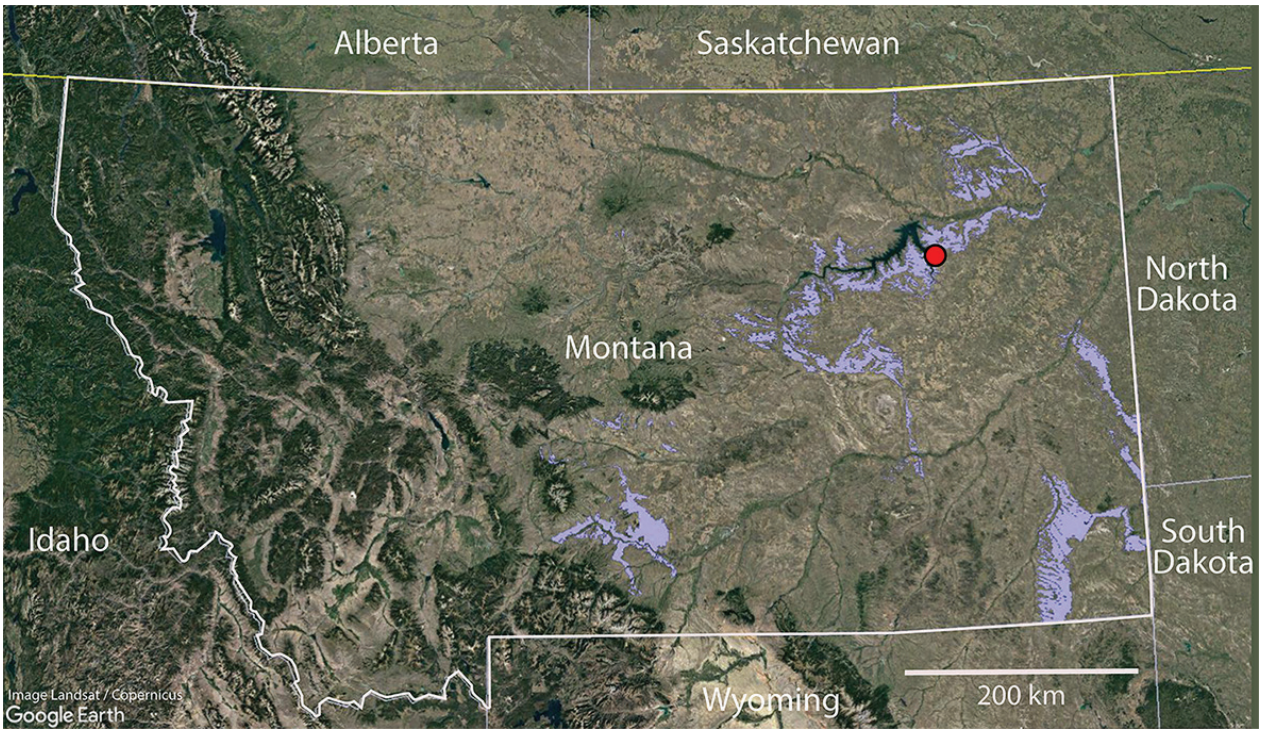

Figure 1. Index map of locality V-1994096 in the Hell Creek Formation, northeast Montana. Blue areas indicate Hell Creek Formation exposures in Montana and the red dot indicates the Bug Creek Anthills assemblage. Base satellite map generated with Google Earth V 7.3.4.8248. (March 20, 2022). Montana, United States. Camera: 929 km, 46°54'58"N, 109°48'21"W. Landsat/Copernicus 2022. http://www.earth.google.com [20 March 2022].

in past surveys of Hell Creek Fm. turtles, despite being readily identifiable (Holroyd et al. 2014). Besides RAM 27109, the only other turtles identifiable from Bug Creek Anthills locality V-1994096 are from indeterminate trionychid (softshell turtle) fragments. However, the coeval small mammal assemblage from Bug Creek Anthills is exceptional in diversity and abundance, with numerous multituberculate (11 genera), marsupial (6 genera) and eutherian (9 genera) taxa identified to species level–see faunal list of Lofgren (1995: 70) and relevant taxonomic updates in Wilson (2014: table 1). According to RAM collections records, indeterminate crocodilian, champsosaurid, amphibian and squamate material has also been recovered from locality V-1994096, as well as a presbyornithid bird. Finally, chondrichthyan and osteichthyan fishes are represented, including Actinopterygii, Amiidae and Lepisosteidae.

Materials and methods

Screenwashing techniques described by McKenna (1965) were employed at Bug Creek Anthills locality V-1994096 in 1994; however, the size of the specimen (larger than ~ 1 cm^2) indicates it was probably surface collected (Lofgren, pers. comm.). Linear measurements were taken using Neiko (China) #01417A 6" Digital Calipers and depth measurements were performed with an iGaging (USA) # 35-125 Digital Electronic Indicator. Some distances and angles were measured from high quality digital photographs using IMAGEJ (Rasband 1997–2016). The plot and regression line of anterior plastral lobe measurements were generated in Microsoft EXCEL (v. 2203). I use the taxonomic scheme of turtles presented by Joyce (2007, 2017) unless otherwise specified and I adhere to Phylocode guidelines (e.g. Laurin et al. 2005; Joyce et al. 2020, 2021). Following Hutchison and Bramble (1981) and most modern authors, the two pairs of scales present on the anterior plastron are termed gular and extragular scales, where the gulars are located anteromedially to the extragular scales and both sets of scales are anterior to the entoplastron. Classification of ichnological pits follows Hutchison and Frye (2001).

Institutional abbreviations

CMN, Canadian Museum of Nature (formerly NMC), Ottawa, Canada; **NMC**, National Museum of Canada, Ottawa, Canada; **PTRM**, Pioneer Trails Regional Museum, Bowman, North Dakota, USA; **RAM**, Raymond M. Alf Museum of Paleontology, Claremont, California, USA; **ROM**, Royal Ontario Museum, Ontario, Canada; **RSKM**, Royal Saskatchewan Museum, Saskatchewan, Canada; **TMP**, Royal Tyrell Museum of Palaeontology, Alberta, Canada; **UALVP**, University of Alberta Laboratory of Vertebrate Paleontology, Alberta, Canada; **UCMP**, University of California Museum of Paleontology, Berkeley, California, USA; **USNM**, National Museum of Natural History, Washington D.C., USA.

Systematic paleontology

Testudinata Batsch, 1788 (sensu Joyce, Parham & Gauthier, 2004)
Paracryptodira Gaffney, 1975 (sensu Joyce, Parham, Anquetin, Claude, Danilov, Iverson, Kear, Lyson, Rabi & Sterli, 2020)
Baenidae Cope, 1873 (sensu Joyce, Anquetin, Cadena, Claude, Danilov, Evers, Ferreira, Gentry, Georgialis, Lyson, Pérez-García, Rabi, Vitek & Parham, 2021)

Boremys Lambe, 1906b

Boremys pulchra Lambe, 1906a

Type specimen. CMN 1130, a plastron and anterior half of carapace (Lambe 1902: fig. 8; Lambe 1906a: pls. 3.4, 4).

Type locality and stratum. Near the mouth of Berry Creek, Red Deer River, Dinosaur Provincial Park, Alberta, Canada; Dinosaur Park (formerly Judith River) Formation, Judith River Group, Campanian, Late Cretaceous (Lambe 1906a; Brinkman and Nicholls 1991; Eberth and Hamblin 1993).

Material. RAM 27109, a near-complete anterior plastral lobe, comprised of co-ossified entoplastron, epiplastra and partial hyoplastra (Fig. 2).

Description. RAM 27109 is a well preserved, mostly complete anterior plastral lobe (Fig. 2). The pattern of sulci at the anterior end of the ventral side of the lobe closely matches that of *Boremys pulchra*, as reconstructed by Brinkman and Nicholls (1991: fig. 7B) (Fig. 2A–C). The epiplastra, entoplastron and hyoplastra of RAM 27109 are completely fused, with no visible sutures (Fig. 2A, C). Archibald (1977) considered lack of shell fusion a derived character in *Boremys*, but most *Boremys pulchra* shells examined by Brinkman and Nicholls (1991) were fused. Considering that baenid turtles exhibit determinate growth and co-ossify as adults and that RAM 27109 is similar in size and proportions to other *B. pulchra* specimens, RAM 27109 can be considered a nearly full-sized adult (Hutchison 1984) (Fig. 3, Table 1). Smaller size is a primary diagnostic character for this species and Brinkman and Nicholls (1991) regard 320 mm as the maximum mid-line carapace length for *B. pulchra*. Similarly, Joyce and Lyson (2015) found 300 mm as the carapace length dividing *B. pulchra* from the congeneric *B. grandis*. Using the proportions of the reconstructed shell of *B. pulchra* from Brinkman and Nicholls (1991), the mid-line carapace length of RAM 27109 is estimated to be ~ 200 mm, similar to Campanian *B. pulchra* specimens (Brinkman and Nicholls 1991; Joyce and Lyson 2015) (Fig. 3, Table 1). The presence of anterior plastral scalloping (lateral epiplastral projections) and straight extragular-humeral sulci further differentiate RAM 27109 from *B. grandis* (Gilmore 1935). I consider the reconstruction of Brinkman and Nicholls (1991: fig. 7B) probably more representative than that presented by Gaffney (1972: fig. 40) because it is more recent and based on more specimens (NMC 2281, ROM 5115, TMP 90.119.6, UALVP 9, UCMP 130155). The current specimen and reconstructions of *B. pulchra* vary in the degree of curvature between the gular-extragular and extragular-humeral sulci, as well as the degree of lateral projection on the epiplastra (Gaffney 1972; Brinkman and Nicholls 1991). Given the uncertainty regarding sutures due to shell fusion, I interpret these last minor morphological differences as probable individual variation (Gaffney 1972; Brinkman and Nicholls 1991).

RAM 27109 is subtriangular in shape with a bilateral pair of rounded lobes (the anterior of which is smaller) projecting laterally from the epiplastra to form distinct anterior plastral scalloping (Fig. 2B–E). Each laterally projecting lobe is upturned dorsally and protrudes slightly beyond a rounded ridge on the dorsal surface of the plastron which runs along the bases of the lobes (Fig. 2D–E). This 3–4 mm wide ridge likely marked the transition between the scale-covered lobes and the body wall (Fig. 2E). The dorsal surface of the anterior plastral lobe is otherwise flat and even, apart from a ~ 1 mm tall ridge along the posterior portion of the anterior plastral lobe mid-line, which likely represents a reduced homologue of the posterior process of the entoplastron that is present in basal testudinatans (Gaffney 1990: figs. 91–92; Szczygielski and Sulej 2019: fig. 6) (Fig. 2D–E). The mid-line ridge reaches a maximum width of 4.3 mm and it diminishes anteriorly across the inferred length of the entoplastron, terminating at approximately the anterior end of this bone (Fig. 2D–E). At this level, there is a small round pit (diameter = ~ 3 mm) on each side of the mid-line ridge (Fig. 2D–E). Anterior to the hyoplastra, the muscles supracoracoideus anterior and deltoideus clavicularis possibly attached to the anterior plastral lobe near the mid-line (Zhu 2011). The functions of these muscles are adduction and retraction of the humerus, which are important in aquatic locomotion of turtles (Walker 1973; Zhu 2011).

Table 1. Measurements of anterior plastral lobes (maximum lengths and widths) of *Boremys pulchra* Lambe, 1906a specimens. Additional data from Brinkman and Nicholls (1991: table 2). Graph ID numbers correspond with those in Figure 3. All measurements are from specimens collected in Dinosaur Provincial Park, Alberta (Dinosaur Park Formation, middle Campanian), except RAM 27109. All measurements in mm.

Graph ID	Specimen	Length mm	Width mm
1	RAM 27109	54	61
2	NMC 2281	64	57
3	USNM 8803	64	94
4	UALVP 9	56	59
5	TMP 88.36.111	52	50
6	TMP 90.119.6	68	80
7	TMP 74.10.1	55	56
8	TMP 75.11.46	53	61
9	TMP 88.2.10	65	75

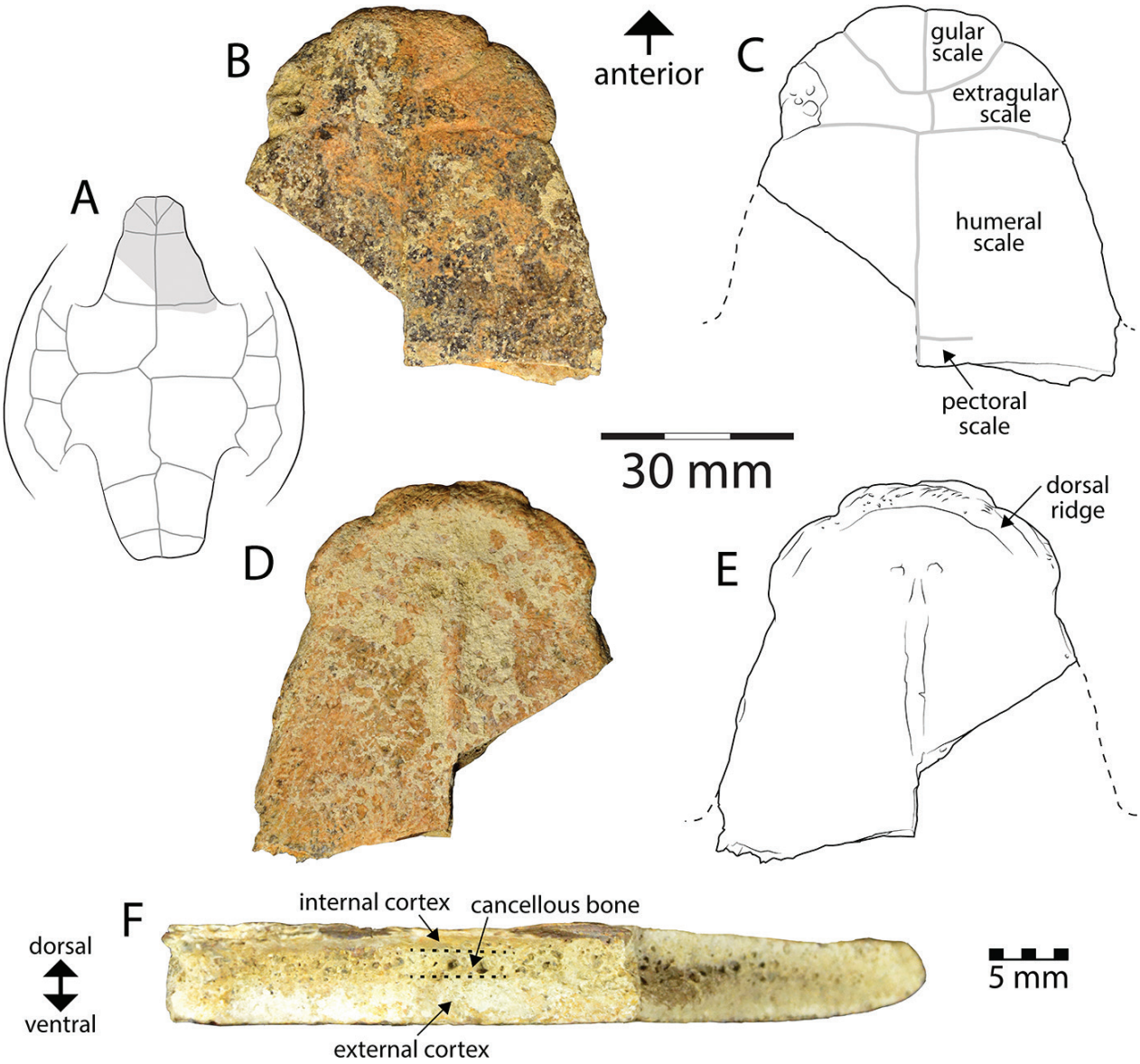

Figure 2. RAM 27109, anterior plastral lobe of *Boremys pulchra* Lambe, 1906a. **A.** Reconstructed *B. pulchra* carapace of Brinkman and Nicholls (1991), with shaded area representing RAM 27109; **B.** Photograph in ventral view; **C.** Line drawing in ventral view; **D.** Photograph in dorsal view; **E.** Line drawing in dorsal view; **F.** Proximal (broken) cross section of anterior plastral lobe. Light grey lines represent sulci and dashed lines in **C** and **E** show missing edges. In **F**, dotted lines indicate boundaries between interior bone layers. 5 mm scale applies to **F** only.

The posterior end of the anterior plastral lobe is broken cleanly in an approximately straight line perpendicular to the mid-line on the left side (Fig. 2F). On the right side, the break angles anterolaterally at approximately 53° from the mid-line (Fig. 2B–E). Both breaks provide a view into the interior anatomy of the anterior plastron, but few details of the microanatomy can be assessed (Fig. 2F). The bone exhibits a diploë structure typical of turtles, with compact external and internal cortices enclosing an interiormost region of cancellous bone (Scheyer 2007) (Fig. 2F). The primary comparative data available regarding baenid shell histology is from carapacial and plastral material of *Boremys* sp. from the Late Cretaceous Dinosaur Park Formation in Alberta, Canada (Scheyer 2007). Compared to *Neurankylus* sp. and *Plesiobaena* sp., *Boremys* sp. (and *Chisternon* sp.) is reported to have less compact bone, thinner cortices and a well-developed cancellous interior, with larger marrow cavities in cancellous bone and higher vascularisation in compact bone (Scheyer 2007). Such detailed microanatomical morphology cannot be ascertained from RAM 27109; however, there is distinct cancellous bone with prominent marrow cavities in the interiormost region of approximately the middle third of the lobe (Fig. 2F). Trabeculae are larger towards the mid-line and are generally round to ovoid and the lateral plastral margins consist of only compact bone, without a cancellous interior (Fig. 2F). Near the mid-line, the well-developed external cortex is approximately 2.7 times thicker than the internal cortex (Fig. 2F). This disparity between external and internal cortical thickness

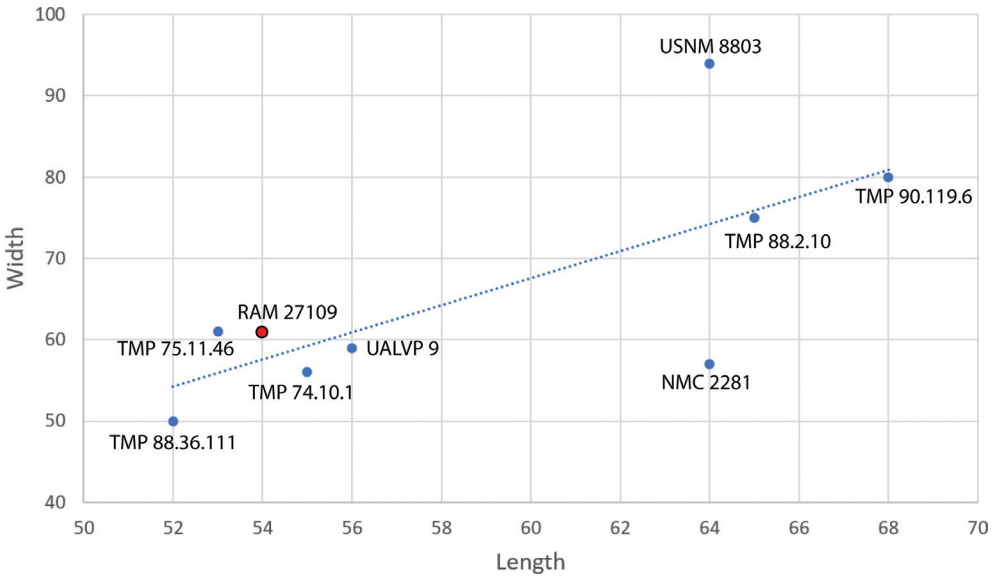

Figure 3. Maximum length/width (mm) plot of the anterior plastral lobe in *Boremys pulchra* Lambe, 1906a specimens (Brinkman and Nicholls 1991: table 2). Values are provided in Table 1. All measurements, except RAM 27109 (in red), are from specimens collected in Dinosaur Provincial Park, Alberta (Dinosaur Park Formation, middle Campanian). For the dotted blue regression line, $R^2 = 0.5246$.

is similar to that of a costal from *Denazinemys nodosa* Gilmore, 1916 in the late Campanian Fruitland Formation, where the exterior cortex is significantly thicker than the internal cortex and trabeculae are mostly small and circular (Lichtig and Lucas 2017).

Results

The posterior half of the posterior lobe of anterior scalloping (lateral epiplastral projection) on the right ventral side of RAM 27109 exhibits distinct pits, which are interpreted as a cluster of at least four ectoparasitic bore marks (Figs 2A, B, 4). The marks are shallow (non-penetrative) and have simple profiles and rounded hemispherical termini (Fig. 4A). They can be classified as Type II pits according to the classification of Hutchison and Frye (2001), which are circular to ovoid with rounded bottoms (Fig. 4A). Measurements for individual marks are provided in Table 2. Pit dimensions range from 1.2–2.8 mm in diameter and from 1.8–3.2 mm in depth (Fig. 4, Table 2). The marks are adjacent to each other along the slope of a bevel at the plastral margin and only on the ventral side. Abraded areas, lateral and anterior to the cluster, may have contained additional small marks, but their borders have been taphonomically obscured (Fig. 4A). Mark #1 is the only pit that has an unabraded border and, thus, a more precise depth, but the remaining pits occur along a curved surface with worn edges, making their depths (and hence diameter/depth ratios) less reliable (Fig. 4, Table 2).

The morphology and size of the bore marks on RAM 27109 are consistent with *Karethraichnus lakkos* Zonneveld, Bartels, Gunnell and McHugh, 2016, a common ectoparasitic ichnotaxon on turtles and tortoises from Cretaceous and Tertiary deposits in North America and Africa (Zonneveld et al. 2016, 2021; Adrian et al. 2021). Congeneric ichnospecies are also known from a Campanian dermochelyid (marine) turtle in Japan and from Late Pleistocene armadillos in Brazil (Sato and Jenkins 2020; Moura et al. 2021). Tracemakers usually associated with *K. lakkos* include leeches and ixodid arthropods (ticks), which are known to feed on blood sinuses within shell bone, especially at sulci between epidermal scales (Siddall and Gaffney 2004; Zonneveld et al. 2016, 2021). Bore marks of *K. lakkos* are only emplaced in locations accessible on living turtles–external surfaces of the carapace and plastron, especially at marginal or lip areas (Zonneveld et al. 2016). Thus, *K. lakkos* is associated with the activities of parasites instead of postmortem scavengers or synmortem predators (Zonneveld et al. 2016).

Table 2. Measurements of bore marks (in mm) on ventral surface of RAM 27109 (see Fig. 4). Marks are attributed to the ectoparasitic ichnotaxon *Karethraichnus lakkos* Zonneveld, Bartels, Gunnell & McHugh, 2016.

Mark #	Diameter mm	Depth mm	Diameter/Depth
1	2.8	1.8	1.56
2	1.3	2.0	0.65
3	1.2	3.2	0.38
4	1.4	2.3	0.61

Discussion

Taxonomic and temporal assignment of RAM 27109, and stratigraphic range extension

Though *Boremys pulchra* is primarily known from the Campanian, fossil material attributable to *Boremys* sp. has also been reported from Maastrichtian deposits of North Dakota, eastern Montana and southern Saskatchewan, the Paleocene of North Dakota (Lyson et al. 2011)

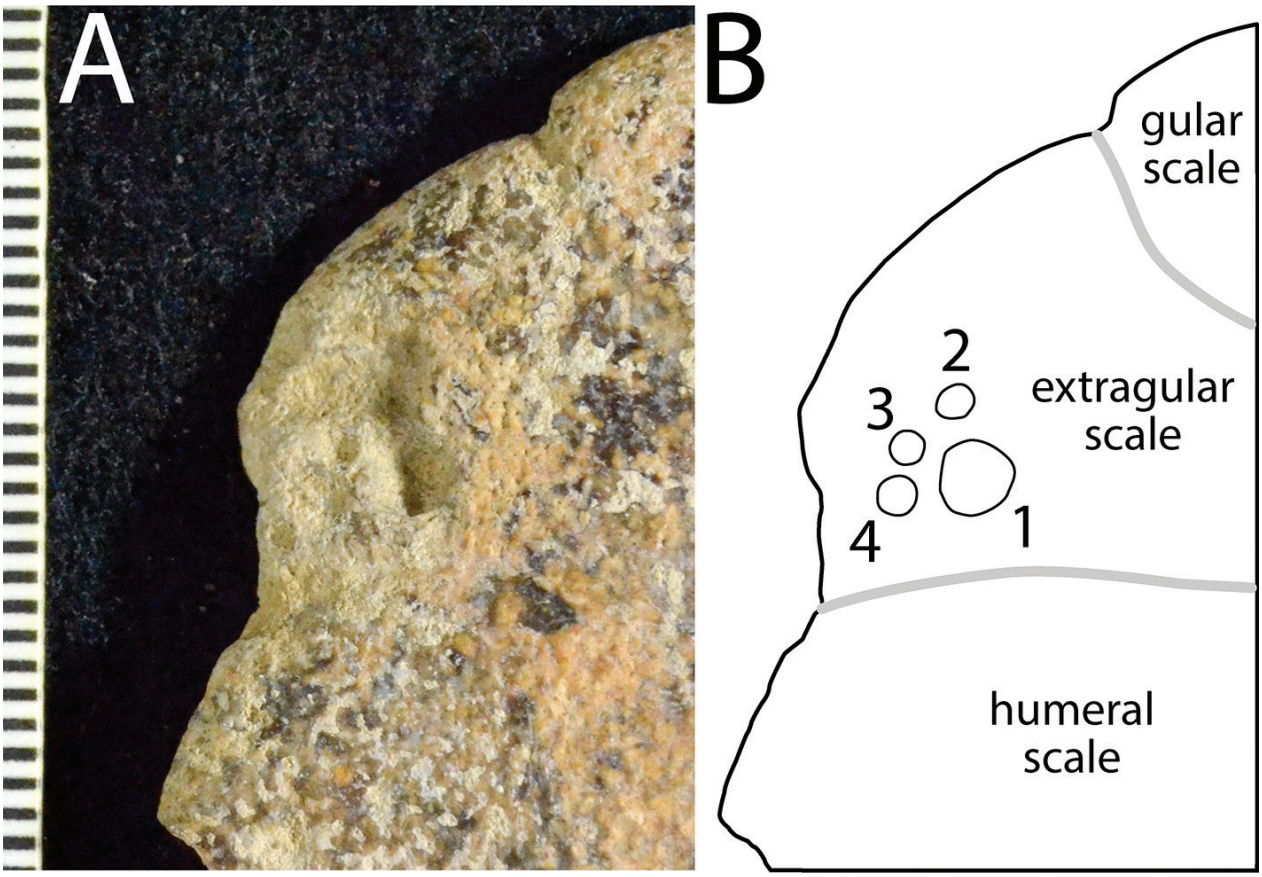

Figure 4. Ectoparasitic bore traces attributed to the ichnotaxon *Karethraichnus lakkos* Zonneveld, Bartels, Gunnell and McHugh, 2016. **A.** Close-up photograph under oblique lighting; **B.** Line drawing. Grey lines indicate sulci and measurements of marks are provided in Table 2.

and the Paleocene of Colorado (Hutchison and Holroyd 2003). For the *Boremys* material described by Lyson et al. (2011), species designation was not possible due to the presence of open sutures and central plastral fontanelles between the mesoplastra, which could be indicators of skeletal immaturity or possible autapomorphies for a new Maastrichtian/Puercan taxon.

The only character in the phylogenetic matrix of Lyson et al. (2011) that is coded differently between *Boremys pulchra* and *Boremys* sp. is a carapacial trait (#44, vertebral scale shape) and, thus, cannot be applied to the plastral specimen RAM 27109. This makes body size within *Boremys* an established morphological difference between its species that is not reflected in the phylogenetic matrix of Lyson et al. (2011). Carapace size is considered (#40) in the more recent baenid matrix of Lyson et al. (2016), but *Boremys* sp. is not included, so the character only distinguishes between *B. pulchra* and *B. grandis*. The remarkable overall similarity between the coding for *B. pulchra* and *Boremys* sp. in multiple baenid matrices makes shell size the only published diagnostic difference between the two taxa, as applicable to the plastron. Shell size is, therefore, the only morphological basis available in the current study to differentiate RAM 27109 from the *Boremys* sp. of Lyson et al. (2011). The only published carapace length of *Boremys* sp. (PTRM 16156, 31.8 cm) is above the upper threshold (30 cm) of *B. pulchra* body size and probably represents a juvenile individual, due to large plastral fontanelles and open sutures (Lyson et al. 2011; Joyce and Lyson 2015). Thus, the adult size of *Boremys* sp. is not known and may be closer to the larger *B. grandis* than *B. pulchra* (Lyson et al. 2011). The consistency of size between RAM 27109 and *B. pulchra* (Table 1), coupled with high similarity of their anterior plastral pholidoses, allows referral of the current specimen to that taxon. However, there is a margin of uncertainty due to the lack of other diagnostic morphology in the partial RAM 27109. Future discoveries (i.e. the skull or more complete shells of *Boremys* sp.) and analysis of other undescribed Maastrichtian *Boremys* sp. material may clarify our understanding of the lineage following the Campanian and additional stratigraphic revisions may be necessary.

RAM 27109 is referred to *B. pulchra*, based on its small adult size and anterior plastral morphology, consistent with Campanian representatives of the species (Gaffney 1972; Brinkman and Nicholls 1991). Its presence in the uppermost Cretaceous deposits of the Hell Creek Formation at Bug Creek Anthills makes it the youngest known specimen of *B. pulchra*, although extensive reworking of uppermost Maastrichtian rocks in this unit only allows for definitive attribution to rocks which are latest Maastrichtian in age (Lofgren 1995). However, the presence of the genus above the K–Pg boundary, the

presence of *B. pulchra* in the latest Maastrichtian (established here) and the known survival of most Hell Creek Fm. baenids into the Paleocene (Lyson and Joyce 2009b; Lyson et al. 2011; Holroyd et al. 2014; Joyce and Lyson 2015), suggests that *B. pulchra* also survived the K–Pg extinction event. Generally, turtles fared well during the K–Pg extinction event, with a survival rate of 84% at the generic level (Hutchison and Archibald 1986; Lofgren 1995; Lyson et al. 2011; Holroyd et al. 2014).

Pathologies

Haematophagous leeches are the most common ectoparasites of modern aquatic reptiles and amphibians, including freshwater turtles (Sawyer 1986; Readel et al. 2008). Leeches can cause anaemia and bacterial and fungal infections in captive hosts and are also known vectors for haematoparasites, which can be transmitted intra- and interspecifically (Telford 1984; Readel et al. 2008). Leech loads vary significantly between modern turtle species and are higher on bottom-walking taxa, which live in close contact with the substrate inhabited by leeches and ponds with high turbidity (Ryan and Lambert 2005; Readel et al. 2008). Some studies have reported higher leech intensity (or associated haemogregarine parasites) in female turtles, possibly due to their frequently larger body size (McKnight et al. 2021). Despite common hypotheses, mean leech intensity in modern taxa is not affected by aerial basking and does not vary with turtle abundance, amount of edge vegetation or number of available basking sites (Readel et al. 2008; McKnight et al. 2021). Baenids, in general, are considered bottom-dwelling turtles that favoured running water and articulated specimens are found predominantly in sandy sediments (Hutchison and Archibald 1986; Holroyd and Hutchison 2002; Lyson et al. 2021). *Karethraichnus*, in particular, has also been reported on baenid fossils from the Eocene Green River Basin in Wyoming and Uinta Formation of Utah, though it has been more frequently documented in the geoemydids *Echmatemys* and *Bridgeremys* (Zonneveld et al. 2016; Adrian et al. 2021). Considered together, these factors suggest that *B. pulchra* may have been exposed to more parasite-bearing substrate due to potential bottom-walking, but its leech loads may have been mitigated by a higher energy, fluvial depositional setting. Further studies should examine the effect of haematophagous parasites on the health, behaviour and physiology of wild turtles, as well as the morphology of modern parasitic traces on turtle shell bone.

Conclusions

The presence of *Boremys pulchra* in the Bug Creek Anthills assemblage of Montana establishes the taxon through the latest Maastrichtian and also potentially extends the stratigraphic range of the taxon through the K–Pg boundary into the Puercan NALMA. Due to temporal uncertainty at Bug Hills Anthills localities caused by reworking of Paleocene fossils into the uppermost Maastrichtian deposits, this extension can only include the latest Cretaceous deposits, consistent with prior treatment of turtle taxa from Bug Creek Anthills (see Holroyd and Hutchison 2002). Thus, the current study extends the stratigraphic range of *B. pulchra* by at least 5 million years. Further, considering that multiple specimens of *Boremys* sp. have been identified from Paleocene deposits (Hutchison and Holroyd 2003; Lyson et al. 2011; Joyce and Lyson 2015) and the high rate of baenid survivorship through the K–Pg extinction event (Hutchison and Archibald 1986; Lyson and Joyce 2009b; Lyson et al. 2011; Holroyd et al. 2014), the present study increases the likelihood that *B. pulchra* also survived the K–Pg boundary. Given the exclusively southern distribution of the large-bodied *B. grandis*, the consistently northern range of the small *B. pulchra* and the reconstructed ancestral range of *Boremys* in Montana (Lively 2013), it is probable that the larger *Boremys* sp. material described by Joyce and Lyson (2011) represents a new northern taxon of intermediate size.

If *Boremys pulchra* did, indeed, survive the K–Pg extinction, it would be the tenth surviving baenid taxon to do so, joining *Neurankylus eximius* Lambe, 1902, *Cedrobaena brinkman* Lyson & Joyce, 2009b, *Cedrobaena putorius* Lyson & Joyce, 2009b, *Palatobaena cohen* Lyson & Joyce, 2009a, *Eubaena cephalica* Hay, 1904, *Stygiochelys estesi* Gaffney & Hiatt, 1971, *Goleremys mckennai* Hutchison, 2004, *Saxochelys gilberti* Lyson, Saylor & Joyce, 2019 and *Boremys* sp. (Lyson et al. 2011; Joyce and Lyson 2015). Survival of aquatic vertebrates across the K–Pg boundary has been related to adaptation in mutable, locally heterogeneous aquatic environments that experienced fluctuating paleotemperature patterns, which characterise the latest Cretaceous deposits in the northern Great Plains of North America (Fastovsky 1990; Holroyd and Hutchison 2002; Holroyd et al. 2014). Additional confirmed Maastrichtian *B. pulchra* specimens may allow more robust comparison between Campanian and later forms. Specific adaptations to post-Campanian paleoenvironments, such as swimming ability, feeding ecology or bottom walking, may also be elucidated by additional morphological study. Finally, further collection of turtle fossils in localities near the Cretaceous/Paleocene transition and detailed examination of specimens currently in collections (including material from microvertebrate sites) may alter the stratigraphic ranges of other north Laramidian turtles, including those that are small and/or rare, like *B. pulchra*.

Acknowledgements

I would like to thank Dr Andrew Farke, Gabe Santos, and Bailey Jorgensen (Raymond M. Alf Museum of Paleontology) for their assistance and access to collections. I also appreciate consultation provided by Drs Don Lofgren, Greg Wilson and Heather Smith during the preparation of the manuscript. Additionally, Drs Emily Bamforth and Thomasz Szczygielski provided helpful feedback and guidance that greatly improved the quality of this publication.

References

Adrian B, Smith HF, Hutchison JH, Townsend KEB (2021) Geometric morphometrics and anatomical network analyses reveal ecospace partitioning among geoemydid turtles from the Uinta Formation, Utah. The Anatomical Record 305: 1359–1393. https://doi.org/10.1002/ar.24792

Archibald DJ (1977) Fossil Mammalia and Testudines of the Hell Creek Formation, and the Geology of the Tullock and Hell Creek Formations, Garfield County. University of California, Berkeley.

Archibald DJ (1981) The earliest known Paleocene fauna and its implications for the Cretaceous–Tertiary boundary. Nature 208: 650–652. https://doi.org/10.1038/291650a0

Archibald DJ (1982) A study of Mammalia and geology across the Cretaceous–Tertiary boundary in Garfield County, Montana. University of California Publications in Geological Sciences 122: 1–286.

Archibald DJ, Lofgren DL (1990) Mammalian zonation near the Cretaceous–Tertiary boundary. Geological Society of America, Special Paper 243: 31–50. https://doi.org/10.1130/SPE243-p31

Batsch AJGC (1788) Versuch einer Anleitung, zur Kenntniß und Geschichte der Thiere und Mineralien, für akademische Vorlesungen entworfen, und mit den nöthigsten Abbildungen versehen. Erster Theil. Allgemeine Geschichte der Natur; besondre der Säugthiere, Vögel, Amphibien und Fische. Akademische Buchhandlung, Jena. https://doi.org/10.5962/bhl.title.79854

Brinkman DB, Nicholls EL (1991) Anatomy and relationships of the turtle *Boremys pulchra* (Testudines: Baenidae). Journal of Vertebrate Paleontology 11: 302–315 https://doi.org/10.1080/02724634.1991.10011400

Cifelli RL, Eberle JJ, Lofgren DL, Lillegraven JA, Clemens WA (2004) Mammalian biochronology of the latest Cretaceous. In: Woodburne MO (Ed.) Late Cretaceous and Cenozoic Mammals of North America: Biostratigraphjy and Geochronology. Columbia University Press, New York, 21–42. https://doi.org/10.7312/wood13040-004

Cope ED (1873 [1872]) Descriptions of some new Vertebrata from the Bridger Group of the Eocene. Palaeontological Bulletin 1: 1–6.

Eaton JG, Kirkland JI, Doi K (1989) Evidence of reworked Cretaceous fossils and their bearing on the existence of Tertiary dinosaurs. Palaios 4: 281–286. https://doi.org/10.2307/3514776

Eberth DA, Hamblin AP (1993) Tectonic, stratigraphic, and sedimentologic significance of a regional discontinuity in the upper Judith River Group (Belly River wedge) of southern Alberta, Saskatchewan, and northern Montana. Canadian Journal of Earth Sciences 30: 174–200. https://doi.org/10.1139/e93-016

Fastovsky DE (1987) Paleoenvironments of vertebrate-bearing strata during the Cretaceous-Paleogene transition, eastern Montana and western North Dakota. Palaios 2: 282–295. https://doi.org/10.2307/3514678

Fastovsky DE (1990) Rocks, resolution, and the record: A review of depositional constraints on fossil assemblages at the terrestrial Cretaceous/Paleogene boundary, eastern Montana and western North Dakota. In: Sharpton VL, Ward PD (Eds) Global catastrophes in Earth history: An interdisciplinary conference on impacts, volcanism, and mass mortality. Geological Society of America Special Paper 247: 541–547. https://doi.org/10.1130/SPE247-p541

Gaffney ES (1972) The systematics of the North American family Baenidae (Reptilia, Cryptodira). Bulletin of the American Museum of Natural History 147: 1–84.

Gaffney ES (1975) A phylogeny and classification of the higher categories of turtles. Bulletin of the American Museum of Natural History 155: 387–436.

Gaffney ES (1990) The comparative osteology of the Triassic turtle *Proganochelys*. Bulletin of the American Museum of Natural History 194: 1–263.

Gaffney ES, Hiatt R (1971) A new baenid turtle from the Upper Cretaceous of Montana. American Museum Novitates 2443: 1–9.

Gilmore CW (1916) Contributions to the geology and paleontology of San Juan County, New Mexico. 2. Vertebrate faunas of the Ojo Alamo, Kirtland, and Fruitland formations. United States Geological Survey Professional Paper 98: 279–308. https://doi.org/10.3133/pp98Q

Gilmore CW (1920) New fossil turtles, with notes on two described species. Proceedings of the United States National Museum 56: 113–132. https://doi.org/10.5479/si.00963801.56-2292.113

Gilmore CW (1935) On the Reptilia of the Kirtland Formation of New Mexico, with descriptions of new species of fossil turtles. Proceedings of the United States National Museum 83: 159–188. https://doi.org/10.5479/si.00963801.83-2978.159

Hay OP (1904) On some fossil turtles belonging to the Marsh collection in Yale University Museum. American Journal of Science 18: 261–276. https://doi.org/10.2475/ajs.s4-18.106.261

Holroyd PA, Hutchison JH (2002) Patterns of geographic variation in latest Cretaceous vertebrates: Evidence from the turtle component. Geological Society of America Special Paper 361: 179–190. https://doi.org/10.1130/0-8137-2361-2.177

Holroyd PA, Wilson GP, Hutchison JH (2014) Temporal changes within the latest Cretaceous and early Paleogene turtle faunas of northeastern Montana. In: Wilson GP, Clemens WA, Horner JR, Hartman JH (Eds) Through the end of the cretaceous in the type locality of the Hell Creek Formation in Montana and adjacent areas. Geological Society of America Special Paper, 299–312. https://doi.org/10.1130/2014.2503(11)

Hutchison JH (1984) Determinate growth in the Baenidae (Testudines): Taxonomic, ecologic, and stratigraphic significance. Journal of Vertebrate Paleontology 3: 148–151. https://doi.org/10.1080/02724634.1984.10011968

Hutchison JH (2004) *Goleremys mckennai*, gen. et sp. n., (Baenidae: Testudines) from the Paleocene of California. Bulletin of the Carnegie Museum of Natural History 36: 91–96. https://doi.org/10.2992/0145-9058(2004)36[91:ANEGMG]2.0.CO;2

Hutchison JH, Bramble DM (1981) Homology of the Plastral Scales of the Kinosternidae and Related Turtles. Herpetologica 37: 73–85.

Hutchison JH, Archibald DJ (1986) Diversity of turtles across the Cretaceous/Tertiary boundary in Northeastern Montana. Palaeogeography, Palaeoclimatology, Palaeoecology 55: 1–22. https://doi.org/10.1016/0031-0182(86)90133-1

Hutchison JH, Frye FL (2001) Evidence of pathology in early Cenozoic turtles. Paleobios 21: 12–19.

Hutchison JH, Holroyd PA (2003) Late Cretaceous and early Paleocene turtles of the Denver Basin, Colorado. Rocky Mountain Geology 38: 121–142. https://doi.org/10.2113/gsrocky.38.1.121

Hutchison JH, Knell MJ, Brinkman DB (2013) Turtles from the Kaiparowits Formation, Utah. In: Titus AL, Loewen MA (Eds) At the top of the Grand Staircase: the Late Cretaceous of Southern Utah. Indiana University Press, Bloomington, IN, 295–318.

Joyce WG (2007) Phylogenetic relationships of Mesozoic turtles. Bulletin of the Peabody Museum of Natural History 48: 1–102. https://doi.org/10.3374/0079-032X(2007)48[3:PROMT]2.0.CO;2

Joyce WG (2017) A review of the fossil record of basal Mesozoic turtles. Bulletin of the Peabody Museum of Natural History 58: 65–113. https://doi.org/10.3374/014.058.0105

Joyce WG, Lyson TR (2015) A review of the fossil record of turtles of the clade Baenidae. Bulletin of the Peabody Museum of Natural History 56: 147–183. https://doi.org/10.3374/014.056.0203

Joyce WG, Parham JF, Gauthier JA (2004) Developing a protocol for the conversion of rank-based taxon names to phylogenetically define clade names, as exemplified by turtles. Journal of Paleontology 78: 989–1013. https://doi.org/10.1666/0022-3360(2004)078%3C0989:DAPFTC%3E2.0.CO;2

Joyce WG, Parham JF, Anquetin J, Claude J, Danilov IC, Iverson JB, Kear BP, Lyson TR, Rabi M, Sterli J (2020) Testudines. In: de Queiroz K, Cantino PD, Gauthier JA (Eds) Phylonyms– A companion to the PhyloCode. CRC Press, Boca Raton, 1049–1051. https://doi.org/10.1201/9780429446276

Joyce WG, Anquetin J, Cadena E-A, Claude J, Danilov IC, Evers SW, Ferreira GS, Gentry AD, Georgialis G, Lyson TR, Pérez-García A, Rabi M, Sterli J, Vitek NS, Parham JF (2021) A nomenclature for fossil and living turtles using phylogenetically defined clade names. Swiss Journal of Palaeontology 140: 1–45. https://doi.org/10.1186/s13358-020-00211-x

Lambe LM (1902) New genera and species from the Belly River Series (mid-Cretaceous). Contributions to Canadian Paleontology 3: 25–81.

Lambe LM (1906a) Boremys, a new chelonian genus from the Cretaceous of Alberta. Ottawa Naturalist 19: 232–234.

Lambe LM (1906b) Description of new species of *Testudo* and *Baëna* with remarks on some Cretaceous forms Ottawa Naturalist 19: 232–234.

Lambe LM (1914) On a new species of *Aspideretes* from the Belly River Formation of Alberta, with further information regarding the structure of the carapace of *Boremys pulchra*. Transactions of the Royal Society of Canada 8: 11–16. https://doi.org/10.5962/bhl.title.62151

Laurin M, de Queiroz K, Cantino P, Cellinese N, Olmstead R (2005) The PhyloCode, type, ranks, and monophyly: a response to Pickett. Cladistics 21: 605–607. https://doi.org/10.1111/j.1096-0031.2005.00090.x

Lichtig AJ, Lucas SG (2017) Sutures of the shell of the Late Cretaceous-Paleocene baenid turtle *Denazinemys*. Neues Jahrbuch für Geologie und Paläontologie - Abhandlungen 283: 1–8. https://doi.org/10.1127/njgpa/2017/0622

Lively JR (2013) New baenid turtles from the Cretaceous Kaiparowits Formation of southern Utah: Implications for Laramidian biogeography. Masters Thesis, University of Utah, Salt Lake City, Utah, USA.

Lively JR (2016) Baenid turtles of the Kaiparowits Formation (Upper Cretaceous: Campanian) of southern Utah, USA. Journal of Systematic Palaeontology 14: 891–918. https://doi.org/10.1080/14772019.2015.1120788

Lofgren DL (1995) The Bug Creek problem and the Cretaceous–Tertiary transition at McGuire Creek, Montana. University of California Publications Geological Sciences 140: 1–185.

Lyson TR, Joyce WG (2009a) A new species of *Palatobaena* (Testudines: Baenidae) and a maximum parsimony and bayesian phylogenetic analysis of Baenidae. Journal of Paleontology 83: 457–470. https://doi.org/10.1666/08-172.1

Lyson TR, Joyce WG (2009b) A revision of *Plesiobaena* (Testudines: Baenidae) and an assessment of baenid ecology across the K/T boundary. Journal of Paleontology 83: 833–853. https://doi.org/10.1666/09-035.1

Lyson TR, Joyce WG, Knauss GE, Pearson DA (2011) *Boremys* (Testudines, Baenidae) from the latest Cretaceous and Early Paleocene of North Dakota: An 11-million-year range extension and an additional K/T survivor. Journal of Vertebrate Paleontology 21: 729–737. https://doi.org/10.1080/02724634.2011.576731

Lyson TR, Sayler JL, Joyce WG (2019) A new baenid turtle, *Saxochelys gilberti*, gen. et sp. nov., from the uppermost Cretaceous (Maastrichtian) Hell Creek Formation: Sexual dimorphism and spatial niche partitioning within the most speciose group of Late Cretaceous turtles. Journal of Vertebrate Paleontology 39: e1662428. [1–18] https://doi.org/10.1080/02724634.2019.1662428

Lyson TR, Petermann H, Toth N, Bastien S, Miller IM (2021) A new baenid turtle, *Palatobaena knellerorum* sp. nov., from the lower Paleocene (Danian) Denver Formation of south-central Colorado, U.S.A. Journal of Vertebrate Paleontology: e1925558. https://doi.org/10.1080/02724634.2021.1925558

McKenna MC (1965) Collecting microvertebrate fossils by washing and screening. In: Kummer B, Raup D (Eds) Handbook of Paleontological Techniques. W.H. Freeman, San Francisco, 193–203.

McKnight DT, Wirth W, Schwarzkopf L, Nordberg EJ (2021) Leech removal is not the primary driver of basking behavior in a freshwater turtle. Ecology and Evolution 11: 10936–10946. https://doi.org/10.1002/ece3.7876

Moura JF, Nascimento CSI, Peixoto BdCPeM, de Barros GEB, Robbi B, Fernandes MA (2021) Damaged armour: Ichnotaxonomy and paleoparasitology of bioerosion lesions in osteoderms of Quaternary extinct armadillos. Journal of South American Earth Sciences 109: 103255. https://doi.org/10.1016/j.jsames.2021.103255

Parks WA (1933) New species of dinosaurs and turtles from the Upper Cretaceous formations of Alberta. University of Toronto Studies, Geological Series 34: 3–33.

Rasband WS (1997–2016) ImageJ. U. S. National Institutes of Health, Bethesda, MD, USA.

Readel AM, Phillips CA, Wetzel MJ (2008) Leech parasitism in a turtle assemblage: Effects of host and environmemtal characteristics. Copeia 2008: 227–233. https://doi.org/10.1643/CH-06-212

Ryan JR, Lambert A (2005) Prevalence and colonization of *Placobella* on two species of freshwater turtles (*Graptemys geographica* and *Sternotherus odoratus*). Journal of Herpetology 39: 284–287. https://doi.org/10.1670/180-04N

Sato K, Jenkins RG (2020) Mobile home for pholadoid boring bivalves: First example from a Late Cretaceous sea turtle in Hokkaido Japan. Palaois 35: 228–236. https://doi.org/10.2110/palo.2019.077

Sawyer RT (1986) Ecology of freshwater leeches. In: Sawyer RT (Ed.) Leech Biology and Behaviour. Clarendon Press, Oxford, 524–590.

Scheyer TM (2007) Comparative bone histology of the turtle shell (carapace and plastron): implications for turtle systematics, functional morphology and turtle origins. PhD Thesis, University of Bonn, Bonn, Germany.

Siddall ME, Gaffney ES (2004) Observations on the leech *Placobdella ornata* feeding from bony tissue of turtles. The Journal of Parasitology 90: 1186–1188. https://doi.org/10.1645/GE-277R

Sloan RE, Van Valen L (1965) Cretaceous mammals from Montana. Science 148: 220–227. https://doi.org/10.1126/science.148.3667.220

Storer JE (1991) The mammals of the Gryde local fauna, Frenchman Formation (Maastrichtian: Lancian), Saskatchewan. Journal of Vertebrate Paleontology 11: 350–369. https://doi.org/10.1080/02724634.1991.10011403

Sullivan RM, Jasinkski SE, Lucas SG (2013) Re-Assessment of Late Campanian (Kirtlandian) turtles from the Upper Cretaceous Fruitland and Kirtland Formations, San Juan Basin, New Mexico. In: Brinkman DB, Gardner JD, Holroyd PA (Eds) Morphology and Evolution of Turtles. Springer Science & Business Media, Dordrecht, 337–386. https://doi.org/10.1007/978-94-007-4309-0_20

Szczygielski T, Sulej T (2019) The early composition and evolution of the turtle shell (Reptilia, Testudinata). Palaeontology 62: 375–415. https://doi.org/10.1111/pala.12403

Telford Jr SR (1984) Haemoparasites of reptiles. In: Hoff GL, Frey FL, Jacobson ER (Eds) Diseases of Amphibians and Reptiles. Plenum Press, New York, 385–518. https://doi.org/10.1007/978-1-4615-9391-1_20

Walker JWF (1973) The locomotor apparatus of Testudines. In: Gans C, Parsons TS (Eds) Biology of the Reptilia. Academic Press, New York, NY, 1–51.

Wilson GP (2014) Mammalian extinction, survival, and recovery dynamics across the Cretaceous-Paleogene boundary in northeastern Montana, USA. The Geological Society of America Special Paper 503: 365–392. https://doi.org/10.1130/2014.2503(15)

Zhu H (2011) Plastron reduction and associated myology in turtles, and its implications for functional morphology and natural history. Masters Thesis, Marshall University, Huntington, West Virginia, USA.

Zonneveld J-P, Bartels WS, Gunnell GF, McHugh LP (2016) Borings in early Eocene turtle shell from the Wasatch Formation, South Pass, Wyoming. Journal of Paleontology 89: 802–820. https://doi.org/10.1017/jpa.2015.61

Zonneveld J-P, AbdelGawad MK, Miller ER (2021) Ectoparasitic borings, mesoparasitic borings, and scavenging traces in early Miocene turtle and tortoise shell: Moghra Formation, Wadi Moghra, Egypt. Journal of Paleontology 96: 304–322. https://doi.org/10.1017/jpa.2021.92

Fossil Record 25 (2) 2022, 287–305 | DOI 10.3897/fr.25.82469

PENSOFT

für Natur MUSEUM FÜR NATURKUNDE BERLIN

A case of frozen behaviour: A flat wasp female with a beetle larva in its grasp in 100-million-year-old amber

Christine Kiesmüller[1], Joachim T. Haug[2,3], Patrick Müller[4], Marie K. Hörnig[1]

1 *University of Greifswald, Zoological Institute and Museum, Cytology and Evolutionary Biology, Soldmannstr. 23, 17489 Greifswald, Germany*
2 *Ludwig-Maximilians-Universität München (LMU Munich), Biocenter, Großhaderner Str. 2, 82152 Planegg-Martinsried, Germany*
3 *GeoBio-Center der LMU München, Richard-Wagner-Str. 10, 80333 München, Germany*
4 *Kreuzbergstr. 90, 66482 Zweibrücken, Germany*

https://zoobank.org/D5DB0BBC-B925-40D3-8F67-56C69C54AC36

Corresponding author: Christine Kiesmüller (christine.kiesmueller@palaeo-evo-devo.info)

Academic editor: Alexander Schmidt ♦ **Received** 18 February 2022 ♦ **Accepted** 25 August 2022 ♦ **Published** 16 September 2022

Abstract

Parasitism, a malignant form of symbiosis, wherein one partner, the parasite, derives benefits to the detriment of another, the host, is a widespread phenomenon. Parasitism sensu lato is understood here to include many phenomena, like parasitoidism, kleptoparasitism, phoresy and obligate parasitism. Insecta has many in-groups that have evolved a parasitic life-style; one of the largest in-groups of these is probably the group of Hymenoptera. Bethylidae, the group of flat wasps, is a smaller in-group of Aculeata, the group of hymenopterans with venom stings; representatives of Bethylidae are parasitic. They are more specifically larval ectoparasitoids, meaning that their immature stages are externally developing parasites that kill their host organism at pupation (end of interaction). They mostly parasitise immature representatives of Coleoptera and Lepidoptera. Female flat wasps search for a host for their progeny, paralyse it with their venom sting and then oviposit onto it.

Herein we describe one of the oldest findings of parasitic interactions of parasitoid wasps with their progenies' hosts, specifically a flat wasp female grasping and (potentially) stinging a beetle immature in Cretaceous Kachin (Myanmar) amber (ca. 100 million years old). This finding indicates that this type of parasitic interaction existed since the Cretaceous, temporally close to the earliest findings of representatives of Bethylidae.

Key Words

Bethylidae, Coleopteran larva, Kachin amber, parasitism, parasitoid wasp, syninclusion

Introduction

Reconstruction of behaviour of extinct organisms

Studying behaviour and trophic interactions of extinct animals can only be done indirectly amid demands for several different approaches (see below; Hörnig et al. 2022) and combinations of these. Spatially close fossilisations of several individuals of the same or different species (group fossilisation), e.g. as syninclusions in amber, are especially interesting in this context, as they can give valuable hints to biotic interactions. Group fossilisation of individuals of different species can indicate predator-prey interactions and thus can help to reconstruct food-webs, but is rarely discussed in this context in the fossil record (examples below; see discussion in Hörnig et al. 2020; Haug JT et al. 2022). Some of these cases of group fossilisation can also fall into the category of the so-called 'frozen behaviour' (Boucot 1990; examples in e.g. Arillo 2007; Boucot and Poinar 2010; Hsieh and Plotnik 2020).

Frozen behaviour refers to "behaviorally critical specimens in which an organism(s) is preserved while actually doing something (such as two insects in copula)" (Boucot 1990, p. 3), which thus may provide insight into potential behavioural patterns. This 'best case scenario' is, however, not widely preserved in the fossil record. Within

euarthropods, especially cases of insects preserved in amber have been documented, e.g. during mating (Weitschat and Wichard 2002; Grimaldi and Engel 2005; Weitschat 2009; Boucot and Poinar 2010; Gröhn 2015; Fischer and Hörnig 2019), hatching (Weitschat 2009; Boucot and Poinar 2010; Gröhn 2015; Hörnig et al. 2019; Pérez-de la Fuente et al. 2019), feeding (Grimaldi 1996; Weitschat and Wichard 2002; Boucot and Poinar 2010; Gröhn 2015; Wang et al. 2016; Hörnig et al. 2020) and other behaviours (Boucot and Poinar 2010; Hsieh and Plotnik 2020).

There are also more indirect indications of behaviour or lifestyles that can be preserved in the fossil record. Trace fossils (ichnofossils; e.g. fossilised animal tracks) or feeding damage (on animals or plants) can be indicators for behaviour (compare e.g. Hsieh and Plotnik 2020 and references therein; but see e.g. Hasiotis 2003 for limitations of ichnofossils specifically). Functional morphology can also provide insight into potentially exhibited behaviours by comparison with extant organisms with similar morphologies to the fossilized organism (Reif 1983; Thomason 1997; Haug JT et al. 2012; Hörnig et al. 2016, 2018). Though if the fossil is e.g. only incompletely preserved and no inferences from functional morphology (or other indications mentioned above) can be made, the concept of the 'extant phylogenetic bracket' (Witmer 1995) can be used to estimate potentially exhibited behavioural patterns by comparing the fossilised organism with its closest extant relatives. The reliability of these approaches varies considerably for every case, however, and a combination of several approaches discussed thoroughly is useful for the reconstruction of behavioural aspects of extinct organisms (Hörnig et al. 2013, 2017, 2018, 2022; Zippel et al. 2021).

With regard to ancestral food webs, reliable reconstruction of predator-prey interactions based on cases of group fossilisation is challenging and often remains speculative. More obvious are examples where the individuals are in direct contact for extended time spans, as is often the case for parasites and their host(s).

Parasitism—a multitude of concepts

Finding clear characteristics of parasitism appears to be difficult (van der Wal and Haug JT 2019). There are many characterisations, "probably as many […] as there are books on parasitism" (Price 1980, p. 4). Most of these characterisations have in common that parasitism sensu lato (s.l.) is an interaction between two organisms wherein one (the parasite) derives benefits (mostly nutrients) and the other (the host) detriments from the interaction, including also that the parasite has certain morphological adaptations to such a lifestyle (e.g. Price 1980; Paracer and Ahmadjian 2000; Daintith and Martin 2010; Goater et al. 2014). Some authors also include the intimacy or dependency of the interaction into their characterisation (e.g. Olsen 1974).

These more general characterisations of parasitism have the consequence that they include phenomena that have been traditionally separate (e.g. herbivory) (as discussed in Poulin 2011; van der Wal and Haug JT 2019). Furthermore, parasitism is frequently seen as a trophic interaction (e.g. Grissell 1999; Lafferty and Kuris 2002; Goater et al. 2014). This may be true for most organisms that are called parasites (or derivatives of that), but some phenomena, especially within social (Wheeler 1928; Lucius et al. 2017) or behavioural (Poulin 2011) parasitism (e.g. kleptoparasitism or better kleptobiosis, but cf. Breed et al. 2012, brood parasitism (Litman 2019)) are not trophic interactions but interactions on the same trophic level (like e.g. competition; Nentwig et al. 2017).

There are many different approaches in how to differentiate between different types of parasites (s.l.). There are e.g. obligate versus facultative parasites, life-stage dependent parasites (larval versus adult parasites), temporary versus periodic versus permanent parasites (based on the length of interaction between parasite and host) or based on the cost of the parasitic interaction for the host (e.g. kleptobiosis, phoresy versus parasitic castrators, parasitoids) (compare e.g. Rothschild and Clay 1957). Parasitoids e.g. reduce their host's fitness to zero by killing them at the end of their interaction and thus costing the host immensely.

A parasite can belong to multiple of these subdivisions at the same time; e.g. representatives of Strepsiptera (especially of Mengenillidae) are obligate, larval endoparasitic castrators (e.g. Kathirithamby 2009). There are a few works that tried to unite all these concepts into one (Lafferty and Kuris 2002; Poulin 2011), but these works have focused mainly on parasitism as a trophic interaction and thus excluded other forms that are associated with parasitism (Poulin 2011). Here, we understand parasitism s.l. in its widest characterisation, including phenomena such as social parasitism, parasitoidism, phoresy and, of course, parasitism sensu stricto, which includes (mostly) permanent and obligate parasites.

Flat wasps and their parasitoid immatures

Flat wasps (Bethylidae) are rather small wasps of about 1–20 mm body length (Azevedo et al. 2018) that owe their common name to their dorso-ventrally flattened body. They are an in-group of Aculeata (wasps with venom sting), wherein they are part of Chrysidoidea. Together with their sister-group Chrysididae, flat wasps account for most species within Chrysidoidea today (Goulet and Huber 1993; but see e.g. Haug JT et al. 2016 for the logical incorrectness of this statement).

The oldest known flat wasp fossils are from the Lower Cretaceous (ca. 130 million years old), with at least twenty-two described species so far (amber only), half of which are from Myanmar amber (Azevedo et al. 2018; Engel 2019; Colombo et al. 2020; Jouault et al. 2020, 2021; Jouault and Brazidec 2021; see also Lepeco and Melo 2021

for taxonomic changes within fossil Bethylidae). Beyond this, they have been also abundant in Cenozoic Lagerstätten (ca. 66 million years old) (e.g. Brues 1939).

Flat wasps are larval parasitoids of holometabolan insect immatures (mostly coleopteran and lepidopteran larvae) and their adults are mostly smaller than their future offspring's hosts (Gauld and Bolton 1988), which the females paralyse with their venom sting (Powell 1938; Finlayson 1950; Schaefer 1962; Evans 1964; Kühne and Becker 1974; Gordh and Medved 1986; Griffiths and Godfray 1988; Abraham et al. 1990; Howard et al. 1998). Since the host immatures often occur in more cryptic or concealed habitats, like soil, stems, wood or seeds (Evans 1964; Gauld and Bolton 1988; Howard and Flinn 1990), flat wasp adults may show additional adaptations for entering these habitats (Williams 1919; Gordh and Medved 1986), such as fossorial (digging, burrowing) forelegs and reduced wings (Evans 1964). Some flat wasps even exhibit subsocial behaviours (Evans 1964), additional (to parasitoidism) maternal care (Casale 1991; Hu et al. 2012; Yang et al. 2012; Tang et al. 2014) and many engage in prey carriage and some also in a sort of nest building (Finlayson 1950; Evans 1964; Rubink and Evans 1979; Howard et al. 1998; for review of prey carriage in wasps in general see e.g. Evans 1962). Yet, studies of behaviour and also their biology at large are mostly restricted to species of agricultural importance, as their immatures parasitise some crop and storage pests (Kühne and Becker 1974; Gordh and Hawkins 1981; Gordh 1998; Cheng et al. 2004; Gao et al. 2016; Jucker et al. 2020).

The immatures' host is often permanently paralysed (Finlayson 1950; Schaefer 1962; Lauzière et al. 2000; Amante et al. 2017; but there are exceptions: e.g. Kühne and Becker 1974; Gordh and Medved 1986; Witethom and Gordh 1994; Mayhew and Heitmans 2000); the flat wasp female then either carries them away to a sort of nest, where they can accumulate multiple potential host individuals for their progeny, or they oviposit onto them on site. The emerging immature(s) either attaches itself to its host or the mother bites the immatures' host to provide the immature easier access for feeding (e.g. Kühne and Becker 1974; Hu et al. 2012). The immature develops externally on its host as an ectoparasitoid and eventually kills it before it pupates (Powell 1938; Schaefer 1962; Kühne and Becker 1974; Gordh and Hawkins 1981; Abraham et al. 1990; Casale 1991; Cheng et al. 2004).

Here we report a flat wasp female that is supposedly in the process of stinging a coleopteran immature, as syninclusions in 100-million-year-old Kachin (Myanmar) amber.

Material and methods

Material

The study is based on one piece of amber from Kachin State (Myanmar) ("Burmese amber"), which is part of the State Natural History Museum, Braunschweig (Staatliches Naturhistorisches Museum Braunschweig), stored under the accession number SNHM-6014. The piece was legally purchased by one of the authors (PM) in 2016.

The amber originates from the Noije Bum hill locality, in the Southwest corner of the Hukawng Valley in Kachin State, Northern Myanmar, South Asia. The amber locality was 'first' discovered (by Europeans) and intensively mined in the 19th and 20th century (Poinar 2019; Cruickshank and Ko 2003; Zherikhin and Ross 2000). It was assumed to be Eocene (33.9–56 million years old) (Chhibber 1934 in Grimaldi et al. 2002) to Miocene (3–23 million years old; Noetling 1893) in age, although Cockerell (1917a, 1917b) already questioned this, given numerous insect inclusions representing exclusively Mesozoic (66–252 million years old) groups (also discussed in Cruickshank and Ko 2003; Shi et al. 2012). In addition, an enclosed ammonite (Yu et al. 2019) as well as zircon dating (Shi et al. 2012) and the (potential) Cretaceous age of the embedding rock matrix (Cruickshank and Ko 2003) support the now widely accepted Cenomanian to Albian age (mid-Cretaceous; 94–113 million years old) of the amber.

The Hukawng Valley locality is a major Lagerstätte of Cretaceous amber in Southeastern Asia and contains a very diverse (palaeo-)biota (Grimaldi et al. 2002; Ross 2021). The palaeoenvironment of Kachin amber has been postulated to be subtropical to tropical (Grimaldi et al. 2002; Yu et al. 2019) consistent with its near equatorial (palaeo-)latitude (Grimaldi et al. 2002; Martínez-Delclòs et al. 2004), potentially nearshore, marine or lagoon (Cruickshank and Ko 2003; Yu et al. 2019) and potentially part of the past 'supercontinent' Gondwana (Poinar 2019).

Methods

The amber piece was photographed using a Keyence VHX-6000 light microscope (equipped with 20–2000 times magnification lenses). In order to reduce reflections and enhance the contrast, the specimens were photographed with a drop of distilled water and an above placed cover slip. Images were recorded in different focal planes (z-stacks) with different illuminations and then combined to a single image with extended field of depth in the microscope's accompanying software.

Additionally, it was photographed with a Canon EOS 70D reflex camera equipped with an MP-E 65 mm macro objective and a Macro Twin Lite MT-24 EX flash light for close-up images. The specimen was mounted and photographed as described above. The generated images (z-stacks) were stacked (fused) with CombineZP and stitched (xy-plane; merged) with Adobe Photoshop CS4 (compare e.g. Haug C et al. 2011).

In addition, the piece was documented with µCT (XRadia MicroXCT-200, Carl Zeiss Microscopy GmbH, Jena, Germany). The tomography was performed with a 4× objective; the X-ray source settings were 40 kV, 200 µA and 8.0 W. The exposure time was 2.5 s; the system-based pixel size is 5.0073 µm, with an image size of 1015 × 1015 px.

The tomographic images were reconstructed with XMReconstructor software (Carl Zeiss Microscopy GmbH, Jena, Germany), resulting in image stacks (TIFF format). Projections were recorded with Binning 2, tomographic images were reconstructed with Binning 1 (full resolution). Volume renderings were performed using Drishti (ver. 2.7) and Amira 6.1; surface reconstructions, as well as horizontal, vertical and longitudinal virtual sections were generated in Amira 6.1. All obtained images were optimised for colour balance, saturation and sharpness and arranged into figures using Adobe Photoshop CS2 and CS4.

Herein we used insect terminology with corresponding neutral euarthropod terminology in brackets, to ensure mutual understanding within the whole arthropod community. Also terminology of Crustacea sensu lato (CT) is pointed out where it differs from insect terminology (IT), as insects are an in-group of Crustacea sensu lato. Special hymenopteran (HY) (after Lanes et al. 2020) and coleopteran terminology (CO) (after Klausnitzer 1978; Crowson 1981) is also pointed out, where necessary and differing from insect terminology.

Results

Description of specimen SNHM-6014

There are two syninclusions in very close proximity in the amber piece: a hymenopteran adult and a coleopteran immature. The walking appendages of the hymenopteran adult appear to hold the coleopteran immature and its stinger is (seemingly) inserted within the coleopteran immature (compare Figs 1–4 for overview and details especially in Figs 5, 6).

Description of the hymenopteran adult

Hymenopteran adult well-preserved on one side (Figs 1, 2, 4), other side with parts of head, thorax and most of the appendages (including wings) not included in the amber piece (compare Fig. 4B,C); about 3 mm long; not depressed, body surface apparently smooth.

Head: Head (ocular segment and post-ocular segments 1–5) about 0.4 mm long and wide; square-shaped in ventral view and ovoid in lateral view; postero-lateral corners (IT: parts of gena) projecting slightly ventrally in lateral view (Fig. 1D); setae sparsely present. Large compound eyes (ocular segment); ovoid in lateral view; with numerous ommatidia (Fig. 1D). Antenna (appendage of post-ocular segment 1; CT: antennula) attached to head anterior to compound eye and very close to mouthparts (Figs 1D, 2A and 4D, turquoise); groove ventral to attachment area discernible; five elements discernible (probably not completely preserved), all elongated rectangular in lateral view; most proximal antenna element 1 (IT: scapus) about 3× wider than long; element 2 (IT: pedicellus) much shorter and about as wide as long; elements 3–5 (IT: flagellomeres 1–3) as wide as long, though slightly smaller than the pedicellus.

Mouth parts: labrum (sclerite of ocular segment) and appendages of post-ocular segments 3–5 attached and directed anteriorly (head prognathous (IT); compare with Figs 1D, 2A, 4D):

Labrum (sclerite of ocular segment) not discernible. Clypeus (associated sclerite of labrum) triangular in frontal view (Fig. 4D), with potentially ridge (HY: median clypeal carina) medially.

Mandibles (appendages of post-ocular segment 3) (Fig. 4D, indigo blue) rectangular in frontal view with rounded corners; median edge with about 4 discernible protrusions (IT: teeth) medially, overlapping medially about one third its width; each mandible about 1.5× wider than long. Further associated structures (hypopharynx; CT: paragnaths) not discernible. Space between attachment of mandibles and compound eye (HY: malar space) short, less than half the proximal width of the mandible.

Of the maxilla (appendage of post-ocular segment 4; CT: maxillula) only distal part (IT: maxillary palp) discernible (Fig. 4D, bluish violet); 5 elements of maxillary palp discernible, all elongated rectangular in frontal view with rounded corners; element 1(?)–2 of maxillary palp about 2× longer than wide, but element 1(?) potentially not entirely discernible; elements 3–5(?) of maxillary palp all about 3× longer than wide; most distal element 5(?) of maxillary palp with rounded tip.

Of the labium (appendage of post-ocular segment 5; CT: maxilla) also only distal parts (IT: labial palps) discernible (Fig. 4D, reddish violet), median parts concealed underneath mandibles; at least 2 elements of labial palp discernible, also both rectangular with rounded corners in frontal view; element 1(?) of labial palp about 2× longer than wide, but potentially not entirely discernible; element 2(?) of labial palp about 3× longer than wide with rounded, but blunt tip.

Mesosoma (anterior trunk tagma): Post-ocular segments 6–9 (HY: mesosoma, IT: thorax and first abdomen segment) altogether ovoid with tapering, pronounced tips in lateral view (Figs 1, 2, 4); about 1 mm long and 0.4 mm wide at its widest; only sparsely setae present, where discernible; laterally on thorax with large structure discernible mostly in volume rendering of µCT-images (Figs 4, 5C, 8) (probably artefact caused by leaked out body fluids during taphonomic processes; compare also with Fig. 1A), obscuring lateral thorax view.

Prothorax (post-ocular segment 6) dorsally apparently trapezoid with two right angles medially (as discernible); ventrally one half of the sclerite (HY: propleuron) also trapezoid with two right angles medially, sclerites conjoined medially; sternite (IT/HY: prosternum) not discernible medially.

First walking appendage (IT: foreleg) attached posteriorly to propleura; about 1.4 mm long; 5 major elements discernible; element 1 (IT: coxa) trapezoid with rounded corners, two right angles medially in anterior view, proximal edge about 2× longer than distal edge; element 2

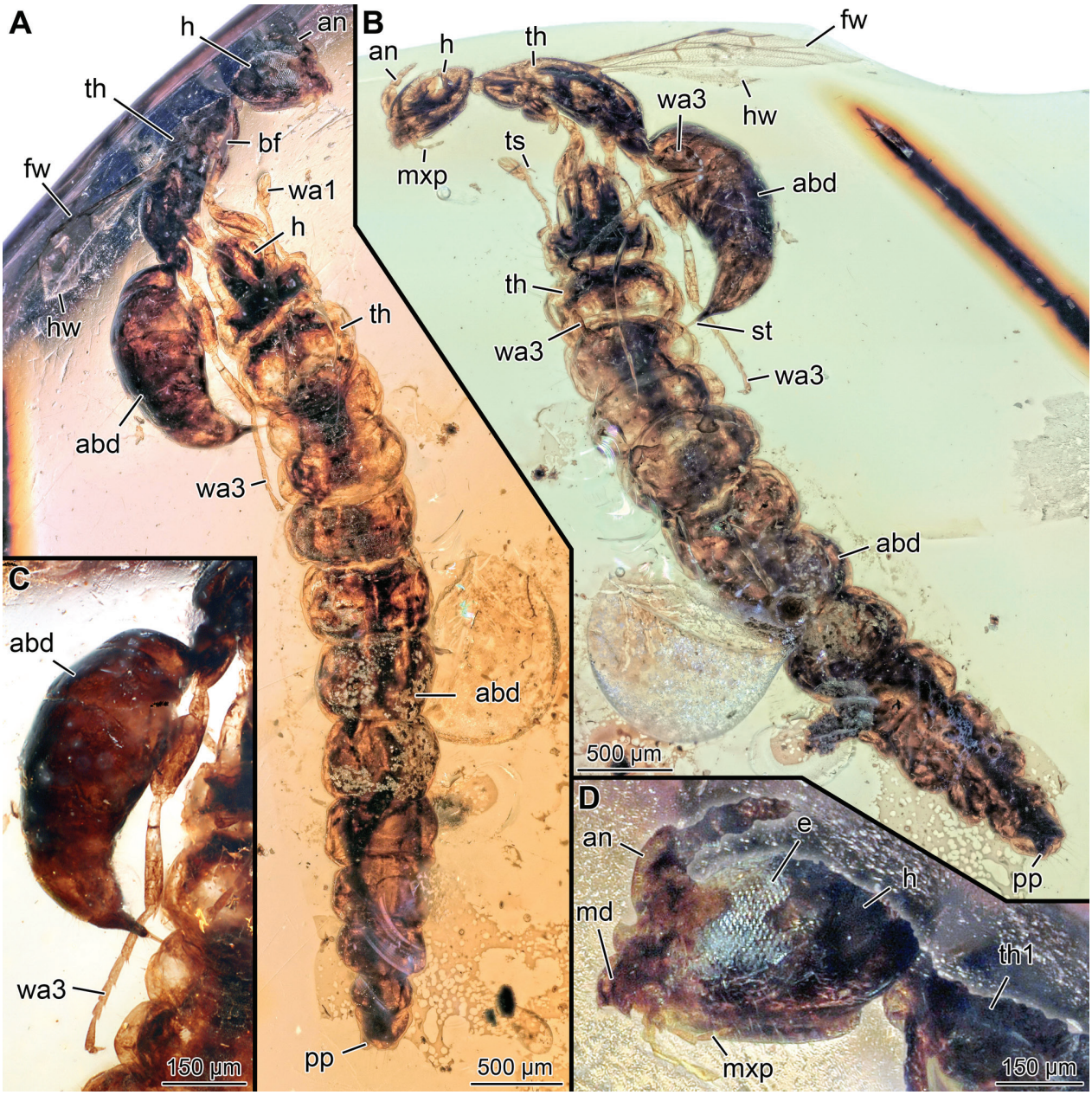

Figure 1. Photograph of amber piece SNHM-6014 with an adult hymenopteran and an immature coleopteran. **A.** Overview side 1 (coleopteran immature in dorsal, hymenopteran adult in lateral view); **B.** Overview side 2 (coleopteran immature in ventral, hymenopteran adult in lateral view); **C**. Detail of hymenopteran adult stinging coleopteran immature (side 1); **D**. Detail hymenopteran head (side 1), mirrored. **abd** – abdomen; **an** – antenna; **bf** – leaked body fluid; **e** – complex eye; **fw** – forewing; **h** – head; **hw** – hind wing; **pp** – pygopodium/postpedes; **th** – thorax; **ts** – tibial spur; **st** – sting (modified ovipositor of hymenopterans); **wa** – walking appendage.

(IT: trochanter) elongated ovoid in lateral view, widening distally to about 2× proximal width, about 4× longer than wide at its narrowest; element 3 (IT: femur) elongated ovoid in lateral view, more than 2× longer than wide at its widest; element 4 (IT: tibia) elongated rectangular with rounded corners in lateral view, more than 4× longer than wide, with one large spine (IT: tibial spur; HY: calcar, i.e. antenna cleaning apparatus) at its median distal corner and more distally a smaller spine with a quarter the length of the larger spine; element 5 (IT: tarsus) subdivided into 5 elements, all rectangular in lateral view; tarsus element 1 by far longest, with two setae at its most distally and about 4× longer than wide; tarsus element 2 slightly longer than wide; tarsus elements 3–4 both as long as wide and thus more square-shaped; tarsus element 5 more trapezoid than rectangular in lateral view with a wider distal than proximal edge and more than 2× longer than wide, with distally two claws and rounded structure in between (IT: arolium), not discernible whether claws simple or with median protrusions (IT/HY: teeth); foreleg with sparse setae.

Mesothorax (post-ocular segment 7) dorsally rectangular (not entirely discernible due to preservation), potentially slightly longer than wide. Dorsally, forewings

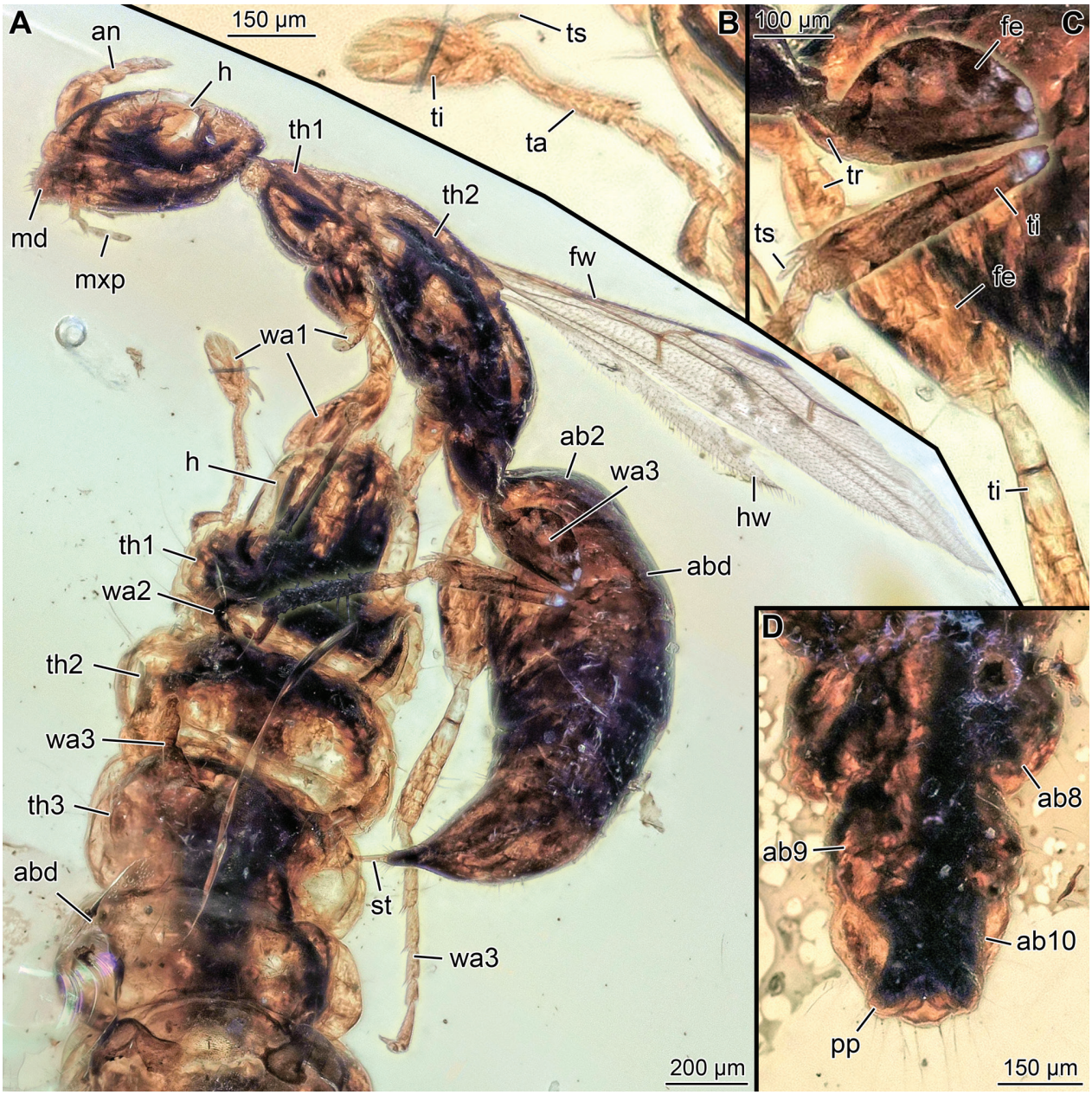

Figure 2. Detailed view on hymenopteran adult of Fig. 1 (side 2). **A.** Close-up overview of hymenopteran adult; **B.** Detailed view on distal part of first walking appendage shown in A; **C.** Detailed view on proximal part of third walking appendage of hymenopteran adult; **D.** Detailed view on posterior end of abdomen of the coleopteran immature. **ab** – abdomen segment; **abd** – abdomen; **an** – antenna; **fe** – femur; **fw** – forewing; **h** – head; **hw** – hind wing; **md** – mandible; **mxp** – maxillary palp; **pp** – pygopodium/postpedes; **th** – thorax; **ti** – tibia; **tr** – trochanter; **ts** – tibial spur; **st** – sting (modified ovipositor of hymenopterans); **wa** – walking appendage.

attaching at border between (possibly) artefactual structure and dorsal sclerite; one forewing preserved, but incomplete (distal part missing, including vein of poststigmal abscissa of $R1_2v$); anterior edge of wing straight (where preserved); vein C_2v not clearly visible; pterostigma (thickened and dark patch at the end of R1) present distally on the anterior edge and elongate ovoid in lateral view; at least four closed cells (encased on all sites by veins) present (R_2c, $1R1_2c$, $1M_2c$ and $1Cu_2c$); additionally cell C_2c potentially obscured, cell $2R1_2c$ distally not preserved (but presumed closed); cell $2Cu_2c$ apparently open; cell $1R1_2c$ pentagonal in dorsal view; all veins apparently tubular (i.e. with distinctly apparent hollow interior), except potentially present vein M_2v (vein $Rs+M_2v$ distally apparently splitting in anterior Rs_2v vein and posteriorly into two M_2v veins (potentially reaching wing margin, though also potentially folding pattern)) and potentially also A_2v; setae all over forewing; longer setae at the anterior and posterior edge.

Mesopectus (sclerite on ventral side of post-ocular segment 7) rectangular, probably 2× wider than long (incompletely preserved); second walking appendage (IT: midleg) attached latero-posteriorly to mesopectus, about 1.3 mm long; coxa circular in anterior view, about as wide

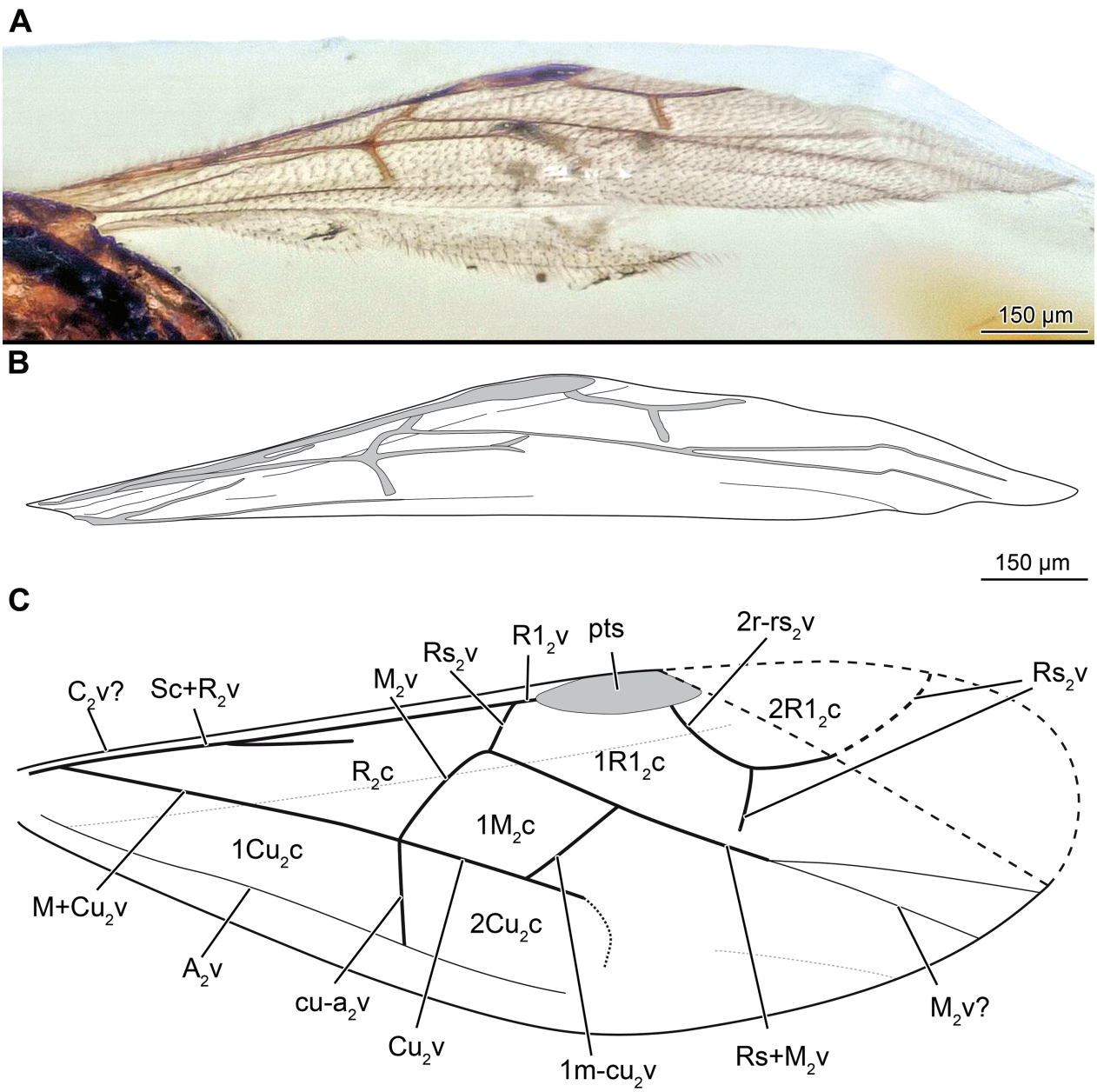

Figure 3. Forewing of hymenopteran adult. **A.** Photograph in dorso-posterior view on forewing; **B.** Drawing of A; **C.** Reconstruction of wing shown in A, B. **1Cu$_2$c** – First cubital cell; **1M$_2$c** – First medial cell; **1R1$_2$c** – First radial cell 1; **2Cu$_2$c** – Second cubital cell; **2R1$_2$c** – Second radial cell 1; **2r-rs$_2$v** – Second radial cross vein; **A$_2$v** – Anal vein; **C$_2$v** – Costal vein (note that it was not discernible in A); **Cu$_2$v** – Cubital vein; **cu-a$_2$v** – cubito-anal vein; **pts** – pterostigma; **M$_2$v** – Median vein; 1**m-cu$_2$v** – medio-cubital vein; **M+Cu$_2$v** – Median+Cubital vein; **R1$_2$v** – prestigmal abscissa of radial vein 1 (in this case); **R$_2$c** – Radial cell; **Rs$_2$v** – radial sector veins; **Rs+M$_2$v** – Radial sector + Median vein; **Sc+R$_2$v** – Subcostal + Radial vein.

as long; trochanter circular in median view, about one third as long as coxa; femur ovoid in lateral view, about 3× longer than wide; tibia elongated rectangular in lateral view, about 5.5× longer than wide and with no spines, spurs or setae discernible (possibly due to obstructed view in that area); tarsus with 5 elements, overall similar to tarsus of foreleg, setae present mostly at the median distal most corner of at least the three most proximal tarsus elements, further setae not discernible; tarsus element 2–3 about 2× longer than wide; tarsus element 5 similar to that of foreleg, but about 3× longer than wide.

Metathorax (post-ocular segment 8) dorsally rectangular, much wider than long; incompletely preserved laterally and partly covered by a similar artefact as mesothorax (see above). One hind wing present (but incomplete preserved); no wing venation discernible, except one possible vein at anterior edge of hind wing (compare Figs 2A, 3); potentially 'fused' vein of Costa+Subcosta+Radius; setae all over hind wing; longer setae at posterior(?) edge of the wing.

Circular sclerite on ventral metathorax (IT/HY: metasternum or metasternal plate) discernible in between midlegs; third walking appendage (IT: hindleg) attached

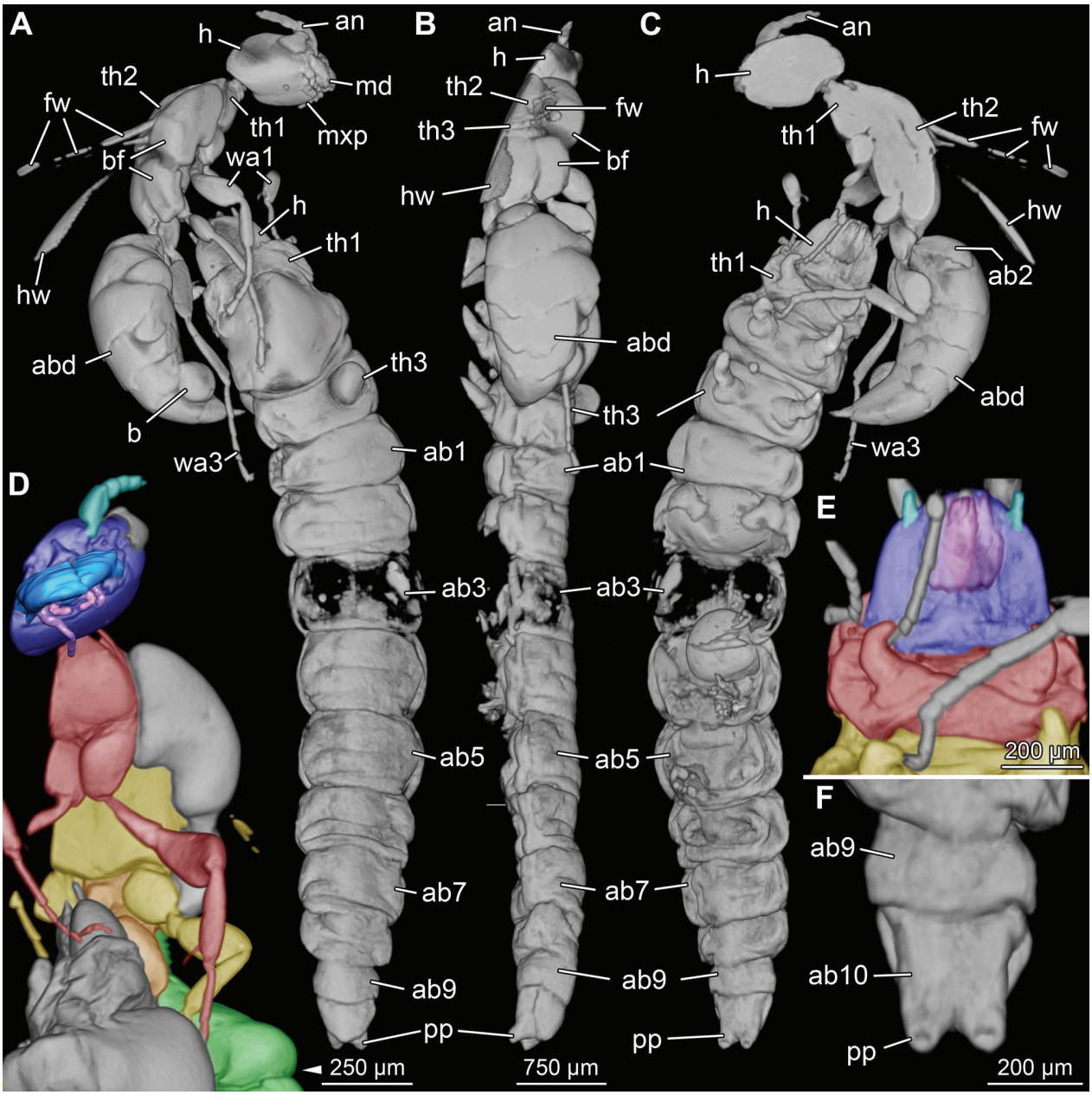

Figure 4. Volume rendering (mostly Drishti 2.7) of µCT of amber piece SNHM-6014. **A–C.** Overview of hymenopteran adult and coleopteran immature; **A.** Dorsal view of coleopteran immature (side 1 of Fig. 1A); **B.** Dorsal view of hymenopteran adult; **C.** Ventral view of coleopteran immature (side 2 of Fig. 1B); **D.** Ventral view of mirrored, colour-marked anterior part of the hymenopteran adult; mouth parts 3D-reconstructed and image of volume rendering taken in Amira 6.1; **blue** – head; **turquoise** – antenna; **indigo blue** – mandible; **violet** – maxilla; **red** – prothorax; **yellow** – mesothorax; **orange** – metathorax; **green** – abdomen. **E.** Detailed colour-marked, ventral view of anterior part of coleopteran immature; same colour-coding as in D. **F.** Detailed, ventral view of mirrored, posterior part of coleopteran immature. **ab** – abdomen segment; **abd** – abdomen; **an** – antenna; **b** = artefact (possible air bubble or similar); **bf** – artefact (possible leaked body fluid or similar); **fw** – forewing; **h** – head; **hw** – hind wing; **md** – mandible; **mxp** – maxillary palp; **pp** – pygopodium/postpedes; **th** – thorax; **wa** – walking appendage.

latero-posteriorly to that ventral sclerite and about 1.6 mm long; coxa ovoid in anterior view, more than 2× longer than wide at its widest; trochanter trapezoid in lateral view with longer posterior edge, about 1.5× longer than wide at its widest; femur ovoid in lateral view, about 2.5× longer than wide at its widest; tibia elongated rectangular in lateral view, widening slightly distally, with two spines of different lengths at its median distal most corner; spine more distally (IT/HY: tibial spur) more than 2× longer than shorter one, tibia about 6× longer than wide at its widest; tarsus with 5 elements, overall similar to tarsus of foreleg, tarsus elements 1–3 each with about two setae at median distal most corner, further setae not discernible, tarsus element 1 6× longer than wide and half as wide as the tibia, tarsus element 2 3× longer than wide, tarsus element 3 more than 3× longer than wide and tarsus element 4 about 2× longer than wide, tarsus element 5 4× longer than wide at its widest.

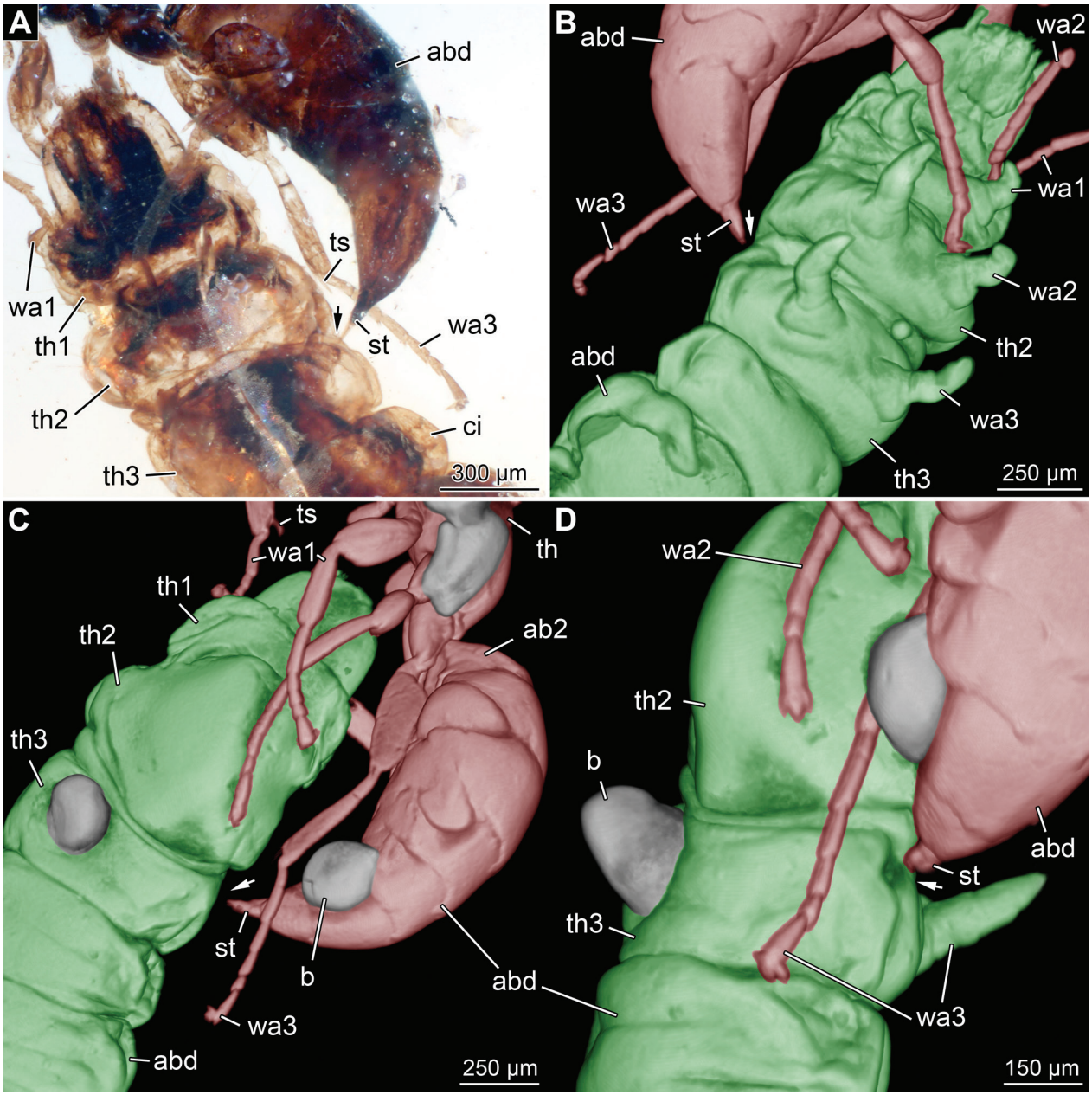

Figure 5. Detail of hymenopteran adult stinging coleopteran immature; arrows point to supposed puncture site. **A.** Photograph in same view as in Fig. 1B; **B–D.** Colour-marked, mirrored volume rendering of µCT of amber piece SNHM-6014 (Drishti 2.7); in **green** coleopteran immature, in **red** hymenopteran adult; **B.** Ventral view of coleopteran immature; **C, D.** Dorsal view of coleopteran immature. **ab** – abdomen segment; **abd** – abdomen; **b** – artefact (possible air bubble or similar); **ci** – coleopteran immature; **st** – sting (modified ovipositor of hymenopterans); **th** – thorax; **ts** – tibial spur; **wa** – walking appendage.

Post-ocular segment 9 (HY: propodeum, IT: abdomen segment 1) only dorsally discernible (HY: metapectal-propodeal complex; note that it is a complex composed of the third thorax and first abdomen segment); rectangular shaped in dorsal view, about 1.5× longer than wide (but incompletely preserved); convexly curved in lateral view and smooth with no posterior spines.

Metasoma (posterior trunk tagma): Metasoma (post-ocular segments 10–19; HY: metasoma segment 1–10; IT: abdomen segments 2–11) attached anteriorly to the mesosoma very ventrally; about 1.6 mm long and 0.5 mm wide at its widest; overall ovoid in lateral view with a very pointy posterior end; curving ventrally, especially posteriorly; only sparsely setae present, where discernible, mostly towards posterior.

Tergite of post-ocular segment 10 (HY: metasoma segment 1; IT: abdomen segment 2) half circular in dorsal view with a small anterior protrusion (petiolate structure; part of the ‘wasp waist’), about 0.2 mm long; sternite circular in ventral view with also small anterior protrusion (petiolate structure); no appendages.

Post-ocular segments 11–14 (HY: metasoma segments 2–5, IT: abdomen segment 3–6) dorsally all rectangular and wider than long; no appendages. Tergite of post-ocular segment 11 (HY: metasoma segment 2; IT: abdomen segment 3) 3× wider than long, 0.25 mm long; sternite of

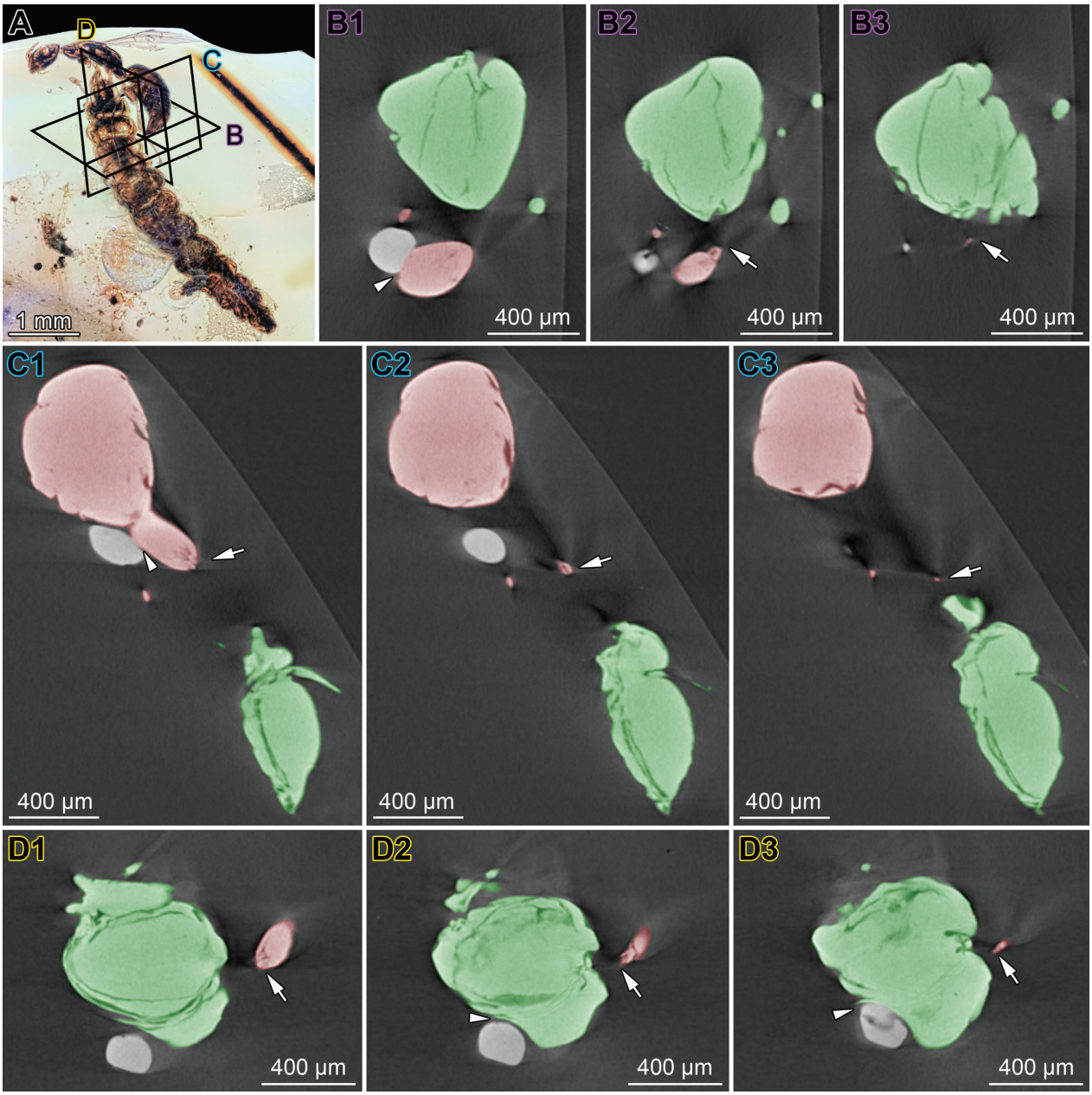

Figure 6. Details of supposed puncture site in the coleopteran immature by the sting of the hymenopteran adult. **A.** Overview photograph; lines within point out section planes of B–D; **B–D.** Colour-marked virtual sections based on µCT of amber piece SNHM-6014 (Amira 6.1); in **green** coleopteran immature, in **red** hymenopteran adult; arrows point towards sting of hymenopteran adult; arrowhead pointing towards connection or disconnection between artefact (possible air bubble or leaked body fluid etc.) and each insect respectively; **B.** Transverse sections through coleopteran immature; 1–3 anterior to posterior sections; **C.** Frontal sections through coleopteran immature; 1–3 dorsal to ventral sections; **D.** Sagittal sections through coleopteran immature; 1–3 lateral to median sections.

post-ocular segment 11 pentagonal with a straight anterior edge and a pointed posterior edge, about as long as wide, tergite wider than sternite, also in subsequent three segments; tergite of post-ocular segment 12 (HY: metasoma segment 3; IT: abdomen segment 4) 2× wider than long, about 0.3 mm long, sternite rectangular, about 3.3× wider than long; tergites of post-ocular segments 13–14 (HY: metasoma segments 4–5; IT: abdomen segments 5–6) about 2.5× wider than long each, metasoma tergite 4 about 0.2 mm long, metasoma tergite 5 about 0.1 mm long, sternites rectangular and 3× wider than long.

Sclerites of post-ocular segments 15–16 (HY: metasoma segments 6–7, IT: abdomen segment 7–8) trapezoid in dorsal view with a longer anterior edge each; dorsal discernible sclerite of abdomen segment 7 slightly wider than long, about 0.2 mm long; dorsal discernible sclerite of abdomen segment 8 1.5× wider than long, 0.08 mm long, ventrally with no apparent segment border between these segments, trapezoid and posterior edge about one quarter width of anterior edge, also no apparent distinction into tergite and sternite; sting (modified ovipositor; appendages of abdomen segments 8 and 9 (post-ocular

segments 16–17; HY: metasoma segments 7–8)) elongated rectangular in lateral view, tapering distally, about 0.2 mm long; consisting of three discernible structures (IT: valvulae), anteriorly broadly connected with abdomen (IT: third valvulae) and posteriorly with distinct sclerotised structure (IT: first and second valvulae; HY: terebra), structure bipartite and side by side without gap, distal tip not discernible.

Description of the coleopteran immature

Coleopteran immature well preserved (compare Figs 1A, B, 2A, D, 4, 5); about 4.7 mm long; slightly dorso-ventral depressed; apparently smooth, but with many very small processes all over the tergites and sternites.

Head: Head (ocular segment and post-ocular segments 1–5) pentagonal in dorsal view with very rounded but pointed anterior edge (Figs 2A, 4E (blue)); about 0.4 mm long and 0.3 mm wide; dorsally potential moult lines discernible (IT/CO: epicranial frontal sutures), area anteriorly to that less than half the length of the head; lateral to ventral sclerite of head (IT: parietale) apparently ventrally not meeting medially, as additional sclerite (CO: gular plate (?)) present there (Figs 2A, 4E); that sclerite overall about trapezoid in ventral view, more than 2× wider than long.

Stemmata (ocular segment) very laterally discernible (but number of ocelli not discernible).

Antenna (appendage of post-ocular segment 1; CT: antennula) about 0.1 mm long; attached laterally on the anterior edge of head (Fig. 4E, turquoise); elongated rectangular in ventral view with 3 elements; antenna element 1 slightly longer than wide; antennal elements 2–3 about as wide as long each; antenna element 3 tapering into a pointed tip and laterally with one seta (CO: supplemental process).

Mouth parts: labrum (sclerite of ocular segment) and appendages of post-ocular segments 3–5 mostly discernible; attached ventrally and directed anteriorly (as is head: prognathous (IT)):

Labrum (sclerite of ocular segment) and mandibles (appendages of post-ocular segment 3) and associated structures not discernible; labrum potentially discernible at tip of head (Fig. 2A), mandibles potentially obscured by posterior mouthparts.

Maxilla (appendage of post-ocular segment 4; CT: maxillula) elongated rectangular in ventral view, with 2 elements; about two thirds the head length (Fig. 4E, bluish violet); proximal element of maxilla (IT: stipes) more than 2× longer than wide, wider than distal element; distal element tapering distally, forking into two tips (probably medially galea and lacinia (IT) and laterally maxillary palp (IT)); about 2× longer than wide at its widest; medially no further structures discernible.

Labium (appendage of post-ocular segment 5; CT: maxilla) elongated rectangular in ventral view (Fig. 4E, reddish violet); length about two thirds of the head length; 4 elements discernible: 2 proximal elements (submentum and mentum (?) (IT), anteriorly to gular plate (?)), one medio-distal element (praementum (?) (IT)) and one distal element (the labial palps (?) (IT); laterally on each side respectively); medio-distal element forking at its distal end into two tips; other details not discernible.

Thorax: Thorax (post-ocular segments 6–8; pro-, meso- and metathorax; Figs 4, 5); all thorax segments (mostly) rectangular with very rounded corners in dorsal view; much wider than long; overall about 0.9 mm long and about 0.6 mm wide at its widest.

Prothorax (post-ocular segment 6) more than 3× wider than long; first walking appendage (IT: foreleg) about 0.1 mm long, with 4 discernible elements: element 1 (IT: coxa) rectangular in posterior view, about 2.5× wider than long; element 2 (IT: trochanter) square-shaped in posterior view, about as long as wide; element 3 (IT: femur) trapezoid in posterior view with longer lateral than median edge, slightly wider than long; element 4 (IT/CO: tibio-tarsus(?)) triangular in posterior view with blunt tip, one claw (IT: praetarsus and claw (?)) discernible at its tip.

Mesothorax (post-ocular segment 7) pentagonal with very rounded corners in dorsal view, projecting slightly anteriorly dorsally; slightly wider than long in dorsal view and in ventral view more than 4× wider than long; convexly curved in lateral view; second walking appendage (IT: midleg) overall similar to foreleg, but about 0.2 mm long.

Metathorax (post-ocular segment 8) 3× wider than long in dorsal view and 2.3× wider than long in ventral view; third walking appendage (IT: hindleg) similar in appearance to midleg, but about 0.3 mm long.

Abdomen: Abdomen (post-ocular segments 9–19) overall very elongated rectangular, tapering distinctly posteriorly; about 3.4 mm long and 0.8 mm wide at its widest; segments all rectangular, wider than long; tergites and sternites not apparently different in form.

Tergites and sternites of abdomen segments 1–9 (post-ocular segment 9–17) all about 1.4–3× wider than long; no dorsal or posterior protrusions present on abdomen segment 9.

Tergite of trunk end (possible conjoined region of abdomen segments 10 and 11; post-ocular segments 18 and 19) slightly wider than long (at the widest point), with very rounded posterior edge, tapering posteriorly; posterior edge with at least 4 setae protruding posteriorly; more than 1.5× wider than long dorsally; two posterior directed protrusions (CO: pygopodia/postpedes(?)) ventrally with blunt end, making up about the last third of the ventral segment (Figs 2D, 4F).

Discussion

Phylogenetic position

The hymenopteran female clearly is a representative of Apocrita and can be assigned to its in-group Chrysidoidea based on the following characteristics (after key in Goulet and Huber 1993): head not globular, but flat and

square-shaped (compare Figs 1D, 4A, 8A); head prognathous; malar space without depression; body hair (setation) sparse or short; forewing with three or more cells, pterostigma present and a tubular vein (C_2v or C+R_2v) on antero-basal part of wing (compare Fig. 3); coxa of hindleg strongly narrowed and tarsus cylindrical; metasoma very ventrally attached to mesosoma, without constriction between abdomen segments 2 and 3 and abdomen tergite 2 not longer than abdomen tergite 3.

Within Chrysidoidea, it is a representative of the group Bethylidae (flat wasps) due to the following characteristics (after key in Goulet and Huber 1993): sternum of prothorax small (often concealed; cf. Fig. 4D); trochanter of foreleg attached postero-laterally on the coxa and tibia of this leg slender; metasoma with seven externally discernible tergites. Additionally, also these characteristics can be seen (after Azevedo et al. 2018): head with well-developed compound eyes (Fig. 1D); dorsal pronotal area present (Fig. 4C) and metasternal plate large (Fig. 4D); forewing with no to seven closed cells (here: four discernible, but potentially six or even seven; compare Fig. 3) and hind wing with no closed cells (compare Fig. 3A; though hind wing incomplete); femur of foreleg swollen (in females; Figs 1A,B, 2) and foreleg with calcar (antenna cleaning apparatus; compare Fig. 2B); second abdomen segment anteriorly very narrow ("petiolar-shaped") (Fig. 2A).

Within Bethylidae, it is potentially a representative of Holopsenellinae Engel, Ortega & Azevedo, 2016 (Azevedo et al. 2018) due to the forewing with a tubular Rs+M_2v vein and (potentially) seven closed cells. The forewing of the herein described hymenopteran female has at least four closed cells definitely discernible (R_2c, 1$R1_2$c, 1M_2c and 1Cu_2c). The Costal cell (C_2c) is not discernible, but that is most likely because of the postero-dorsal view on the forewing (compare Fig. 3) and not an actual absence. The second Radial 1 cell (1$R2_2$c) is also only proximally discernible as the wing in its distal portion is cut off; but it is present and likely also closed. The second Cubital cell (2Cu_2c) is discernible, but apparently not closed. But in this area of the wing there is either a small stone or an air-bubble preserved which obstructs the view there (compare Figs 2A, 3A), so this cell (2Cu_2c) may potentially also be closed.

Within the Holopsenellinae, it seems to be most closely related to either *Cretabythus sibiricus* Evans, 1973 or *Holopsenelliscus pankowskiorum* Engel, 2019 (after key in Jouault et al. 2020). It shares the following characteristics with *C. sibiricus*: antenna elements slightly longer than wide; mandible with four teeth (apical one longest); reduced clypeus (with potential median clypeal carina); short malar space; coxae of fore- and hindleg on continuous line, coxae of midleg slightly separated from that; mesopleurae smooth; tibial spur formula also potentially matching (1-2-2, here: 1-?-2), longer spur of tibia of hindleg 0.4× length of distal element of same leg; forewing venation remarkable similar (except for the potential M_2v present in the new specimen), hind wing with strong anterior vein margin and without cells (as far as can be seen in the new specimen); metanotum(?) discernible as thin band anterior to propodeum; metasoma slender and without unusual modifications (smooth integument). *C. sibiricus* is so far only known from one adult male from Taimyr amber (Evans 1973), is slightly smaller than the female described herein (2.5 mm of *C. sibiricus*, 3 mm of the new specimen) and features dentate claws which are lacking in the latter.

A comparison of the new specimen with *H. pankowskiorum* reveals the following shared characteristics: scapus distinctly enlarged compared with pedicellus and flagellum; clypeus not projected forward, anterior margin not emarginate (i.e. with indentation); genae broad; mandible short and thick (but *H. pankowskiorum* has only three teeth) and not obscured by the clypeus; femora distinctly swollen (particularly femur of foreleg); tibiae elongated (though more in the new specimen than in *H. pankowskiorum*), tibial spur formula also potentially matching (1-2-2, here: 1-?-2); proximal tarsus element slender, longer than wide and longest tarsus element; claws short, gently curved and simple (without teeth); forewing with closed 2$R1_2$c and pterostigma wider than long (but pterostigma in the new specimen longer than in *H. pankowskiorum*), other forewing venation remarkable similar (also potentially present M_2v); first metasomal tergite without ridge (transverse carina). *H. pankowskiorum* is also known from Kachin amber (Engel 2019). However, *H. pankowskiorum* differs from the new specimen in the following characteristics (Engel 2019): slightly longer (3.75 mm, new specimen just 3 mm); compound eyes circular (new specimen ovoid and shorter than in *H. pankowskiorum*); mandibles with three teeth (new specimen with four); shape of 1M_2c differs slightly, pterostigma length (longer in new specimen), M_2v not reaching wing margin (as it potentially does in new specimen); propodeum as wide as long (new specimen longer than wide); metasoma not petiolate (here distinctly so).

In summary, the herein described flat wasp cannot be confidently assigned to *C. sibiricus* or *H. pankowskiorum*, but neither can its inclusion in either of the two species or their genera be ruled out, as taxonomically relevant characters are only incompletely preserved. Owing to these uncertainties, we refrain from describing a new species or genus based on the new specimen.

The other individual can be unambiguously identified as a coleopteran (=beetle) immature due to its three well-articulated walking appendages and absence of other appendages posterior to the thorax (with the exception of the last externally discernible abdomen segment). Thorax appendages with four elements and a claw indicate that it is a representative of the group Polyphaga. Further identification of the immature is challenging; so far, the ample larval beetle fauna in Myanmar has not been treated in detail and the specimen lacks prominent features that would enable pinpointing of closer relationships to a specific in-group of Polyphaga. Especially the suboptimal structural resolution of the mouthparts proves detrimental in this context.

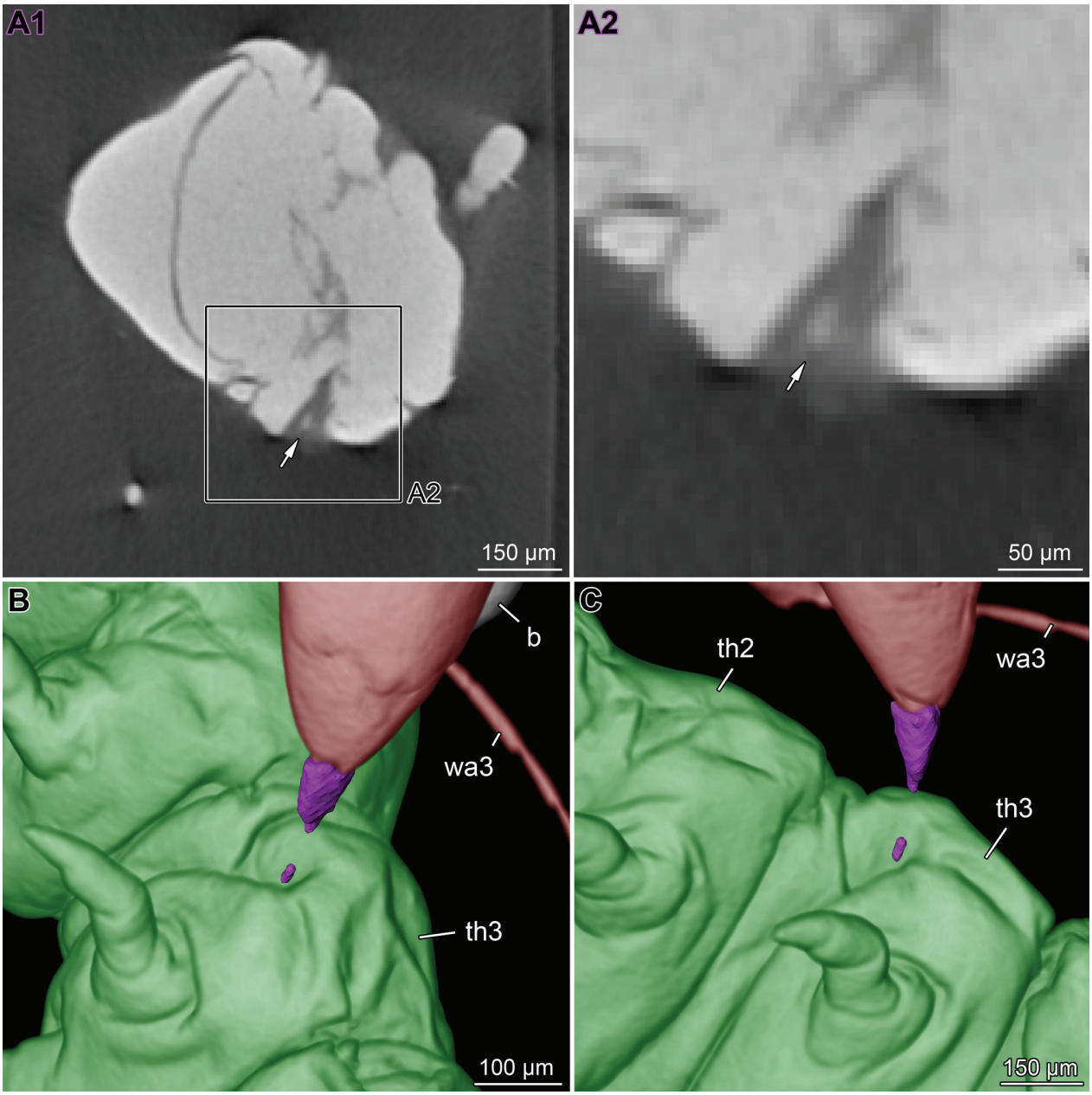

Figure 7. Details of supposed puncture site in the coleopteran immature by the sting of the hymenopteran adult (taken in Amira 6.1). **A.** Virtual section based on µCT of amber piece SNHM-6014; transverse section through the coleopteran immature; arrow points toward supposed rest of the hymenopteran sting in the puncture site; **A1.** Overview image; **A2.** Detailed view of puncture site; **B, C.** Colour-marked volume rendering of µCT of amber piece SNHM-6014 in slightly different views; in **green** coleopteran immature, in **red** hymenopteran adult, in **violet** the sting (3D reconstruction based on µCT). **b** – artefact (possible air bubble or similar); **th** – thorax segment; **wa** – walking appendage.

Interpretation of the amber piece

The hymenopteran female and the coleopteran immature are in direct contact with each other. The hymenopteran's tarsi, especially the distal portion with the claws, are positioned in between segmental borders or in folds of the membranous area of the head and anterior thorax region of the coleopteran (Figs 1B, 2, 4C–E, 5A, B), possibly to facilitate better grasping of the immature. Extant females of Bethylidae tend to grasp their progeny's coleopteran hosts during their initial attack with either both their mandibles and their legs (Mertins 1980; Abraham et al. 1990; Howard et al. 1998), just the legs (Gordh and Medved 1986 [indirectly inferred]; Amante et al. 2017) or just the mandibles (Kühne and Becker 1974; Gordh and Hawkins 1981).

Additionally, the sting (modified ovipositor) of the wasp seems to be inserted into the metathorax of the coleopteran. This is clearly discernible in the macrophotographs (compare Figs 1, 2A, 5A), but less apparent in the µCT data (compare Figs 4–6), which might be a result of too low contrast in X-ray due to preservation of this fine structure (as has been shown for other structures; see

Rühr and Lambertz 2019). However, there appears to be a small structure within the apparent puncture site that may belong to the sting (compare Fig. 7), being located where the tip of its sting (specifically the terebra) would be expected by extrapolation (Fig. 7B,C). Regardless of whether this small structure indeed represents the sting's tip or not, it appears that the sting of the wasp applied pressure onto the metathorax of the coleopteran and most likely also penetrated it, as a well-defined pressure site is present (esp. Figs 5D, 6B3, 7A, see also macrophotographs Figs 1, 2).

Notably, the amber displays no discernible layers around both insects, indicating that either the embedding in the resin was sudden and fast or that they did not move (much) during the process (incl. wriggling of the coleopteran immature as defensive behaviour; compare with Kühne and Becker 1974; Mertins 1980; Hu et al. 2012; Polaszek et al. 2019, S1 video). Together with the positioning of the wasp's sting and legs, this leaves two alternative explanations for the behaviour captured in the piece.

1) The wasp may have been caught in the process of paralysing the coleopteran. Since some extant representatives of Bethylidae sit and wait on the host until it is fully paralysed after the sting (Evans 1964; Kühne and Becker 1974; Abraham et al. 1990; Howard et al. 1998; Lauzière et al. 2000), a similar behaviour may explain the apparent lack of movement in the syninclusions studied here.

2) Other extant representatives of Bethylidae are motionless during oviposition, which may last several minutes (Gordh and Medved 1986; Abraham et al. 1990). Accordingly, it would be likewise possible that the wasp was in the process of ovipositing onto the coleopteran instead. As evidence against this, the body posture of the fossil wasp (compare Figs 1, 2A) lacks some of the characteristics typically observed in extant flat wasps during oviposition, such as the telescoped and arched metasomal segments, as well as a contorted hypopygium (last externally discernible abdomen segment) that permits egg extrusion (Gordh and Medved 1986). Furthermore, the sting is not always inserted into the host, but sometimes just closely pressed to it during oviposition (Gordh and Medved 1986). Thus, it is more probable that the herein described female wasp was preserved while stinging the coleopteran immature, rather than ovipositing onto it.

Parasitism/Parasitoidism in the fossil record

Direct interactions between parasites/parasitoids and their hosts in the fossil record are rare, but not completely unknown. Relatively well-documented examples of such interactions are e.g. nematodan worms parasitizing different insects (endoparasitism), primarily representatives of Diptera (flies and mosquitoes), Formicidae (in-group of Hymenoptera; ants) and Hemiptera (true bugs) (e.g. Grimaldi 1996; Poinar 2003; Poinar and Buckley 2006; Arillo 2007; see also Boucot and Poinar 2010 and references therein), with numerous cases of the nematodes emerging from their hosts preserved in amber. Similarly common are mites and ticks (ectoparasitism) as temporary parasites (see van der Wal and Haug JT 2019; Hörnig et al. 2020 for discussion of the term) especially on representatives of dipterans, moths (Lepidoptera) and scale insects (in-group of Hemiptera) (Arillo 2007; Boucot and Poinar 2010).

The majority of hymenopterans are parasitic, specifically parasitoid (e.g. Rasnitsyn 1980). In fact, parasitoidism is widely assumed to be the key innovation underlying the massive radiation within Hymenoptera (Gaston 1991; Davis et al. 2010; Huber 2017) which began in the Mesozoic (Rasnitsyn 1980; Rasnitsyn and Quicke 2002). Most likely, it evolved only once within the group Vespina (Orussoidea+Apocrita; e.g. Rasnitsyn 1980; Gauld and Bolton 1988; Whitfield 2003) and some in-groups of Apocrita (specifically within the Aculeata) have secondarily lost it again (e.g. Snelling 1981; Anderson 1984; Gauld and Bolton 1988; Danforth 2002). Due to the early origin of parasitoidism within Hymenoptera, we should expect to find such parasitoid wasps regularly as fossils.

In line with this notion, the majority of the fossil hymenopterans hitherto described do indeed represent parasitoids. Beyond this, there are even some examples of direct interaction between the larval parasitoid or its parent and its host. There are two reports of wasps embedded during (supposed) oviposition: a representative of Stigmaphronidae (Arillo 2007; previously assigned to Megaspilidae by Alonso et al. 2000) ovipositing into(/onto?) a dipteran (Alonso et al. 2000, fig. 12-1) in Spanish amber (Álava) and a representative of Ichneumonidae ovipositing into a caterpillar (Wunderlich 1986 in Arillo 2007) in Baltic amber. Furthermore, there are other representatives of Ichneumonidae, which have also been found in direct interaction with their host, namely: an immature attached to a spider in Dominican amber (Poinar 1992 in Arillo 2007) and a cocoon adjacent to the seemingly depleted eggs of a spider in Baltic amber (Poinar 2004 in Arillo 2007; Boucot and Poinar 2010, fig. 60). An immature representative of the related group Braconidae has also been described emerging from an ant in Baltic amber (Poinar and Miller 2002).

Another well recorded group within amber is Dryinidae. The immatures of its extant representatives are ectoparasitic (and/or endoparasitic) on auchenorrhynchans (in-group of Hemiptera) (Goulet and Huber 1993; Olmi and Virla 2006; Guglielmino et al. 2013) and there are multiple syninclusions in Dominican amber that illustrate corresponding parasitism of immature representatives of Drynidiae on representatives of Fulgoroidea (in-group of Auchenorrhyncha; Poinar 1992, fig. 140, Poinar and Poinar 1999, fig. 140, and Ross 1998, fig. 73, in Arillo 2007; Poinar 2001; Grimaldi and Engel 2005, fig. 11.37; Boucot and Poinar 2010, fig. 56) and Cicadellidae (also in-group of Auchenorrhyncha; Grimaldi 1996, p. 97).

An unidentified hymenopteran immature is depicted in Boucot and Poinar (2010, fig. 58) emerging from an adult trichopteran (caddiesfly) (also described in Poinar and Anderson 2005 in Boucot and Poinar 2010) in Baltic amber.

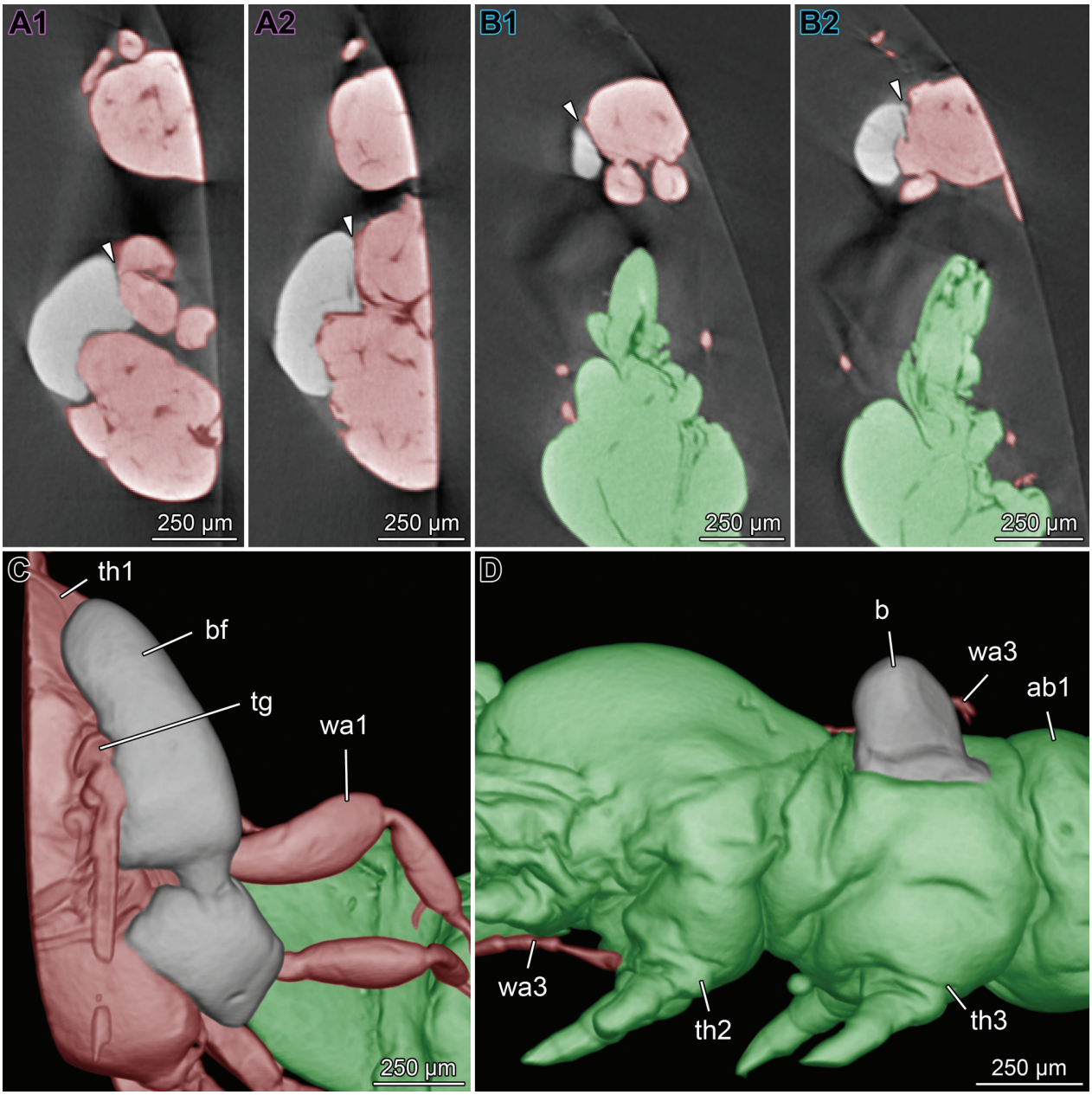

Figure 8. Details of artefacts on the hymenopteran adult and the coleopteran immature in amber piece SNHM-6014 (taken in Amira 6.1). **A, B.** Virtual section based on µCT of amber piece SNHM-6014; in **green** coleopteran immature, in **red** hymenopteran adult; arrowhead pointing towards connection or disconnection between artefact (possible air bubble or leaked body fluid etc.) and the hymenopteran adult. **A.** Sagittal sections through hymenopteran adult; 1–2 ventral to dorsal sections; **B.** Transverse sections through hymenopteran adult; 1–2 anterior to posterior sections; **C, D.** Colour-marked volume rendering of µCT of amber piece SNHM-6014; in **green** coleopteran immature, in **red** hymenopteran adult; **C.** Dorsal view on thorax of hymenopteran adult and artefacts there; **D.** Lateral view on mirrored thorax of coleopteran immature and artefacts there. **ab** – abdomen segment; **b** – artefact (possible air bubble or similar); **bf** – artefact (possible leaked body fluid or similar); **tg** – tegula (part of wing joint area); **th** – thorax segment; **wa** – walking appendage.

Conclusions

Examples of group fossilisation as cases of 'frozen behaviour' are of high value for the reconstruction of behavioural aspects and the evolution of lifestyles. Even if many species of fossil insects, and particularly hymenopterans (almost 2,500 fossil species; Aguiar et al. 2013), have been described, our knowledge about their way of life, including intra- and interspecific interactions, is still very limited.

Adding further findings, such as the here represented specimen, will help to reach a better understanding of the food-web and therefore ecological impact of different arthropod groups in deep-time. This is especially important as the currently available data on food-webs of palaeo-ecosystems does not allow us to conclude a comprehensive view of interactions between extinct organism groups.

The specimen herein is, besides the representative of the Stigmaphronidae with a dipteran specimen in Spanish

amber (Alonso et al. 2000; Arillo 2007), one of the oldest examples of interaction of an adult hymenopteran with a putative host of their immatures and the oldest documentation of an interaction of flat wasps (Bethylidae) and coleopteran immatures. This indicates that the interaction between parasitoid flat wasp immatures and coleopteran immatures, as seen today, already existed at least about 100 million years ago.

Acknowledgments

CK is kindly funded by the Landesgraduiertenförderung MV. The Volkswagen Foundation kindly funds JTH with a Lichtenberg Professorship. Micro-computed tomography was performed at the Imaging Center of the Department of Biology, University of Greifswald (DFG INST 292/119-1 FUGG; DFG INST 292/120-1 FUGG). We thank C. Haug, Munich, and G. Brenneis, Greifswald, for their help and suggestions improving the manuscript. CK, JTH and MKH thank J. M. Starck, Munich, and S. Harzsch, Greifswald, for their continuous support. We would also like to thank an anonymous reviewer for helpful comments that helped improve the manuscript. We highly appreciate the effort of all people involved in providing open access, open source and low cost software.

References

Abraham YJ, Moore D, Godwin G (1990) Rearing and aspects of biology of *Cephalonomia stephanoderis* and *Prorops nasuta* (Hymenoptera: Bethylidae) parasitoids of the coffee berry borer, *Hypothenemus hampei* (Coleoptera: Scolytidae). Bulletin of Entomological Research 80(2): 121–128. https://doi.org/10.1017/S000748530001333X

Alonso J, Arillo A, Barrón E, Corral JC, Grimalt J, López JF, López R, Martínez-Delclós X, Ortuño V, Peñalver E, Trincão PR (2000) A new fossil resin with biological inclusions in Lower Cretaceous deposits from Álava (Northern Spain, Basque-Cantabrian Basin). Journal of Paleontology 74(1): 158–178. https://doi.org/10.1017/S0022336000031334

Amante M, Schöller M, Hardy ICW, Russo A (2017) Reproductive biology of *Holepyris sylvanidis* (Hymenoptera: Bethylidae). Biological Control 106: 1–8. https://doi.org/10.1016/j.biocontrol.2016.12.004

Anderson M (1984) The evolution of eusociality. Annual Review of Ecology and Systematics 15: 165–189. https://doi.org/10.1146/annurev.es.15.110184.001121

Aguiar AP, Deans AR, Engel MS, Forshage M, Huber JT, Jennings JT, Johnson NF, Lelej AS, Longino JT, Lohrmannm V, Mikó I, Ohl M, Rasmussen C, Taeger A, Yu DSK (2013) Order Hymenoptera. In: Zhang Z-Q (Ed.) Animal biodiversity: an outline of higher-level classification and survey of taxonomic richness (Addenda 2013). Zootaxa 3703(1): 51–62. https://doi.org/10.11646/zootaxa.3703.1.12

Arillo A (2007) Paleoethology: Fossilized behaviours in amber. Geologica Acta 5(2): 159–166. https://doi.org/10.1344/105.000000301

Azevedo CO, Alencar IDCC, Ramos MS, Barbosa DN, Colombo WD, Vargas JMR, Lim J (2018) Global guide of the flat wasps (Hymenoptera, Bethylidae). Zootaxa 4489(1): 1–294. https://doi.org/10.11646/zootaxa.4489.1.1

Boucot AJ (1990) Evolutionary Paleobiology of Behavior and Coevolution. Elsevier Science Publishers B.V., Amsterdam (Netherlands), 725 pp.

Boucot AJ, Poinar Jr GO (2010) Fossil Behavior Compendium. 1st Edn. CRC Press, Boca Raton (Florida, USA), 324 pp. https://doi.org/10.1201/9781439810590

Breed MD, Cook C, Krasnec MO (2012) Cleptobiosis in social insects. Psyche: A Journal of Entomology 2012(Special Issue): e484765. https://doi.org/10.1155/2012/484765

Brues CT (1939) New Oligocene Braconidae and Bethylidae from Baltic Amber. Annals of the Entomological Society of America 32(2): 251–263. https://doi.org/10.1093/aesa/32.2.251

Casale A (1991) Some notes on the parental and parasocial behaviour of *Sclerodermas domesticus* Latreille (Hymenoptera Bethylidae). Ethology Ecology & Evolution 3(sup1): 34–38. https://doi.org/10.1080/03949370.1991.10721905

Cheng LL, Howard RW, Campbell JF, Charlton RE, Nechols JR, Ramaswamy SB (2004) Mating behavior of *Cephalonomia tarsalis* (Ashmead) (Hymenoptera: Bethylidae) and the effect of female mating frequency on offspring production. Journal of Insect Behavior 17(2): 227–245. https://doi.org/10.1023/B:JOIR.0000028572.76021.d9

Cockerell TDA (1917a) Arthropods in Burmese amber. Psyche: A Journal of Entomology 24: 40–45. https://doi.org/10.1155/1917/83242

Cockerell TDA (1917b) Arthropods in Burmese amber. American Journal of Science s4-44(263): 360–368. https://doi.org/10.2475/ajs.s4-44.263.360

Colombo WD, Gobbi FT, Perkovsky EE, Azevedo CO (2020) Synopsis of the fossil Pristocerinae (Hymenoptera, Bethylidae), with description of two new genera and six species from Burmese, Taimyr, Baltic and Rovno ambers. Historical Biology 33(9): 1736–1752. https://doi.org/10.1080/08912963.2020.1733551

Crowson RA (1981) The Biology of the Coleoptera. Academic Press, London (UK), 802 pp. https://doi.org/10.1016/C2013-0-07304-5

Cruickshank RD, Ko K (2003) Geology of an amber locality in the Hukawng Valley, Northern Myanmar. Journal of Asian Earth Sciences 21: 441–455. https://doi.org/10.1016/S1367-9120(02)00044-5

Daintith J, Martin EA (2010) A Dictionary of Science (Oxford Paperback Reference). 6th Edn. Oxford University Press, Oxford (UK), 900 pp.

Danforth BN (2002) Evolution of sociality in a primitively eusocial lineage of bees. Proceedings of the National Academy of Sciences of the United States of America (PNAS) 99(1): 286–290. https://doi.org/10.1073/pnas.012387999

Davis RB, Baldauf SL, Mayhew PJ (2010) The origins of species richness in the Hymenoptera: Insights from a family-level supertree. BioMed Central (BMC) Evolutionary Biology 10(1): e109. https://doi.org/10.1186/1471-2148-10-109

Engel MS (2019) A holopsenelline wasp in mid-Cretaceous amber from Myanmar (Hymenoptera: Bethylidae). Palaeoentomology 002(2): 199–204. https://doi.org/10.11646/palaeoentomology.2.2.10

Evans HE (1962) The evolution of prey-carrying mechanisms in wasps. Evolution 16(4): 468–483. https://doi.org/10.2307/2406179

Evans HE (1964) A synopsis of the American Bethylidae (Hymenoptera, Aculeata). Bulletin of the Museum of Comparative Zoology, Harvard University 132(1): 1–222. https://www.biodiversitylibrary.org/item/25435#page/11/mode/1up

Evans HE (1973) Cretaceous aculeate wasps from Taimyr, Siberia (Hymenoptera). Psyche: A Journal of Entomology 80: 166–178. https://doi.org/10.1155/1973/16876

Finlayson LH (1950) The Biology of *Cephalonomia waterstoni* Gahan (Hym., Bethylidae), a Parasite of *Laemophloeus* (Col., Cucujidae). Bulletin of Entomological Research 41(1): 79–97. https://doi.org/10.1017/S0007485300027498

Fischer TC, Hörnig MK (2019) Mating moths (Tineidae, Ditrysia, Lepidoptera) preserved as frozen behavior inclusion in Baltic Amber (Eocene). Palaeontologia Electronica 22.1.7: 1–10. https://doi.org/10.26879/829

Gao SK, Wei K, Tang YL, Wang XY, Yang ZQ (2016) Effect of parasitoid density on the timing of parasitism and development duration of progeny in *Sclerodermus pupariae* (Hymenoptera: Bethylidae). Biological Control 97: 57–62. https://doi.org/10.1016/j.biocontrol.2016.03.003

Gaston KJ (1991) The Magnitude of Global Insect Species Richness. Conservation Biology 5(3): 283–296. https://doi.org/10.1111/j.1523-1739.1991.tb00140.x

Gauld I, Bolton B [Eds] (1988) The Hymenoptera. British Museum (Natural History) Oxford University Press, New York (USA), 332 pp.

Goater TM, Goater CP, Esch GW (2014) Parasitism. The diversity and ecology of the animal parasites. 2nd Edn. Cambridge University Press, Cambridge (UK), 498 pp. https://doi.org/10.1017/CBO9781139047876

Gordh G (1998) A New Species of *Sierola* Parasitic on Moth Larvae in Western Australia (Hymenoptera: Bethylidae). Proceedings of the Hawaiian Entomological Society 33: 83–88. http://hdl.handle.net/10125/16306

Gordh G, Hawkins B (1981) *Goniozus emigratus* (Rohwer), a primary external parasite of *Paramyelois transitella* (Walker), and comments on bethylids attacking Lepidoptera (Hymenoptera: Bethylidae; Lepidoptera: Pyralidae). Journal of the Kansas Entomological Society 54(4): 787–803. https://www.jstor.org/stable/25084238

Gordh G, Medved RE (1986) Biological notes on *Goniozus pakmanus* Gordh (Hymenoptera: Bethylidae), a parasite of pink bollworm, *Pectinophora gossypiella* (Saunders)(Lepidoptera: Gelechiidae). Journal of the Kansas Entomological Society 59(4): 723–734. https://www.jstor.org/stable/25084850

Goulet H, Huber JT [Eds] (1993) Hymenoptera of the world: An identification guide to families. Canada Communication Group Publishing, Ottawa (Canada), 668 pp. https://cfs.nrcan.gc.ca/publications?id=35617

Griffiths NT, Godfray HCJ (1988) Local mate competition, sex ratio and clutch size in bethylid wasps. Behavioral Ecology and Sociobiology 22(3): 211–217. https://doi.org/10.1007/BF00300571

Grimaldi DA (1996) Amber: Window to the Past. Harry N. Abrams/American Museum of Natural History, New York (USA), 216 pp.

Grimaldi DA, Engel MS (2005) Evolution of the Insects. Cambridge University Press, New York (USA), 755 pp.

Grimaldi DA, Engel MS, Nascimbene PC (2002) Fossiliferous Cretaceous Amber from Myanmar (Burma): Its Rediscovery, Biotic Diversity, and Paleontological Significance. American Museum Novitates 2002(3361): 1–71. https://doi.org/10.1206/0003-0082(2002)361%3C0001:FCAFMB%3E2.0.CO;2

Grissell EE (1999) Hymenopteran biodiversity: some alien notions. American Entomologist 45(4): 235–244. https://doi.org/10.1093/ae/45.4.235

Gröhn C (2015) Einschlüsse in Baltischem Bernstein. 1st Edn. Wacholtz Verlag/Murmann Publishers, Kiel/Hamburg (Germany), 424 pp. [in German]

Guglielmino A, Olmi M, Bückle C (2013) An updated host-parasite catalogue of world Dryinidae (Hymenoptera: Chrysidoidea). Zootaxa 3740(1): 1–113. https://doi.org/10.11646/zootaxa.3740.1.1

Hasiotis ST (2003) Complex ichnofossils of solitary and social soil organisms: Understanding their evolution and roles in terrestrial paleoecosystems. Palaeogeography, Palaeoclimatology, Palaeoecology 192(1–4): 259–320. https://doi.org/10.1016/S0031-0182(02)00689-2

Haug C, Mayer G, Kutschera V, Waloszek D, Maas A, Haug JT (2011) Imaging and documenting gammarideans. International Journal of Zoology 2011: e380829. [9 pp] https://doi.org/10.1155/2011/380829

Haug JT, Haug C, Garwood RJ (2016) Evolution of insect wings and development—new details from Palaeozoic nymphs. Biological Reviews 91(1): 53–69. https://doi.org/10.1111/brv.12159

Haug JT, Waloszek D, Maas A, Liu Y, Haug C (2012) Functional morphology, ontogeny and evolution of mantis shrimp-like predators in the Cambrian. Palaeontology 55: 369–399. https://doi.org/10.1111/j.1475-4983.2011.01124.x

Haug JT, Kiesmüller C, Haug GT, Haug C, Hörnig MK (2022) A fossil aphidlion preserved together with its prey in 40 million-year-old Baltic amber. Palaeobiodiversity and Palaeoenvironments: 1–9. https://doi.org/10.1007/s12549-021-00521-z

Hörnig MK, Haug JT, Haug C (2013) New details of *Santanmantis axelrodi* and the evolution of the mantodean morphotype. Palaeodiversity 6: 157–168.

Hörnig MK, Haug JT, Haug C (2017) An exceptionally preserved 110 million years old praying mantis provides new insights into the predatory behaviour of early mantodeans. PeerJ Life & Environment 5: e3605. https://doi.org/10.7717/peerj.3605

Hörnig MK, Fischer TC, Haug JT (2019) Caught in the act of hatching—a group of heteropteran nymphs escaping from their eggs preserved in Dominican amber. Palaeodiversity 12(1): 123–134. https://doi.org/10.18476/pale.v12.a12

Hörnig MK, Haug C, Schneider JW, Haug JT (2018) Evolution of reproductive strategies in dictyopteran insects—clues from ovipositor morphology of extinct roachoids. Acta Palaeontologica Polonica 63(1): 1–24. https://doi.org/10.4202/app.00324.2016

Hörnig MK, Haug C, Müller P, Haug JT (2022) Not quite social—possible cases of gregarious behaviour of immatures of various lineages of Insecta in 100-million-year-old amber. Bulletin of Geoscience 97(1): 69–87. https://doi.org/10.3140/bull.geosci.1818

Hörnig MK, Sombke A, Haug C, Harzsch S, Haug JT (2016) What nymphal morphology can tell us about parental investment—a group of cockroach hatchlings in Baltic Amber documented by a multi-method approach. Palaeontologia Electronica 19.1.6A: 1–20. https://doi.org/10.26879/571

Hörnig MK, Kiesmüller C, Müller P, Haug C, Haug JT (2020) A new glimpse on trophic interactions of 100-million-year old lacewing larvae. Acta Palaeontologica Polonica 65(4): 777–786. https://doi.org/10.4202/app.00677.2019

Howard RW, Flinn PW (1990) Larval trails of *Cryptolestes ferrugineus* (Coleoptera: Cucujidae) as kairomonal host-finding cues for the parasitoid *Cephalonomia waterstoni* (Hymenoptera: Bethylidae). Annals of the Entomological Society of America 83(2): 239–245. https://doi.org/10.1093/aesa/83.2.239

Howard RW, Charlton M, Charlton RE (1998) Host-finding, host-recognition, and host-acceptance behavior of *Cephalonomia tarsalis* (Hymenoptera: Bethylidae). Annals of the Entomological Society of America 91(6): 879–889. https://doi.org/10.1093/aesa/91.6.879

Hsieh S, Plotnick RE (2020) The representation of animal behaviour in the fossil record. Animal Behaviour 169: 65–80. https://doi.org/10.1016/j.anbehav.2020.09.010

Hu Z, Zhao X, Li Y, Liu X, Zhang Q (2012) Maternal Care in the Parasitoid *Sclerodermus harmandi* (Hymenoptera: Bethylidae). PLoS ONE 7(12): e51246. https://doi.org/10.1371/journal.pone.0051246

Huber JT (2017) Biodiversity of Hymenoptera. In: Fottit RG, Adler PH (Eds) Insect Biodiversity: Science and Society. Vol. I, 2nd Edn. John Wiley & Sons Ltd., West Sussex (UK), 419–461. https://doi.org/10.1002/9781444308211.ch12

Jouault C, Brazidec M (2021) A new protopristocerine wasp (Hymenoptera: Bethylidae) from the mid-Cretaceous Burmese amber. Annales de Paléontologie 107(4): 102522. https://doi.org/10.1016/j.annpal.2021.102522

Jouault C, Perrichot V, Nel A (2021) New flat wasps from mid-Cretaceous Burmese amber deposits highlight the bethylid antiquity and paleobiogeography (Hymenoptera: Chrysidoidea). Cretaceous Research 123(21): 104772. https://doi.org/10.1016/j.cretres.2021.104772

Jouault C, Ngô-Muller V, Pouillon J-M, Nel A (2020) New Burmese amber fossils clarify the evolution of bethylid wasps (Hymenoptera: Chrysidoidea). Zoological Journal of the Linnean Society 191(4): 1044–1058. https://doi.org/10.1093/zoolinnean/zlaa078

Jucker C, Hardy IC, Malabusini S, de Milato S, Zen G, Savoldelli S, Lupi D (2020) Factors affecting the reproduction and mass-rearing of *Sclerodermus brevicornis* (Hymenoptera: Bethylidae), a natural enemy of exotic flat-faced longhorn beetles (Coleoptera: Cerambycidae: Lamiinae). Insects 11(10): e657. [22 pp] https://doi.org/10.3390/insects11100657

Kathirithamby J (2009) Host-Parasitoid Associations in Strepsiptera. Annual Review of Entomology 54(1): 227–249. https://doi.org/10.1146/annurev.ento.54.110807.090525

Klausnitzer B (1978) Ordnung Coleoptera (Larven). Springer-Science+Business Media, B.V., Dordrecht (Netherlands), 378 pp. https://doi.org/10.1007/978-94-009-9975-6 [in German]

Kühne H, Becker G (1974) Zur Biologie und Ökologie von *Sclerodermа domesticum* Latreille (Bethylidae, Hymenoptera), einem Parasiten holzzerstörender Insektenlarven. Zeitschrift für Angewandte Entomologie 76: 278–303. https://doi.org/10.1111/j.1439-0418.1974.tb01888.x [in German]

Lafferty KD, Kuris AM (2002) Trophic strategies, animal diversity and body size. Trends in Ecology and Evolution 17(11): 507–513. https://doi.org/10.1016/S0169-5347(02)02615-0

Lanes GO, Kawada R, Azevedo CO, Brothers DJ (2020) Revisited morphology applied for Systematics of flat wasps (Hymenoptera, Bethylidae). Zootaxa 4752(1): 1–127. https://doi.org/10.11646/zootaxa.4752.1.1

Lauzière I, Pérez-Lachaud G, Brodeur J (2000) Behavior and Activity Pattern of *Cephalonomia stephanoderis* (Hymenoptera: Bethylidae) Attacking the Coffee Berry Borer, *Hypothenemus hampei* (Coleoptera: Scolytidae). Journal of Insect Behavior 13(3): 375–395. https://doi.org/10.1023/A:1007762202679

Lepeco A, Melo GAR (2021) The wasp genus †*Holopsenella* in mid-Cretaceous Burmese amber (Hymenoptera: †Holopsenellidae stat. nov.). Cretaceous Research 131: 105089. https://doi.org/10.1016/j.cretres.2021.105089

Litman JR (2019) Under the radar: Detection avoidance in brood parasitic bees. Philosophical Transactions of the Royal Society B: Biological Sciences 374: 20180196. https://doi.org/10.1098/rstb.2018.0196

Lucius R, Loos-Frank B, Lane RP, Poulin R, Roberts CW, Grencis RK (2017) The Biology of Parasites. Wiley-VCH Verlag GmbH & Co. KGaA, Weinheim (Germany), 452 pp.

Martínez-Delclòs X, Briggs DEG, Peñalver (2004) Taphonomy of insects in carbonates and amber. Palaeogeography, Palaeoclimatology, Palaeoecology 203(1–2): 19–64. https://doi.org/10.1016/S0031-0182(03)00643-6

Mayhew PJ, Heitmans WRB (2000) Life history correlates and reproductive biology of *Laelius pedatus* (Hymenoptera: Bethylidae) in The Netherlands. European Journal of Entomology 97(3): 313–322. https://doi.org/10.14411/eje.2000.048

Mertins JW (1980) Life history and behavior of *Laelius pedatus*, a gregarious bethylid ectoparasitoid of Anthrenus verbasci. Annals of the Entomological Society of America 73(6): 686–693. https://doi.org/10.1093/aesa/73.6.686

Nentwig W, Bacher S, Brandl R (2017) Ökologie kompakt. 4th Edn. Springer Spektrum, Berlin/Heidelberg (Germany), 369 pp. https://doi.org/10.1007/978-3-662-54352-8 [in German]

Noetling F (1893) On the Occurrence of Burmite, a new Fossil Resin from Upper Burma. Records of the Geological Survey of India 26(1): 31–40.

Olmi M, Virla E (2006) Familia Dryinidae. In: Fernández F, Sharkey MJ (Eds) Introducción a los Hymenoptera de la Región Neotropical. Serie Entomología Colombiana. Sociedad Colombiana de Entomología y Universidad Nacional de Colombia, Bogotá D. C. (Columbia), 401–418. https://repository.agrosavia.co/handle/20.500.12324/34432 [in Spanish]

Olsen OW (1974) Animal parasites. Their Life Cycles and Ecology. 3rd Edn. Dover Publications Inc., New York (USA), 562 pp.

Paracer S, Ahmadjian V (2000) Symbiosis. An Introduction to Biological Associations. 2nd Edn. Oxford University Press, Inc., New York (USA), 291 pp.

Pérez de la Fuente R, Engel MS, Azar D, Peñalver E (2019) The hatching mechanism of 130-million-year-old insects: an association of neonates, egg shells and egg bursters in Lebanese amber. Palaeontology 62(4): 547–559. https://doi.org/10.1111/pala.12414

Poinar Jr GO (2001) Dominican amber. In: Briggs DEG, Crowther PR (Eds) Paleobiology II. Blackwell Science Ltd., Oxford (UK), 362–364. https://doi.org/10.1002/9780470999295.ch86

Poinar Jr GO (2003) Trends in the evolution of insect parasitism by nematodes as inferred from fossil evidence. Journal of Nematology 35(2): 129–132. https://www.ncbi.nlm.nih.gov/pubmed/19265986

Poinar Jr GO (2019) Burmese amber: evidence of Gondwanan origin and Cretaceous dispersion. Historical Biology 31(10): 1304–1309. https://doi.org/10.1080/08912963.2018.1446531

Poinar Jr GO, Miller JC (2002) First fossil record of endoparasitism of adult ants (Formicidae: Hymenoptera) by Braconidae (Hymenoptera). Annals of the Entomological Society of America 95(1): 42–43. https://doi.org/10.1603/0013-8746(2002)095[0041:FFROEO]2.0.CO;2

Poinar Jr GO, Buckley R (2006) Nematode (Nematoda: Mermithidae) and hairworm (Nematomorpha: Chordodidae) parasites in Early Cretaceous amber. Journal of Invertebrate Pathology 93(1): 36–41 https://doi.org/10.1016/j.jip.2006.04.006.

Polaszek A, Almandhari T, Fusu L, Al-Khatri SAH, Al Naabi S, Al Shidi RH, Hardy ICW (2019) *Goniozus omanensis* (Hymenoptera: Bethylidae) an important parasitoid of the lesser date moth *Batrachedra amydraula* Meyrick (Lepidoptera: Batrachedridae) in Oman. PLoS ONE 14(12): e0223761. https://doi.org/10.1371/journal.pone.0223761

Poulin R (2011) Chapter 1—The many roads to parasitism. A tale of convergence. In: Rollinson D, Hay SI (Eds) Advances in

Parasitology. 1st Edn., Vol. 74, Iss. C. Elsevier Ltd., Oxford (UK), 1–40. https://doi.org/10.1016/B978-0-12-385897-9.00001-X

Powell D (1938) The Biology of *Cephalonomia tarsalis* (Ash.), a Vespoid Wasp (Bethylidae: Hymenoptera) Parasitic on the Sawtoothed Grain Beetle. Annals of the Entomological Society of America 31(1): 44–49. https://doi.org/10.1093/aesa/31.1.44

Price PW (1980) Evolutionary Biology of Parasites. Monographs in Population Biology Vol. 15. Princeton University Press, Princeton (New Jersey, USA), 256 pp.

Rasnitsyn AP (1980) Proizhojdenie i evoliutia pereponchatokrilih nasekomih [= The Origin and Evolution of the Hymenopterous Insects]. Akademia Nauk SSSR, Trudi Paleonotologhicheskogo Instituta, Tom 174 [= Transactions of the Paleontological Institute, Academy of Sciences of the USSR, Vol. 174]. Izdatelstvo "Nauka" [= "Science" Publishing House], Moscow (Russia), 192 pp. [in Russian]

Rasnitsyn AP, Quicke DL (2002) History of insects. Kluwer Academic Publishers, Dordrecht (Netherlands), 517 pp. https://doi.org/10.1007/0-306-47577-4

Reif W-E (1983) Functional morphology and evolutionary biology. Paläontologische Zeitschrift 57(3–4): 255–266. https://doi.org/10.1007/BF02990316

Ross AJ (2021) Burmese (Myanmar) amber taxa. on-line supplement v.2021.1, 27 pp. http://www.nms.ac.uk/explore/stories/natural-world/burmese-amber/

Rothschild M, Clay T (1957) Fleas, Flukes & Cuckoos. A Study of Bird Parasites. The Macmillan Company, New York (USA), 305 pp. https://www.biodiversitylibrary.org/item/28804#page/7/mode/1up

Rubink WL, Evans HE (1979) Notes on the nesting behavior of the Bethylid wasp, *Epyris eriogoni* Kieffer, in Southern Texas. Psyche: A Journal of Entomology 86(4): 313–319. https://doi.org/10.1155/1979/58308

Rühr PT, Lambertz M (2019) Surface contrast enhancement of integumentary structures in X-ray tomography. Journal of Anatomy 235(2): 379–385. https://doi.org/10.1111/joa.13008

Schaefer CH (1962) Life History of *Conophthorus radiatae* (Coleoptera: Scolytidae) and its Principal Parasite, *Cephalonomia utahensis* (Hymenoptera: Bethylidae). Annals of the Entomological Society of America 55(5): 569–577. https://doi.org/10.1093/aesa/55.5.569

Shi G, Grimaldi DA, Harlow GE, Wang J, Wang J, Yang M, Lei W, Li Q, Li X (2012) Age constraint on Burmese amber based on U-Pb dating of zircons. Cretaceous Research 37: 155–163. https://doi.org/10.1016/j.cretres.2012.03.014

Snelling RR (1981) Systematics of social Hymenoptera. In: Hermann HR (Ed.) Social insects. Vol. II, 2nd Edn. Academic Press Inc., New York (USA), 369–453. https://doi.org/10.1016/B978-0-12-342202-6.50012-5

Tang X, Meng L, Kapranas A, Xu F, Hardy ICW, Li B (2014) Mutually beneficial host exploitation and ultra-biased sex ratios in quasisocial parasitoids. Nature Communications 5: e4942. https://doi.org/10.1038/ncomms5942

Thomason J [Ed.] (1997) Functional Morphology in Vertebrate Paleontology. 1st Paperback Edn. Cambridge University Press, New York (USA), 277 pp.

van der Wal S, Haug JT (2019) Letter to the editor referencing "The apparent kleptoparasitism in fish-parasitic gnathiid isopods". Parasitology Research 118(5): 1679–1682. https://doi.org/10.1007/s00436-019-06281-2

Wang B, Xia F, Engel MS, Perrichot V, Shi G, Zhang H, Chen J, Jarzembowski EA, Wappler T, Rust J (2016) Debris-carrying camouflage among diverse lineages of Cretaceous insects. Science Advances 2(6): e1501918. https://doi.org/10.1126/sciadv.1501918

Weitschat W (2009) Jäger, Gejagte, Parasiten und Blinde Passagiere–Momentaufnahmen aus dem Bernsteinwald. Denisia 26/Kataloge der oberösterreichischen Landesmuseen Neue Serie 86(2009): 243–256. [in German]

Weitschat W, Wichard W (2002) Atlas of Plants and Animals in Baltic Amber. Verlag Dr. Friedrich Pfeil, München (Germany), 256 pp.

Wheeler WM (1928) The Social Insects. Their Origin and Evolution. Kegan Paul, Trench, Trubner & Co. Ltd./Harcourt, Brace and Company, London (UK)/New York (USA), 378 pp. https://www.biodiversitylibrary.org/item/238968#page/7/mode/1up

Whitfield JB (2003) Phylogenetic insights into the evolution of parasitism in Hymenoptera. In: Advances in Parasitology. Vol. 54. Elsevier Ltd., Oxford (UK), 69–101. https://doi.org/10.1016/S0065-308X(03)54002-7

Williams FX (1919) *Epyris extraneus* Bridwell (Bethylidae), a Fossorial Wasp That Preys on the Larva of the Tenebrionid Beetle, *Gonocephalum seriatum* (Boisduval). Proceedings of the Hawaiian Entomological Society 4(1): 55–63. http://hdl.handle.net/10125/15656

Witethom B, Gordh G (1994) Development and Life Table of *Gonzozus thallandensis* Gordh & Witethom (Hymenoptera: Bethylidae), A Gregarious Ectoparasitoid Of A Phycitine Fruit Borer (Lepidoptera: Pyralidae). Journal of the Science Society of Thailand 20: 101–114. https://doi.org/10.2306/scienceasia1513-1874.1994.20.101

Witmer LM (1995) The Extant Phylogenetic Bracket and the importance of reconstructing soft tissues in fossils. In: Thomason J (Ed.) Functional Morphology in Vertebrate Paleontology. Cambridge University Press, Cambridge (UK), 19–33.

Yang Z-Q, Wang X-Y, Yao Y-X, Gould JR, Cao L-M (2012) A New Species of *Sclerodermus* (Hymenoptera: Bethylidae) Parasitizing *Agrilus planipennis* (Coleoptera: Buprestidae) From China, With a Key to Chinese Species in the Genus. Annals of the Entomological Society of America 105(5): 619–627. https://doi.org/10.1603/AN12017

Yu T, Thomson U, Mu L, Ross R, Kennedy J, Broly P, Xia F, Zhang H, Wang B, Dilcher D (2019) An ammonite trapped in Burmese amber. Proceedings of the National Academy of Sciences 116(23): 11345–11350. https://doi.org/10.1073/pnas.1821292116

Zherikhin VV, Ross AJ (2000) A review of the history, geology and age of Burmese amber (Burmite). Bulletin of the Natural History Museum, London (Geology Series) 56(1): 3–10. https://www.biodiversitylibrary.org/page/40537672#page/5/mode/1up

Zippel A, Kiesmüller C, Haug GT, Müller P, Weiterschan T, Haug C, Hörnig MK, Haug JT (2021) Long-headed predators in Cretaceous amber—fossil findings of an unusual type of lacewing larva. Palaeoentomology 004(5): 475–498. https://doi.org/10.11646/palaeoentomology.4.5.14

Fossil Record 25 (2) 2022, 307–330 | DOI 10.3897/fr.25.83276

PENSOFT

für Natur MUSEUM FÜR NATURKUNDE BERLIN

Revision of the *Semicytherura henryhowei* group (Crustacea, Ostracoda) with the new records from Korea

Anna B. Jöst[1], Taihun Kim[2], Hyun-Sung Yang[2], Do-Hyung Kang[2], Ivana Karanovic[1,3,4]

1 *Department of Life Science, College of Natural Sciences, Hanyang University, Seoul, 04763, Republic of Korea*
2 *Jeju Marine Research Center, Korea Institute of Ocean Science and Technology, Jeju 63349, Republic of Korea*
3 *Research Institute for Convergence of Basic Science, Hanyang University, Seoul, 04763, Republic of Korea*
4 *Institute for Marine and Antarctic Studies, University of Tasmania, Private Bag 49, 7001, Hobart, Tasmania, Australia*

https://zoobank.org/BF8C7768-181B-4A75-9CF4-9C6F3DC6D559

Corresponding authors: Anna B. Jöst (annajoest@outlook.com), Ivana Karanovic (ivana@hanyang.ac.kr)

Academic editor: Carolin Haug ♦ **Received** 8 March 2022 ♦ **Accepted** 5 October 2022 ♦ **Published** 4 November 2022

Abstract

The genus *Semicytherura* Wagner, 1957 has nearly 300 species, is common in shallow and marginal marine habitats, and has a worldwide distribution. It is divided into several species groups, of which the *Semicytherura henryhowei* Hanai & Ikeya, 1977 group is one of the most frequently recorded in temperate Asia. A previous study indicated that many of its members are actually species complexes, and that several morphotypes could be distinguished by carapace shape and ornamentation. We review these complexes and conclude that the *henryhowei* group currently contains 29 species, nine of which are undescribed. We also provide an illustrated guide and a key to species, based on newly standardized carapace ridge terminology. This enabled us to describe one new species from the extant (i.e., present-day) sediments in Jeju Island, Korea, *S. kiosti* **sp. nov.** We also found one juvenile valve of *S. kazahana* Yamada, Tsukagoshi & Ikeya, 2005, the first official illustrated record of this species from Korean waters. Our revised spatial and temporal distributions of fossil and extant records from this group provide new insights into trans-Arctic interchange of ostracod fauna from the Late Miocene onwards.

Key Words

Benthic Ostracoda, identification key, MarineGEO ARMS, new species, taxonomy, trans-Arctic interchange

Introduction

Semicytherura Wagner, 1957 is a podocopid ostracod genus, belonging to the family Cytheruridae. It comprises at least 291 species, 126 of which are known only from the fossil record. A total of 283 of these species are listed in the World Register of Marine Species (Brandão et al. 2022), whereas at least the following eight are missing: *Semicytherura leptosubundata* (Ozawa & Kamiya, 2008), *S. obitsuensis* (Nakao & Tsukagoshi, 2020), *S. pseudoundata* Irizuki & Yamada in Irizuki et al. (2004), *S. robustundata* (Ozawa & Kamiya, 2008), *S. skippa* (Hanai, 1957), *S. subslipperi* Ozawa & Kamiya, 2008, *S. tanimurai* (Ozawa & Kamiya, 2008), and *S. tetragona* (Hanai, 1957). The last species was described as *Cytherura tetragona* Hanai, 1957 and is still listed as such in the World Register of Marine Species (Brandão et al. 2022). However, *Cytherura* Sars, 1866 and *Semicytherura* show distinctive differences in carapace features, like hingement and calcified inner lamella (Wagner 1957; Athersuch et al. 1989; Whatley and Cusminsky 2010). Based on these, *Cytherura tetragona* should be re-assigned to *Semicytherura*, as already adopted by some ostracodologists [e.g., Yamada et al. (2005)].

There are more than 40 species of *Semicytherura* (including records in open nomenclature) reported from Japan and adjacent areas (Yamada et al. 2005). However, reports specifically from Korean waters are uncertain. The only officially published and illustrated species reported from Korea is a specimen assigned to *S. minaminipponica*

(Ishizaki, 1981) from the Plio-Pleistocene deposits of Jeju Island (Paik and Lee 1988). The study also mentions *S. henryhowei* Hanai & Ikeya in Hanai et al. 1977, as well as seven undescribed species left in the open nomenclature, but no images or illustrations are provided. Several other papers have been published that mention various *Semicytherura* species from Korea, but none of them offer taxonomic proof. For example, Ikeya and Cronin (1993) report *S. miurensis* (Hanai, 1957) in their factor 6 assemblage from the Korean Peninsula, in addition to another 15 *Semicytherura* species from both Japan and Korea but they do not specify which species occur where (Ikeya and Cronin 1993). Lee et al. (2000) list the following fossil species from the Korea's East coast: *S. elongata* (Edwards, 1944), *S.* cf. *elongata*, *S.* cf. *subundata* (Hanai, 1957), *S. wakamurasaki* Yajima, 1982, *S.* cf. *wakamurasaki*, and *S. daishakaensis* (Tabuki, 1986) (typographical error in Lee et al. 2000: *S. daishakensis*). They also list these extant (i.e., present-day) species: *S. hanaii* Ishizaki, 1981, *S.* cf. *henryhowei*, *S.* cf. *hiberna* Okubo, 1980, *S. miurensis*, *S.* cf. *miurensis*, *S. polygonoreticulata*, and *S.* cf. *sabula* (Frydl, 1982) (Lee et al. 2000). Schornikov and Zenina (2008) mention *S. kazahana* Yamada, Tsukagoshi & Ikeya, 2005, *S. mukaishimensis* Okubo, 1980, and *S. polygonoreticulata* (Ishizaki & Kato, 1976) occurring along the coastal zone of Jeju Island. Additionally, Yamada et al. (2005) refer to an unpublished Korean record of *S. kazahana* by Lee (1990; unpublished) as *Semicytherura* sp. B. Here, we provide the first published record including illustrations of *S. kazahana* from Korean waters.

Semicytherura species can be grouped based on their general shape and dominant carapace features. Yamada et al. (2005) report five species groups from Japan and adjacent areas: the *henryhowei*, *miurensis*, *skippa*, *hanaii*, *tetragona*, and *sabula* group. Here, we focus on species from the *henryhowei* group, which comprises animals of sub-rectangular to sub-trapezoid shape (right valves tend to be more sub-trapezoid and left valves more sub-rectangular), with thick carapace and a system of broad ridges (carinae) and a horizontal caudal process with varying degree of conspicuousness.

Prior to the study of Yamada et al. (2005), several *S. henryhowei* morphotypes have been recognized (see e.g., Okubo 1980). Phenotypic plasticity is rather common in shallow marginal marine genera [for detailed discussion on morphological variation in marginal marine ostracods, see Jöst et al. (2021)], and *Semicytherura* species primarily inhabit inner bays, tolerating brackish environments, and are often associated with plants (Boomer and Eisenhauer 2002; Szczechura and Aiello 2003; Yamada et al. 2005; Schellenberg 2007). Yamada et al. (2005) studied more than 200 specimens of different *S. henryhowei* morphotypes from Japan and found that they are, in fact, four separate species: *S. henryhowei*, *S. kazahana*, *S. slipperi* Yamada, Tsukagoshi & Ikeya, 2005, and *S. sasameyuki* Yamada, Tsukagoshi & Ikeya, 2005. Besides differences in the soft-body morphology, the species can be distinguished by differences in the carapace pore system, and ridge pattern (Yamada et al. 2005). Prior to this, Irizuki et al. (2004) described *Semicytherura pseudoundata* Irizuki & Yamada, 2004 from the Early Miocene deposit of Japan. They noted its close morphological similarity to *S. henryhowei* and *S. undata* (Sars, 1866), but described it as new, based on the distinct differences in the ventral ridge (Irizuki et al. 2004). Additionally, Ozawa and Kamiya (2008) added four new Pleistocene species, following the application of the distinct ridge patterns as a species-specific taxonomic character introduced by Yamada et al. (2005). They described *S. robustundata* Ozawa & Kamiya, 2008, *S. subslipperi* Ozawa & Kamiya, 2008, *S. leptosubundata* Ozawa & Kamiya, 2008, and *S. tanimurai* Ozawa & Kamiya, 2008 as new members of the *henryhowei* group. Yamada and Tsukagoshi (2010) added two more extant species, *S. maxima* Yamada & Tsukagoshi, 2010 and *S. ikeyai* Yamada & Tsukagoshi, 2010. They also conducted a comparative morphological study to determine which of the species belongs to the *henryhowei* group. As a result, besides the above mentioned 12 species, the following 20 are also considered members (see Appendix 1): *S. balrogi* Brouwers, 1994; *S. subundata* (Hanai, 1957); *S.* aff. *S. henryhowei* sensu Cronin and Ikeya (1987); *S.* aff. *henryhowei* sensu Irizuki (1994); *S.* cf. *henryhowei* sensu Cronin (1989); *S. neosubundata* (Ishizaki, 1966); *S. simplex* (Brady & Norman, 1889); *Semicytherura* sp. 1–5 sensu Irizuki (1994); *Semicytherura* sp. sensu Irizuki et al. (2005); *Semicytherura* sp. 1 sensu Yasuhara and Irizuki (2001); *Semicytherura* sp. 2 sensu Yamada et al. (2002); *Semicytherura* sp. 1–2 sensu Ozawa et al. (2008); *Semicytherura* sp. A sensu Cronin and Ikeya (1987); *Semicytherura* sp. B sensu Whatley and Boomer (1995); and *Kangarina* sp. B sensu Valentine (1976) (Yamada and Tsukagoshi 2010).

The first treatise list reporting members of the *S. henryhowei* group included 30 species, whereas 20 of these were left in the open nomenclature (Yamada et al. 2005) (Appendix 1). This list was later revised and eight of these 20 open-nomenclature-records were identified to the species level (Yamada and Tsukagoshi 2010). However, four records previously left in the open nomenclature were added, six species records were re-assigned to other species, and several new species were added. Finally, the updated list contains 32 species in total, of which 16 were left in the open nomenclature and another 16 were identified (Yamada and Tsukagoshi 2010) (Appendix 1).

Here, following the scheme of the species-specific ridge pattern, we conducted a revision of the updated treatise list by Yamada and Tsukagoshi (2010) and found that, amongst the records of *S. henryhowei*, there are two occurrences where the specimens belong to a different species (see Table 1). We also found that seven of the sixteen species left in the open nomenclature belong to already described species of the *henryhowei* group, whereas nine species are new to science (Table 1). Additionally, we recognized six more species records that also belong to the *henryhowei* group, that were not included in the list of members by Yamada and Tsukagoshi (2010) [*S. quadraplana* Allison & Holden, 1971; *S. kaburagawensis* Tanaka, 2013; *S. usuigawensis* Tanaka, 2013;

Semicytherura sp. A and B sensu Yamada et al. (2004); and *Hemicytherura* sp. 3 sensu Ikeya and Itoh (1991)] (Appendix 1).

Our taxonomic revision changes the known geological age of *S. tanimurai*, *S. kazahana/sasameyuki*, and *S. undata*, as well as the geological age and spatial distribution of *S. balrogi* and *S. ikeyai*. Revised distribution and remarks on the geological age are discussed with updated (paleo-)distribution maps. Additionally, we describe one new species belonging to the *henryhowei* group, *S. kiosti* sp. nov. Jöst and Karanovic, and show the first official record of *S. kazahana* from Korean waters. Finally, we generated an identification key to the species of this group, including illustrations of all known members to aid future taxonomic research.

Methods

Project

The material provided here was collected as a part of an ongoing project that collaborates with the Marine Global Earth Observatory (MarineGEO) program and in partnership with the Korea Institute of Ocean Science and Technology (KIOST) on Jeju Island, Republic of Korea (ROK). The MarineGEO is under the umbrella of the Smithsonian's global Tennenbaum Marine Observatories Network (TMON) with its headquarters in Washington, D.C., USA (https://marinegeo.si.edu/). It is the first long-term research program with partners from all over the world, applying a standardized method of sampling (ARMS, Fig. 1) to study coastal marine biodiversity. Its main aim is to understand the role of biodiversity in sustaining resilient marine ecosystems. As such, a thorough taxonomic knowledge of the current species is indispensable.

Samples

Specimens were collected either from an Autonomous Reef Monitoring Structure (ARMS) (Fig. 1A, B, E), or from the sediment scoop samples (i.e., surface sediments) near the ARMS in August, 2019. The ARMS are standardized, three-dimensional samplers of marine biodiversity that are non-destructive to the environment. They are shelf-like units made of stacks of plates with different sized spacers in between the plates. Plate by plate, the units are assembled under water and left there, passively collecting the sample (i.e., surface and sedimentation-derived sediments) (Fig. 1C–E). For this study, ARMS were deployed by scuba at 19 m at Seongsan, Jeju Island, South Korea (Fig. 2) on the 3rd of October, 2018 and left under the water until retrieval on August 20th, 2019. On board the boat, the ARMS unit was immediately transferred to a recovery bin and submerged in the filtered seawater. Upon arrival on shore, the unit was disassembled inside the recovery bin and anything on and in between the plates was fixed with 99% ethanol. Living and dead ostracods were wet-picked in 99% ethanol from the 100–500 µm size fractions of the material collected by the ARMS unit and the scoop sample, respectively. Five of the 7 specimens presented here were recovered from the ARMS sample. Two specimens were recovered from a sediment scoop sample. The scoop sample was collected by SCUBA from the sea floor next to the ARMS structure during retrieval. A 50 mL conical tube was used to scoop up the sediment. Picking and sorting were done using a stereomicroscope (Olympus SZX12) in the Laboratory of Animal Systematics and Phylogeny at Hanyang University, ROK. Each disarticulated valve is counted as one specimen. One articulated male adult carapace was found and opened for the scanning electron microscope (SEM) imaging (LV: # 109_1 (lost during imaging); RV: 109_2).

Table 1. Revised species assignments of the members of the *Semicytherura henryhowei* group. Bold font indicates specimens of the treatise list by Yamada and Tsukagoshi (2010).

Author name	Species name	Revised species name
Cronin and Ikeya (1987)	***Semicytherura* aff. *S. henryhowei***	*S. balrogi*
Cronin and Ikeya (1987)	***Semicytherura* sp. A**	*Semicytherura* sp. nov.
Cronin (1989)	***Semicytherura* cf. *S. henryhowei***	*Semicytherura* sp. nov.
Ikeya and Itoh (1991)	*Hemicytherura* sp. 3	*S. kiosti* sp. nov. Jöst & Karanovic
Irizuki (1994)	***Semicytherura henryhowei***	*S. balrogi*
Irizuki (1994)	***Semicytherura* aff. *S. henryhowei***	*Semicytherura* sp. nov.
Irizuki (1994)	***Semicytherura* sp. 1**	*Semicytherura* sp. nov.
Irizuki (1994)	***Semicytherura* sp. 2**	*Semicytherura* sp. nov.
Irizuki (1994)	***Semicytherura* sp. 3**	*S. undata*
Irizuki (1994)	***Semicytherura* sp. 4**	*Semicytherura* sp. nov.
Irizuki (1994)	***Semicytherura* sp. 5**	*Semicytherura* sp. nov.
Irizuki et al. (2005)	***Semicytherura* sp.**	*S. kazahana*
Ozawa et al. (2008)	***Semicytherura* sp. 1**	*Semicytherura* sp. nov.
Ozawa et al. (2008)	***Semicytherura* sp. 2**	*Semicytherura* sp. nov.
Whatley and Boomer (1995)	***Semicytherura* sp. B**	*S. ikeyai*
Yajima (1988)	***Semicytherura henryhowei***	*S. sasameyuki/ S. kazahana*
Yamada and Tsukagoshi (2010)	***Kangarina* sp. B sensu Valentine (1976)**	*S. balrogi*
Yamada et al. (2002)	***Semicytherura* sp. 2**	*S. tanimurai*
Yamada et al. (2004)	*Semicytherura* sp. A	*S. sasameyuki/ S. kazahana*
Yamada et al. (2004)	*Semicytherura* sp. B	*S. slipperi*
Yasuhara and Irizuki (2001)	***Semicytherura* sp. 1**	*S. kazahana*

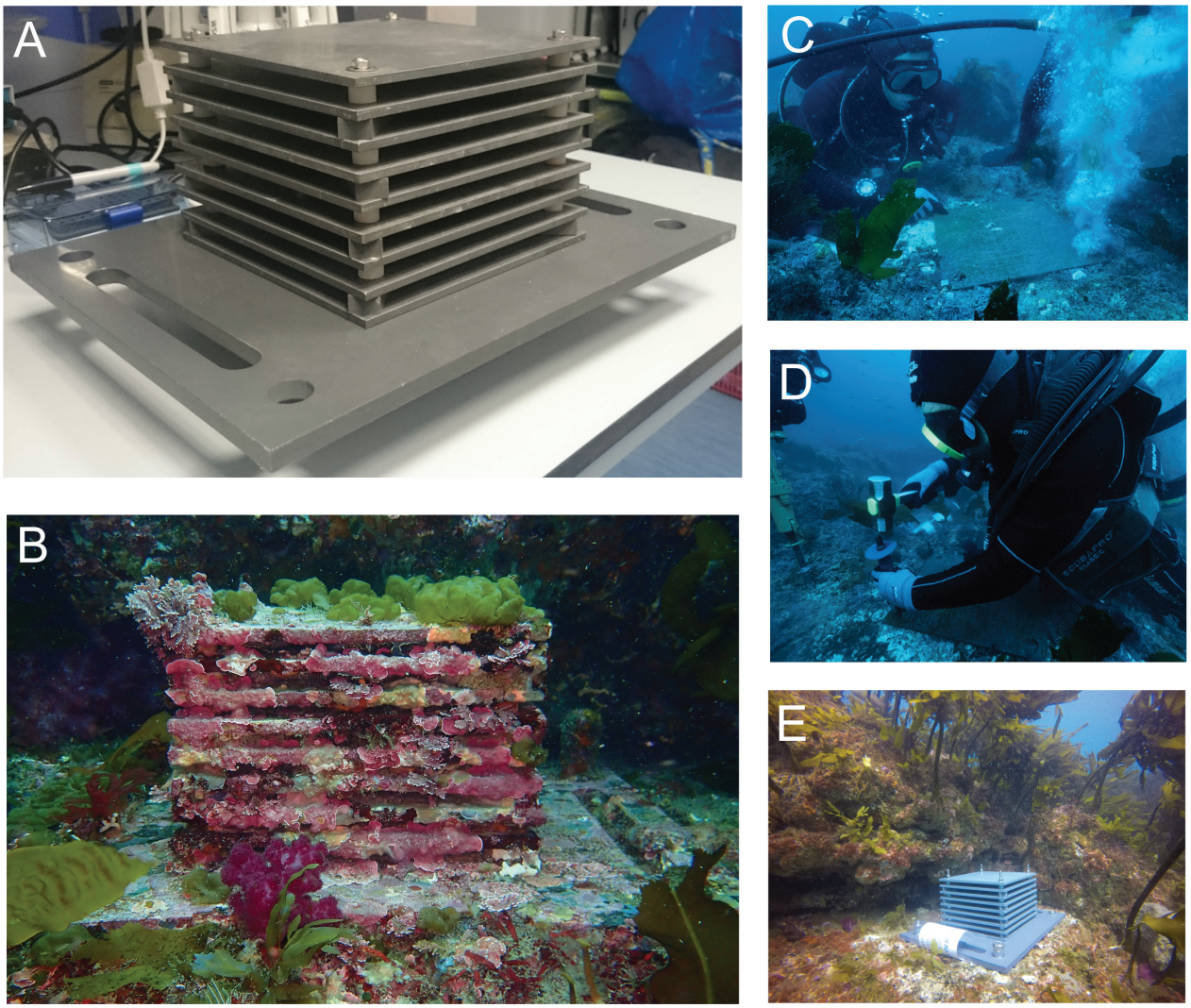

Figure 1. Autonomous Reef Monitoring Structure (ARMS). **A.** Assembled ARMS; **B.** ARMS after one year of deployment at Seongsan (representative photo); **C–E.** ARMS installation by SCUBA (representative photos).

The SEM images were taken at Eulji University, ROK, with a Hitachi S-4700 scanning electron microscope after platinum coating.

The type material of *Semicytherura kiosti* sp. nov. (holotype: one male ARV, # 109_2; paratypes: five RVs (# 68 female A, # 108 male A, # 177 female A-1, # 239 female A-2, # 240 female A) and our specimen of *S. kazahana*, are deposited in the National Institute of Biological Resources (NIBR) in Incheon, ROK (deposition number *S. kiosti*: DSEVIV0000003716; *S. kazahana*: DSEVIV0000003720). The new species is registered with ZooBank (*LSID.* urn:lsid:zoobank.org:act:DAA1DAD2-32A5-4F02-8143-D0D158F8568B).

Maps and plot

Sampling location and geographic distribution of selected species were mapped with the software QGIS (version 3.16.8 Hannover; 1989, 1991, Free Software Foundation, Inc.). Continent shapefiles were acquired through open sources at https://www.igismap.com, country specific shapefiles through https://gadm.org/download_country_v3.html. Map depicting trans-Arctic interchange through time were generated with MapCreator (version 2.0; personal edition) and edited with vector graphics software Inkscape (0.92.1 version 3; 2007, Free Software Foundation, Inc.). Length/height plot was generated with SigmaPlot (version 10.0; 2006, Systat Software, Inc.) and edited with Inkscape 0.92.

Abbreviations

ALV Adult left valve;
ARV Adult right valve;
A-1 A-1 instar (last juvenile molt before adult);
A-2 A-2 instar (second-last molt before adult).

Data availability

Specimens are deposited at the National Institute of Biological Studies (NIBR, Incheon, South Korea) under the deposition numbers DSEVIV0000003716 (*S. kiosti*

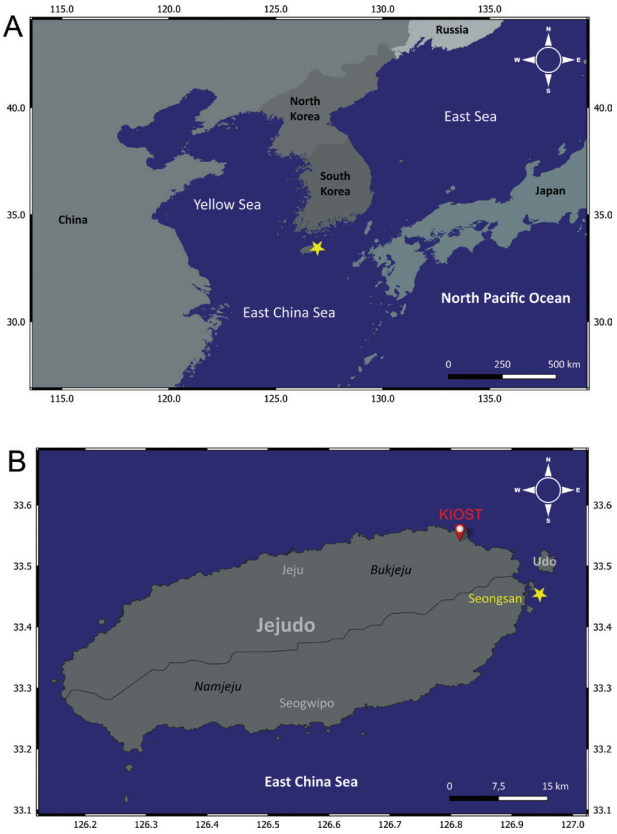

Figure 2. Map of sampling location. **A.** Overview of Korea including adjacent countries and seas; **B.** Overview of Jeju Island with sampling location in yellow. Yellow star denotes the deployment site of the ARMS; red location pin icon points at the location of the Korea Institute of Ocean Science and Technology (KIOST) on Jeju Island; grey shades denote land masses, blue denotes seas. Coordinates given in decimal degrees.

sp. nov.) and DSEVIV0000003720 (*S. kazahana*). This published work and the nomenclatural acts it contains, have been registered in ZooBank (LSID. urn:lsid:zoobank.org:act:DAA1DAD2-32A5-4F02-8143-D0D158F8568B).

Results

Yamada and Tsukagoshi (2010) provided a treatise list of all published members of the *henryhowei* group, and included a total of 32 species: 16 named and 16 left in the open nomenclature. We studied all species and identified all unnamed species based on distinctive ridge pattern and prominent carapace characteristics. A schematic explanation of the ridge terminology is given in Fig. 3. Additionally, we added seven more species, previously not included in the treatise list, namely *Semicytherura* sp. 1 sensu Yamada et al. (2002), *Semicytherura quadraplana* Allison & Holden, 1971, *Hemicytherura* sp. 3 sensu Ikeya and Itoh 1991, *Semicytherura kaburagawensis* Tanaka, 2013, *Semicytherura usuigawensis* Tanaka, 2013, and *Semicytherura* sp. A and B sensu Yamada et al. (2004) (Appendix 1). The following species assignments were concluded (see also Table 1):

S. henryhowei sensu Irizuki (1994) (pg. 13, pl. 3, figs 1, 2) is most likely *S. balrogi* Brouwers, 1994

The two valves pictured clearly show the anterior longitudinal ridge extending past the anterior third and connecting with the dorsal margin at the posterodorsal corner, which is characteristic for specimens of *S. balrogi* (Fig. 4P). True, *S. henryhowei* does not have such a long, smooth anterior longitudinal ridge (Fig. 4F). Additionally, *S. henryhowei* has a thin ridge branching off the dorsal margin at two-thirds of the valve length, in front of the posterodorsal corner, connecting with the anterior subvertical ridge within the dorsal half (Fig. 4F). The imaged left valve (fig. 1; Irizuki, 1994) shows no posterior subvertical ridge, whereas the right valve shows an inconspicuous, short posterior subvertical ridge, not merging with the ventral ridge. Both, *S. henryhowei* and *S. balrogi* lack the posterior subvertical ridge.

Semicytherura aff. *S. henryhowei* sensu Cronin and Ikeya (1987) (pg. 83, pl. 3, fig. 13) is most likely *S. balrogi*

The pictured left valve shows a conspicuous, long, arching anterior longitudinal ridge, running from the mid-height at the anterior margin to the posterodorsal corner without prominent ridges connecting it with the ventral ridge, which is typical of *S. balrogi* (Fig. 4P).

Kangarina sp. B sensu Valentine (1976) (pl. 5, fig. 15) is probably *S. balrogi*

The pictured right valve has four anteroventral marginal denticles, a long anterior longitudinal ridge, and a ventral ridge that starts off anteriorly at the height of the third anteroventral marginal denticle, slightly arching toward the ventral margin, then both merging within the posterior third of the valve, before ascending toward the posterior ridge. All these characteristics are distinct patterns found in *S. balrogi* (Fig. 4P).

S. henryhowei sensu Ikeya and Itoh (1991) (pg. 143, fig. 22C) is most likely *S. ikeyai* Yamada & Tsukagoshi (2010)

The pictured left valve is characterized by a continuous anterior longitudinal ridge that connects with the dorsal margin at the posterior half, in front of the posterodorsal corner, which is typical for *S. ikeyai* (Fig. 4N).

Semicytherura sp. B sensu Whatley and Boomer (1995) (pg. 255, pl. 1, figs 6, 7) is most likely *S. ikeyai*

The pictured right and left valves show an anterior longitudinal ridge ascending in a nearly straight manner from the

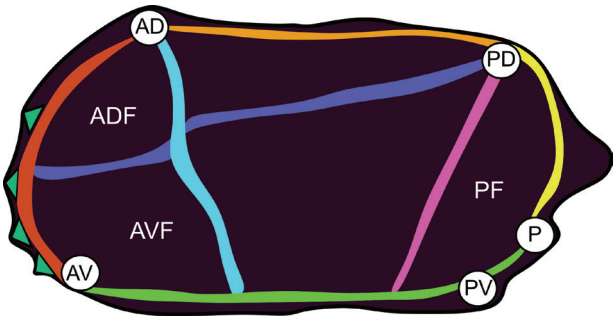

Figure 3. Schematic drawing for terminology of major ridges (carinae) of the *Semicytherura henryhowei* group. Red: anterior ridge; orange: dorsal ridge; yellow: posterior ridge; green: ventral ridge; pink: posterior subvertical ridge; blue: anterior sublongitudinal ridge; turquoise: posterior subvertical ridge; Green triangles: anteroventral marginal denticles (crenulations); white dots: corners; AD: Anterodorsal; PD: posterodorsal; P: posterior; PV: posteroventral; AV: anteroventral; ADF: anterodorsal fossa; AVF: anteroventral fossa; PF: posterior fossa.

anterior margin at mid-height of the valve to the end of the anterior third above mid-height, where the anterior subvertical ridge crosses in the posteroventral direction and a thin ridge splits from the anterior half of the anterior subvertical ridge, and merging, as dorsal continuation of the anterior longitudinal ridge, with the dorsal margin in front of the posterodorsal corner. The ventral ridge is comparably thin. These are typical morphological traits of *S. ikeyai* (Fig. 4N). In case of the specimens of Whatley and Boomer (1995), the ridge connecting the anterior subvertical ridge with the dorsal margin is rather inconspicuous.

Semicytherura sp. sensu Irizuki et al. (2005) (pg. 42, pl. 4, fig. 7) is most likely *S. kazahana* Yamada, Tsukagoshi & Ikeya, 2005

The pictured right valve has a short anterior longitudinal ridge, which, with the anterior subvertical ridge, splits the anterior half of the valve into two fossae. The posterior ridge connecting the ventral ridge with the dorsal ridge is distinct. The ventral half of the anterior subvertical ridge is wider than the dorsal half. There appears to be five marginal anteroventral denticles, although the anterior edge of the specimen is not clear. All these characteristics resemble *S. kazahana* (Fig. 4H).

Semicytherura sp. 3 sensu Irizuki (1994) (pg. 13, pl. 3, figs 8–11) is most likely *S. undata* (Sars, 1866)

The imaged right and left valves have the ventral ridge typical for *S. undata* (Fig. 4L). It starts from, or close to, the anteroventral margin and runs in a slightly convex curve above the ventral margin until the anterior third to half of the valve length. From there, it descends in a straight, diagonal line toward the ventral margin until merging with it and terminating at or behind the posterior third of the valve length. The subvertical dorsal ridge, however, is lacking in some specimens [pl. 3, figs 9–11 (Irizuki 1994)], which is uncharacteristic for *S. undata*. One pictured left valve [pl. 3, fig. 8 (Irizuki 1994)] has a short subvertical dorsal ridge, as typical for specimens of *S. undata* (Fig. 4L). The dorsal ridge of *S. undata* is characterized by a prominent, very short, "comma-shaped" ridge in the posteroventral area, which all specimens here show, although to a varying extent (Irizuki 1994).

Semicytherura sp. B sensu Yamada et al. (2004) is most likely *S. slipperi* Yamada et al., 2005

The pictured left valves (pg. 383, text-figs 2C, E) are characterized by a short anterior longitudinal ridge, steeply running upward in a straight fashion, thickening toward its posterior end at the anterior third of the valve-length (Fig. 4D). The posterior subvertical ridge is lacking. The ventral part of the anterior subvertical ridge is not a smooth continuation of the slightly curved, prominent dorsal part, but connecting to the ventral ridge in a rather inconspicuous zig-zag manner. Four anteroventral marginal denticles are present (Yamada et al. 2004).

Semicytherura sp. A sensu Yamada et al. (2004) is either *S. sasameyuki*, or *S. kazahana* Yamada, Tsukagoshi & Ikeya, 2005

The pictured left valve (pg. 383, text-fig. 2A) shows the typical ridge pattern of *S. kazahana* [pg. 247, fig. 2C, pg. 253, fig. 6; (Yamada et al. 2005)] and *S. sasameyuki* [pg. 247, fig. 2D; pg. 255, fig. 8; (Yamada et al. 2005)]. The anterior subvertical ridge smoothly connects to the anterior longitudinal ridge with its dorsal part, and to the ventral ridge with its ventral part. The posterior subvertical ridge is smooth, tapering toward ventral and connecting with the ventral ridge. The four comparably large, acuminate, anterior marginal denticles can indicate the specimen's association to both, *S. sasameyuki* (Fig. 4J), which always shows four marginal denticles, as well as to *S. kazahana* (Fig. 4H), which may either show four or five marginal denticles, or none at all (see pg. 243, fig. 6A–D, four denticles; E, zero denticles; F, five denticles; Yamada et al. 2005). For a definite distinction between the two species, soft-body analysis is necessary.

Semicytherura sp. 1 sensu Yasuhara and Irizuki (2001) is most likely *S. kazahana*

The pictured adult left and juvenile right valves (pg. 93, pl. 11 figs 7, 8) show the typical ridge pattern of *S. kazahana* and *S. sasameyuki* (Yamada et al. 2005). However, the adult valve shows the presence of four anteroventral marginal denticles (pg. 93, pl. 11, fig. 7), whereas they are absent

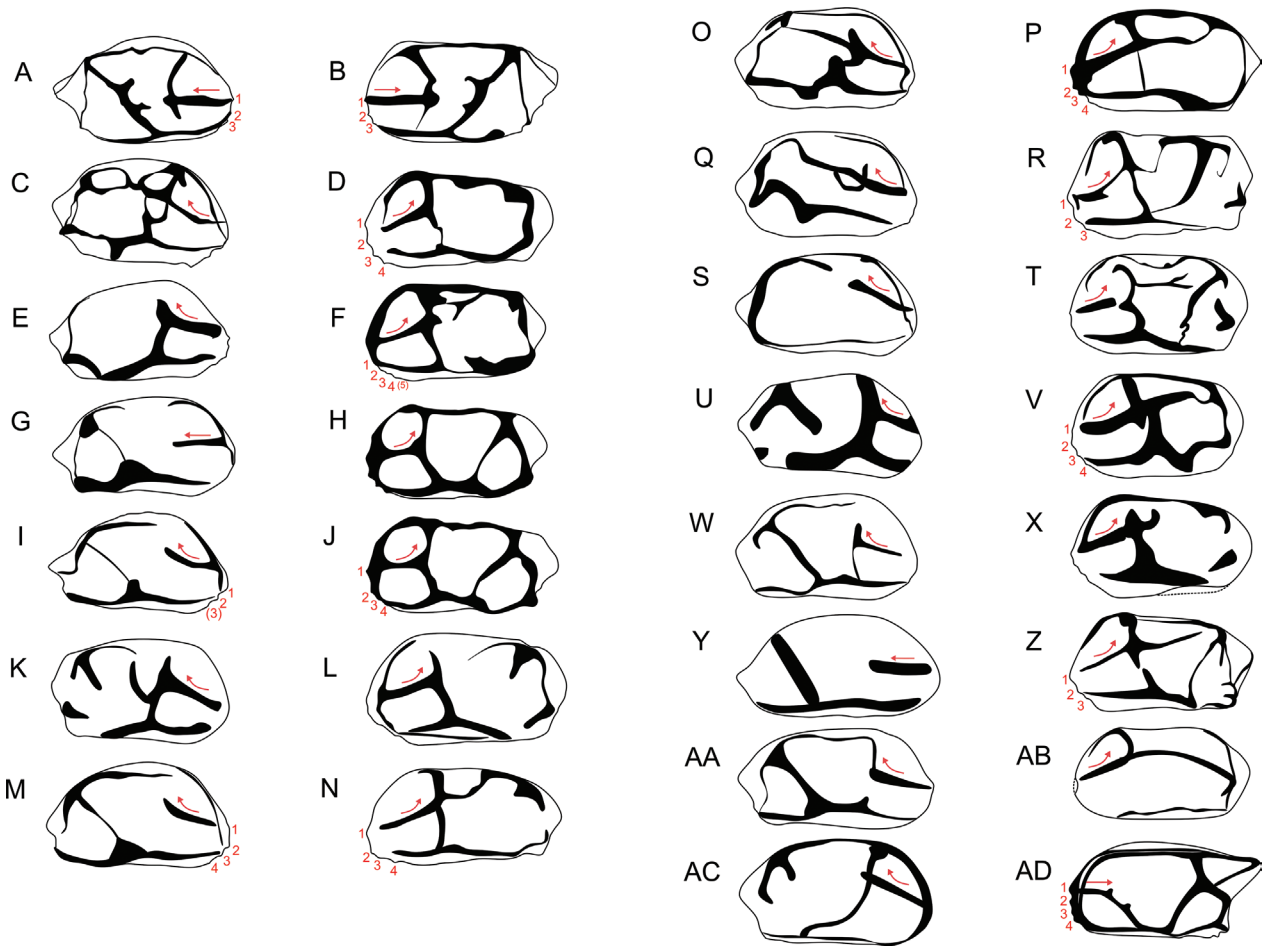

Figure 4. Illustrated guide of major ridge systems of the *Semicytherura henryhowei* species complex. **A.** *Semicytherura kiosti* sp. nov. Jöst and Karanovic male ARV; based on # 109_2 herein; **B.** *Semicytherura kiosti* sp. nov. Jöst and Karanovic male ALV; based on # 109_1 herein; **C.** *Semicytherura robustundata* Ozawa & Kamiya, 2008 ARV; based on Ozawa and Kamiya 2008; **D.** *Semicytherura slipperi* Yamada, Tsukagoshi & Ikeya, 2005 ALV; based on Yamada et al. 2005; **E.** *Semicytherura subslipperi* Ozawa & Kamiya, 2008 ARV; based on Ozawa and Kamiya 2008; **F.** *Semicytherura henryhowei* Hanai, 1977 ALV; based on Yamada et al. 2005; **G.** *Semicytherura leptosubundata* Ozawa & Kamiya ARV; based on Ozawa and Kamiya 2008; **H.** *Semicytherura kazahana* Yamada, Tsukagoshi & Ikeya, 2005 ALV; based on Yamada et al. 2005; **I.** *Semicytherura subundata* (Hanai, 1957) ARV; based on Ozawa and Kamiya 2008; **J.** *Semicytherura sasameyuki* Yamada, Tsukagoshi & Ikeya, 2005 ALV; based on Yamada et al. 2005; **K.** *Semicytherura tanimurai* Ozawa & Kamiya, 2008 ALV; based on Ozawa and Kamiya 2008; **L.** *Semicytherura undata* (Sars, 1865) ARV; based on Cronin and Ikeya 1987; **M.** *Semicytherura maxima* Yamada & Tsukagoshi, 2010 ARV; based on Yamada and Tsukagoshi 2010; **N.** *Semicytherura ikeyai* Yamada & Tsukagoshi, 2010 ARV; based on Yamada and Tsukagoshi 2010; **O.** *Semicytherura* sp. nov. sensu Irizuki 1994 (*S.* sp. 4) ALV; based on Irizuki 1994; **P.** *Semicytherura balrogi* Brouwers, 1994 ARV; based on Brouwers 1994; **Q.** *Semicytherura* sp. nov. sensu Irizuki 1994 (*S.* sp. 5) ALV; based on Irizuki, 1994; **R.** *Semicytherura* sp. nov. sensu Cronin and Ikeya 1987 (*S.* sp. A) ARV; based on Cronin and Ikeya 1987; **S.** *Semicytherura* sp. nov. sensu Cronin 1989 (*S.* sp. cf. *henryhowei*) ALV; based on Cronin 1989; **T.** *Semicytherura* sp. nov. sensu Irizuki 1994 (*S.* sp. 2) ARV; based on Irizuki 1994; **U.** *Semicytherura simplex* (Brady & Norman, 1889) ALV; based on Hu 1978; **V.** *Semicytherura* sp. nov. sensu Ozawa et al. 2008 (*S.* sp. 1) ARV; based on Ozawa et al. 2008; **W.** *Semicytherura pseudoundata* Irizuki & Yamada, 2004 ALV; based on Irizuki et al. 2004; **X.** *Semicytherura* sp. nov. sensu Ozawa et al. 2008 (*S.* sp. 2) ARV; based on Ozawa et al. 2008; **Y.** *Semicytherura neosubundata* (Ishizaki, 1966) ALV; based on Ishizaki 1966; **Z.** *Semicytherura* sp. nov. sensu Irizuki 1994 (*S.* sp. aff. *henryhowei*) ARV; based on Irizuki 1994; **AA.** *Semicytherura kaburagawensis* Tanaka, 2013 RV; based on Tanaka and Hasegawa 2013; **AB.** *Semicytherura* sp. nov. sensu Irizuki 1994 (*S.* sp. 1) ALV; based on Irizuki 1994; **AC.** *Semicytherura usuigawensis* Tanaka, 2013 RV; based on Tanaka and Hasegawa 2013; **AD.** *Semicytherura quadraplana* Allison & Holden, 1971 ALV; based on the original drawing in Allison and Holden 1971. Red arrows indicate whether anterior sublongitudinal ridge is horizontal or sloped; red numbers indicate the anteroventral marginal denticles.

in the juvenile valve (pg. 93, pl. 11, fig. 8 in Yasuhara and Irizuki 2001). This variation in number of anteroventral denticles indicates that the specimens of Yasuhara and Irizuki (2001) belong to *S. kazahana* (Fig. 4H), unless they present juvenile and adult of separate species. However, although the geographical distribution of *S. kazahana* and *S. sasameyuki* overlaps, their microhabitats differ with the former being a phytal species typical of rocky shore

environments, and the latter living on the silty sands of inner bays (Yamada et al. 2005). This speaks for the presence of just one of the two species, here *S. kazahana*, due to the varying number of anteroventral marginal denticles.

S. henryhowei sensu Yajima (1988) is either *S. sasameyuki*, or *S. kazahana*

The pictured right valve (pg. 1076, pl. 1, fig. 12) shows a prominent posterior subvertical ridge, which is absent in *S. henryhowei* (Fig. 4F). Additionally, *S. henryhowei* has small, rounded, anterior marginal denticles, whereas this specimen shows four distinct and pointy anterior denticles. The ridge pattern, and number and shape of anteroventral denticles, marks this specimen as, either *S. sasameyuki* or *S. kazahana*. Whereas *S. sasameyuki*, so far, has only been reported from extant sediments of Japan, *S. kazahana* has a Pleistocene record from Korea (Lee 1990, unpublished), an extant Japanese distribution (Yamada et al. 2005; living specimens collected 1977–2000), as well as an extant Korean distribution (this study; valves collected 2019). Our species re-assignment indicates a Japanese Miocene existence of either of the species.

Semicytherura sp. 2 sensu Yamada et al. (2002) is most likely *S. tanimurai* Ozawa & Kamiya, 2008

The pictured right valve exhibits a prominent anterior subvertical ridge with a posterior branch at its dorsal half (pg. 122, pl. 1, fig. 16; Ozawa and Kamiya 2008), typical of *S. tanimurai* (Fig. 4K). Although this upward-curved branch is sharper, more like a V-shape in *S. tanimurai* (Fig. 5A), whereas this specimen shows a rounder U-shape (Fig. 5B). Additionally, the ventral ridge is slightly different at its posterior half, as it continues to the posterior tip of the ventral margin (anteroventral corner) (Fig. 5B), whereas in *S. tanimurai* it discontinues after merging with the ventral margin ahead of the anteroventral corner (Fig. 5A). Hence, our species re-assignment to *S. tanimurai* is tentative.

Hemicytherura sp. 3 sensu Ikeya and Itoh 1991 is most likely *S. kiosti* Jöst & Karanovic, sp. nov.

The pictured right valve (pg. 138, fig. 17A) shows all distinct carapace characteristics of *S. kiosti* sp. nov.: three small anteroventral marginal denticles, a prominent posterior subvertical ridge starting at the posterodorsal corner and merging with the ventral ridge at around mid-length, a posterior ridge connecting posterodorsal and posteroventral corners in a straight line, and a horizontal, straight, and short sublongitudinal anterior ridge (Fig. 4B, AA).

The following three species were not included in the list of members of the *S. henryhowei* complex by Yamada and Tsukagoshi (2010), however, based on their prominent ridge systems, they also belong to this species group (Fig. 4AA, AC, AD).

Semicytherura kaburagawensis Tanaka, 2013

The species is characterized by a broad, sigmoid ventral ridge that starts as a thin ridge at anteroventral margin, running parallel to ventral margin toward posterior, growing broader and forming a sigmoid curve at posterior third of carapace length at merging point with subvertical dorsal ridge (pg. 144, fig. 4.2 in Tanaka and Hasegawa 2013). Subvertical dorsal ridge prominent, starting from posterodorsal corner in a bifurced manner (Fig. 4AA). Posterior ridge branch thin, merging with ventral ridge at posteroventral corner; subvertical dorsal ridge branch thick, merging with ventral ridge at posterior third of carapace length. Posterior ridge, subvertical dorsal ridge, and ventral ridge form a rectangular posterodorsal fossa. Anterior sublongitudinal ridge short, mildly arched, slightly ascending, terminating at anterior third of carapace length. Posterior half of subvertical dorsal ridge running from anterodorsal corner (eye tubercle according to type description) ventrally, in a straight, horizontal line, merging with dorsal end of anterior sublongitudinal ridge. Anterior half of subvertical dorsal ridge not observed.

Semicytherura usuigawensis Tanaka, 2013

The species is characterized by a long, sigmoid subvertical dorsal ridge, running from posterodorsal corner ventrally through anterior sublongitudinal ridge, and merging with ventral ridge at posterior third of carapace length (pg. 144, fig. 4.3 in Tanaka and Hasegawa 2013). Posterior subvertical ridge very short. Posterior ridge broad, terminalizing at mid-height. Elliptical anterodorsal fossa (Fig. 4AC).

Semicytherura quadraplana Allison & Holden, 1971

The species is characterized by four anteroventral marginal denticles, a downward arching anterior sublongitudinal ridge that fuses with the ventral half of its anterior subvertical ridge, which, in turn, connects to the ventral ridge within the anterior half of the carapace length (pg. 194, fig. 20b in Allison and Holden 1971). The dorsal half of the anterior subvertical ridge is very short, the posterior subvertical ridge bifurcate, forming an elliptical posterodorsal fossa (Fig. 4AD).

The following nine species did not fit the ridge pattern of any of the known species of the group, hence are undescribed species of the *henryhowei* group:

Semicytherura sp. 1 (pg. 13, pl. 3, fig. 6), *Semicytherura* sp. 2 (pg. 13, pl. 3, fig. 7), *Semicytherura* sp. 4 (pg. 13, pl. 3, figs 12–15), and *Semicytherura* sp. 5 (pg. 13, pl. 3, figs 16, 17) sensu Irizuki (1994)

Semicytherura sp. 1 is too poorly preserved to make any definite statements. However, it appears to exhibit a long anterior longitudinal ridge, arching over the entire length of the valve exterior and terminating when merging with the dorsal ridge below the caudal process (Fig. 4AB). This is a unique feature, not observed in any of the other species of the *S. henryhowei* complex. *Semicytherura* sp. 2 has a conspicuous anterior subvertical ridge shaped like a large "3" (Fig. 4T). Additionally, it sports two, horizontal dorsal ridges, the one closer to the dorsal margin is curved, and the one below is straight and forking at its dorsal end. *Semicytherura* sp. 4 (Fig. 4O) sports a long anterior longitudinal ridge, as do *S. balrogi*, *S. robustundata*, and *S. ikeyai* among the described species of the *S. henryhowei* group. Unlike the three described species, however, its dorsal branch at the anterior third of the anterior longitudinal ridge is short and does not merge with the dorsal margin. Additionally, its anterior subvertical ridge that connects the anterior longitudinal ridge with the ventral ridge is not straight as in *S. balrogi* (Fig. 4P) and *S. ikeyai* (Fig. 4N), but more of a zig-zag line, similar to *S. robustundata* (Fig. 4C). However, whereas in *S. robustundata* this connection is described as a "U-shape" and a "T-shape" (upside-down T) (Fig. 6B), here, it is a hook-shape and upside-down T or Y (Fig. 6A). *Semicytherura* sp. 5 (Fig. 4Q) is characterized by a long anterior longitudinal ridge ascending from mid-height at the anterior margin to the posterodorsal corner, parallel to the likewise ascending ventral ridge, which is situated above the ventral margin (Fig. 4Q). This main pattern of two long, parallel ridges running across the valve is very conspicuous and characteristic of this undescribed species.

Semicytherura sp. A of Cronin and Ikeya (1987) (pg. 83, pl. 3, fig. 10)

The pictured left valve has a very prominent, thick posterior subvertical ridge, tapering toward its ventral tip (Fig. 4R). The ventral ridge is straight, horizontal, and tapering toward posterior. The anterior longitudinal ridge starts below the mid-height of the valve at the ventral margin, and ascends as a curve toward the anterior third of the valve length, where it connects with the anterior subvertical ridge above the mid-height of the valve. Behind the anterior subvertical ridge, it continues in a thin, zig-zag fashion, merging with the dorsal margin/ridge at the mid-length of the valve. The caudal process is broadly triangular, inconspicuous, above the mid-height. The carapace surface is covered in fine pits and thin reticulation.

Semicytherura cf. *S. henryhowei* of Cronin (1989) (pg. 135, pl. 3, figs 3, 4)

The pictured right and left valves are characterized by the absence of the anterior and posterior subvertical ridges (Fig. 4T). The valves are less ornamented by thick ridges, but rather show near-circular inflations in their posterior and anterior halves. The anterior longitudinal ridge starts from the anterior margin at the mid-height of the valve, and ascends toward the end of the anterior third of the valve length, on top of the anterior inflation. A deep, median sulcus separates the anterior longitudinal ridge from its continuation, which merges with the dorsal ridge slightly in front of the posterodorsal corner. The carapace is ornamented by fine pits and thin reticulation.

Semicytherura sp. 1 of Ozawa et al. (2008) (pg. 167, pl. 2, figs 14, 15)

The pictured right and left valves are characterized by comparably thick ridges (Fig. 4V). The ventral ridge is distinct, rising from the anterior to the end of the anterior third of the valve length, where the anterior subvertical ridge connects with it at its peak. It then drops in a straight line to the ventral margin, from where it rises again in a curved fashion to the dorsal corner. The anterior sublongitudinal ridge is long, thick, but its posterior end is either thinner and lower where it connects with the posterodorsal corner (pg. 167, pl. 2, fig. 14; Ozawa et al. 2008), or it terminates as a thick ridge without connecting to the posterodorsal corner (pg. 167, pl. 2, fig. 15; Ozawa et al. 2008). Both valves have four anteroventral marginal denticles.

Semicytherura sp. 2 of Ozawa et al. (2008) (pg. 167, pl. 2, fig. 16)

The pictured left valve lacks a prominent posterior subvertical ridge, and the anterior sublongitudinal ridge continues after the anterior subvertical ridge as a short, upward-curved extension (Fig. 4X). The carapace is ornamented by fine pits and reticulation.

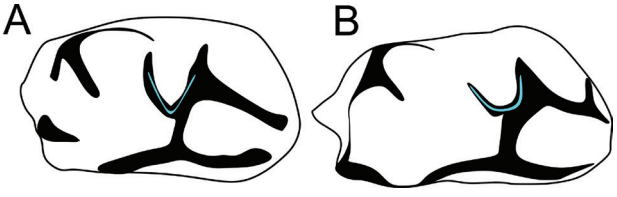

Figure 5. Shape details of posterodorsal branch of anterior subvertical ridge in *Semicytherura* sp. 2 sensu Yamada et al. 2002 proposed *S. tanimurai* Ozawa & Kamiya, 2008 and *S. tanimurai* original type. A. *Semicytherura tanimurai* Ozawa & Kamiya, 2008. B. *Semicytherura* sp. 2 sensu Yamada et al. 2002 proposed *S. tanimurai* Ozawa & Kamiya, 2008. Turquoise highlights the specific shape caused by the different angles, the dorsal branch forks off the anterior subvertical ridge in both specimens.

Semicytherura aff. *henryhowei* of Irizuki (1994) (pg. 13, pl. 3, fig. 3)

The pictured left valve shows an anterior sublongitudinal ridge that continues as a thinner ridge after the crossing of the anterior subvertical ridge. The posterior sublongitudinal ridge is present, but inconspicuous (Fig. 4Z). True, *S. henryhowei* has a short anterior sublongitudinal ridge, terminating when crossing with the anterior subvertical ridge at the end of the anterior third of the valve length, and the posterior subvertical ridge is absent (Fig. 4F). Additionally, *S. henryhowei* has either four or five anteroventral marginal denticles, whereas this species has three (Fig. 4Z).

Key to the species of the *henryhowei* group based on the most prominent carapace characteristics

1 Anterior sublongitudinal ridge horizontal, straight 2
– Anterior sublongitudinal ridge ascending or descending, either in straight line or curved 5
2 Anterior subvertical ridge absent 3
– Anterior sublongitudinal ridge connected to anterior subvertical ridge 4
3 Posterior subvertical ridge prominent, straight; ventral ridge of moderate width (Fig. 4Y) ..... *Semicytherura neosubundata* (Ishizaki, 1966)
– Posterior subvertical ridge thin or inconspicuous; ventral ridge alate (Fig. 4G) ..... *Semicytherura leptosubundata* (Ozawa & Kamiya, 2008)
4 Ventral half of anterior subvertical ridge connected to dorsal ridge; 3 anteroventral marginal denticles (Fig. 4A, B) ..... *Semicytherura kiosti* sp. nov. Jöst & Karanovic
– Ventral half of anterior subvertical ridge short or absent; 4 anteroventral marginal denticles (Fig. 4AD) ..... *Semicytherura quadraplana* Allison & Holden, 1971
5 Anterior sublongitudinal ridge short, terminating at anterior third of valve length; anterior subvertical ridge absent 6
– Anterior sublongitudinal ridge posteriorly connected to other ridge/ridges going in posterior direction and/or anterior subvertical ridge present 8
6 Posterior subvertical ridge present 7
– Posterior subvertical ridge absent (Fig. 4S) ..... *Semicytherura* sp. nov. sensu Cronin 1989 (*Semicytherura* sp. cf. *henryhowei*)
7 Four anteroventral marginal denticles (Fig. 4M) ..... *Semicytherura maxima* Yamada & Tsukagoshi, 2010
– Less than four anteroventral marginal denticles (Fig. 4I) ..... *Semicytherura subundata* (Hanai, 1957)
8 Posterior subvertical ridge absent or short (not connected to ventral ridge) 15
– Posterior subvertical ridge long, connecting posterodorsal corner to ventral ridge 9
9 Posterior fossa present 10
– Posterior fossa absent 13
10 Anterior sublongitudinal ridge long; three anteroventral marginal denticles (Fig. 4Z) ..... *Semicytherura* sp. nov. sensu Irizuki, 1994 (*Semicytherura* sp. aff. *henryhowei*)
– Anterior sublongitudinal ridge short, terminating at anterior third of valve length 11
11 Anterior subvertical ridge connected to ventral ridge 12
– Anterior subvertical ridge not connected to ventral ridge; dorsal half of anterior subvertical ridge straight, vertical, connected to anterodorsal corner (Fig. 4AA) ..... *Semicytherura kaburagawensis* Tanaka, 2013
12 Zero, four, or five anteroventral marginal denticles; in dorsal view, three pores along exterior margin and two pores anterior along interior margin (Fig. 4H) ..... *Semicytherura kazahana* Yamada, Tsukagoshi & Ikeya, 2005
– Four anteroventral marginal denticles; in dorsal view, four pores along exterior margin and one pore anterior along interior margin (Fig. 4J) ..... *Semicytherura sasameyuki* Yamada, Tsukagoshi & Ikeya, 2005
13 Anterior subvertical ridge with prominent, short posterior half not connected to anterodorsal corner, and thin ventral half connecting with ventral ridge (Fig. 4W) ..... *Semicytherura pseudoundata* Irizuki & Yamada, 2004
– Anterior subvertical ridge connecting anterodorsal corner with ventral ridge 14
14 Ventral ridge prominent, thick (Fig. 4T) ..... *Semicytherura* sp. nov. sensu Irizuki 1994 (*Semicytherura* sp. 2)
– Ventral ridge with thick anterior half, thin posteriorly from merging point with anterior subvertical ridge (Fig. 4R) ..... *Semicytherura* sp. nov. sensu Cronin and Ikeya 1987 (*Semicytherura* sp. A)
15 Posterior ridge long, connecting posterodorsal corner with posteroventral corner (Fig. 4L) ... *Semicytherura undata* (Sars, 1866)
– Posterior ridge short, not reaching posteroventral corner 16
16 Bifurced ridge from posterodorsal corner; posterior ridge branch longer than posterior subvertical ridge branch (Fig. 4AC) ..... *Semicytherura usuigawensis* Tanaka, 2013
– Bifurced ridge from posterodorsal corner; posterior ridge branch shorter than posterior subvertical ridge branch 17
17 Anterior subvertical ridge with posterodorsal branch at ventral half; dorsal half short (Fig. 4K) ..... *Semicytherura tanimurai* (Ozawa & Kamiya, 2008)
– Anterior subvertical ridge without posterodorsal branch at ventral half; dorsal half long, connecting with dorsal margin/anterodorsal corner (Fig. 4U) ..... *Semicytherura simplex* (Brady & Norman, 1889)

18 Anterior subvertical ridge connecting with dorsal margin/ridge 22
– Anterior subvertical ridge short, not connecting with dorsal margin/ridge 19
19 Anterior sublongitudinal ridge long, connecting anterior margin/ridge with posterodorsal corner 20
– Anterior sublongitudinal ridge short, terminalizing at least within anterior half of carapace length 21
20 Anterior subvertical ridge connecting to ventral ridge (Fig. 4O) ..... *Semicytherura* sp. nov. sensu Irizuki 1994 (*Semicytherura* sp. 4)
– Anterior subvertical ridge not connecting to ventral ridge (Fig. 4Q) ..... *Semicytherura* sp. nov. sensu Irizuki 1994 (*Semicytherura* sp. 5)
21 Anterior longitudinal ridge terminating at mid-length of valve; distinct dorsal ridge; short posterior ridge not connected with posteroventral corner (Fig. 4X) ..... *Semicytherura* sp. nov. sensu Ozawa et al. 2008 (*Semicytherura* sp. 2)
– Anterior longitudinal ridge terminating at anterior third of valve length; no obvious dorsal ridge; thin posterior ridge connected with posteroventral corner (Fig. 4E) ..... *Semicytherura subslipperi* Ozawa & Kamiya, 2008
22 Anterior sublongitudinal ridge short, terminating within anterior half of valve length 23
– Anterior sublongitudinal ridge long, either connecting to other ridges/margins or terminating at posterior third of valve length 24
23 Short, thin, bifurced ridge branching off dorsal ridge in anteroventral direction at posterior third of valve length; four or five anteroventral marginal denticles (Fig. 4F) ..... *Semicytherura henryhowei* Hanai & Ikeya in Hanai et al. 1977
– Dorsal ridge without branches at posterior third of valve length; four anteroventral marginal denticles (Fig. 4D)..... *Semicytherura slipperi* Yamada, Tsukagoshi & Ikeya, 2005
24 Anterior subvertical ridge connecting with ventral ridge 25
– Ventral half of anterior subvertical ridge absent; posterior part of long anterior longitudinal ridge connecting with posterior ridge (Fig. 4AB)..... *Semicytherura* sp. nov. sensu Irizuki 1994 (*Semicytherura* sp. 1)
25 Posterior part of long anterior sublongitudinal ridge either connecting with posterodorsal corner or terminating within posterior third of valve length 26
– Posterior part of long anterior sublongitudinal ridge connecting with dorsal margin/ ridge at posterior third of valve length; four anteroventral marginal denticles (Fig. 4N) ..... *Semicytherura ikeyai* Yamada & Tsukagoshi, 2010
26 Ventral half of anterior subvertical ridge simple, thin, straight line, connecting to ventral ridge; four anteroventral marginal denticles (Fig. 4P)..... *Semicytherura balrogi* Brouwers, 1994
– Ventral half of anterior subvertical ridge no simple, thin, straight line 27
27 Ventral half of anterior subvertical ridge connecting to ventral ridge as U-shape on top of upside-down T-shape (Figs 4C, 6b)..... *Semicytherura robustundata* (Ozawa & Kamiya, 2008)
– Ventral half of anterior subvertical ridge thick, short; thick ridge connecting posterior part of long anterior sublongitudinal ridge to ventral ridge as upside-down Y-shape (Figs 4V, 6a)..... *Semicytherura* sp. nov. sensu Ozawa et al. 2008 (*Semicytherura* sp. 1)

Systematics

Description of the group's characteristics

Superfamily CYTHERACEA Baird, 1850
Family CYTHERURIDAE Müller, 1894
Subfamily CYTHERURINAE Müller, 1894
Genus *SEMICYTHERURA* Wagner, 1957

The *Semicytherura henryhowei* Hanai & Ikeya, 1997 species group

Revised diagnosis of the species group. External view. Thick carapace, sub-rectangular to sub-trapezoid in lateral view (right valves more sub-trapezoid, left valves more sub-rectangular). External ornamentation of prominent ridges including anterior ridge from anteroventral to anterodorsal corner (Fig. 3, red), anterior longitudinal ridge (short or long, horizontal or arched; Fig. 3, blue), ventral ridge from anteroventral to posteroventral or posterior corner, depending on species-specific length of ridge (Fig. 3, green), posterior ridge from posterior to posterodorsal corner (Fig. 3, yellow), dorsal ridge from posterodorsal to anterodorsal corner (Fig. 3, orange), anterior subvertical ridge from anterodorsal corner to ventral ridge (depending on species-specific length of ridge) at anterior half of valve (Fig. 3, turquoise), and posterior subvertical ridge from posterodorsal corner to ventral ridge (depending on species-specific length of ridge) at posterior half of valve (Fig. 3, purple). Ridges vary in length and degree of conspicuousness. Not all ridges are present in all species. In species where anterior subvertical ridge is connected with dorsal and/or ventral ridge(s), anterior fossa(e) form (Fig. 3). Anterior fossa(e) elliptic/rectangular (*S. subslipperi*, Fig. 4E, ventral only; *S. usuigawensis*, Fig. 4AC, dorsal only; *S. kazahana*, Fig. 4H; *S. sasameyuki*, Fig. 4J; *S. simplex*, Fig. 4U) to triangular/trapezoid (*S. kiosti* sp. nov., Fig. 4A, B, dorsal only; *S. henryhowei*, Fig. 4D) in shape. Likewise, prominent posterior ridge, as well as distinct posterior subvertical ridge connecting with ventral ridge, form a posterior fossa (e.g., *S. kiosti* sp. nov., Fig. 4A, B; *S. kazahana*, Fig. 4H; *S. sasameyuki*,

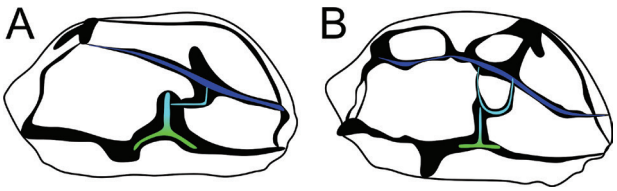

Figure 6. Connection details between anterior sublongitudinal ridge and ventral ridge in *Semicytherura robustundata* Ozawa & Kamiya, 2008 and *Semicytherura* sp. nov. sensu Irizuki 1994 (*S.* sp. 4). **A.** *Semicytherura* sp. nov. sensu Irizuki 1994 (*S.* sp. 4); **B.** *Semicytherura robustundata* Ozawa & Kamiya, 2008. Blue denotes the anterior sublongitudinal ridge; green denotes the ventral ridge; turquoise denotes the connecting ridge system.

Fig. 4J; *S. kaburagawensis*, Fig. 4AA; *S. quadraplana*, Fig. 4AD). Anterior margin with zero up to five denticles ventrally (Fig. 3, green triangles). Horizontal caudal process with varying degree of conspicuousness; generally, at or above mid-height.

Internal view. Recurved inner lamella not present in all species of the group; lacking in at least the following species: *S. balrogi*, *S. simplex*. Recurved inner lamella subject to sexual dimorphism in at least the following species: *S. kiosti* sp. nov., *S. slipperi*, *S. maxima*, *S. ikeyai*.

Description of species

Semicytherura kazahana Yamada, Tsukagoshi & Ikeya, 2005

Fig. 7

Note. First published record of the species from Korean waters. NIBR deposition number: DSEVIV0000003720.

Synonymy. (*Semicytherura henryhowei* sensu Yajima 1988: pg. 1076, pl. 1, fig. 12); (This specimen is either *S. kazahana* or *S. sasameyuki*, see Discussion). *Semicytherura quadrata* sensu Ishizaki 1968: pg. 20, pl. 4, figs 11, 12. *Semicytherura* sp. B sensu Lee 1990 (unpublished): pl. 27, figs 12, 13. *Semicytherura* sp. 1 sensu Yasuhara and Irizuki 2001: pg. 93, pl. 11, fig. 8. *Semicytherura kazahana* Yamada, Tsukagoshi & Ikeya, 2005: pgs 247, 253, 254, figs 2C, 6, 7.

Diagnosis. Juvenile. Sub-rectangular to sub-trapezoid lateral outline, as typical for species of the *S. henryhowei* group. Anteroventral margin here without crenulations [there are records of specimens showing four or five anteroventral marginal denticles; see Yamada et al. (2005)]. Carapace surface finely pitted. Dorsal margin weakly descending toward posterior. Acute caudal process at mid-height. Ventral margin weakly descending toward anterior. Thick, prominent ridges on carapace, as typical for the *S. henryhowei* group.

Anterior longitudinal ridge short, slightly ascending in straight line until posterior end of anterior one-third of valve length. Prominent, continuous ventral ridge running horizontally in antero-posterior direction, curving at posterior third of valve length. Two elliptical fossae in anterior half; sub-trapezoid fossa in posterior half.

Material. Juvenile, right valve # 70, from ARMS sediment (i.e., surface and sedimentation-derived sediments).

Locality and age. Seongsan (성산), Jeju Island, ROK (33°27'13"N, 126°56'45"E) (Fig. 2), 19 m water depth. Extant (collection date 2019; surface and sedimentation-derived sediments, valve only, no soft body).

Description. Heavily calcified, thick valve, sub-rectangular in lateral view. Maximum height at anterior third. Dorsal margin is weakly ascending towards posterior. Ventral margin is weakly descending towards posterior. Anterodorsal margin is smooth, obliquely rounded; anteroventral margin without visible marginal denticles, but partially broken; posterior margin is slightly curved above the caudal process. Acute posterior caudal process at mid-carapace.

The carapace surface is covered in fine pits and pores with sensory hairs. Valve with thick ridges; ventral ridge prominent; slightly ascending toward posterior third; then describing a steep drop toward the edge of the ventral margin and ascending again in a straight line toward the posterior margin, resembling the lower loop of a large S-shape; the upper loop of the S-shape is the thick posterior end of the dorsal ridge at the posterodorsal corner; interconnection between posterodorsal and posteroventral loops by a thin descending posterior subvertical ridge, completing the S-shape; anterior longitudinal ridge short; starting at mid-height from anterior margin, slightly ascending until terminating at posterior end of anterior third of valve length; dorsal half of anterior subvertical ridge steeply running upward and bending backward to anterodorsal corner, forming elliptical, anterodorsal fossa; ventral half of anterior subvertical ridge less prominent, zig-zag course, connecting to ventral ridge at mid-length of carapace, forming elliptical, anteroventral fossa.

Reticulation. Surface finely pitted (Fig. 7D, E) with prominent, species-specific ridge system.

Pores. Some simple pores with sensory hairs (Fig. 7D).

Hingement. Merodont hinge with a socket at each end of a ridge structure in the right valve (Fig. 7C) [not collected, but complementary negative structures in the left valve (tooth at each end of a groove)]. Typical for genus. Hingeline arched.

Adductor muscle scars. Not observed.

Recurved inner lamella. Absent in juveniles [see e.g., *S. subundata* in Ozawa and Kamiya (2008), pg. 143, fig. 4; *S. kiosti* Jöst & Karanovic sp. nov., Fig. 12 herein].

Dimensions. Carapace dimensions: length: 0.3064 mm, height: 0.166 mm.

Occurrence. Extant sediments, Korea (this study; surface and sedimentation-derived sediments collected 2019), and Japan (Yamada et al. 2005; living specimens, surface sediment collection: 1977–2000); Pleistocene sediments, Korea (Lee, 1990; unpublished); (potentially) Miocene sediments, Japan (Yajima 1988) (after species re-assignment, this study; uncertain whether *S. kazahana* or *S. sasameyuki*, see Discussion).

Remarks. Our specimen greatly resembles the juvenile specimen of *Semicytherura* sp. 1 sensu Yasuhara and

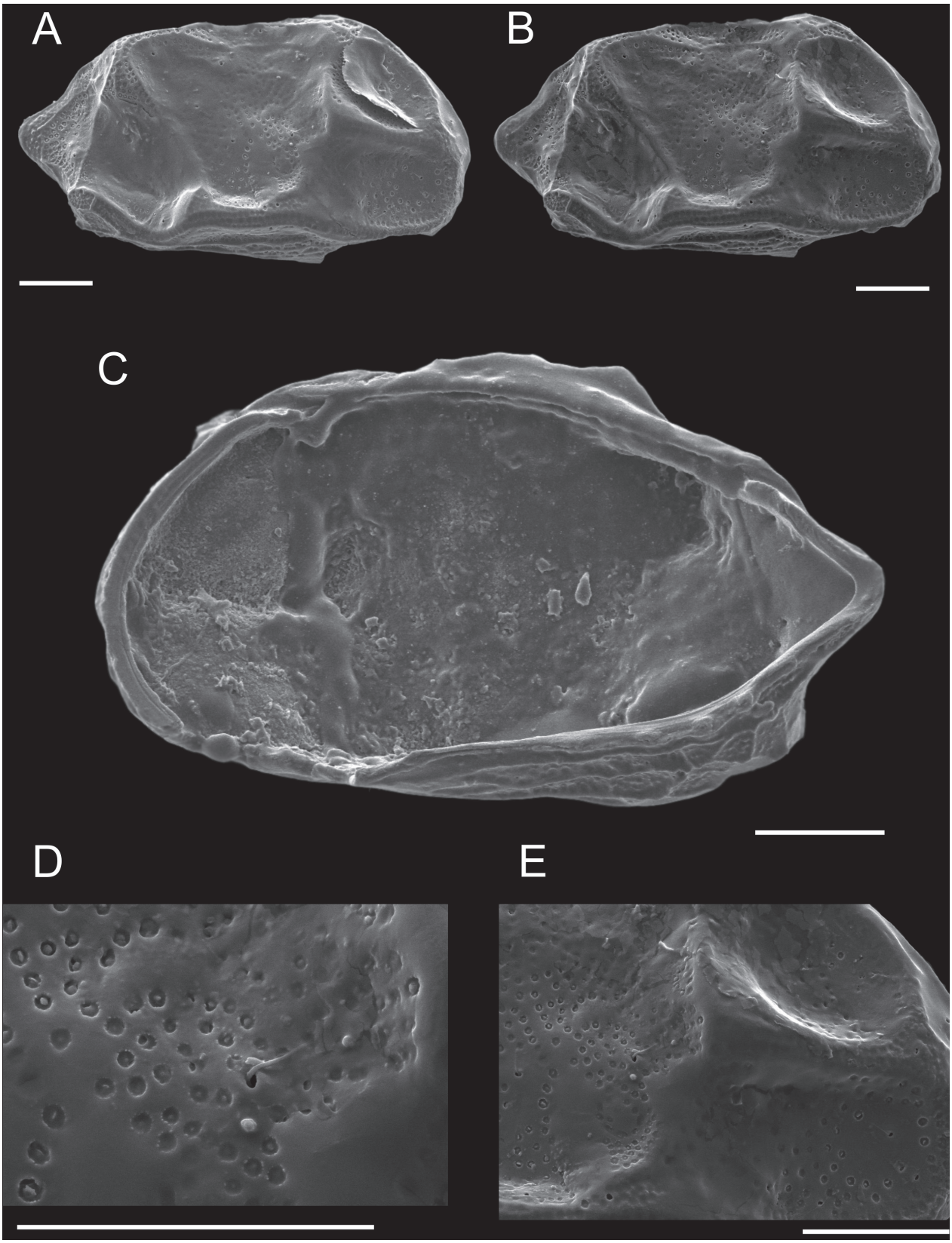

Figure 7. *Semicytherura kazahana* external and internal lateral views. **A–E.** Specimen # 70 A-1RV; **A–B, D–E.** Lateral external view; **D.** Details of pore with sensory hair and pitted carapace surface; **E.** Details d anterior subvertical ridge; **C.** Lateral internal view. Scale bars: 50 µm.

Irizuki 2001 (pg. 93, pl. 11, fig. 8), which was assigned to *S. kazahana* herein. The specimen of Yasuhara and Irizuki displays small, rounded anterior marginal denticals, which are absent in our specimen. However, *S. kazahana* has shown to display differing numbers of crenulations along its anterior margin (Yamada et al. 2005).

***Semicytherura kiosti* Jöst & Karanovic, sp. nov.**

https://zoobank.org/DAA1DAD2-32A5-4F02-8143-D0D158F8568B

Figs 8–12

Note. NIBR deposition number: DSEVIV0000003716.

Synonymy. *Hemicytherura* sp. 3 sensu Ikeya and Itoh 1991: pg. 138, fig. 17A.

Etymology. After the collaborating institution, Korea Institute of Ocean Science and Technology (KIOST), who provided the samples and funding for the MarineGEO project in Korea.

Diagnosis. Sub-rectangular lateral outline (especially LV), as typical for species of the *S. henryhowei* group. Anteroventral margin with three crenulations (denticles). Carapace surface roughly pitted with finer, smaller pits at marginal areas. Dorsal margin straight, horizontal. Broadly acute caudal process above mid-height. Ventral margin straight, horizontal, but posterior half obscured by ventral ridge. Thick, prominent ridges on carapace, as typical for the *henryhowei* group. Prominent posterior subvertical ridge forming large, subtriangular fossa in posterior half of valve. Prominent, horizontal, straight anterior longitudinal ridge forming large, subtrapezoid fossa with dorsal half of anterior subvertical ridge.

Holotypes. Two valves: adult male left valve, # 109_1 (lost, only SEM) and right valve, # 109_2 from ARMS sediment (i.e., surface and sedimentation-derived sediments).

Paratypes. Five valves: # 68 (female ARV) and # 108 (male ARV) from ARMS sediment (i.e., surface and sedimentation-derived sediments), and # 177 (female A-1RV), # 239 (female A-2RV), # 240 (female ARV) from scoop sediment (i.e., surface sediment).

Type deposition. Specimens are deposited at the National Institute of Biological Studies (NIBR, Incheon, South Korea) under the deposition number DSEVIV0000003716.

Type locality and age. Seongsan (성산), Jeju Island, ROK (33°27'13"N, 126°56'45"E) (Fig. 2), 19 m water depth. Extant (collection date 2019; surface and sedimentation-derived sediments; valves only, no soft bodies).

Description. Heavily calcified, thick valve, sub-rectangular (LV) to ovoid (RV) in lateral view. Right valve larger than left valve (see Fig. 8, length/height plot, # 109_1 and # 109_2). Maximum height at anterodorsal corner. Dorsal margin is horizontal, straight, parallel to ventral margin. Ventral margin is obscured by overhanging ventral ridge at posterior half. Anterodorsal margin is smooth, obliquely rounded; antero-ventral margin with three small, acute marginal denticles; posterior margin is ascending in a straight line above the caudal process. Broadly acute posterior caudal process above mid-carapace.

The carapace surface is covered in rough pits, and pores with sensory hairs. Finer, smaller pits at marginal areas. Valve with thick ridges; anterior sublongitudinal ridge short, horizontal, straight line, terminating at anterior third of valve length; prominent posterior subvertical ridge connecting posterodorsal corner with ventral ridge at mid-length of valve; posterior ridge branching off posterodorsal corner and running in a straight, vertical manner to posterior corner; posterior subvertical ridge, posterior ridge and posterior half of ventral ridge form large, subtriangular fossa; anterior longitudinal ridge, dorsal half of anterior subvertical ridge, and anterodorsal margin form large, subtrapezoid fossa. Right valves slightly higher and longer than left valves. Females longer and slightly higher than males (see length/height plot, Fig. 8).

***Reticulation*.** Surface covered in large pits with prominent, species-specific ridge system.

***Pores*.** Some simple pores with sensory hairs.

***Hingement*.** Merodont hinge with a socket at each end of a ridge structure in the right valve (Figs 9A, C, 10B, F, I). Complementary negative structures in the left valve (tooth at each end of a groove) (no SEM). Typical for genus. Hingeline arched.

***Adductor muscle scars*.** Vertical row of 4 adductor scars in ventro-median area (Fig. 9). Uppermost and lowermost scar less elongate in comparison with the middle two scars. At least 8 dorsal scars in upper half of valve (Fig. 11B). 2 mandibular scars slightly below, in front of adductor scars (Fig. 11F, blue arrows). 2 frontal scars in front of two uppermost adductor scars (Fig. 11F, white arrows).

***Recurved inner lamella*.** Strongly recurved in male adult (#109_2); absent in female adult (#240); not developed at juvenile stages (# 239) yet (Fig. 12).

Dimensions. Carapace dimensions of holotype: female ARV (# 240): length: 0.330 mm, height: 0.197 mm. Carapace dimensions of paratypes: female ARV: (# 68): length: 0.329 mm, height: posterior margin obscured by glue, ~ 0.196? mm; male ALV (# 109_1): length: 0.306 mm, height: 0.162 mm; male ARV (# 109_2): length: 0.308, height: 0.182 mm; male ARV (# 108): length: 0.310 mm, height: 0.185 mm; female A-2RV (# 239): length: 0.262 mm, height: 0.153 mm; female A-1RV (#177): length: 0.291 mm, height: 0.175 mm (Fig. 8).

Occurrence. Extant sediments, Korea (Jeju Island; surface and sedimentation-derived sediments collected 2019) and Japan (Sendai Bay, Matsushima Bay, Pacific Ocean; surface sediments collected 1985, 1986, 1988).

Remarks. The present species is characterized by a short, straight, horizontal anterior longitudinal ridge (Fig. 4B, AA). Of all known members of the *henryhowei* group, *Semicytherura kiosti* shares this trait only with *S. leptosubundata* (Fig. 4G) and *S. neosubundata* (Fig. 4Y). Morphological distinction between the three species based on prominent ridge patterns is straightforward. *Semicytherura kiosti* has an obvious anterior subvertical ridge, which is lacking in the other two species. *Hemicytherura* sp. 3 sensu Ikeya and Itoh 1991 is identical to our specimens of *S. kiosti* (fig. 17A in Ikeya and Itoh 1991). *Hemicytherura* Elofson, 1941 can easily be differentiated from the other members of the *Semicytherura henryhowei* group by the carapace surface features. Species of *Hemicytherura*, do exhibit something like ridges, but these do not resemble the characteristic ridge system of thick carinae of the *S. henryhowei* group. Rather, *Hemicytherura* is categorized by the characteristic fossa reticulation units that form around pores (Tanaka et al. 2011). Species of the *S. henryhowei* complex also show a less coarsely pitted surface ornamentation when compared to the *Hemicytherura* species.

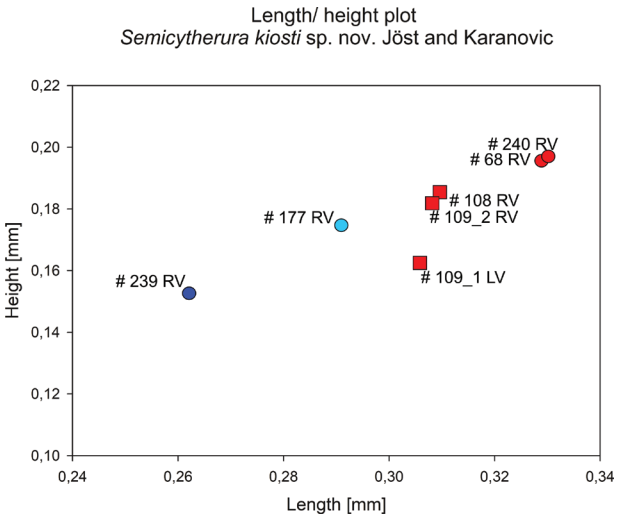

Figure 8. Length/height plot of *Semicytherura kiosti* sp. nov. Jöst & Karanovic. Circles indicate female, squares indicate males. Adult valves depicted in red, juveniles in blue: light blue: A-1 stage, dark blue: A-2 stage; LV indicates left valve, RV indicates right valve.

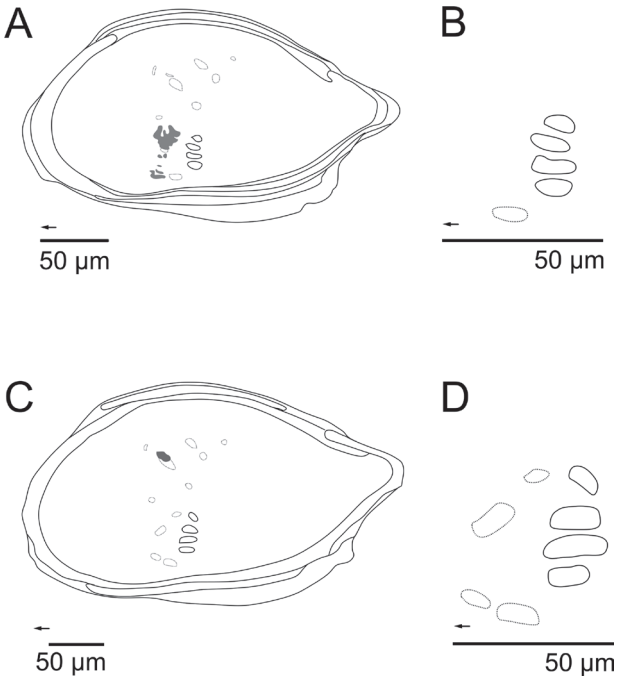

Figure 9. Line drawings of *Semicytherura kiosti* sp. nov. Jöst & Karanovic internal view with details on muscle imprints. **A, B.** Specimen # 239 juvenile (A-2, female) RV lateral internal view; **C, D.** Specimen # 240 female ARV lateral internal view. **A.** Lateral internal view of RV; **B.** Adductor muscle scar cluster in bold, one of two mandibular muscle scars depicted as dotted line; **C.** Lateral internal view of RV; **D.** Adductor muscle scar cluster in bold, two mandibular muscle scars depicted as dotted line. Dotted line indicates frontal, mandibular, and dorsal muscle scars; bold line indicates adductor muscle scars; females lacking strongly recurved inner lamella as observed in adult male. Arrow indicates anterior direction. Grey shaded shapes indicate dirt covering muscle scars. Scale bars: 50 µm.

Discussion

According to the key to Cytheruridae genera (see Athersuch et al. 1989), *Semicytherura* can be easily distinguished from all other genera by its conspicuously recurved posterior inner lamella, which is sometimes referred to as "marginal infoldment" (Ozawa and Kamiya 2008). A detailed study on its ultrastructure showed that it is a prismatic structure, different from the epidermis in other podocopid ostracods (Yamada et al. 2004), hence the term "prismatic layer" (Yamada et al. 2005). More recently, it was recognized that this layer may be sexually dimorphic in some species (Yamada et al. 2005; Whatley and Cusminsky 2010). While Whatley and Cusminsky (2010) mention three species in which males lack the recurved inner lamella, we checked the literature and found that at least 11 species express sexual dimorphism in this characteristic trait. In *Semicytherura slipperi* Yamada, Tsukagoshi & Ikeya, 2005 (see pg. 252, fig. 5A–D in Yamada et al. 2005), *S. maxima* Yamada & Tsukagoshi, 2010 (see pg. 293, figs 2G, H, 3C, D), *S. clavata* (Brady, 1880) (see Whatley and Cusminsky 2010; no internal view provided in original description), and *S. contraria* (Zhao & Whatley, 1989) (see pg. 175, pl. 1, fig. 14), males show a more pronounced expression than females. In *S. obitsuensis* (Nakao & Tsukagoshi, 2020) (see pg. 5, fig. 4B), *S. ikeyai* Yamada & Tsukagoshi, 2010 (see pg. 297, figs 11G, H, 12C, D), and *S. kiosti* sp. nov. Jöst & Karanovic (Fig. 12), females completely lack the recurved inner lamella. Also, adult females of *S. balrogi* Brouwers, 1994 lack the recurved inner lamella, although no information was given for males (pl. 6, figs 1, 2). Furthermore, *S. tauronae* Brouwers, 1994 (pl. 1, fig. 4), *S. henryi* (Brouwers, 1994) (pl. 6, figs 3, 4), *S. simplex* (Hu, 1978) (pg. 134, text-fig. 5B), and *S. skagwayensis* Brouwers, 1994 (pl. 6, fig. 5) also do not exhibit this character in adult valves of, at least, in one sex (Brouwers 1994). These observations call for a revision of the identification key by Athersuch et al. (1989). However, this is beyond the scope of our paper.

Detailed discussions on the speciation process of the *S. henryhowei* group, including geological and geographical distribution maps, as well as implications for the group's species diversity, are provided by Yamada et al. (2005; figs 11, 12), and Yamada and Tsukagoshi (2010; fig. 19). The authors also introduced subgroups based on differences in the carapace surface ornamentation, and further found that, although sharing a common ancestor in the North West Pacific, up until the Early Miocene, the species of each subgroup show distinct ecological differences (Yamada and Tsukagoshi 2010). Yamada et al. (2005) also discussed the phenomenon of trans-Arctic migration of ostracod fauna from the North West Pacific through the Bering Sea to the North Atlantic Ocean using the *S. henryhowei* group as a higher taxon. However, a distinction on species level within the group was not conducted. As a full review of the geographical and geological distribution of all 29 species of the *henryhowei* group is beyond the scope of this paper, here we focus on the species that, following the species-reassignments herein, underwent interesting changes in respect to the geological ages and/or (paleo-)distributions. We dis-

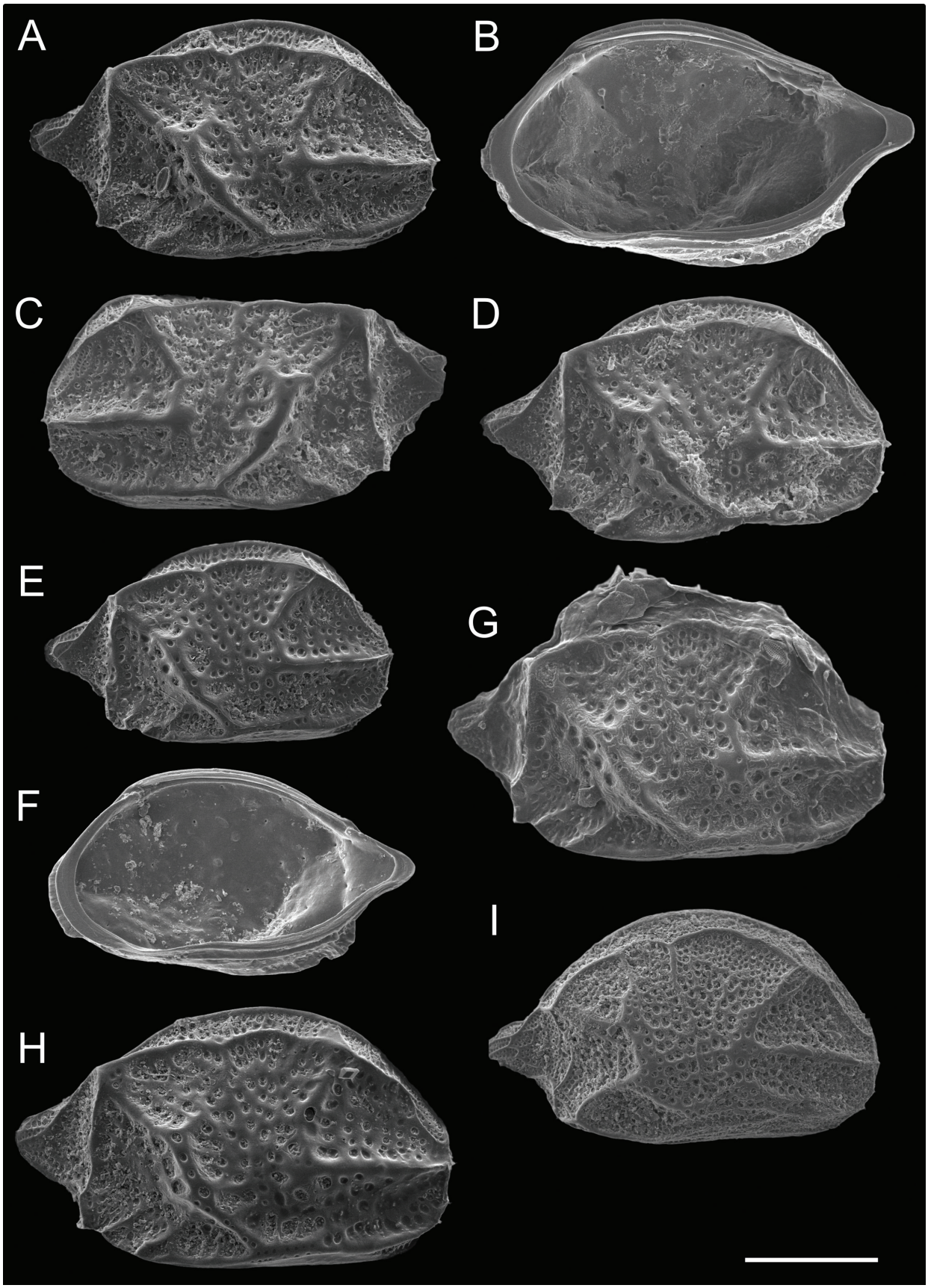

Figure 10. *Semicytherura kiosti* sp. nov. Jöst & Karanovic external and internal lateral views. **A–C.** Specimen # 109 adult male; **A, B.** # 109_2 RV; **A.** lateral external view; **B.** lateral internal view; **C.** # 109_1 LV, lateral external view; **D.** Specimen # 108 male ARV, lateral external view; **E, F.** Specimen # 239 female A-2RV; **E.** lateral external view; **F.** lateral internal view; **G.** Specimen # 68 female ARV, lateral external view; **H.** Specimen # 240 female ARV, lateral external view; **I.** Specimen # 177 female A-1RV, lateral external view. Scale bar: 100 μm.

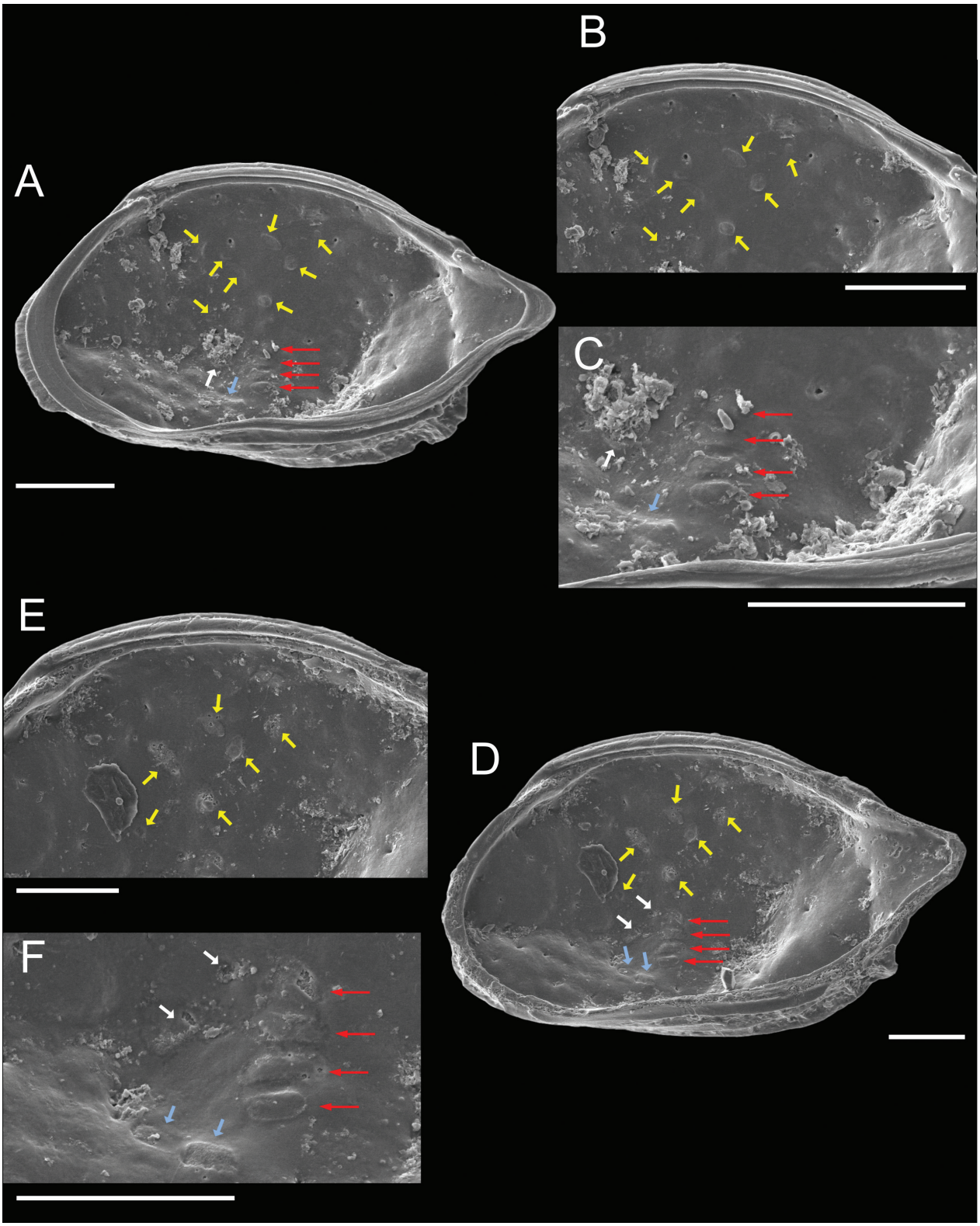

Figure 11. *Semicytherura kiosti* sp. nov. Jöst & Karanovic muscle scar details. **A–C.** Specimen # 239 female A-2RV lateral internal view; **D–F.** Specimen # 240 female ARV lateral internal view. Red arrows indicate adductor muscle scars; yellow arrows indicate dorsal muscle scars; blue arrows indicate mandibular muscle scars; white arrows indicate frontal muscle scars. Not all muscle scars simultaneously visible in both specimens. Scale bars: 50 µm.

covered changes to the geological distribution in at least five members of the species complex (*S. balrogi*, *S. ikeyai*, *S. tanimurai*, *S. sasameyuki/kazahana*, *S. undata*). In at least three of them (*S. balrogi*, *S. ikeyai*, *S. undata*), these changes also affected their geographical distribution. In respect to *S. balrogi* and *S. undata*, our findings give new insights into trans-Arctic interchange of ostracod fauna on species level. Details are discussed for each species separately.

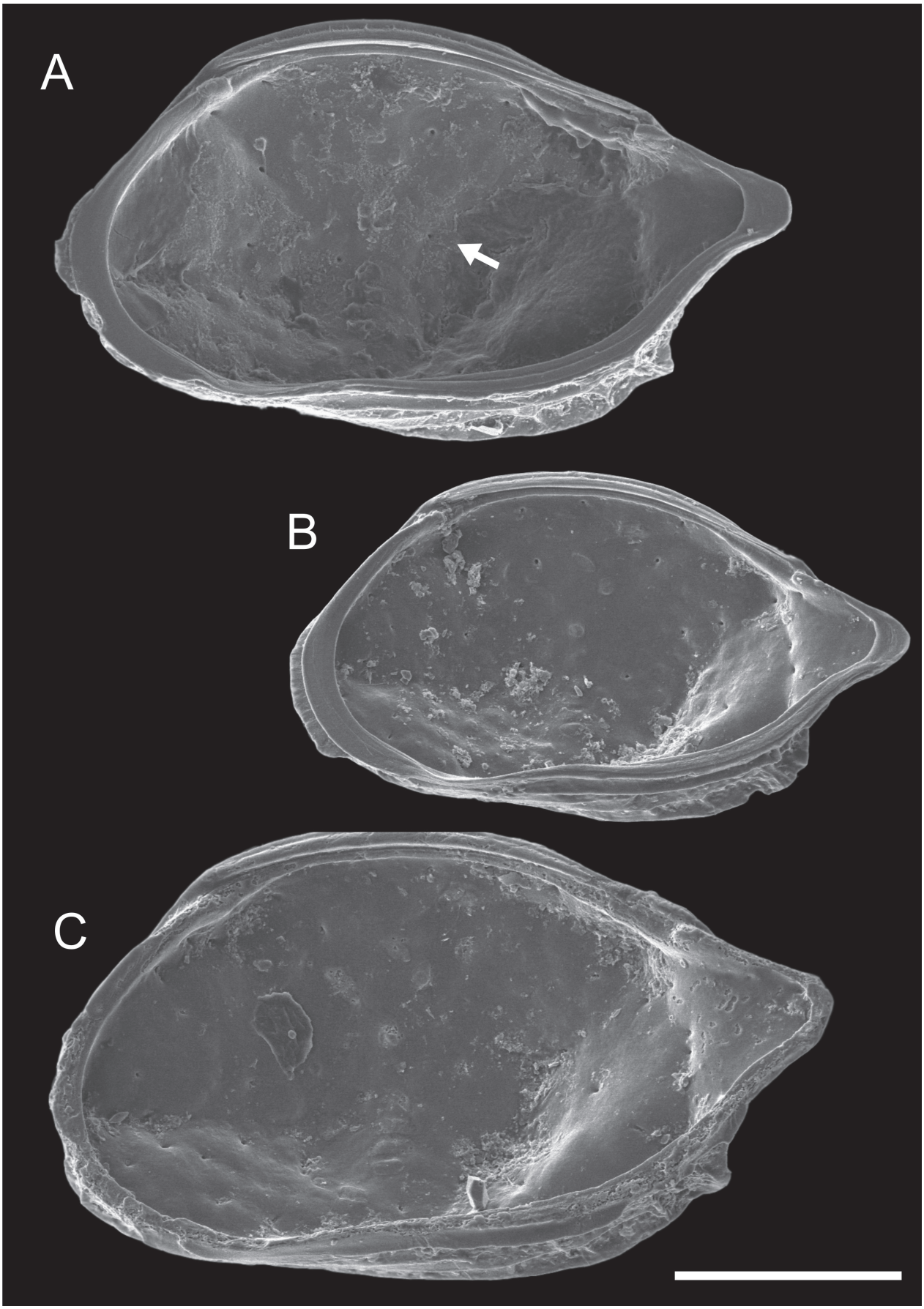

Figure 12. *Semicytherura kiosti* sp. nov. Jöst & Karanovic internal view details, recurved inner lamella. **A.** Male adult right valve (# 109_2) depicting strongly recurved inner lamella (white arrow); **B.** Female juvenile right valve (# 239) lacking recurved inner lamella; **C.** Female adult right valve (# 240) lacking recurved inner lamella.

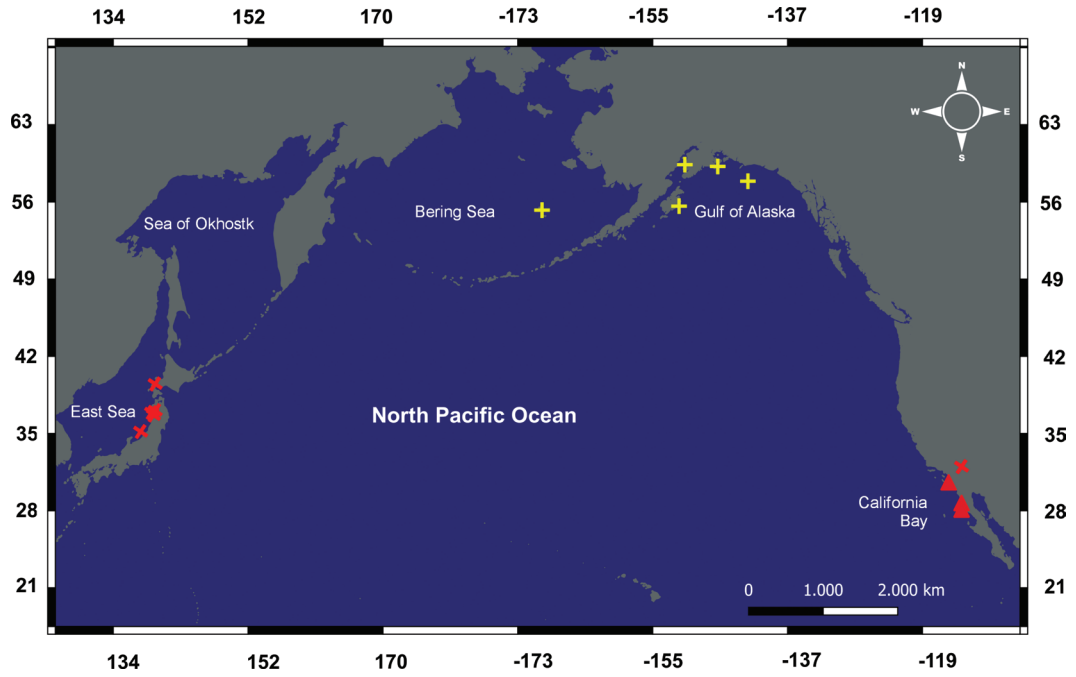

Figure 13. (Paleo-)distribution of *Semicytherura balrogi* Brouwers, 1994. Yellow denotes known records, red denotes new (re-assigned) records. Cross (red) and plus (yellow) denote new and known fossil records, respectively; triangle (red) denotes (new) extant records (for sample details, see Valentine 1976; Brouwers 1981, 1982a, b, 1983).

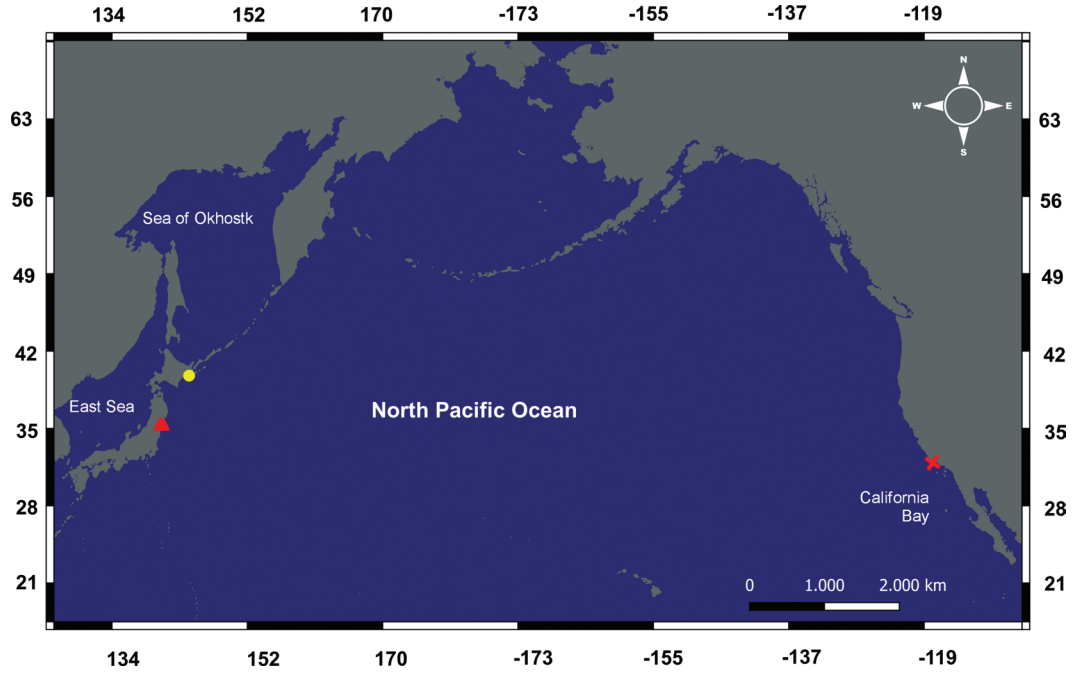

Figure 14. (Paleo-)distribution of *Semicytherura ikeyai* Yamada & Tsukagoshi, 2010. Yellow denotes known records, red denotes new (re-assigned) records. Cross (red) denotes (new) fossil records, triangle (red) and dot (yellow) denote extant (i.e., valves from 1985, 1986, 1988; living from 1992) new and known records, respectively.

Semicytherura aff. *undata* was reported from high latitudes in North America (Fig. 13, yellow) from the Pleistocene through the Holocene (Brouwers 1994). Our revision indicates that *S.* aff. *undata* is actually *S. balrogi*, and after the assessment of its records, we can conclude that *S. balrogi* also appears at lower latitudes of North America, from the Early Pleistocene and the Holocene, respectively (Valentine 1976) (Fig. 13, red). Additionally, we added the Miocene (Irizuki 1994) and the Pleistocene (Cronin & Ikeya, 1987) records from Japan (Fig. 13, red crosses). According to these new insights, *S. balrogi* first occurred in the North Pacific around Japan during the Miocene, and from there, spread in a circumpolar fashion into the North Atlantic, where it occurs as far south as California Bay (Valentine 1976; Brouwers 1981, 1982a, b, 1983).

Semicytherura ikeyai was described from the extant sediments (i.e., living specimens collected 1992) of the Eastern North Pacific in Akkeshi Bay, Japan (Yamada

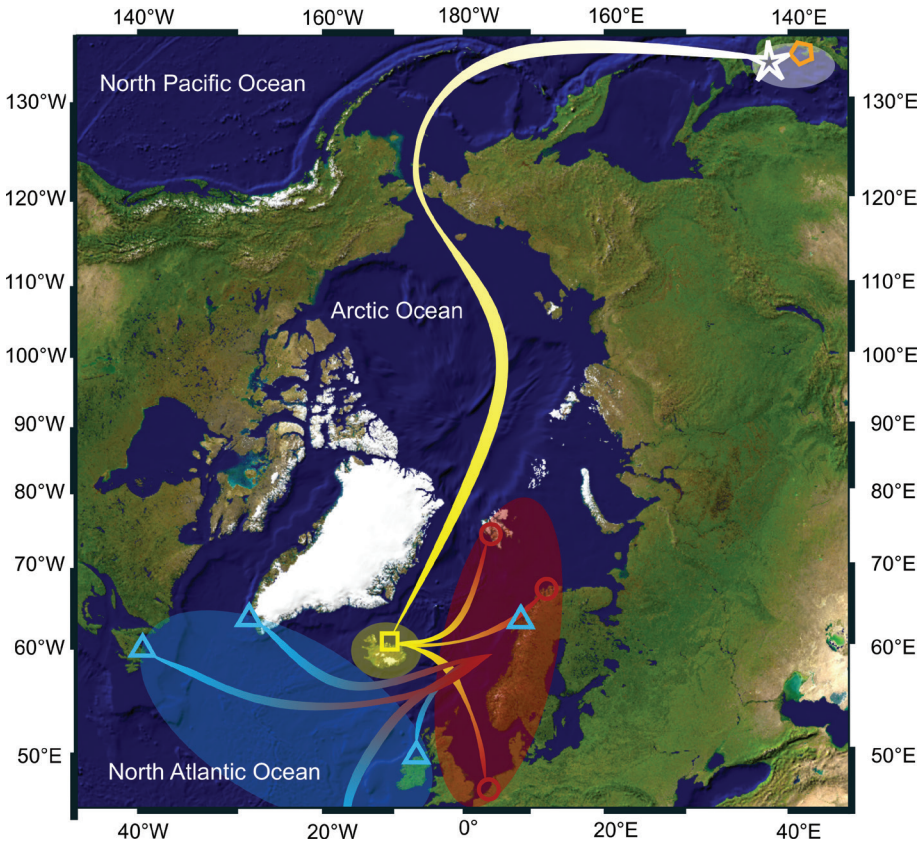

Figure 15. Trans-Arctic Interchange demonstrated on (paleo-)records of *Semicytherura undata* (Sars, 1866). White star denotes re-assigned Miocene record; yellow rectangle denotes Pliocene record; orange pentagon denotes Pleistocene records; red circles denote Holocene records; light-blue triangles denote modern records. Shaded areas indicate assumed area of occurrence based on records. Lines indicate possible migration routes, color-coded by temporal scheme.

and Tsukagoshi 2010) (Fig. 14, yellow). Our results added others extant (i.e., primarily valves collected 1985, 1986, 1988) Japanese records (Ikeya and Itoh 1991), and extended its distribution further south than previously reported, to the Sendai and Matsushima Bay area (Fig. 14, red triangle). Additionally, we report the first fossil record of the species from the Pleistocene core sediments of ODP site 893 in California Bay, which is also the first known occurrence from the Western North Pacific (Fig. 14, red cross) (Whatley and Boomer 1995).

Semicytherura tanimurai is an extinct species occurring in the Pleistocene formations of Japan (Ishizaki and Matoba 1985; Ozawa 1996; Ozawa and Kamiya 2008). Here, we add an older Japanese record from the Pliocene Sasaoka Formation (Yamada et al. 2002).

Semicytherura sasameyuki and *S. kazahana* are inner bay species commonly known from the extant silty-sand surface sediments of Japan (living specimens collected 1977–2000; Yamada et al. 2005). *Semicytherura kazahana* is also known from Pleistocene (Lee 1990; unpublished), as well as extant sediments (this study) of Korea. Here, we add an older Japanese record from the Miocene (Yajima, 1988). As *S. sasameyuki* and *S. kazahana* are difficult to clearly distinguish based on carapace features only, the latter record is not certain.

Semicytherura undata is a species with primarily circumpolar (paleo-)distribution, but also occurring as far south as South-West France (Guillaume et al. 1985). This record should be revised in the future, since the species seems to be a predominantly cold water inhabitant. Its known geological age dates back to the Pliocene of Iceland (Cronin 1991) (Fig. 15, yellow square), with the Pleistocene records from Japan (Cronin and Ikeya 1987; Ozawa and Kamiya 2005) (Fig. 15, orange pentagon), the Holocene records from the Netherlands (Wagner 1957), Norway (Neale and Howe 1975), and Spitzbergen (Hartmann 1992) (Fig. 15, red circles), and an extant distribution including the waters around Great Britain (Brady 1868; Athersuch et al. 1989), North America (Cronin 1989), Norway (Sars 1926; Freiwald and Mostafawi 1998), France (Guillaume et al. 1985), and Greenland (Penney 1989) (Fig. 15, turquoise triangles). According to this, the species first occurred in the North Atlantic during the Pliocene, and from there, spread to the North Pacific via the Bering Strait before its closure during the Pleistocene glaciations. However, our taxonomic revision revealed a Miocene record from the North Pacific (Japan) (Irizuki 1994), significantly changing the current view on evolution and migration patterns of this species (Fig. 15, white star). Our new insights indicate that *S. undata* originated in the North Pacific (Fig. 15, white shaded ellipse) during the Miocene and spread to the North Atlantic through the Arctic during the Late Miocene opening of the Bering Strait (5.32 Myr ago) (Gladenkov et al. 2002) (Fig. 15, white to

yellow route). This major geological event led to a connection between the North Pacific and the North Atlantic waters, which, especially for Asian and North American biotas, is of a great paleogeographic and biogeographic significance (Marincovich and Gladenkov 1999). Our interpretation is supported by the Pliocene record from Iceland (Fig. 15, yellow rectangle), located within the North Atlantic gateway to the Arctic (Cronin 1991), as well as its Holocene distribution, which is primarily focused in the sub-polar North Atlantic (Fig. 15, red circles). *Semicytherura undata* is the 14th known cold water ostracod species involved with the trans-Arctic interchange, in addition to 13 such species reported by Irizuki (1994).

Conclusions

Thorough taxonomic and systematic revisions are essential for an accurate documentation of the past and present biodiversity, with the ultimate aim to assess the impact of environmental disruptions on the species extinction and distribution. In this paper, we use homologous ornamentation patterns found across the *Semicytherura henryhowei* species group, the most common and diverse representatives of this ostracod genus. The genus and the entire order where it belongs (Cytheroidea) are best known from the fossil record, and have been important tools and proxies in paleostudies. Therefore, understanding shell morphology is important for a proper assessment of biodiversity and paleoclimate across geological ages. Our revision resulted in 29 species belonging to the *henryhowei* group, from 32 reported before (Appendix 1). By providing a taxonomic key to this group, we facilitate future species identifications. In addition, we describe one new species, as well as one new species record from Jeju Island in Korea, collected as a part of the MarineGEO ARMS project. Our taxonomic revision concluded changes in current species assignments, which resulted in the new insights regarding oldest records of *S. tanimurai* and *S. sasameyuki/kazahana*. Additionally, both geological age and spatial (paleo)distribution of *S. balrogi*, *S. ikeyai*, and *S. undata* are revised. The temporal distribution was adjusted from the Pleistocene to the Miocene, highlighting the importance of opening and closing of the Bering Strait for the faunal exchange in the Northern Hemisphere.

Acknowledgements

We thank the KIOST staff assisting sample collection and processing, and Mr. Junho Kim at Eulji University (ROK) for assisting the SEM imaging preparations. We are truly thankful for the helpful feedback provided by Thomas M. Cronin, as well as the critical comments by one anonymous reviewer regarding a previous version of this manuscript, which decisively improved this current work. We also thank the editor, Dr. Carolin Haug, and one anonymous reviewer for their comments on the current version of the manuscript; and Zdravka Zorkova and Polina Petrakieva for copy editing and layout, respectively. The study described in this article was partially supported by grants from the Brain Pool Program through NRF funded by the Ministry of Science and ICT (reference code: 2019H1D3A1A01070922 to ABJ), and by the Korea Institute of Ocean Science and Technology (reference codes: PEA0016 and PEA0025).

References

Allison EC, Holden JC (1971) Recent ostracodes from Clipperton Island Eastern tropical Pacific. Transactions of the San Diego Society of Natural History 16: 165–214. https://doi.org/10.5962/bhl.part.15458

Athersuch J, Horne DJ, Whittaker JE (1989) Marine and brackish water ostracods (superfamilies Cypridacea and Cytheracea) – keys and notes for the identification of the species. Kermack DM, Barnes RSK (Eds). Synopses of the British Fauna 43: 1–351.

Baird W (1850) The Natural History of the British Entomostraca. Ray Society, London, 364 pp. https://doi.org/10.5962/bhl.title.39641

Boomer I, Eisenhauer G (2002) Ostracod faunas as palaeoenvironmental indicators in marginal marine environments. In: The Ostracoda. Applications in Quaternary Research, 135–149. https://doi.org/10.1029/131GM07

Brady GS (1868) A synopsis of the recent British Ostracoda. The Intellectual Observer 12: 110–130. https://doi.org/10.5962/bhl.title.84654

Brady GS (1880) Report on the Ostracoda dredged by H.M.S Challenger during the years 1873–1876. Edinburgh: Neill, 1880–1895, Great Britain, 228 pp. https://doi.org/10.5962/bhl.title.6513

Brady GS, Norman AM (1889) A Monograph of the Marine and Freshwater Ostracoda of the North Atlantic and of North Western Europe. Sect I. Podocopa. Scientific Transactions of the Royal Dublin Society 2: 63–27.

Brandão SN, Antonietto LS, Nery DG, Karanovic I (2022) World Ostracod Database, Ostracoda.

Brouwers EM (1981) Tabulation of the ostracode assemblages and associated organisms from selected bottom grab samples taken in the Northeast Gulf of Alaska, F.R.S. Townsend Cromwell cruise EGAL-75-KC, 1975. United States Department of the Interior Geological Survey. Open-File Report. https://doi.org/10.3133/ofr811314

Brouwers EM (1982a) Tabulation of the ostracode assemblages and associated fauna and flora from Van Veen samples taken in the northeast Gulf of Alaska, R/V Discovery cruise DC2-80-EG, June, 1980. U.S. Geological Survey Open-File Report, 82–390. https://doi.org/10.3133/ofr82390

Brouwers EM (1982b) Tabulation of the ostracode assemblages and associated organisms from selected bottom grab samples taken in the northeast Gulf of Alaska, F.R.S. Townsend Cromwell cruise EGAL-75-KC, 1975, Part II. U.S. Geological Survey Open-File Report, 82–949. https://doi.org/10.3133/ofr82949

Brouwers EM (1983) Occurrence and distribution chart of ostracodes from the northeast Gulf of Alaska: U.S. Geological Survey Miscellaneous Field Studies Map MF-1518.

Brouwers EM (1994) Systematic paleontology of Quaternary ostracode assemblages from the Gulf of Alaska, Part 3 – family Cytheruridae. U.S. Geological Survey Professional Paper 1544: 102 pp. https://doi.org/10.3133/pp1544

Cronin TM (1989) Paleozoogeography of postglacial Ostracoda from Northeastern North Atlantic. In: Gadd NR (Ed.) The Late Quaternary Development of the Champlain Sea Basin. Geological Association of Canada, 125–144.

Cronin TM (1991) Pliocene shallow water paleoceanography of the North Atlantic Ocean based on marine ostracodes. Quaternary Science Reviews 10(2–3): 175–188. https://doi.org/10.1016/0277-3791(91)90017-O

Cronin TM, Ikeya N (1987) The Omma-Manganji ostracod fauna (Plio-Pleistocene) of Japan and the zoogeography of circumpolar species. Journal of Micropalaeontology 6(2): 65–88. https://doi.org/10.1144/jm.6.2.65

Elofson O (1941) Zur Kenntnis der marinen Ostracoden Schwedens mit besonderer Berücksichtigung des Skagerraks. Zoologiska Bildrag från Uppsala 19: 215–534.

Freiwald A, Mostafawi N (1998) Ostracods in a cold-temperate coastal environment, Western Troms, Northern Norway: Sedimentary aspects and assemblages. Facies 38(1): 255–274. https://doi.org/10.1007/BF02537368

Frydl PM (1982) Holocene ostracods in the southern Boso peninsula. University Museum, University of Tokyo. Bulletin 20: 61–144.

Gladenkov AY, Oleinik AE, Marincovich Jr L, Barinov KB (2002) A refined age for the earliest opening of Bering Strait. Palaeogeography, Palaeoclimatology, Palaeoecology 183(3–4): 321–328. https://doi.org/10.1016/S0031-0182(02)00249-3

Guillaume MC, Peypouquet J, Tetart J (1985) Quaternaire et Actuel. In: Oertli HJ (Ed.) Atlas des Ostracodes de France (Paléozoique-Actuel). Bulletin des Centres de Recherches Exploration, Production Elf-Aquitaine 9: 337–377.

Hanai T (1957) Studies on the Ostracoda from Japan III. Subfamilies Cytherurinae G. W. Müller (emend. G. O. Sars 1925) and Cytheropterinae n. subfam. Journal of the Faculty of Science. University of Tokyo 11: 11–36.

Hanai T, Ikeya N, Ishizaki K, Sekiguchi Y, Yajima M (1977) Checklist of Ostracoda from Japan and its adjacent seas. University Museum, University of Tokyo. Bulletin 12: 1–119.

Hartmann G (1992) Zur Kenntnis der rezenten und subfossilen Ostracoden des Liefdefjords (Nordspitzbergen, Svålbard). I. Teil. Mit einer Tabelle subfossil nachgewiesener Foraminiferen. Mitteilungen des hamburgischen zoologischen Museums 89: 181–225.

Hu C-H (1978) Studies on Ostracodes from the Toukoshan Formation (Pleistocene), Miaoli District, Taiwan. Petroleum Geology of Taiwan 15: 127–166.

Ikeya N, Cronin TM (1993) Quantitative analysis of Ostracoda and water masses around Japan: Application to Pliocene and Pleistocene paleoceanography. Micropaleontology 39(3): 263–281. https://doi.org/10.2307/1485900

Ikeya N, Itoh H (1991) Recent Ostracoda from the Sendai Bay region, Pacific coast of northeastern Japan. Reports of Faculty of Science, Shizuoka University 25: 93–145.

Irizuki T (1994) Late Miocene ostracods from the Fujikotogawa Formation, northern Japan – with reference to cold water species involved with trans-Arctic interchange. Journal of Micropalaeontology 13(1): 3–15. https://doi.org/10.1144/jm.13.1.3

Irizuki T, Yamada K, Maruyama T, Ito H (2004) Paleoecology and taxonomy of Early Miocene Ostracoda and paleoenvironments of the eastern Setouchi Province, central Japan. Micropaleontology 50(2): 44. https://doi.org/10.2113/50.2.105

Irizuki T, Matsubara T, Matsumoto H (2005) Middle Pleistocene Ostracoda from the Takatsukayama Member of the Meimi Formation, Hyogo Prefecture, western Japan: Significance of the occurrence of *Sinocytheridea impressa*. Paleontological Research 9(1): 37–54. https://doi.org/10.2517/prpsj.9.37

Ishizaki K (1966) Miocene and Plioccene ostracodes from the Sendai area, Japan. The science reports of the Tohoku University 37: 131–163.

Ishizaki K (1968) Ostracodes from Uranouchi Bay, Kochi Prefecture, Japan. The science reports of the Tohoku University 40: 1–45.

Ishizaki K (1981) Ostracoda from the East China Sea. Tohoku University Scientific Reports 51: 37–65.

Ishizaki K, Kato M (1976) The basin development of the diluvium Furuya mud basin, Shizuoka Prefecture, Japan, based on faunal analysis of fossil ostracodes. Takayanagi Y, Saito T (Eds). Progress in Micropaleontology: 118–143.

Ishizaki K, Matoba Y (1985) Akita (Early Pleistocene cold, shallow water Ostracoda). In: The Committee of the 9th International Symposium on Ostracoda (Eds) Guidebook of Excursions for the 9th International Symposium on Ostracoda, Shizuoka, 12 pp.

Jöst AB, Hong Y, Karanovic I (2021) First description of soft body parts of *Ambtonia* Malz and *Nipponocythere* Ishizaki (Ostracoda) from Korea with details on the genera's geographic and paleogeographic distribution. Marine Micropaleontology 174: 102029. https://doi.org/10.1016/j.marmicro.2021.102029

Lavrova TV, Lutaenko KA, Silina AV, Evseev GA, Dautova TN, Jeon Y-J, Heo S-J (2008) Marine biodiversity and bioresources of North-Eastern Asia. Conference Paper.

Lee E-H (1990 unpublished) Pleistocene Ostracoda from the marine sedimentary strata of the Cheju Island, Korea. Department of Geology, Graduate School of Korea University, 400 pp.

Lee E-H, Huh M, Schornikov EI (2000) Ostracod fauna from the East Sea coast of Korea and their distribution – preliminary study on Ostracoda as an indicator of water pollution. Journal of the Geological Society of Korea 36: 435–472.

Marincovich Jr L, Gladenkov AY (1999) Evidence for an early opening of the Bering Strait. Nature 397(6715): 149–151. https://doi.org/10.1038/16446

Müller GW (1894) Die Ostracoden des Golfes von Neapel und der angrenzenden Meeres-Abschnitte. R. Friedländer & Sohn, Berlin, 586 pp.

Nakao Y, Tsukagoshi A (2020) A new species of *Semicytherura* (Crustacea: Ostracoda: Cytheroidea) from Obitsu River Estuary (central Japan) and its microhabitat. Species Diversity 25(1): 1–9. https://doi.org/10.12782/specdiv.25.1

Neale JW, Howe HV (1975) The marine Ostracoda of Russian Harbour, Novaya Zemlya, and other high latitude faunas. Bulletins of American Paleontology 65: 381–431.

Okubo I (1980) Six species of the subfamily Cytherurinae Müller, 1894, in the Inland Sea, Japan (Ostracoda). Publications of the Seto Marine Biological Laboratory 25(1–4): 7–26. https://doi.org/10.5134/175996

Ozawa H (1996) Ostracode fossils from the Late Pliocene to Early Pleistocene Omma Formation in the Hokuriku District, Central Japan. Scientific Reports of the Kanazawa University 41: 77–115.

Ozawa H, Kamiya T (2005) The effect of glacio-eustatic sea-level change on Pleistocene cold-water ostracod assemblages from the Japan Sea. Marine Micropaleontology 54(3–4): 167–189. https://doi.org/10.1016/j.marmicro.2004.10.002

Ozawa H, Kamiya T (2008) Taxonomy and palaeobiogeographical significance of four new species of *Semicytherura* (Ostracoda, Crustacea) from the Early Pleistocene Omma Formation of the Japan Sea coast. Journal of Micropalaeontology 27(2): 135–146. https://doi.org/10.1144/jm.27.2.135

Ozawa H, Nagamori H, Tanabe T (2008) Pliocene ostracods (Crustacea) from the Togakushi area, central Japan; palaeobiogeography of trans-Arctic taxa and Japan Sea endemic species. Journal of Micropalaeontology 27(2): 161–175. https://doi.org/10.1144/jm.27.2.161

Paik K-H, Lee E-H (1988) Plio-Pleistocene ostracods from the Sogwipo Formation, Cheju Island, Korea. In: Developments in Palaeontology and Stratigraphy. Evolutionary biology of ostracoda: its fundamentals and applications: Proceedings of the ninth International Symposium on Ostracoda, 541–556. https://doi.org/10.1016/S0920-5446(08)70207-3

Penney DN (1989) Recent shallow marine ostracoda of the Ikerssuak (Bredefjord) district, Southwest Greenland. Journal of Micropalaeontology 8(1): 55–75. https://doi.org/10.1144/jm.8.1.55

Sars GO (1866) Oversigt af Norges marine Ostracoder. Forhandlinger i Videnskabs-Selskabet i Christiania, 1–144.

Sars GO (1926) An account of the Crustacea of Norway with short descriptions and figures of all species, Vol 9, Ostracoda. Parts 11, 12, Cytheridae (continued). Bergen Museum, Bergen, 177–208.

Schellenberg SA (2007) Marine Ostracods. In: Encyclopedia of Quaternary Science. Elsevier, 2046–2062. https://doi.org/10.1016/B0-444-52747-8/00249-0

Schornikov EI, Zenina MA (2008) Ostracods of the coastal zone of Jeju Island, Korea. In: Lavrova TV, Lutaenko KA, Silina AV, Evseev GA, Dautova TN, Jeon Y-J, Heo S-J. Marine biodiversity and bioresources of North-Eastern Asia. Conference Paper.

Szczechura J, Aiello G (2003) The ostracod genus *Nipponocythere* Ishizaki, 1971 from the Middle Miocene of the Fore-Carpathian Depression, Central Paratethys; its origin and paleoenvironment. Geologica Carpathica 54: 9–20.

Tabuki R (1986) Plio- Pleistocene Ostracoda from the Tsugaru Basin, North Honshu, Japan. Bulletin of College of Education. University of the Ryukyus Repository 29: 27–160.

Tanaka G, Hasegawa Y (2013) Miocene ostracods from the Itahana Formation in the Tomioka District, Gunma Prefecture, Central Japan: Paleoenvironmental significance and systematics. Paleontological Research 17(2): 138–172. https://doi.org/10.2517/1342-8144-17.2.138

Tanaka G, Kaseda Y, Ikeya N (2011) Reclassification of the genus *Hemicytherura* (Crustcea, Ostracoda) from Japan and the surrounding regions. Bulletin of Gunma Museum of Natural History 15: 19–42. https://doi.org/10.2517/1342-8144-15.4.213

Valentine PC (1976) Zoogeography of Holocene Ostracoda off Western North America and paleoclimatic implications. Geological Survey Professional Paper 916: 81. https://doi.org/10.3133/pp916

Wagner CW (1957) Sur les Ostracodes du Quaternaire récent des Pays-Bas et leur utilisation dans l'étude géologique des dépots holocenes. Université de Paris, A. 707: 1–259.

Whatley RC, Boomer ID (1995) Autochthonous and allochthonous Qauternary Ostracoda from site 893, Santa Barbara Basin. In: Kennett JP, Baldauf JG, Lyle M (Eds) Proceedings of the Ocean Drilling Program, 146 Part 2 Scientific Results. Proceedings of the Ocean Drilling Program. Ocean Drilling Program. https://doi.org/10.2973/odp.proc.sr.146-2.1995

Whatley R, Cusminsky G (2010) *Semicytherura* Wagner: Its inner lamella and its close allies. Journal of Micropalaeontology 29(1): 1–4. https://doi.org/10.1144/jm.29.1.1

Yajima M (1988) Preliminary notes on the Japanese Miocene Ostracoda. In: Developments in Palaeontology and Stratigraphy. Elsevier, 1073–1085. https://doi.org/10.1016/S0920-5446(08)70240-1

Yamada S, Tsukagoshi A (2010) Two new species of *Semicytherura* (Podocopa: Ostracoda) from Akkeshi Bay, Hokkaido, Japan, with comments on their speciation and related species. Zoological Science 27(3): 292–302. https://doi.org/10.2108/zsj.27.292

Yamada K, Irizuki T, Tanaka Y (2002) Cyclic sea-level changes based on fossil ostracode faunas from the Upper Pliocene Sasaoka Formation, Akita Prefecture, northeast Japan. Palaeogeography, Palaeoclimatology. Palaeoecology 185(1–2): 115–132. https://doi.org/10.1016/S0031-0182(02)00281-X

Yamada S, Tsukagoshi A, Ikeya N (2004) Ultrastructure of the carapace in some *Semicytherura* species (Ostracoda: Crustacea). Micropaleontology 50(4): 381–389. https://doi.org/10.2113/50.4.381

Yamada S, Tsukagoshi A, Ikeya N (2005) Taxonomy, morphology and speciation of the *Semicytherura henryhowei* group (Crustacea, Ostracoda). Hydrobiologia 538(1–3): 243–265. https://doi.org/10.1007/s10750-004-4970-4

Yasuhara M, Irizuki T (2001) Recent Ostracoda from the northeastern part of Osaka Bay, southwestern Japan. Journal of Geosciences (Prague) 44: 57–95.

Zhao Q, Whatley R (1989) Recent Podocopid Ostracoda of the Sedili River and Jason Bay, Southeastern Malay Peninsula. Micropaleontology 35(2): 168–187. https://doi.org/10.2307/1485467

Appendix 1

Table A1. Treatise list reporting *Semicytherura henryhowei* group.

Author name	Species name Yamada et al. 2005	Species name Yamada and Tsukagoshi 2010	Species name Jöst et al., this study	Locality	Geologic time
Allison and Holden (1971)	Not included	Not included	*S. quadraplana*	Tropical East Pacific	Extant
Athersuch et al. (1989)	*S. undata*	*S. undata*	*S. undata*	British	Extant
Brady (1868)	*C. undata*	*C. undata*	*C. undata*	British	Extant
Brouwers (1994)	*S. balrogi*	*S. balrogi*	*S. balrogi*	North America	Holocene
Cronin and Ikeya (1987)	*S. subundata*	*S. subundata*	*S. subundata*	Japan/ Omma-Manganji	Pleistocene
Cronin and Ikeya (1987)	*S.* aff. *henryhowei*	*S.* aff. *henryhowei*	*S. balrogi*	Japan/ Omma-Manganji	Pleistocene
Cronin and Ikeya (1987)	*S.* sp. A	*S.* sp. A	*S.* sp. nov.	Japan/ Omma-Manganji	Pleistocene
Cronin and Ikeya (1987)	Not included	*S. undata*	*S. undata*	Japan/ Omma-Manganji	Pleistocene
Cronin (1989)	*S. undata*	*S. undata*	*S. undata*	North America	Extant
Cronin (1989)	*S.* cf. *henryhowei*	*S.* cf. *henryhowei*	*S.* sp. nov.	North America	Extant
Cronin (1991)	*S. undata*	*S. undata*	*S. undata*	Iceland	Pliocene
Freiwald and Mostafawi (1998)	*S. undata*	*S. undata*	*S. undata*	North Norway	Extant
Guillaume et al. (1985)	*S. undata*	*S. undata*	*S. undata*	South-west France	Extant
Hanai (1957)	*C. quadrata*	*S. henryhowei*	*S. henryhowei*	Japan (Hayama)	Extant
Hanai (1957)	*C. subundata*	*C. subundata*	*C. subundata*	Japan/ Sawane	Pleistocene

Author name	Species name Yamada et al. 2005	Species name Yamada and Tsukagoshi 2010	Species name Jöst et al., this study	Locality	Geologic time
Hanai (1961)	*S. quadrata*	Not included	Not included	Japan (Hayama)	Extant
Hanai (1961)	*S. subundata*	Not included	Not included	Japan/ Sawane	Pleistocene
Hanai et al. (1977)	*S. henryhowei*	Not included	Not included	Japan (Hayama)	Extant
Hartmann (1992)	*S. undata*	*S. undata*	*S. undata*	Spitzbergen	Holocene
Hu (1978)	*S. simplex*	*S. simplex*	*S. simplex*	Southern Taiwan	Pleistocene
Hu (1981)	*S. simplex*	*S. simplex*	*S. simplex*	Southern Taiwan	Pleistocene
Hu (1984)	*S. simplex*	*S. simplex*	*S. simplex*	Southern Taiwan	Pleistocene
Ikeya et al. (1985)	*S. henryhowei*	*S. henryhowei*	*S. henryhowei*	Japan (Hamana-ko)	Extant
Ikeya et al. (1985)	*S.* sp. D	*S. sasameyuki*	*S. sasameyuki*	Japan (Hamana-ko)	Extant
Ikeya and Itoh (1991)	*S. henryhowei*	*S. henryhowei*	*S. henryhowei*	Japan (Sendai Bay)	Extant
Ikeya and Itoh (1991)	Not included	Not included	*S. kiosti* sp. nov. Jöst and Karanovic (*Hemicytherura* sp. 3)	Japan (Sendai Bay)	Extant
Ikeya and Suzuki (1992)	*S. henryhowei*	*S. henryhowei*	*S. henryhowei*	South West Japan Sea	Extant
Irizuki (1994)	*S. henryhowei*	*S. henryhowei*	*S. balrogi*	Japan/ Fujikotogawa	Miocene
Irizuki (1994)	*S.* aff. *henryhowei*	*S.* aff. *henryhowei*	*S.* sp. nov.	Japan/ Fujikotogawa	Miocene
Irizuki (1994)	*S. subundata*	*S. subundata*	*S. subundata*	Japan/ Fujikotogawa	Miocene
Irizuki (1994)	*S.* sp. 1	*S.* sp. 1	*S.* sp. nov.	Japan/ Fujikotogawa	Miocene
Irizuki (1994)	*S.* sp. 2	*S.* sp. 2	*S.* sp. nov.	Japan/ Fujikotogawa	Miocene
Irizuki (1994)	*S.* sp. 3	*S.* sp. 3	*S. undata*	Japan/ Fujikotogawa	Miocene
Irizuki (1994)	*S.* sp. 4	*S.* sp. 4	*S.* sp. nov.	Japan/ Fujikotogawa	Miocene
Irizuki (1994)	*S.* sp. 5	*S.* sp. 5	*S.* sp. nov.	Japan/ Fujikotogawa	Miocene
Irizuki et al. (1994)	Not included	*S. pseudoundata*	*S. pseudoundata*	Japan/ Toyama	Miocene
Irizuki et al. (2005)	Not included	*S.* sp.	*S. kazahana*	Japan/ Meimi	Pleistocene
Irizuki (2007)	Not included	*S. subundata*	*S. subundata*	Japan/ Kuwae	Pliocene
Ibid.	Not included	*S. subslipperi*	*S. subslipperi*	Japan/ Kuwae	Pliocene
Ishizaki (1966)	*Cytherura neosubundata*	*Cytherura neosubundata*	*Cytherura neosubundata*	Japan/ Tatsunokuchi	Pliocene
Ishizaki (1966)	*S. quadrata*	*S. henryhowei*	*S. henryhowei*	Japan/ Hatatate	Miocene
Ishizaki (1968)	*S. quadrata*	*S. kazahana*	*S. kazahana*	Japan (Uranouchi Bay)	Extant
Ishizaki (1971)	*S. quadrata*	*S. sasameyuki*	*S. sasameyuki*	Japan (Aomori Bay)	Extant
Ishizaki and Matoba (1985)	*S. henryhowei*	*S. tanimurai*	*S. tanimurai*	Japan/ Sasaoka	Pleistocene
Ishizaki and Matoba (1985)	*S. subundata*	*S. subundata*	*S. subundata*	Japan/ Shibikawa	Pleistocene
Lee (1990)	*S.* sp. B	*S. kazahana*	*S. kazahana*	Korea (Jeju Island)	Pleistocene
Neale and Howe (1975)	*S. undata*	*S. undata*	*S. undata*	North Norway	Holocene
Okubo (1980)	*S. henryhowei*	*S. sasameyuki*	*S. sasameyuki*	Japan (Seto Inland Sea)	Extant
Ozawa (1996)	*S. subundata*	*S. subundata*	*S. subundata*	Japan/ Omma-Manganji	Pleistocene
Ozawa (1996)	*S.* cf. *undata*	*S. robustundata*	*S. robustundata*	Japan/ Omma-Manganji	Pleistocene
Ozawa (1996)	*S.* sp. 4	*S. subslipperi*	*S. subslipperi*	Japan/ Omma-Manganji	Pleistocene
Ozawa (1996)	*S.* sp. 5	*S. leptosubundata*	*S. leptosubundata*	Japan/ Omma-Manganji	Pleistocene
Ozawa (1996)	*S.* sp. 6	*S. tanimurai*	*S. tanimurai*	Japan/ Omma-Manganji	Pleistocene
Ozawa and Kamiya (2005)	Not included	*S. robustundata*	*S. robustundata*	Japan/ Omma-Manganji	Pleistocene
Ozawa and Kamiya (2005)	Not included	*S. leptosubundata*	*S. leptosubundata*	Japan/ Omma-Manganji	Pleistocene
Ozawa and Kamiya (2005)	Not included	*S. subslipperi*	*S. subslipperi*	Japan/ Omma-Manganji	Pleistocene
Ozawa and Kamiya (2005)	Not included	*S. undata*	*S. undata*	Japan/ Omma-Manganji	Pleistocene
Ozawa and Kamiya (2008)	Not included	*S. robustundata*	*S. robustundata*	Japan/ Omma-Manganji	Pleistocene
Ozawa and Kamiya (2008)	Not included	*S. subslipperi*	*S. subslipperi*	Japan/ Omma-Manganji	Pleistocene
Ozawa and Kamiya (2008)	Not included	*S. leptosubundata*	*S. leptosubundata*	Japan/ Omma-Manganji	Pleistocene
Ozawa and Kamiya (2008)	Not included	*S. tanimurai*	*S. tanimurai*	Japan/ Omma-Manganji	Pleistocene
Ozawa et al. (2008)	Not included	*S. subundata*	*S. subundata*	Japan/ Ogikubo	Pliocene
Ozawa et al. (2008)	Not included	*S.* sp. 1	*S.* sp. nov.	Japan/ Ogikubo	Pliocene
Ozawa et al. (2008)	Not included	*S.* sp. 2	*S.* sp. nov.	Japan/ Ogikubo	Pliocene
Penney (1989)	*S. undata*	*S. undata*	*S. undata*	Greenland	Extant
Sars (1926)	*C. undata*	*S. undata*	*S. undata*	Norway	Extant
Tanaka and Hasegawa (2013)	Not included	Not included	*S. kaburagawensis*	Japan/ Itahana	Miocene
Tanaka and Hasegawa (2013)	Not included	Not included	*S. usuigawensis*	Japan/ Itahana	Miocene
Tsukagoshi and Kamiya (1996)	*S.* aff. *henryhowei*	*S. sasameyuki*	*S. sasameyuki*	Japan (Maizuru Bay)	Extant
Valentine (1976)	*Kangarina* sp. B	*Kangarina* sp. B	*S. balrogi*	North America	Holocene
Wagner (1957)	*S. undata*	*S. undata*	*S. undata*	Netherlands	Holocene
Whatley and Boomer (1995)	*S.* sp. B	*S.* sp. B	*S. ikeyai*	ODP site 893	Pleistocene
Yajima (1988)	*S. henryhowei*	*S. henryhowei*	*S. sasameyuki/ kazahana*	Japan/ Mizunami	Miocene
Yamada and Tsukagoshi (2010)	Not included	*S. maxima*	*S. maxima*	Japan (Akkeshi Bay)	Extant
Yamada and Tsukagoshi (2010)	Not included	*S. ikeyai*	*S. ikeyai*	Japan (Akkeshi Bay)	Extant
Yamada et al. (2002)	*S. subundata*	*S. subundata*	*S. subundata*	Japan/ Sasaoka	Pliocene
Yamada et al. (2002)	*S.* sp. 1	*S. subslipperi*	*S. subslipperi*	Japan/ Sasaoka	Pliocene
Yamada et al. (2002)	*S.* sp. 2	*S.* sp. 2	*S. tanimurai*	Japan/ Sasaoka	Pliocene
Yamada et al. (2004)	Not included	Not included	*S. sasameyuki/ kazahana* (*S.* sp. A)	Japan/ fish tank University of Tsukuba	Extant
Yamada et al. (2004)	Not included	Not included	*S. slipperi* (*S.* sp. B)	Japan(Akkeshi Bay)	Extant
Yamada et al. (2005)	*S. henryhowei*	*S. henryhowei*	*S. henryhowei*	Japan (Hayama)	Extant
Yamada et al. (2005)	*S. slipperi*	*S. slipperi*	*S. slipperi*	Japan (Akkeshi Bay)	Extant
Yamada et al. (2005)	*S. kazahana*	*S. kazahana*	*S. kazahana*	Japan (Aburatsubo Bay)	Extant
Yamada et al. (2005)	*S. sasameyuki*	*S. sasameyuki*	*S. sasameyuki*	Japan (Maizuru Bay)	Extant
Yamane (1998)	*S. henryhowei*	*S. sasameyuki*	*S. sasameyuki*	Japan (Seto Inland Sea)	Extant
Yasuhara and Irizuki (2001)	Not included	*S. henryhowei*	*S. henryhowei*	Japan (Osaka Bay)	Extant
Yasuhara and Irizuki (2001)	Not included	*S.* sp. 1	*S. kazahana*	Japan (Osaka Bay)	Extant

Fossil Record 25 (2) 2022, 331–343 | DOI 10.3897/fr.25.90692

PENSOFT

für Natur MUSEUM FÜR NATURKUNDE BERLIN

The geologically oldest specimen of *Pterodactylus*: a new exquisitely preserved skeleton from the Upper Jurassic (Kimmeridgian) Plattenkalk deposits of Painten (Bavaria, Germany)

Felix J. Augustin[1], Panagiotis Kampouridis[1], Josephina Hartung[1], Raimund Albersdörfer[2], Andreas T. Matzke[1]

1 *Department of Geosciences, University of Tübingen, Hölderlinstraße 12, 72074 Tübingen, Germany*

2 *Dinosaurier Museum Altmühltal, Dinopark 1, 85095 Denkendorf, Germany*

https://zoobank.org/E342050A-E2C2-47F4-A315-09B507E6D267

Corresponding author: Felix J. Augustin (felix.augustin@uni-tuebingen.de)

Academic editor: Johannes Müller ♦ **Received** 22 July 2022 ♦ **Accepted** 7 November 2022 ♦ **Published** 28 November 2022

Abstract

Pterodactylus from the uppermost Jurassic of southern Germany represents one of the most iconic pterosaurs, due to its status of being the first member of the Pterosauria to have been described and named. During the early phase of pterosaur research, *Pterodactylus* was a wastebasket taxon containing dozens of sometimes distantly related assigned species. Decades later, a comprehensive revision of the genus significantly reduced the number of species. To date, only one species remains in the genus, *Pterodactylus antiquus*, although the referral of several specimens to this taxon and the taxonomic relationships of them is still debated. Thus far, the genus has been only reported from the Upper Jurassic Plattenkalk deposits of Bavaria, and all of these occurrences are Tithonian in age. Here we describe the first record of *Pterodactylus* from the Torleite Formation near Painten (Bavaria), which represents the first occurrence of the genus from the Kimmeridgian. The specimen is a complete, articulated and exquisitely preserved skeleton of a small-sized individual. Aside from its old geological age, it is a typical representative of the genus, greatly resembling other specimens from younger strata. Certain characters, such as the overall size, skull length, relative orbit size, and phalangeal formula indicate that the specimen from Painten represents a juvenile to young subadult individual, an ontogenetic stage rarely found among *Pterodactylus* specimens. The find significantly expands the temporal range of the taxon and represents one of the best-preserved specimens of the genus reported so far.

Key Words

Kimmeridgian, Pterodactyloidea, *Pterodactylus*, Pterosauria, Solnhofen Archipelago, Upper Jurassic

Introduction

The very first pterosaur that was scientifically described and named, and which thus led to the recognition of this extremely diverse group of flying reptiles that dominated the skies of the Mesozoic, was *Pterodactylus* from the famous Upper Jurassic Plattenkalk deposits of southern Germany, although the affinities of the first specimens have caused considerable debate (Collini 1784; Cuvier 1809; Wellnhofer 2008a). The earliest finds of *Pterodactylus* date back to the 18th century but the precise date of their discovery remains difficult to establish (Ősi et al. 2010; Tischlinger 2020). Usually, the holotype specimen of *Pterodactylus antiquus* or 'Mannheim Exemplar' (BSP AS.I.739), found between 1767 and 1784, is regarded as the first discovered pterosaur fossil (Wellnhofer 1970, 1978, 2008a), although the holotype of *Pterodactylus micronyx* or 'Pester Exemplar' (ELTE V 256) was found between 1757 and 1779 and thus might have been found earlier (Ősi et al. 2010). First described by Cosimo Alessandro Collini in 1784, the 'Mannheim Exemplar' was originally regarded as an aquatic vertebrate with uncertain relationships (Collini 1784), before the German naturalist Johann Hermann

identified the animal as a flying vertebrate, although he regarded it as a mammal (Taquet and Padian 2004). The French naturalist and founder of comparative anatomy, Georges Cuvier, finally recognized the reptilian affinities of the specimen and later coined the term 'pterodactyle' for it (Cuvier 1809), which was later latinized into *Pterodactylus*. In the following years, however, the specimen was still variably regarded as a mammal or bird by some researchers like the German naturalist Samuel Thomas von Soemmerring, who regarded it as a bat and erected the species '*Ornithocephalus*' *antiquus* for it (Soemmerring 1812), the first binomial name for a pterosaur. Even more confusion was involved in the classification of the 'Pester Exemplar' that was initially identified as a crustacean by the Italian naturalist Ignazio Born (1779), and only over 70 years later its true affinities were recognized by Herrmann von Meyer, who used it as the holotype for the new species *Pterodactylus micronyx* (Meyer 1856).

After the initial discoveries of the Mannheim and Pester specimens, numerous additional specimens of *Pterodactylus* were discovered in the Solnhofen area from the beginning of the 19th century onward, including some with preserved soft tissues (Abel 1925), making '*Pterodactylus*' one of the best-known pterosaur genera early on. Partly due to its iconic status of being the first known pterosaur genus, *Pterodactylus* became a wastebasket taxon, especially during the 19th century. Numerous, even rather distantly related taxa, have originally been placed in the genus *Pterodactylus*, many of them, however, representing nomina dubia and species assignable to other genera. In 1970, Wellnhofer in his monograph on the pterodactyloids from the Franconian laminated limestone, provided a taxonomic revision of the genus and listed a total of six valid species for *Pterodactylus* (Wellnhofer 1970). Of these, five species have subsequently been moved to other genera, including *P. suevicus* (*Cycnorhamphus suevicus*, Bennett 1996a), *P. elegans* (*Ctenochasma elegans*, Jouve 2004), *P. micronyx* (*Aurorazhdarcho micronyx*, Bennett 2013a), *P. longicollum* (*Ardeadactylus longicollum*, Bennett 2013a), and *P. kochi* (*Diopecephalus kochi*, Vidovic and Martill 2018). Recently, there has been substantial discussion about the taxonomic status and validity of *P. kochi* and it is now either regarded as a junior synonym of *P. antiquus* or as belonging to a separate genus (see below). Although '*Pterodactylus*' has been reported also from France, England, Portugal and Tanzania, all of these finds were subsequently referred to other genera or to indeterminate pterodactyloids (see Barrett et al. 2008 and references therein). Therefore, *Pterodactylus* is currently known only from Bavaria and all of the reported finds are of Tithonian age (Barrett et al. 2008; Bennett 2013a). In this paper, we report the geologically oldest specimen of *Pterodactylus* from the Kimmeridgian and the first report of the genus from the Upper Jurassic Torleite Formation.

Institutional abbreviations

BMMS, Bürgermeister Müller Museum Solnhofen, Solnhofen, Germany; **BSPG**, Bayerische Staatssammlung für Paläontologie und Geologie, Munich, Germany; **DMA**, Dinosaurier Museum Altmühltal, Denkendorf, Germany; **ELTE**, Eötvös Loránd University, Budapest, Hungary; **JME**, Jura Museum Eichstätt, Eichstätt, Germany; **RGM**, Rijksmuseum van Geologie en Mineralogie, Leiden, Netherlands; **SM**, Senckenberg Museum, Frankfurt, Germany; **SMNS**, Staatliches Museum für Naturkunde Stuttgart, Stuttgart, Germany; **TM**, Teyler Museum, Haarlem, Netherlands.

Geological setting

The specimen described herein was found near Painten, a small town situated in the southern part of the Franconian Alb in central Bavaria (Fig. 1). The Franconian Alb forms, together with the Swabian Alb (its western continuation in the state of Baden-Württemberg), a low mountain range in southern Germany that extends from the southwest to northeast and is composed of Lower to Upper Jurassic marine sedimentary rocks. A number of uppermost Jurassic localities on the Franconian and Swabian Alb have yielded abundant and exceptionally well-preserved fossils of plants, invertebrates and vertebrates. These sites are generally characterized by an extremely fine-grained, laminated and planar limestone usually lacking bioturbation. This laminated limestone is often called by its German name 'Plattenkalk' (Viohl 2015b). The most important fossil localities, which also yielded the majority of the historical finds including the first specimens of *Pterodactylus* mentioned above, are located in the southern part of the Franconian Alb near Solnhofen and Eichstätt. The fossil treasures of this area were recognized early on, when the fine-grained limestone was mined in numerous small and large quarries for building stones and later for lithographic plates. Aside from the region near Solnhofen and Eichstätt, several other localities of the southern Franconian Alb yielded a rich fossil assemblage with a similar preservation, including (from southwest to northeast) Daiting, Schamhaupten, Painten, Kelheim, Jachenhausen, Zandt and Brunn (Fig. 1). Together, the Plattenkalk deposits of the southern Franconian Alb form the 'Solnhofen Archipelago', also referred to as the 'Solnhofen Limestone'. Two other important fossil sites preserving a similarly rich and well-preserved fauna are located on the northern Franconian Alb near Wattendorf, respectively on the southwestern part of the Swabian Alb near Nusplingen (Fig. 1).

Although these sites are overall similar, some significant differences are noteworthy with respect to lithology, age and fossil composition. As outlined above, the deposits are all composed of fine-grained limestones, the so-called Plattenkalk, yet the amount of silica and mud as well as the thickness of the limestone layers is highly variable, likely reflecting slightly distinct depositional environments (Viohl 2015b). Moreover, the different fossil sites of the Solnhofen Archipelago belong to at least four distinct formations – from oldest to youngest, the Torleite (Malm Epsilon), Geisental (Malm Zeta 1), Painten (Malm Zeta 1), Altmühltal (Malm Zeta 2) and Mörnsheim (Malm Zeta 3) formations – ranging in age from the upper Kimmeridgian to the lower Tithonian (Schweigert 2007, 2015;

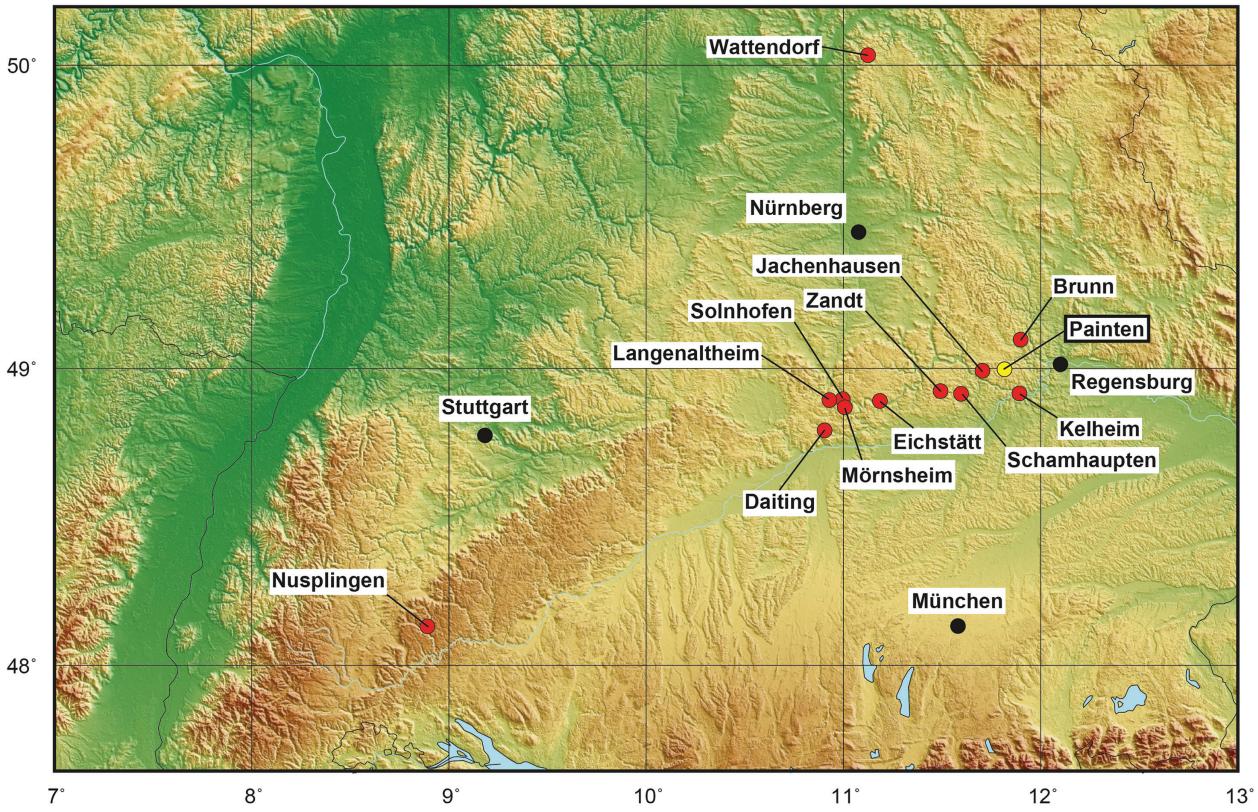

Figure 1. Map of southern Germany with the Franconian and Swabian Alb. The new specimen of *Pterodactylus antiquus* described in this study (DMA-JP-2014/004) was found 2 km northeast of Painten in the Rygol Quarry. The map was created with GMT6 (Wessel et al. 2013).

Niebuhr and Pürner 2014). During the time of deposition in the latest Jurassic, the area of today's southern Germany was situated in a shallow, tropical sea with small and larger islands. In this setting, the 'Plattenkalk' was likely deposited in locally restricted basins or 'Wannen' that were bordered by sponge bioherms and thus were separated from the open sea. The resulting stagnant water conditions in these lagoons coupled with the tropical climate caused the depletion of oxygen and hypersaline conditions near the ground, which, together with rapid sedimentation during periodic storm events, probably led to the exceptional preservation of the fossils (Viohl 2015a).

The faunal assemblage of the Solnhofen Archipelago comprises an extremely diverse array of invertebrates and vertebrates, often showing a spectacular preservation, which made these Upper Jurassic Plattenkalk deposits world famous (especially those of the southern Franconian Alb). Unsurprisingly, terrestrial and aerial vertebrates are more rarely found than marine ones but over the last centuries, numerous specimens have been discovered, including exquisitely preserved rhynchocephalians, squamates, atoposaurid crocodyliforms, theropod dinosaurs, early avialians, and pterosaurs (Wellnhofer 1970, 1975, 2008b; Ostrom 1978; Göhlich and Chiappe 2006; Rauhut et al. 2012, 2019; Frey and Tischlinger 2015; Tischlinger and Rauhut 2015). Among these, pterosaurs represent the most abundant reptile group and in total more than 500 pterosaur specimens are known (Tischlinger and Frey 2015). Interestingly, *Pterodactylus* has so far only been reported from the Solnhofen Archipelago (i.e. sediments of the southern part of the Franconian Alb), and all occurrences are Tithonian in age, ranging from the Malm Zeta 2 to Malm Zeta 3 (Bennett 2013a; Vidovic and Martill 2018).

The new specimen of *Pterodactylus* described herein represents the first occurrence of the genus from the Torleite Formation (Malm Epsilon) and was found in the quarry of the Rygol Company near Painten. The quarry is situated in the northern part of the 'Paintener Wanne', a locally restricted basin covering an area of approximately 15 × 12 km (Albersdörfer and Häckel 2015). The *Pterodactylus* specimen was found at the bottom of the exposed section in the 'Kieselplattenkalk', a 5.9 m thick package of laminated, fine-grained, silicified limestone intercalated with graded turbidite horizons consisting of carbonate debris (Albersdörfer and Häckel 2015; Keupp et al. 2016). Stratigraphically, the 'Kieselplattenkalk' of Painten belongs to the Arnstorf member of the Torleite Formation, which has been assigned to the *Hybnoticeras beckeri* ammonite Zone and the *Lithacoceras ulmense* Subzone, corresponding to a latest Kimmeridgian age (Schweigert 2007; Niebuhr and Pürner 2014). The 'Kieselplattenkalk' of Painten is characterized by an unusually high amount of silica and, in this respect, resembles the roughly coeval 'Plattenkalk' deposits of Schamhaupten and Kelheim (Viohl 2015b).

Although the Rygol Quarry has been operated since the 1950s, fossils only came to light after 2001, when systematic excavations were conducted, first led by the shift worker Wolfgang Häckel and, later, by the private Albersdörfer

institute (Albersdörfer and Häckel 2015). Excavations conducted over the last 20 years yielded a rich and diverse fossil assemblage comprising abundant plant remains, invertebrates (including sponges, corals, crinoids, brachiopods, ammonites, coleoids, gastropods, crustaceans, echinoderms) and vertebrates (Albersdörfer and Häckel 2015; Keupp et al. 2016). Among the latter, fishes are by far the most common group being represented by actinopterygians, chondrichthyans, and coelacanths (Albersdörfer and Häckel 2015). Fossil reptiles are abundant compared to other quarries and include rhynchocephalians, ichthyosaurs, turtles, the thalattosuchians *Cricosaurus albersdoerferi* and *Dakosaurus* sp., atoposaurid neosuchians, pterosaurs and the theropod dinosaur *Sciurumimus albersdoerferi* (Rauhut et al. 2012; Tischlinger and Frey 2013; Albersdörfer and Häckel 2015; Spindler and Albersdörfer 2019; Sachs et al. 2021; Spindler et al. 2021), though it must be noted that most specimens have not been described in detail yet and thus several may represent new taxa. In general, the fossils from the Rygol Quarry are extremely well preserved and relatively abundant, especially those of terrestrial vertebrates. The abundance of plants and terrestrial vertebrates indicates that coastlines must have been located nearby, while the presence of coleoids demonstrates that the local basin ('Paintener Wanne') was connected to the open sea (Röper 2005).

Materials and methods

The specimen described in this paper was found during systematic excavations on the 2nd of June 2014 by Márton Vremir in the Rygol Quarry, approximately 2 km northeast of Painten (49°0'31"N, 11°49'35"E). The pterosaur was meticulously prepared mechanically in more than 120 h by Wolfgang Haeckel under magnification of 26–20×, exclusively using pneumatic tools and needles. The specimen is permanently housed and accessible in the collection of the Dinosaurier Museum Altmühltal in Denkendorf, Bavaria, Germany (DMA) under the collection number DMA-JP-2014/004. In addition, it is guaranteed by contract that the privately owned specimen will always be available for science. The anatomical nomenclature mainly follows Wellnhofer (1985). Anatomical orientations in the wing bones are described according to a laterally extended wing, and therefore, we use the terms dorsal and ventral instead of lateral and medial.

Systematic palaeontology

Pterosauria Kaup, 1834
Pterodactyloidea Plieninger, 1901
Pterodactylidae Bonaparte, 1838
***Pterodactylus* Cuvier, 1809**

***Pterodactylus antiquus* Soemmerring, 1812**
Figs 2–5

Holotype. BSP AS.I.739, an almost complete skeleton including the skull.

Amended diagnosis. Modified after Bennett (2013a): Upper Jurassic pterodactyloid with a slender and elongated rostrum; the dorsal margin of the skull straight to only slightly concave upward; nasoantorbital fenestra length ~20–25% of skull length in large individuals; number of teeth proportional to skull length with up to ~25 teeth

Figure 2. *Pterodactylus antiquus*, DMA-JP-2014/004, from the Upper Jurassic (Kimmeridgian) Torleite Formation of Painten; overview photograph.

per jaw side in large individuals; teeth low conical; teeth largest anteriorly and decreasing in size posteriorly; tooth row length ~75% of jaw length; upper tooth row extending posterior to the anterior margin of the nasoantorbital fenestra; a low sagittal bony crest dorsal to the nasoantorbital fenestra and orbit in large individuals, which apparently lacks the striations seen in *Ctenochasma*, *Germanodactylus*, and *Gnathosaurus*; a soft tissue crest extending dorsally from the bony crest in large individuals; an occipital lappet of soft tissues extending posteriorly from the occipital region; cervical vertebrae 3–7 elongate and neck relatively longer than in *Cycnorhamphus*, *Ctenochasma*, and *Aurorazhdarcho* (shared with "*P.*" *longicollum*); in small specimens, WP2 is 93–96% of WP1 length, in large ones ~91%; in modified Nopcsa curves, WP1–4 lengths typically exhibit a convex upward curve (shared with *Germanodactylus*); in the pes, MtII is longer than MtI or equal to MtI in length; the proximal phalanges of digit I–III show progressive reduction in length whereas those of digits I and IV are subequal (shared with *Germanodactylus*).

Referred material. DMA-JP-2014/004, a nearly complete and articulated skeleton including the complete skull.

Locality. Rygol Quarry near Painten, Niederbayern, Bavaria, Germany.

Stratum. Torleite Formation, *Beckeri* zone, *Ulmense* subzone, upper Kimmeridgian, Upper Jurassic.

Taxonomic remarks. For many decades after its discovery, *Pterodactylus* has been essentially a wastebasket taxon and dozens of species have been assigned to the genus, many of which later turned out to represent rather distantly related taxa. In 1970, Wellnhofer, in his classic monograph on the pterodactyloids from the Solnhofen Limestones, provided a thorough revision of the genus and listed a total of six species: *P. antiquus*, *P. kochi*, *P. longicollum*, *P. suevicus*, *P. micronyx* and *P. elegans* (Wellnhofer 1970). Subsequently, four of these species have been assigned to their own genera, a decision followed by most researchers without much controversy, with *P. suevicus* having been assigned to *Cycnorhamphus* (=*Gallodactylus*) (e.g. Fabre 1976; Wellnhofer 1978; Bennett 1996a, 2013b; Unwin 2003), *P. elegans* to *Ctenochasma* (e.g. Bennett 1996b, 2007; Unwin 2003; Jouve 2004), *P. micronyx* to *Aurorazhdarcho* (Bennett 1996b, 2013a, Hone et al. 2013), and *P. longicollum* to *Ardeadactylus* (Bennett 2013a; Vidovic and Martill 2018). In contrast to this, the taxonomic status of *Pterodactylus kochi* has caused considerable debate recently and it is now usually regarded either as a junior synonym of *P. antiquus* or as belonging to a distinct genus. After the revision of the genus, Mateer (1976) was the first to suggest that *P. kochi* and *P. antiquus* are extremely similar and that the former therefore represents a junior synonym of the latter (although it should be noted that a synonymy of the two species has originally been proposed already by Zittel, 1883). Later, Bennett (1996b) conducted statistical analyses of *Pterodactylus* and other pterodactyloids from the Solnhofen Limestone, likewise concluding that the specimens assigned to *P. kochi* likely represent immature individuals of *P. antiquus*. This view has been also expressed by several other subsequent studies (Jouve 2004; Bennett 2013b, 2018).

Despite the synonymization of *P. kochi* with *P. antiquus*, several later studies have treated the two species as separate taxa (e.g. Frey and Martill 1998; Kellner 2003; Unwin 2003). Recently, Vidovic and Martill (2014) found the holotype of *P. scolopaciceps*, which has been synonymized with *P. kochi* by Zittel (1883) and was listed as such by Wellnhofer (1970), to differ considerably from other *Pterodactylus* specimens and thus assigned it to the new genus *Aerodactylus*. In addition, they assigned a number of other specimens to *Aerodactylus scolopaciceps* that previously were referred to *P. kochi* (Vidovic and Martill 2014). Subsequently, Vidovic and Martill (2018) re-studied several specimens assigned to *Pterodactylus* and found the holotype of *P. kochi* and two referred specimens to differ in several respects from *P. antiquus*. Therefore, they proposed that *P. kochi* actually belongs to a separate genus, *Diopecephalus*, which was originally coined by Harry Govier Seeley in the second half of the 19th century (Vidovic and Martill 2014, 2018). Thus far, a consensus on this topic has not been reached. Regarding the taxonomy of *Pterodactylus*, we here tentatively follow Mateer (1976), Bennett (1996b, 2013b), and Jouve (2004) and consequently regard *P. kochi* as representing a junior synonym of *P. antiquus*, because we find it difficult to differentiate the two taxa based on the proposed diagnoses for the time being.

Comparative description

The specimen consists of a complete, articulated and extremely well-preserved skeleton lying on its right side (Fig. 2). Only a very small portion of the left mandible as well as of the left and right tibia is missing. Otherwise, the skeleton is nearly perfectly preserved with every bone present and in its roughly correct anatomical position. The mandible is slightly detached from the skull and is preserved in ventral view. The hyoid bones are present and, like the mandible, are slightly dislocated ventrally, being preserved between the left and right mandibular rami. The wings are folded with the right wing lying partly under the left one and partly under the body skeleton. The hind limbs extend laterally and both are visible in posterolateral view.

For the comparison below, we largely relied on the classical monograph of Wellnhofer (1970), in which he described every *Pterodactylus* specimen known at the time and additionally provided the most comprehensive overview of the genus including five specimens of *P. antiquus* and 23 specimens of *P.* '*kochi*'. Wellnhofer (1970) also provided detailed measurements for all of these *Pterodactylus* specimens, which formed the basis for the quantitative comparison presented below (for details, see Wellnhofer 1970: chapter 10). Note that we here use the corrected measurements for TM 10341 by Bennett (2013a)

that differ considerably from those listed by Wellnhofer (1970). In order to make the comparison as clear as possible, and because there has been considerable debate on the taxonomy of *Pterodactylus* (see above), we here refer to individual specimens instead of referring simply to *P. antiquus* or *P. kochi*. Moreover, we provide both the specimen number used in the Wellnhofer (1970) monograph (i.e. his 'Exemplar Nr.') and the official repository number. Notably, specimen JME 29.III.1950 (Exemplar Nr. 9), which was originally referred to *P. kochi* by Wellnhofer (1970), has been reassigned to *Germanodactylus cristatus* by Bennett (2006), and we herein follow this referral. When referring to *Pterodactylus* in the comparison below, we include both *P. antiquus* and *P. kochi*, as we tentatively accept the synonymy of the two as outlined above. For an overview of the measurements of the skeleton and individual bones as well as some selected dimensions, see Table 1.

Table 1. Measurements (in mm) of the new *Pterodactylus* specimen from Painten (DMA-JP-2014/004).

skull	48
orbit	10
nasoantorbital fenestra	16
lower jaw	38
mandible symphysis	14
neck	28
Precaudal thoracic vertebral column (PCRW)	33
scapula	13
coracoid	11
humerus	18
radius	25
mc IV	16
wp 1	22.5
wp 2	21.5
wp 3	19.5
wp 4	17
femur	18.5
tibia	23.5

Cranial skeleton

The skull of DMA-JP-2014/004 is complete and exposed in left lateral view (Fig. 3). It has a total length of approximately 48 mm, and thus lies within the lower range previously observed in *Pterodactylus* with reported skull lengths ranging between 23 mm in the smallest specimen (BSPG 1967 I 276, Exemplar Nr. 6) and 149 mm in the largest specimen preserving a complete skull (BMMS 7, without Exemplar Nr.) (Wellnhofer 1970; Bennett 2013a). Like in other specimens of *Pterodactylus*, the orbit is circular in outline and has a diameter of slightly more than 10 mm. The orbit is thus relatively large compared to overall skull length (ca. 20%), likely reflecting the young ontogenetic age of the specimen. Wellnhofer (1970) provided SOL-indices (=Schädel-Orbita-Längen-Index, German for skull-orbit-length index) for the pterodactyloids from the Solnhofen Archipelago, which range from 30 in the smallest individual of *Pterodactylus* (BSPG 1967 I 276, Exemplar Nr. 6; skull length of 23 mm) to 15 in the largest (BSPG 1883 XVI 1, Exemplar Nr. 28; skull length of 113.5). With an SOL-index of 20 and a skull length of 48 mm, the new specimen from Painten matches the observed relationship between SOL-index and skull length for pterodactyloids very well (see Wellnhofer 1970: fig. 17) and falls within the range defined as the transitional ontogenetic stage (between juvenile and adult).

The sclerotic ring is preserved within the dorsal half of the orbit and even the individual sclerotic elements can be discerned, although an exact number of sclerotic elements

Figure 3. *Pterodactylus antiquus*, DMA-JP-2014/004, from the Upper Jurassic (Kimmeridgian) Torleite Formation of Painten; detail photograph of the skull.

cannot be provided due to the small size and imperfect preservation. The sclerotic ring is ellipsoidal in shape being slightly longer than high, although it seems to be diagenetically somewhat compressed dorsoventrally. Judging from other specimens preserving the sclerotic ring like BSPG 1968 I 95 (Exemplar Nr. 2) and SMNS 81775 (without Exemplar Nr.), the sclerotic ring normally has a circular outline and occupies almost the entire orbit (Wellnhofer 1970; Bennett 2006: fig. 6). The nasoantorbital fenestra has an anteroposterior length of 16 mm, occupying around one third of the skull length, which is similar to other *Pterodactylus* specimens including the holotype of *P. antiquus* (BSPG AS I 739, Exemplar Nr. 4) (Wellnhofer 1970). In very young individuals, the ratio between nasoantorbital length and skull length is slightly smaller, around one fifth to one fourth (e.g. BSPG 1967 I 276, Exemplar Nr. 6) (Wellnhofer 1970). The parietal region of the skull posterior to the orbit is rounded. The dorsal margin of the skull is relatively straight and slightly concave. The ventral margin of the skull and the palatal region are completely straight.

The mandible is complete and preserved in ventral view, although it is slightly distorted in a way that the left lateral aspect is partly visible. It has a total length of 38 mm, while the symphysis is 14 mm long, thus occupying slightly more than one third (approximately 37%) of the length of the mandible. In general, it seems as if the symphysis becomes proportionately slightly larger (relative to mandible length) during ontogeny, with the ratio ranging between 37% in small individuals (BSPG 1967 I 276, Exemplar Nr. 6; skull length of 23 mm) and 43% in large individuals (BSPG AS I 739, Exemplar Nr. 4; skull length of 108 mm) (Wellnhofer 1970). The distance between the left and right mandibular ramus at the level of the joint is 7 mm, although this value should be treated with caution due to the slight distortion of the lower jaw. The suture between the mandibular rami is well discernible, being completely straight and extending anteroposteriorly. The paired hyoid bones are located between the posterior parts of the lower jaw and have an elongated, slightly bowed morphology, and thus resemble those of the very small specimen BSPG 1967 I 276 (Exemplar Nr. 6) (Wellnhofer 1970: fig. 5).

The tooth crowns are overall low and conical, just as in all other specimens of *Pterodactylus*. There are 14 teeth preserved in the left upper jaw, extending from the jaw tip up until the anterior third of the nasoantorbital fenestra. The size of the teeth progressively decreases posteriorly – again a feature present in several other *Pterodactylus* specimens including the type specimens of both *P. antiquus* (BSPG AS I 739, Exemplar Nr. 4), and of *P. kochi* (BSPG AS XIX 3, Exemplar Nr. 23) (Wellnhofer 1970: fig. 3, pl. 1–2). In the left lower jaw, 14 teeth are present that gradually become smaller posteriorly and extend for 17 mm measured from the tip of the jaw (roughly 45% of the total mandible length). As was demonstrated by Wellnhofer (1970) as well as later by Jouve (2004) and Bennett (2013a), the tooth count in *Pterodactylus* changes in proportion with the length of the skull and thus the ontogenetic age of the specimen. The number of teeth in the upper jaw ranges between 12 in small individuals (BSPG 1967 I 276, Exemplar Nr. 6; skull length of 23 mm) and 18 in large individuals (BSPG AS I 739, Exemplar Nr. 4; skull length of 108 mm) (Wellnhofer 1970).

Axial skeleton

The neck of DMA-JP-2014/004 (Fig. 4a) comprises seven cervical vertebrae (but see Bennett 2004, 2013a) and has a length of approximately 28 mm, which compares well with other *Pterodactylus* specimens of a similar size such as (the slightly smaller) TM 10341 (Exemplar Nr. 1) that has a neck length of 25.9 mm and a skull length of 44.5 mm (Bennett 2013a). The dorsal series comprises 15 vertebrae, while the number of sacral vertebrae is difficult to assess due to the slightly displaced ilium (Fig. 4a). The combined length of the dorsal and sacral region (= PCRW-length of Wellnhofer 1970 and Bennett 2013a) is 33 mm and thus similar in size but proportionately slightly smaller compared to that of the similarly-sized specimen TM 10341 (Exemplar Nr. 1), in which the dorsal and sacral vertebral column have a combined length of 33.3 mm (Bennett 2013a). The tail of the new specimen from Painten is partially covered by the ilium, and therefore its exact length and the number of caudal vertebrae cannot be reliably determined. The ribs are still attached to their respective vertebrae, are very thin and slightly curved. However, they are partly concealed by the overlying forelimb elements. The overlapping gastralia are present in the abdominal area of the specimen, anteroventrally of the pelvis.

Appendicular skeleton

The forelimbs are complete and mostly articulated, although the right wing is partly underlying the body skeleton (Fig. 4b). The measurements were thus taken from the left forelimb. The scapula and the coracoid are preserved next to each other, the former having a length of 13 mm and the latter of 11 mm, although the coracoid is not fully visible in the left or the right side. The left humerus, which is slightly dislocated from the glenoid, has a length of 18 mm. Radius and ulna are lying next to each other, being completely parallel and more or less equal in length. Both are considerably longer than the humerus with a length of 25 mm. As discussed by Wellnhofer (1970), the wrist of *Pterodactylus* consists of two proximal carpals and four distal carpals. In the new specimen from Painten, the two proximal carpals contact the distal joints of radius and ulna, while the four distal carpals are preserved as small, blocky elements between the proximal carpals and the metacarpals. The four metacarpals are subequal in length and preserved parallel to each other, but metacarpals I–III are much smaller and partly covered by metacarpal IV. The wing metacarpal (i.e. metacarpal IV) is similar in size to, albeit slightly shorter than, the humerus with a length of 16 mm. The pulley-like distal joint of the wing metacarpal is well visible in dorsal view. The phalanges of the wing finger are elongated and rod-like and decrease in

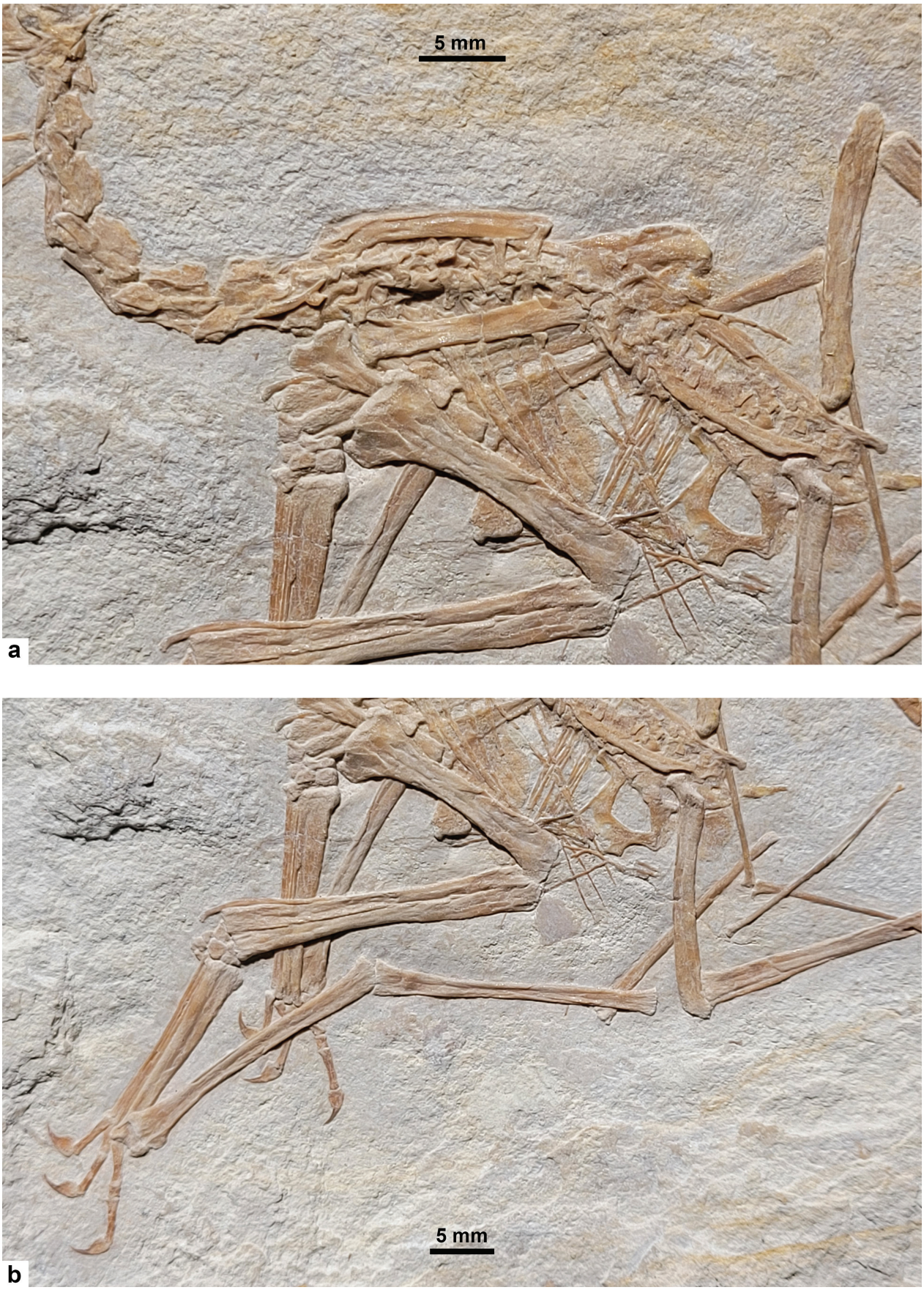

Figure 4. *Pterodactylus antiquus*, DMA-JP-2014/004, from the Upper Jurassic (Kimmeridgian) Torleite Formation of Painten; detail photograph of the axial skeleton (**a**), as well as the forelimbs (**b**).

size distally, with lengths of 22.5 mm (wing phalanx 1), 21.5 mm (wing phalanx 2), 19.5 mm (wing phalanx 3) and 17 mm (wing phalanx 4). The distal-most phalanx of the left wing finger is slightly dislocated from the third one. The right wing is completely articulated but largely hidden under the body skeleton. The other fingers are articulated with their respective metacarpals and are completely preserved. The phalangeal formula of the hand is 2-3-4-4-0, as is typical for pterosaurs. The proportions of the wing of the Painten specimen are very similar to those reported from other specimens of *Pterodactylus*, with the humerus being around a quarter to a third shorter than the radius, the wing metacarpal being similar in size to (albeit slightly smaller than) the humerus, and the wing phalanges becoming progressively but slowly shorter (for a comparison of the forelimb proportions in *Pterodactylus*, see also below).

The pelvis comprises the articulated ilium, which is firmly attached to the sacral vertebrae, the pubis and the ischium (Fig. 5). The hind limbs are both well visible, being stretched out laterally (Fig. 5). The femora are articulated with the pelvis, the slightly demarcated femoral head still being connected to the acetabulum. The femur has a length of 18.5 mm and thus is slightly shorter than the tibia, which has a length of 23.5 mm, a condition also seen in all other *Pterodactylus* specimens (Wellnhofer 1970; Bennett 2013a). The fibula is very thin, tightly attached to the tibia, and only extending for the proximal half of the tibia. The tarsals are tightly interlocked and articulated in the right hind limb, whereas in the left hind limb, the tarsals are somewhat disarticulated. Of the five tarsals (two proximal and three distal ones) typically present in *Pterodactylus* (Wellnhofer 1970), at least four (two proximal and two distal ones) are visible in the specimen from Painten. The feet are again well preserved and articulated, comprising all five metacarpals and all five digits. Among the metatarsals, metatarsal II is the longest, metatarsal I and III are subequal in length and slightly shorter than metatarsal II. Metatarsal IV is shorter than metatarsal I and II, and metatarsal V is considerably shorter than the other metatarsals, being only a small splint-like bone. The first four digits bear small claws, whereas the fifth digit consists only of a single short phalanx. The phalangeal formula is 2-3-3-3-1. As demonstrated by Wellnhofer (1970), the phalangeal formula of *Pterodactylus* is dependent on the ontogenetic age of the animal, varying between 2-3-3-3-1 in juveniles and 2-3-4-4-1 in adults. Therefore, the phalangeal formula of the specimen from Painten again indicates an individual of juvenile to subadult age.

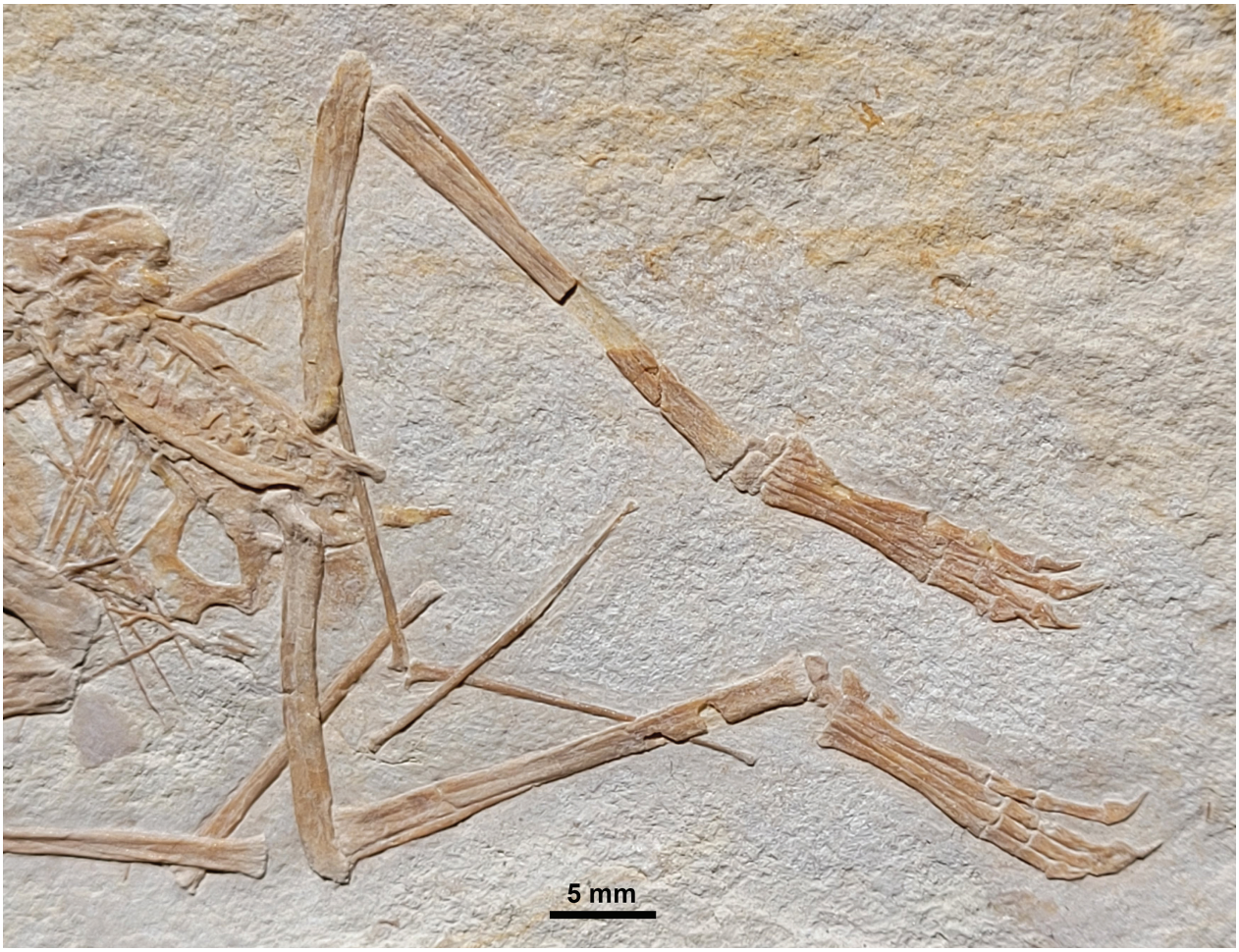

Figure 5. *Pterodactylus antiquus*, DMA-JP-2014/004, from the Upper Jurassic (Kimmeridgian) Torleite Formation of Painten; detail photograph of the hind limbs.

Skeletal proportions and Nopcsa curves

The length of the skull, neck, combined dorsal and sacral vertebral column (=PCRW-length of Wellnhofer 1970 and Bennett 2013a), humerus, radius, wing metacarpal, wing phalanx 1–4, femur and tibia were plotted in order to produce a modified Nopcsa curve (see Bennett 2013a). In this diagram, we also plotted the respective lengths of all other *Pterodactylus* specimens (measurements taken from Wellnhofer 1970 as well as Bennett 2013a for specimen TM 10341 and Frey and Tischlinger 2000 for an uncatalogued specimen stored in a private collection). The resulting Nopcsa diagram (Fig. 6) is essentially an updated version of the one figured by Bennett (2013a: fig. 9). In general, the specimen from Painten, DMA-JP-2014/004, is remarkably similar to the other *Pterodactylus* specimens regarding its skeletal proportions. The skull is the longest element in all specimens, while the neck is significantly shorter. In the large majority of specimens, including DMA-JP-2014/004, the combined length of the dorsal and sacral vertebral column (=PCRW-length) is greater than that of the neck, with some notable exceptions such as the holotype of *P. antiquus* (BSPG AS I 739, Exemplar Nr. 4), in which the PCRW-length is smaller than, or equal to, the length of the neck. Notably, all of these exceptions are relatively large specimens with skull lengths of more than 80 mm. All specimens smaller than that (i.e. having skull lengths below 80 mm) have a neck shorter than their combined dorsal and sacral vertebral column.

In all specimens referred to *Pterodactylus*, the humerus is much shorter than the PCRW-length and the radius is longer than the humerus (Fig. 6). The metacarpal of the wing finger is again considerably shorter than the radius and has a similar size as the humerus in all specimens aside from SM R4074, in which the wing finger metacarpal is comparatively very long, having almost the same length as the radius. In all specimens except SM R4074 (which seems to have an unusually long fourth metacarpal), the first wing finger phalanx is much longer than the wing finger metacarpal. In all specimens of *Pterodactylus*, phalanges 1–4 of the wing finger are progressively shorter, which, in the diagram (Fig. 6), results in a slightly convex and gentle downward curve. The femur is significantly longer than the wing phalanx 4 but shorter than the tibia. In summary, the outline of the Nopcsa curve of the specimen from Painten is nearly identical to that of similarly sized *Pterodactylus* specimens, thus indicating remarkably similar skeletal proportions and placing DMA-JP-2014/004 unequivocally within the genus *Pterodactylus*.

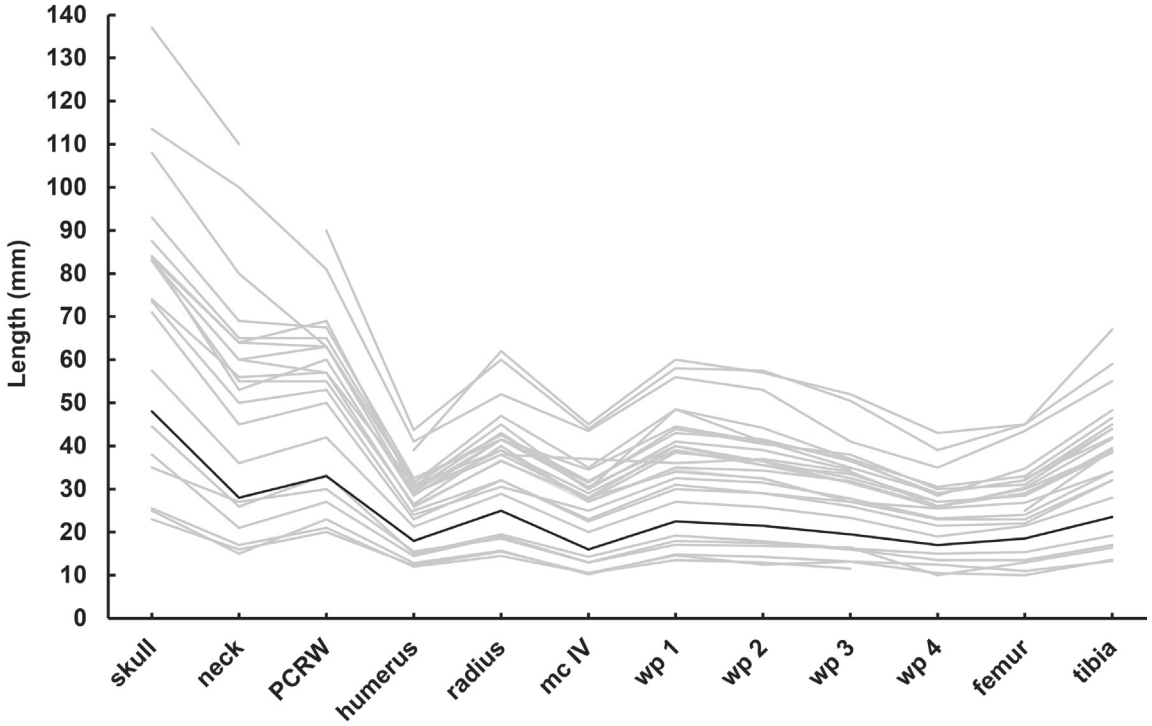

Figure 6. Modified Nopcsa curves of the skeletal proportions of *Pterodactylus antiquus* (including *P. kochi*). The measurements were taken from Wellnhofer (1970) as well as from Frey and Tischlinger (2000). Note that we used the corrected values of TM 10341 (Exemplar Nr. 1) provided by Bennett (2013a) that differ considerably from those listed by Wellnhofer (1970). Specimen JME 29.III.1950 (Exemplar Nr. 9) was excluded because it was shown by Bennett (2006) to belong to *Germanodactylus cristatus*. The heavy black line represents the curve for the new specimen from Painten described herein (DMA-JP-2014/004). The line with the third-largest skull represents the holotype of *P. antiquus* (BSPG AS I 739, Exemplar Nr. 4; skull length of 108 mm), and the line directly below that of the Painten specimen (DMA-JP-2014/004) represents TM 10341 (Exemplar Nr. 1; skull length of 44.5 mm). **Abbreviations**: **mcIV**, metacarpal IV (i.e. the wing finger metacarpal); **PCRW**, combined length of the dorsal and sacral vertebral column (=PCRW-length of Wellnhofer 1970 and Bennett 2013a; praecaudale Rumpfwirbelsäule); **r**, radius; **s**, skull; **t**, tibia; **wp1–4**, wing finger phalanx 1–4.

Discussion and conclusion

The new specimen from Painten is clearly referable to *Pterodactylus antiquus*, based on the diagnosis proposed by Bennett (2013a). More specifically, it has an elongate skull, a slender and elongated rostrum, a straight to only slightly concave dorsal skull margin, low and conical teeth that are large anteriorly and decrease in size posteriorly, an upper tooth row extending to the anterior margin of the nasoantorbital fenestra, wing phalanx 2 being 93–96% (exactly 95.6%) as long as wing phalanx 1, wing phalanges 1–4 exhibiting a convex upward curve in modified Nopcsa curves, and a longer metatarsal II than I (for the diagnosis of *P. antiquus* see also above). Only features listed by Bennett (2013a) as being characteristic of adult individuals and varying across ontogenetic stages (e.g. tooth count, length of nasoantorbital fenestra, presence of a sagittal bony crest), are absent in DMA-JP-2014/004. In addition, the Painten *Pterodactylus* is extremely similar to other specimens assigned to *P. antiquus* (including *P. kochi*), especially those of a similar size and thus ontogenetic stage, with respect to both gross morphology and skeletal proportions (see above). The Painten *Pterodactylus* most likely represents a juvenile to young subadult individual as shown by its overall size, absolute skull length, the size of the orbit (relative to skull length), and phalangeal formula of the pes. Based on the SOL-index of Wellnhofer (1970), the specimen is assignable to the transitional stage ('Übergangsbereich') between juvenile and adult individuals. Interestingly, the DMA-JP-2014/004 falls here into a size range that is relatively rare in the known sample of *Pterodactylus* specimens. So far, only four specimens with a skull length between 30 and 60 mm have been reported, and only one of these falls into the size range between 38 and 57.5 mm (TM 10341, Exemplar Nr. 1; skull length of 44.5 mm).

In general, small and immature individuals dominate the sample of *Pterodactylus* from Solnhofen, whereas large and adult individuals are comparatively rare (Bennett 1996b). The same pattern can also be observed in other pterodactyloids and *Rhamphorhynchus* from the Solnhofen Archipelago (Bennett 1995, 1996b). As observed by Bennett (1996b), the specimens are, however, not evenly distributed across the full size range but predominantly fall into distinct size-classes that are separated by marked gaps. For *Pterodactylus*, these size classes are characterized by a skull length of 15–45 mm and 55–95 mm for the small and large size-classes, respectively (Bennett 1996b). The gaps bounding these size-classes are between 38–57 mm and more than 93 mm skull length. The specimen from Painten (with a skull length of 48 mm) thus is a rare representative of the first gap between the small and large size-classes. Bennett (1996b) interpreted the distinct size-classes as year-classes, which consequently means that DMA-JP-2014/004 was of an intermediate (and rarely found) ontogenetic age at the time of its death, between two consecutive year-classes. In his statistical study on *Rhamphorhynchus* from the Solnhofen Limestone (a taxon showing similar size-classes), Bennett (1995) provided two explanations for the observed size-pattern: either these pterosaurs suffered from seasonal mortalities, or the conditions allowing the preservation of the carcasses were present only seasonally. Seasonal mortality, in turn, could be explained by migratory behaviour of the animals (i.e. they were present in the region only seasonally) or it could mean that the animals died from environmental factors occurring seasonally, such as monsoons or toxic algal blooms (Bennett 1995). Seasonal preservation, on the other hand, would indicate seasonal changes in water quality (Bennett 1995) or seasonal changes of sedimentary influx into the basins (the 'Wannen'). Therefore, both the seasonal mortality hypothesis and the seasonal preservation hypothesis could be explained by the reconstructed seasonal (perhaps monsoonal) climate prevailing at the time of deposition of the Solnhofen Limestone (see above). The dominance of small, immature individuals in the sample of *Pterodactylus* specimens probably reflects their higher vulnerability and/or their higher potential to be preserved in the shallow basins (Bennett 1995).

Interestingly, the tetrapod assemblage from the Plattenkalk deposits of the Painten area appears to be highly distinctive on an alpha-taxonomic level. Although closely related species are also known from other strata of the laminated limestone of the Franconian Alb, several taxa are so far unique to the Painten limestones, including new but so far undescribed turtles (Albersdörfer and Häckel 2015; Spindler and Albersdörfer 2019), a new species of *Cricosaurus* (Sachs et al. 2021), the theropod *Sciurumimus* (Rauhut et al. 2012), a so far undescribed new pro-pterodactyloid (Tischlinger and Frey 2013), and a so far undescribed *Cycnorhamphus*-like pterosaur (Bennett 2013b), among others. The specimen described in this paper represents an intriguing exception because it can be confidently assigned to *Pterodactylus antiquus*, a species otherwise well-known from much younger limestone deposits of the Solnhofen Archipelago referable to the Malm Zeta 2 to Malm Zeta 3 (Bennett 2013a; Vidovic and Martill 2018). The Plattenkalk deposits from Painten (Torleite Formation) have been assigned to the *Beckeri* ammonite zone, the *Ulmense* subzone and the *rebouletianum* ammonite horizon corresponding to the latest Kimmeridgian age. The youngest occurrence of *Pterodactylus antiquus* comes from the Mörnsheim limestone deposits (Wellnhofer 1970), which have been assigned to the Malm Zeta 3, and more specifically, *Hybonotum* ammonite zone, *Moernsheimensis* subzone and *moernsheimensis* ammonite horizon (Schweigert 2015). Therefore, *Pterodactylus antiquus* spans at least six ammonite horizons, which are from oldest to youngest, the *rebouletianum*, *eigeltingense*, *riedlingensis*, *leisackerensis*, *rueppellianus*, and *moernsheimensis* (Schweigert 2007, 2015). Following the reasoning of Rauhut et al. (2018), it is possible to estimate the approximate duration of this timespan based on the assumption of Schweigert (2005), who calculated an average ammonite horizon duration of 165,000 years. This leads to a temporal range for *Pterodactylus antiquus* of roughly one million years. The unique taxonomic composition of the vertebrate fauna from Painten (at least on an alpha-taxonomic level) might be related

to the relatively old geological age of the deposits or, alternatively, to the particular palaeogeographic or palaeoecological characteristics of the Painten basin ('Paintener Wanne'). Ultimately, this could also explain the somewhat unusual ontogenetic age of the *Pterodactylus* specimen described here (see above). However, for the time being, the exact reasons for the distinctiveness of the vertebrate assemblage from Painten cannot be resolved conclusively, as much of the material from there still awaits detailed study. In general, this paper highlights the potential of the Plattenkalk deposits from Painten for yielding important new insights into the vertebrate fauna of the Solnhofen Archipelago but, at the same time, it also illustrates the importance of future work regarding the material.

Acknowledgements

We wish to thank the Painten excavation team, especially Márton Vremir, who discovered the specimen, and his late brother Mátyás Vremir, who organized the team from Romania that contributed to the excavation significantly. We are grateful to Wolfgang Häckel, who skilfully recovered the fossil and who conducted the challenging preparation. Uwe Kirscher (University of Tübingen) kindly helped with the geographic map. Moreover, we are grateful to Frederik Spindler (DMA) for providing access to the specimen. We would like to thank Eberhard Frey for constructive and helpful feedback on the manuscript as well as editor Johannes Müller for his comments and assistance during the publication process.

References

Abel O (1925) On a skeleton of *Pterodactylus antiquus* from the lithographic shales of Bavaria, with remains of skin and musculature. American Museum Novitates 192: 1–12.

Albersdörfer R, Häckel W (2015) Die Kieselplattenkalke von Painten. In: Arratia G, Schultze H-P, Tischlinger H, Viohl G (Eds) Solnhofen: ein Fenster in die Jurazeit. Verlag Dr. Friedrich Pfeil, München, 126–133.

Barrett PM, Butler RJ, Edwards NP, Milner AR (2008) Pterosaur distribution in time and space: An atlas. Zitteliana 28: 61–107.

Bennett SC (1995) A statistical study of *Rhamphorhynchus* from the Solnhofen Limestone of Germany: Year-classes of a single large species. Journal of Paleontology 69(3): 569–580. https://doi.org/10.1017/S0022336000034946

Bennett SC (1996a) On the Taxonomic Status of *Cycnorhamphus* and *Gallodactylus* (Pterosauria: Pterodactyloidea). Journal of Paleontology 70(2): 335–338. https://doi.org/10.1017/S0022336000023441

Bennett SC (1996b) Year-classes of pterosaurs from the Solnhofen Limestone of Germany: Taxonomic and systematic implications. Journal of Vertebrate Paleontology 16(3): 432–444. https://doi.org/10.1080/02724634.1996.10011332

Bennett SC (2004) New information on the pterosaur *Scaphognathus crassirostris* and the pterosaurian cervical series. Journal of Vertebrate Paleontology 24: 38A.

Bennett SC (2006) Juvenile specimens of the pterosaur *Germanodactylus cristatus*, with a review of the genus. Journal of Vertebrate Paleontology 26(4): 872–878. https://doi.org/10.1671/0272-4634(2006)26[872:JSOTPG]2.0.CO;2

Bennett SC (2007) A review of the pterosaur *Ctenochasma*: Taxonomy and ontogeny. Neues Jahrbuch für Geologie und Paläontologie. Abhandlungen 245(1): 23–31. https://doi.org/10.1127/0077-7749/2007/0245-0023

Bennett SC (2013a) New information on body size and cranial display structures of *Pterodactylus antiquus*, with a revision of the genus. Palaontologische Zeitschrift 87(2): 269–289. https://doi.org/10.1007/s12542-012-0159-8

Bennett SC (2013b) The morphology and taxonomy of the pterosaur *Cycnorhamphus*. Neues Jahrbuch für Geologie und Paläontologie. Abhandlungen 267(1): 23–41. https://doi.org/10.1127/0077-7749/2012/0295

Bennett SC (2018) New smallest specimen of the pterosaur *Pteranodon* and ontogenetic niches in pterosaurs. Journal of Paleontology 92(2): 254–271. https://doi.org/10.1017/jpa.2017.84

Bonaparte CL (1838) Synopsis vertebratorum systematis. Amphibiorum. Nuovi Annali Science Naturali Bologna 2: 391–397.

Born I (1779) Zufällige Gedanken über die Anwendung der Konchylien Petrefaktenkude auf die physikalische Erdbeschreibung. Abhandlungen einer Privatgesellschaft 4: 305–312.

Collini CA (1784) Sur quelques Zoolithes du Cabinet d'Histoire naturelle de S. A. S. E. Palatine & de Bavière, à Mannheim. Acta Theodoro-Palatinae Mannheim. Pars Physica 5: 58–103.

Cuvier G (1809) Mémoire sur le squelette fossile d'un reptile volant des environs d'Aichstedt, que quelques naturalistes ont pris pour un oiseau, et dont nous formons un genre de Sauriens, sous le nom de Petro-Dactyle. Annales de Musée d'Histoire Naturelle 13: 424.

Fabre J (1976) Un nouveau Pterodactylidae du gisement de Canjuers (Var) *Gallodactylus canjuersensis* nov. gen., nov. sp. Annales de Paléontologie 62: 35–70.

Frey E, Martill DM (1998) Soft tissue preservation in a specimen of *Pterodactylus kochi* (Wagner) from the Upper Jurassic of Germany. Neues Jahrbuch für Geologie und Paläontologie - Abhandlungen 210(3): 421–441. https://doi.org/10.1127/njgpa/210/1998/421

Frey E, Tischlinger H (2000) Weichteilanatomie der Flugsaurierfüße und Bau der Scheitalkämme: Neue Pterosaurierfunde aus den Solnhofener Schichten (Bayern) und der Crato Formation (Brasilien). Archaeopteryx 18: 1–16.

Frey E, Tischlinger H (2015) Krokodile (Crocodyliformes). In: Arratia G, Schultze H-P, Tischlinger H, Viohl G (Eds) Solnhofen: ein Fenster in die Jurazeit. Verlag Dr. Friedrich Pfeil, München, 448–458.

Göhlich UB, Chiappe LM (2006) A new carnivorous dinosaur from the Late Jurassic Solnhofen archipelago. Nature 440(7082): 329–332. https://doi.org/10.1038/nature04579

Hone DWE, Habib MB, Lamanna MC (2013) An annotated and illustrated catalogue of Solnhofen (Upper Jurassic, Germany) pterosaur specimens at Carnegie Museum of Natural History. Annals of the Carnegie Museum 82(2): 165–191. https://doi.org/10.2992/007.082.0203

Jouve S (2004) Description of the skull of a *Ctenochasma* (Pterosauria) from the latest Jurassic of eastern France, with a taxonomic revision of European Tithonian Pterodactyloidea. Journal of Vertebrate Paleontology 24(3): 542–554. https://doi.org/10.1671/0272-4634(2004)024[0542:DOTSOA]2.0.CO;2

Kaup J (1834) Versuch einer Eintheilung der Säugethiere in 6 Stämme und der Amphibien in 6 Ordnungen. Isis 3: 311–315.

Kellner AWA (2003) Pterosaur phylogeny and comments on the evolutionary history of the group. Geological Society of London, Special Publications 217(1): 105–137. https://doi.org/10.1144/GSL.SP.2003.217.01.10

Keupp H, Hoffmann R, Stevens K, Albersdörfer R (2016) Key innovations in Mesozoic ammonoids: The multicuspidate radula and the calcified aptychus. Palaeontology 59(6): 775–791. https://doi.org/10.1111/pala.12254

Mateer NJ (1976) A statistical study of the genus *Pterodactylus*. Bulletin of the Geological Institutions of the University of Uppsala 6: 97–105.

Meyer H von (1856) Letter on various fossil vertebrates. Neues Jahrbuch für Mineralogie, Geognomie, Geologie, Petrefakt: 826.

Niebuhr B, Pürner T (2014) Plattenkalk und Frankendolomit – Lithostratigraphie der Weißjura-Gruppe der Frankenalb (außeralpiner Oberjura, Bayern). Schriftenreihe der Deutschen Gesellschaft für Geowissenschaften 83: 5–72. https://doi.org/10.1127/sdgg/83/2014/5

Ősi A, Prondvai E, Géczy B (2010) The history of Late Jurassic pterosaurs housed in Hungarian collections and the revision of the holotype of *Pterodactylus micronyx* Meyer 1856 (a 'Pester Exemplar'). Geological Society of London, Special Publications 343(1): 277–286. https://doi.org/10.1144/SP343.17

Ostrom JH (1978) The osteology of *Compsognathus longipes* WAGNER. Zitteliana 4: 73–118.

Plieninger F (1901) Beiträge zur Kenntnis der Flugsaurier. Palaeontographica 48: 65–90.

Rauhut OWM, Foth C, Tischlinger H, Norell MA (2012) Exceptionally preserved juvenile megalosauroid theropod dinosaur with filamentous integument from the Late Jurassic of Germany. Proceedings of the National Academy of Sciences of the United States of America 109(29): 11746–11751. https://doi.org/10.1073/pnas.1203238109

Rauhut OWM, Foth C, Tischlinger H (2018) The oldest *Archaeopteryx* (Theropoda: Avialiae): a new specimen from the Kimmeridgian/Tithonian boundary of Schamhaupten, Bavaria. PeerJ 6: e4191. https://doi.org/10.7717/peerj.4191

Rauhut OW, Tischlinger H, Foth C (2019) A non-archaeopterygid avialan theropod from the Late Jurassic of southern Germany. Worthy T, Tautz D, Worthy T, Oconnor J (Eds). eLife 8: e43789. https://doi.org/10.7554/eLife.43789

Röper M (2005) Field Trip B: East Bavarian Plattenkalk - different types of upper Kimmeridgian to lower Tithonian Plattenkalk deposits and facies. Zitteliana 26: 57–70.

Sachs S, Young MT, Abel P, Mallison H (2021) A new species of *Cricosaurus* (Thalattosuchia, Metriorhynchidae) based upon a remarkably well-preserved skeleton from the Upper Jurassic of Germany. Palaeontologia Electronica 24: 1–28. https://doi.org/10.26879/928

Schweigert G (2005) Calibration of the upper Jurassic in the Stratigraphic Table of Germany 2002 by means of faunal horizons. Newsletters on Stratigraphy 41: 279–286. https://doi.org/10.1127/0078-0421/2005/0041-0279

Schweigert G (2007) Ammonite biostratigraphy as a tool for dating Upper Jurassic lithographic limestones from South Germany first results and open questions. Neues Jahrbuch für Geologie und Paläontologie - Abhandlungen 245(1): 117–125. https://doi.org/10.1127/0077-7749/2007/0245-0117

Schweigert G (2015) Biostratigraphie der Plattenkalke der Südlichen Frankenalb. In: Arratia G, Schultze H-P, Tischlinger H, Viohl G (Eds) Solnhofen: ein Fenster in die Jurazeit. Verlag Dr. Friedrich Pfeil, München, 63–66.

Soemmerring ST (1812) Über einen *Ornithocephalus*. Denkschriften der königlichen bayerischen Akademie der Wissenschaften, mathematisch-physikalische Classe 3: 89–158.

Spindler F, Albersdörfer R (2019) Schatzkammer im Herzen Bayerns. Die einzigartigen Fossilfunde von Painten. Eigenverlag Dinosaurier-Park Altmühltal, Denkendorf, Denkendorf, 70 pp.

Spindler F, Lauer R, Tischlinger H, Mäuser M (2021) The integument of pelagic crocodylomorphs (Thalattosuchia: Metriorhynchidae). Palaeontologia Electronica 24: 1–41. https://doi.org/10.26879/1099

Taquet P, Padian K (2004) The earliest known restoration of a pterosaur and the philosophical origins of Cuvier's Ossemens Fossiles. Comptes Rendus. Palévol 3(2): 157–175. https://doi.org/10.1016/j.crpv.2004.02.002

Tischlinger H (2020) Der „Collini-*Pterodactylus*" – eine Ikone der Flugsaurier-Forschung. Archaeopteryx 36: 16–31.

Tischlinger H, Frey E (2013) Ein neuer Pterosaurier mit Mosaikmerkmalen basaler und pterodactyloider Pterosauria aus dem Ober-Kimmeridgium von Painten (Oberpfalz, Deutschland). Archaeopteryx 31: 1–13.

Tischlinger H, Frey E (2015) Flugsaurier (Pterosauria). In: Arratia G, Schultze H-P, Tischlinger H, Viohl G (Eds) Solnhofen: ein Fenster in die Jurazeit. Verlag Dr. Friedrich Pfeil, München, 459–480.

Tischlinger H, Rauhut OWM (2015) Schuppenechsen (Lepidosauria). In: Arratia G, Schultze H-P, Tischlinger H, Viohl G (Eds) Solnhofen: ein Fenster in die Jurazeit. Verlag Dr. Friedrich Pfeil, München, 448–458.

Unwin DM (2003) On the phylogeny and evolutionary history of pterosaurs. Geological Society of London, Special Publications 217(1): 139–190. https://doi.org/10.1144/GSL.SP.2003.217.01.11

Vidovic SU, Martill DM (2014) *Pterodactylus scolopaciceps* Meyer, 1860 (Pterosauria, Pterodactyloidea) from the Upper Jurassic of Bavaria, Germany: The problem of cryptic pterosaur taxa in early ontogeny. PLoS ONE 9(10): e110646. https://doi.org/10.1371/journal.pone.0110646

Vidovic SU, Martill DM (2018) The taxonomy and phylogeny of *Diopecephalus kochi* (Wagner, 1837) and '*Germanodactylus rhamphastinus*' (Wagner, 1851). Geological Society of London, Special Publications 455(1): 125–147. https://doi.org/10.1144/SP455.12

Viohl G (2015a) Die lithostraigraphischen Plattenkalke im engeren Sinne. In: Arratia G, Schultze H-P, Tischlinger H, Viohl G (Eds) Solnhofen: ein Fenster in die Jurazeit. Verlag Dr. Friedrich Pfeil, München, 78–100.

Viohl G (2015b) Die Plattenkalk-Typen der Südlichen Frankenalb. In: Arratia G, Schultze H-P, Tischlinger H, Viohl G (Eds) Solnhofen: ein Fenster in die Jurazeit. Verlag Dr. Friedrich Pfeil, München, 72–77.

Wellnhofer P (1970) Die Pterodactyloidea (Pterosauria) der Oberjura-Plattenkalke Süddeutschlands. Bayerische Akademie der Wissenschaften, Mathematisch-Naturwissenschaftliche Klasse. Abhandlungen 141: 1–133.

Wellnhofer P (1975) Die Rhamphorhynchoidea (Pterosauria) der Oberjura-Plattenkalke Süddeutschlands. Teil I: Allgemeine Skelettmorphologie. Palaeontographica Abteilung A 148: 1–33.

Wellnhofer P (1978) Handbuch der Paläoherpetologie. Teil 19: Pterosauria. Gustav Fischer Verlag, Stuttgart, 82 pp.

Wellnhofer P (1985) Neue Pterosaurier aus der Santana-Formation (Apt) der Chapada Do Araripe, Brasilien. Palaeontographica Abteilung A 187: 105–182.

Wellnhofer P (2008a) A short history of pterosaur research. Zitteliana 28: 7–19.

Wellnhofer P (2008b) Archaeopteryx: der Urvogel von Solnhofen. Dr. Friedrich Pfeil, München, 256 pp.

Wessel P, Smith WHF, Scharroo R, Luis J, Wobbe F (2013) Generic Mapping Tools: Improved version released. Eos 94(45): 409–410. https://doi.org/10.1002/2013EO450001

Zittel KA (1883) Über Flugsaurier aus dem lithographischen Schiefer Bayerns. Palaeontographica 29: 47–80.